

DEVELOPMENT OF A REINFORCED SYNTHETIC HEART VALVE FOR PERCUTANEOUS DELIVERY

MONICA MARY ROZEIK

This thesis is submitted in partial fulfilment for the degree of
Doctor of Engineering

Department of Biomedical Engineering
Wolfson Centre, 106 Rottenrow, University of Strathclyde, G4 0NW

2013

DECLARATION

This thesis is the result of the author's original research. It has been composed by the author and has not been previously submitted for examination which has led to the award of a degree.

The copyright of this thesis belongs to the author under the terms of the United Kingdom Copyright Acts as qualified by University of Strathclyde Regulation 3.50. Due acknowledgement must always be made of the use of any material contained in, or derived from, this thesis.

Signed:

Date:

ACKNOWLEDGEMENTS

I would firstly like to thank my supervisors for their complete support and knowledge, without which, I would have been unable to complete my thesis. I am indebted to Professor Terry Gourlay, for his guidance and vibrant input of ideas and to Professor David Wheatley for his invaluable experience and contribution to the field of valve development and testing.

I am also indebted to several people who have helped in certain aspects of this thesis; Stephen Murray for his speedy assistance in developing jigs and cutters, David Smith for his aid with the Instron machine, and those who assisted me in the use of laboratory and imaging equipment including John Maclean, Elizabeth Goldie and Drs Louise Birchall, Laurie Shedden, Ashleigh Fletcher, Iain Larmour and Paul Edwards. I would also like to thank Brightwake Ltd. for their assistance in the development of the stents, as well as the EPSRC for their funding in this project.

Furthermore, I would like to thank my family for their continued support; my mother and sisters for always saying the right thing at the right time and my friends for their invaluable company and stress relief.

I would finally like to dedicate this in loving memory of my father who was always full of support and enthusiasm.

ABSTRACT

Approximately 30% of patients with aortic stenosis over the age of 75 years are refused surgery on the grounds of technical or high risk complications. Following the onset of symptoms, prognosis is very poor if left untreated. Transcatheter aortic valves intervention (TAVI) has paved the way for valve replacement in high risk patients without the need for open heart surgery. The current market approved valves can be delivered percutaneously through the femoral artery or transapically to the beating heart, deployed over the calcified leaflets and begin functioning immediately.

Complications with the current TAVI valves include a requirement for a large delivery sheath which leads to major vascular bleeding. Additionally, these valves use pericardial leaflets, which are too thick to collapse into a small catheter and have a propensity to calcify. It is therefore the objective of this thesis to develop an ultra-thin reinforced synthetic leaflet to reduce the delivery profile and facilitate deployment through a peripheral artery. Polyurethane films reinforced with multi-walled carbon nanotubes were solvent cast and tested for changes to the mechanical properties. Dip coated composite valves with varying content of carbon nanotubes were then developed and tested in a high cycle durability tester.

The stiffness of composites was found to improve overall with increasing nanotube content. However, fatigue life was found to be compromised, with only the 0.125% MWNT-TPU composite material having similar fatigue life to the neat TPU. The durability of the leaflets was also severely compromised when the thickness was dropped below 50 μm . Leaflet stresses were also reportedly highest at the commissures and the belly region. A valve having sufficiently thin leaflets (130 μm) was developed from a harder grade of polyurethane and has survived 23 million cycles to date. It is believed that a thin and durable leaflet can be achieved using harder grades of polyurethanes reinforced with low carbon nanotube concentrations.

TABLE OF CONTENTS

| | | |
|-------|---|----|
| 1 | Introduction | 2 |
| 1.1 | The Aortic Valve | 2 |
| 1.1.1 | Gross Anatomy and Location..... | 2 |
| 1.1.2 | Valve Dynamics | 5 |
| 1.1.3 | Structure of the Leaflets | 6 |
| 1.1.4 | Mechanical Properties | 8 |
| 1.2 | Valvular Diseases | 10 |
| 1.2.1 | Bicuspid Aortic Valves | 10 |
| 1.2.2 | Aortic Stenosis | 12 |
| 1.2.3 | Aortic Regurgitation..... | 14 |
| 1.2.4 | Indications for Surgery Based on EOA..... | 14 |
| 1.3 | Aortic Valve Replacement | 16 |
| 1.3.1 | Cardiac Surgery..... | 16 |
| 1.3.2 | Mechanical Valves | 17 |
| 1.3.3 | Bioprosthetic Valves | 19 |
| 1.3.4 | Tissue Engineered Valves | 21 |
| 1.3.5 | Polymeric Valves | 23 |
| 1.3.6 | Complications with AVR..... | 24 |
| 1.4 | Chapter Summary | 26 |
| 2 | Percutaneous Heart Valves | 29 |
| 2.1 | First Generation Percutaneous Heart Valves..... | 30 |
| 2.1.1 | History..... | 30 |
| 2.1.2 | Cribier Edwards Valve | 32 |
| 2.1.3 | CoreValve Prosthesis | 35 |
| 2.2 | Transcatheter Approaches | 37 |
| 2.2.1 | Clinical Evaluation and Imaging..... | 37 |
| 2.2.2 | Antegrade Transseptal Approach..... | 38 |
| 2.2.3 | Transfemoral Retrograde Approach..... | 39 |
| 2.2.4 | Transapical Aortic Intervention | 41 |
| 2.2.5 | Other Transcatheter Approaches..... | 42 |

| | | |
|-------|---|----|
| 2.3 | Repositionable and Retrievable PHVs | 44 |
| 2.4 | Valve in Valve Procedures | 46 |
| 2.5 | Results from the PARTNER Trial..... | 46 |
| 2.6 | Complications..... | 47 |
| 2.7 | Future TAVI..... | 49 |
| 2.8 | Chapter Summary | 49 |
| 3 | Thesis Aims and Objectives..... | 53 |
| 4 | Pericardial Heart Valves | 57 |
| 4.1 | Introduction | 57 |
| 4.2 | Structure and Biochemistry of Pericardium | 58 |
| 4.3 | Mechanical Anisotropy | 59 |
| 4.4 | Sample Preparation..... | 60 |
| 4.5 | Tensile Testing | 62 |
| 4.6 | Results | 64 |
| 4.7 | Discussion | 69 |
| 4.8 | Comparison with Polymeric Leaflets | 72 |
| 4.9 | Chapter Summary | 73 |
| 5 | Principles of Valve Design..... | 75 |
| 5.1 | Introduction | 75 |
| 5.2 | The Dimensions of the Native Aortic Valve | 77 |
| 5.3 | Leaflet Geometry..... | 78 |
| 5.3.1 | Polymeric Valve Geometries | 78 |
| 5.3.2 | The Valve Design..... | 81 |
| 5.4 | Material Considerations | 84 |
| 5.4.1 | Mechanical Properties | 85 |
| 5.4.2 | Leaflet Thickness | 88 |
| 5.4.3 | Fibre Composite Valves..... | 90 |
| 5.4.4 | Leaflet Manufacturing..... | 91 |
| 5.4.5 | Leaflet Calcification and Thrombosis..... | 93 |
| 5.5 | Chapter Summary | 94 |
| 6 | Polymeric Valve Composites..... | 97 |
| 6.1 | Reinforcement of Heart Valves | 97 |

| | | |
|-------|--|-----|
| 6.2 | Introduction to Polyurethane Elastomers | 100 |
| 6.3 | Structure of Nanotubes | 103 |
| 6.4 | Properties of Nanotubes | 105 |
| 6.4.1 | Mechanical Properties | 105 |
| 6.4.2 | Electrical and Thermal Conductivity | 106 |
| 6.4.3 | Biocompatibility | 107 |
| 6.5 | Purification of Nanotubes | 109 |
| 6.6 | Polymer Nanotube Composites | 111 |
| 6.6.1 | Dispersion Techniques in Polymer | 111 |
| 6.6.2 | Alignment of Carbon Nanotubes | 113 |
| 6.6.3 | Mechanical Properties | 115 |
| 6.6.4 | Fatigue Life | 115 |
| 6.7 | Chapter Summary | 116 |
| 7 | Composite Materials Testing | 119 |
| 7.1 | Preparation of Materials | 119 |
| 7.1.1 | Materials | 119 |
| 7.1.2 | Purification of Carbon Nanotubes | 119 |
| 7.2 | Determination of the Tensile Properties of MWNT Composites | 120 |
| 7.2.1 | Estane [®] with Impure Thick MWNTs | 120 |
| 7.2.2 | Carbothane [®] and Elast-Eon [™] MWNT Composites | 121 |
| 7.2.3 | Carbothane PC3595A with Thick Impure MWNTs | 123 |
| 7.3 | Results | 128 |
| 7.3.1 | SEM and Raman Imaging | 128 |
| 7.3.2 | Estane with thick impure MWNT Composites | 131 |
| 7.3.3 | Carbothane / and Elast-Eon / MWNT Composites | 135 |
| 7.3.4 | Carbothane 95A with Thick Impure MWNTs | 140 |
| 7.4 | Discussion | 150 |
| 7.5 | Chapter Summary | 154 |
| 8 | Valve Development and Testing | 156 |
| 8.1 | Valve Fabrication | 156 |
| 8.1.1 | Dip Coating Process | 156 |
| 8.1.2 | Leaflet Thicknesses | 157 |

| | | |
|-------|---------------------------------------|-----|
| 8.2 | Durability Testing..... | 160 |
| 8.2.1 | Set-Up | 161 |
| 8.2.2 | Valves with the Delrin Stent | 165 |
| 8.2.3 | Valves with Polycarbonate Stents..... | 167 |
| 8.3 | Computational Fluid Dynamics..... | 170 |
| 8.3.1 | Introduction to Fluid Dynamics | 170 |
| 8.3.2 | Steady Flow through a Valve..... | 173 |
| 8.3.3 | Unsteady Flow through a Valve..... | 178 |
| 8.3.4 | Model Limitations | 182 |
| 8.4 | Discussion | 183 |
| 8.5 | Chapter Summary | 185 |
| 9 | Discussion and Conclusions..... | 187 |
| 9.1 | Discussion | 187 |
| 9.2 | Future Work | 194 |
| 9.3 | Conclusion..... | 196 |
| 10 | References | 198 |

LIST OF FIGURES

| | |
|--|----|
| Figure 1.1 - Anatomical position of the aortic valve in relation to the left ventricle, left atrium and ascending aorta of the heart. Green line shows the basal attachment of the aortic leaflets (Piazza et al. 2008). | 3 |
| Figure 1.2 - Cut away of the aorta showing the semilunar leaflets, sinuses of Valsalva and the coronary ostia (Grays Anatomy)..... | 4 |
| Figure 1.3 - Leaflet of an aortic valve with visible bundles of collagen fibres. C marks the commissures. | 8 |
| Figure 1.4 - (a) Mechanical response of collagen and elastin during the cardiac cycle and (b) schematic representation of the aortic leaflet during systole and diastole. Reprinted from (Mendelson and Schoen 2006). | 9 |
| Figure 1.5 - Schematic of the bicuspid aortic valve (Siu and Silversides 2010). | 11 |
| Figure 1.6 - Photograph of a minimally diseased aortic valve and a severely calcified aortic valve. Arrow points to lipo-calcific changes to the aortic side although the commissures are spared (Freeman and Otto 2005). | 13 |
| Figure 1.7 - Mechanical heart valves: A. Ball and cage valve, B. Tilting-disc valve and C. Bileaflet valve (Bloomfield 2002)..... | 19 |
| Figure 1.8 - Bioprosthetic valves: a) Medtronic Hancock II Porcine Valve, b) Edwards Pericardial Valve and c) Edwards Prima Plus Stentless Porcine Prosthesis. | 20 |
| Figure 1.9 - Photographs of autologous tissue engineered valve (a) non-woven PGA scaffold coated with P4HB from the (a) aortic and (b) ventricular sides. (c) and (d) after 4 weeks of culturing. Adapted from Mol et al., (2006)..... | 22 |
| Figure 1.10 - Polymeric heart valves; (a) the Elast-Eon valve manufactured by Aortech, (b) the ADAIM Polycarbonate urethane valve and the (c) POSS-PCU valve developed at University College London..... | 24 |
| Figure 2.1 - Percutaneous valve developed by Anderson et al. (a) stent assembly, (b) porcine aortic valve sutured to stent and (c) aortic view of valve (1992)..... | 30 |
| Figure 2.2 - Early percutaneous heart valves; (A) the Bonhoeffer valve, (B) Lutter valve and (C) Paniagua heart valve. | 32 |
| Figure 2.3 - Evolution of the Cribier Edwards valve; (A) first generation equine pericardial valve, (B) SAPIEN valve and (C) the low profile SAPIEN XT valve both with bovine pericardium (Webb and Binder 2012). | 34 |
| Figure 2.4 - (a) First and (b) Third generation of the CoreValve prosthesis, adapted from Grube et al. (2008) and (c) CoreValve® Evolut™ prosthesis..... | 36 |
| Figure 2.5 - Edwards SAPIEN XT delivery; (A) Novaflex balloon catheter in collapsed and expanded state and (B) the Novaflex handle (Willson et al. 2011)..... | 40 |

| | |
|--|----|
| Figure 2.6 - Transapical Valves; (a) Symetis Acurate™, (b) Medronic Engager and (c) 2 nd Generation JenaValve (Sinning et al. 2012)..... | 43 |
| Figure 2.7 - Transcatheter approaches a) Retrograde transfemoral approach, b) Antegrade transseptal approach, (c) trans-aortic approach, (d) trans-subclavian artery and (e) trans-axillary approach (Rodes-Cabau 2012)..... | 43 |
| Figure 2.8 - The Direct Flow PHV; (A) Side view displaying the aortic and ventricular rings and (B) top view in a hydrodynamic testing chamber. | 44 |
| Figure 4.1 - Schematic representation of the layers of pericardium (taken from mediconweb.com)... | 58 |
| Figure 4.2 - Photograph of fresh porcine pericardium and the parallel blade cutter used to cut the strips. | 60 |
| Figure 4.3 – Strips cut from a sheet of pericardium aligned at (a) 0° and (b) 90° to the direction of the fibres. | 62 |
| Figure 4.4 - Porcine pericardium strip sandwiched between frames of sandpaper and clamped on to the Instron grips. | 63 |
| Figure 4.5 – Images from microscope taken of fresh porcine pericardium, descending through its layers (a)-(f). Arrows indicate predominate direction of fibres. Note the change of direction of fibres from (b) to (c). The bundles of fibres appear to be loosely bound. .. | 64 |
| Figure 4.6 - Images from microscope of fixed pericardium descending through the various layers (a)-(f). Arrows indicate predominant direction of fibres. A tighter crimp formation in comparison to the fresh pericardium is apparent by the increased amplitude of the ridges. The resolution decreases as the depth of the images increases. | 65 |
| Figure 4.7 – Graph of the stress-strain relationship for a fixed pericardium strip in the longitudinal and transverse directions. | 67 |
| Figure 4.8 – Graph of the stress-strain relationship for a fresh pericardium in the longitudinal and transverse directions. | 67 |
| Figure 4.9 - Mean (\pm SEM) of the Elastic modulus in MPa of fixed and fresh porcine pericardium (n = 6 for the fixed PP, n = 9 fresh 0° PP and, n = 7 fresh 90° PP). | 68 |
| Figure 4.10 - Mean (\pm SEM) of the Ultimate tensile strength in MPa of fixed and fresh porcine pericardium (n = 6 for the fixed PP, n = 9 fresh 0° PP and, n = 7 fresh 90° PP). | 68 |
| Figure 4.11 – Load – deformation response of polyurethane. | 73 |
| Figure 5.1 - The aortic valve (I) schematic and (II) valve parameters; H – height, R _b – Radius of base, R _c – radius of commissures, ϕ – angle from free edge to plane of commissures, α – angle of base of leaflets to a plane through the commissures (Thubrikar et al. 1981)... | 78 |
| Figure 5.2 - Various design concepts; (a) symmetric and (b) asymmetric valve design by Aortech in a semi-open positions, (c) Bezier surface valve by Mohammadi et al. (2011), (d)-(f) different commissural opening; closed, open and semi-open with flat leaflets, (g) Burrisci valve with open coatpatation regions and a flat surface, (h) ADIAM valve mid open position and (i) Mackay valve. | 81 |

| | |
|---|-----|
| Figure 5.3 - Leaflet design (a) Hyperbolic in the circumferential direction and elliptical in the radial direction (Mackay et al. 1996). (b) Major axis of hyperbole increased. | 83 |
| Figure 5.4 - Photograph of (a) the assembled stent and former used and separate photographs of the (b) polycarbonate stent and (c) stainless steel former. | 84 |
| Figure 5.5 - Creep properties (a) constant stress applied between t_0 and t_1 and (b) strain response. | 86 |
| Figure 5.6 - Stress relaxation properties (a) constant strain applied at t_0 for a length of time and (b) stress response. | 86 |
| Figure 5.7 - The stress-strain relationship of several polyurethane elastomers (Bernacca et al. 2002). | 87 |
| Figure 5.8 - Cross sectional view of a crimped percutaneous valve and catheter assembly (Li and Sun 2010). | 90 |
| Figure 5.9 - Minimum catheter size needed in relation to thickness of valve leaflet with and without a balloon expandable stent based on the model by Li and Sun (2010). | 90 |
| Figure 6.1 - Types of composite reinforcements (Mathworld)..... | 97 |
| Figure 6.2 - Reinforced polymeric heart valves; (a) stentless reinforced valve, (b) side and (c) top view of a stented reinforced valve, (d) LARS mesh reinforced and (e) Dacron reinforced valve. | 99 |
| Figure 6.3 - (a) Formation of a polyurethane segment and (b) schematic of the segmented structure. SS – soft segment. HS – hard segment. Adapted from Crawford et al. (1998). | 100 |
| Figure 6.4 - Conceptual diagrams of (a) single and (b) multi-walled carbon nanotubes and their typical dimensions (Reilly 2007). | 104 |
| Figure 6.5 - Schematic of the hexagonal lattice of the nanotube (Thostenson et al. 2001). | 104 |
| Figure 6.6 - SEM images of platelets adhered on (a) PU or (b) MWNT-PU surface (Meng et al. 2005). | 108 |
| Figure 6.7 - TEM images of: (a) as-produced crude materials, (b) material that was refluxed for 24 h in 3 M HNO ₃ , (c) material produced by treating the HNO ₃ -treated sample in 5 M HCl for 6 h, (d) purified MWNTs produced by oxidizing the acid-treated sample for 60 min in air at 510 °C (Chen et al. 2002). | 110 |
| Figure 6.8 - Carbon nanotube in Estane polymer (a) spin coated on a substrate and (b) SEM photograph of aligned fibres (arrows highlighting direction of fibres). | 114 |
| Figure 7.1 - Acid refluxing process of the carbon nanotubes | 120 |
| Figure 7.2 - Nanotubes dispersed in DMAc solvent (a) before and (b) after sonication | 122 |
| Figure 7.3 - Water bath testing on BOSE ELF system. | 125 |
| Figure 7.4 - Fatigue testing polymer samples between grips of the Bose ELF Tester. | 126 |
| Figure 7.5 - SEM at two different magnifications of thick MWNTs; A & B – Raw form, C & D after acid treatment and E & F following calcination in static air. | 128 |
| Figure 7.6 - SEM images of thin MWNTs at two different magnifications; A & B – Raw form | 129 |
| Figure 7.7 - Raman spectroscopy of the thin (10-15 nm) MWNTs in their raw, acid treated and pure states. | 130 |

| | |
|--|-----|
| Figure 7.8 - Raman spectroscopy of the thick (110-170 nm) MWNTs in their raw, acid treated and pure states. | 130 |
| Figure 7.9 - Stress-strain relationship of Estane with up to 4% MWNTs. | 132 |
| Figure 7.10 – Close up of Figure 7.9. Secant modulus is derived from dividing the stress at 5% strain by 0.05. | 132 |
| Figure 7.11 – Relationship between the secant modulus and the thickness of the samples showing no correlation. R – Repeat composite. | 133 |
| Figure 7.12 - Comparison of the typical mechanical properties of polyurethanes up to 45% strain. . | 134 |
| Figure 7.13 - The average (\pm S.E.M) secant modulus at 5% strain of 1% of MWNT composites having 110 nm and 10 nm diameters. I – Impure nanotubes, P – Pure nanotubes. E5 –Elast-Eon, PC85 and PC95 – Carbothane PC3585A and PC3595A respectively (n=5, * indicates significance difference from neat polymer, $p < 0.05$ based on a one-way ANOVA test). | 135 |
| Figure 7.14 – Stress and strain relationships with time using displacement controlled creep for neat Elast-Eon. Variability in stress at a fixed strain is noticeable. Sample 1 has a reduced stress due to initial tuning of the testing system. | 137 |
| Figure 7.15 – Stress and strain relationships with time using displacement controlled creep for Elast-Eon with impure 110 nm MWNTs. Sample 1 has a reduced stress value due to initial tuning of the test system. | 137 |
| Figure 7.16 - Creep modulus of 1% MWNT composites after 30 seconds. I - Impure nanotubes. P - Pure nanotubes. (n=5 except for PC85-P-110 nm, * indicates significance difference from neat polymer, $p < 0.05$ based on a one-way ANOVA test). | 138 |
| Figure 7.17 – a) ramp graph of strain against time and b) stress response for samples of neat Elast-Eon. | 139 |
| Figure 7.18 - Mean (\pm S.E.M) stiffness against dispersion time (hours) in an ultrasonic bath for 0.5% and 1% fibres. N=5, * represents significant difference ($p < 0.05$) compared to composite at 1 hour sonication time, based on a one-way ANOVA study. | 140 |
| Figure 7.19 - Mean (\pm S.E.M) storage modulus of the 0.5% and 1% fibres after 1 hour and 7.5 hours dispersion time (n=6). | 141 |
| Figure 7.20 - Optical microscope images of the 0.5% (a-d) and 1% (e-h) MWNT composites following 1 (a, e), 3 (b, f), 5 (c, g) and 7.5 hours (d, h) dispersion in an ultrasonic bath (35x magnification). Red circles highlight some of the clusters in the matrix. | 141 |
| Figure 7.21 - Elastic modulus between 0.5 and 1.0 MPa stress with increasing strain rate and nanotube content. N>4, * represents significance, $P < 0.05$, in composite samples only. ** represents significance, $P < 0.01$ in all samples based on a one-way ANOVA study. | 142 |
| Figure 7.22 - Secant Modulus at 5% strain of Carbothane 95A after immersion in distilled water for several days (n=5). | 143 |
| Figure 7.23 - Change of sample thickness (mm) with increasing time in water (n=6). | 144 |

| | |
|--|-----|
| Figure 7.24 – Negative correlation between the percentage stress relaxation and the secant modulus. | 144 |
| Figure 7.25 - Cycles to failure with increasing MWNT content. | 146 |
| Figure 7.26 - SEM images of failed fatigue tested samples at two different magnifications of PC3595A with (a-b) 0%, (c-d) 0.125% and (e-f) 0.25% MWNTs. | 147 |
| Figure 7.27 - Secant modulus at 5% strain for the pure, 0% and composite 1% films several days after gamma irradiation. NS - non sterile and SS – sterile. | 148 |
| Figure 7.28 - Percentage stress relaxation in composites following sterilization. | 149 |
| Figure 7.29 - Secant modulus at 5% strain for composites when crimped under a 1 kg load. * represents significant difference ($p < 0.05$) compared to control based on a one-way ANOVA study. | 149 |
| Figure 8.1 - Former with stent mounted and dipped in (a) an inverted and (b) upright position on the hotplate. | 157 |
| Figure 8.2 - Rigid stents used (a) rapid prototyping, (b) clear polycarbonate stent and (c) Delrin stent. | 158 |
| Figure 8.3 - Developed valves (a) clear polymer, (b) 0.125% 95A-MWNT, (c) 0.5% 95A-MWNT and (d) 1.0% P5A-MWNT. | 158 |
| Figure 8.4 - Thickness distribution of the free edge of leaflets. | 159 |
| Figure 8.5 - Thickness distribution in the belly region of leaflets. | 159 |
| Figure 8.6 - Thickness distribution at the base of leaflets. | 159 |
| Figure 8.7 - General Vi-Vitro set up. | 160 |
| Figure 8.8 - Bellow replacement on durability tester (a) brittle old bellow (blue) alongside a softer new bellow (transparent) and (b) mounted on tester. | 162 |
| Figure 8.9 - Silicone ring mould with a valve-less stent before (a) and after (b) application of silicone. (c) Valve mounted in piston cap. | 162 |
| Figure 8.10 - Top view of Vi-Vitro tester with all 6 valves in situ. | 163 |
| Figure 8.11 - Pressure transducers mounted to top and bottom of valve chambers. | 163 |
| Figure 8.12 - Typical pressure curves in HiCycle chamber displaying a 90 mmHg pressure drop. TVG – transvalvular gradient. | 164 |
| Figure 8.13 - Typical opening pressures of 0% and 0.125% 95A-MWNT valves with varying number of coats. | 164 |
| Figure 8.14 - Initial failure modes of valves with a Delrin stent; leaflet de-bonding from stent. | 165 |
| Figure 8.15 - SEM images of failed samples around the stent post region; (a)-(b) 0% and (c) 1.0% valves, (d) free edge at stent post. | 166 |
| Figure 8.16 - Primary failure mode of valves with a polycarbonate stents; leaflet rupture across belly region. | 167 |
| Figure 8.17 - Failed 0% (a-b) and 1% (c-d) MWNT valves with leaflet ruptures (a) leaflet near base of valve, (b) at polycarbonate stent post, (c) split along the middle and (d) close-up of (c) with evidence of fibre pull-out. | 168 |

| | |
|---|-----|
| Figure 8.18 - Polycarbonate stent fracture with valves. Leaflet ruptured occurred as a secondary failure mode. | 169 |
| Figure 8.19 - Velocity profile of fluid in a pipe; flow is fully developed when the boundary layers merge. The initial plug velocity profile is like that of the aorta (www.learneasy.info). | 171 |
| Figure 8.20 - Top and isometric view of the valve in pipe model with leaflets flat in the radial direction. Third of valve hidden in isometric view to show leaflets. | 174 |
| Figure 8.21 - Velocity vectors of flat and curved leaflet at a cross-section of the pipe at z=0..... | 175 |
| Figure 8.22 - Pressure contours of flat and curved leaflet at a cross-section of the pipe at z=0..... | 176 |
| Figure 8.23 - Shear stresses across walls in flat and curved leaflets. | 177 |
| Figure 8.24 - Contours of the wall shear stress in the flat valve. | 177 |
| Figure 8.25 - Fluent grid model of the valve in pipe with a velocity inlet (blue) and pressure outlet (red). | 179 |
| Figure 8.26 - Maximum facet total pressure in mm of mercury at the inlet, and valve and pipe outlets. | 180 |
| Figure 8.27 - Maximum facet velocity in m/s at the inlet and valve and pipe outlets. | 180 |
| Figure 8.28 - Maximum facet shear stress in Pascals at the inlet and valve and pipe outlets..... | 180 |
| Figure 8.29 - Velocity magnitude at an iso-surface of z=0 for times of 280 ms, 350 ms and 420 ms | 181 |
| Figure 8.30 - Pressure and velocity profiles at at an iso-surface of z=0 for times of 280 ms, 350 ms and 420 ms..... | 181 |
| Figure 8.31 - Contours of wall shear stress (mmHg) at valve outlet. | 182 |

LIST OF TABLES

| | |
|--|-----|
| Table 2.1 - Comparison of some of the current percutaneous valves..... | 51 |
| Table 4.1 – Description of the testing samples..... | 61 |
| Table 4.2 – Summary of results (mean ± SEM) from the tensile testing for each set group. | 66 |
| Table 7.1 - Ratio of intensity bands for thin (high aspect ratio) MWNTs in their raw, refluxed and pure states (n=3). | 131 |
| Table 7.2 - Average ratio of intensity bands (± S.E.) for thick MWNTs in their raw, refluxed and pure states (n=3). | 131 |
| Table 7.3 - Average (± SEM) of the tensile properties of Estane with 1-4% thick and impure MWNTs (n=7-10)..... | 133 |
| Table 7.4 – Percentage stress relaxation (%) in composites (n=5)..... | 138 |
| Table 7.5 – Tear strength (N/mm) of composites (n = 3)..... | 139 |
| Table 7.6 - Results of the mechanical properties of composites at 37°C | 145 |
| Table 7.7 - Summary of results (Mean ± SEM) for fatigue testing batches at 70.1% strain. | 145 |

LIST OF ABBREVIATIONS

| | | |
|------|---|---|
| AS | – | Aortic Stenosis |
| AR | – | Aortic Regurgitation |
| AV | – | Atrioventricular |
| AVR | – | Aortic Valve Replacement |
| BAV | – | Bicuspid Aortic Valve |
| BPV | – | Bovine Pericardial Valve |
| CABG | – | Coronary Artery Bypass Graft |
| CPB | – | Cardiopulmonary Bypass |
| CNT | – | Carbon Nanotubes |
| DFM | – | Direct Flow Medical |
| DMA | – | Dynamic Mechanical Analysis |
| ECM | – | Extracellular Matrix |
| EOA | – | Effective Orifice Area |
| ESV | – | End Systolic Volume |
| Fr | – | French Dimensions |
| GAG | – | Glycosaminoglycan |
| HITS | – | High Intensity Transient Signals |
| LDL | – | Low Density Lipoprotein |
| LV | – | Left Ventricle |
| LVOT | – | Left Ventricular Outflow Tract |
| MSC | – | Mesenchymal Stem Cells |
| MSCT | – | Multi-slice Computed Tomography |
| MRI | – | Magnetic Resonance Imaging |
| MWNT | – | Multi-walled Carbon Nanotubes |
| PAV | – | Porcine Aortic Valve |
| PBS | – | Potassium Buffer Solution |
| PG | – | Proteoglycan |
| PHV | – | Percutaneous Heart Valve |
| PPM | – | Patient-Prosthesis Mismatch |
| PTFE | – | Polytetrafluoroethylene |
| PU | – | Polyurethane |
| PyC | – | Isotropic Pyrolytic Carbon |
| RVP | – | Rapid Ventricular Pacing |
| SWNT | – | Single-walled Carbon Nanotubes |
| TA | – | Transapical |
| TAVI | – | Transcatheter Aortic Valve Intervention |

| | | |
|----------------|---|----------------------------------|
| TEE | – | Transesophageal Echocardiography |
| TEHV | – | Tissue Engineered Heart Valve |
| TF | – | Transfemoral |
| T _g | – | Glass Transition Temperature |
| TPG | – | Transvalvular Pressure Gradient |
| TPU | – | Thermoplastic Polyurethane |
| TTE | – | Transthoracic Echocardiography |
| UTS | – | Ultimate Tensile Strength |
| VEC | – | Valvular Endocardial Cells |
| VIC | – | Valvular Interstitial Cells |
| VC | – | Vena Contracta |
| VTI | – | Velocity Time Integral |

CHAPTER 1:

INTRODUCTION

1 INTRODUCTION

1.1 THE AORTIC VALVE

The aortic valve is subjected to opening and closing approximately 103,000 times a day and about 3.7 billion times in an average life-span. It directs a one way forward flow of blood from the left ventricle of the heart to the rest of the body with minimal regurgitation and pressure drop (Thubrikar 1990). These delicate and thin leaflet structures are subjected to a lot of rapid tensile, shear and bending stresses. Historically, they were considered to react passively to regulate the flow of blood to keep us alive. However, it is now readily becoming accepted that the aortic valve undergoes a series of complex operations at the cellular and molecular level to maintain their function in the extreme hemodynamic and mechanical environments (El-Hamamsy et al. 2010). In diseased valves, their function is compromised leading to complications such as heart failure and eventual death if left untreated. In severe cases, valve replacement is the gold standard treatment.

A correct understanding of the anatomy of the aortic root is vital when considering the design of a prosthetic valve. This is of particular importance when implanting a heart valve through a transcatheter intervention which sandwiches the native leaflets between the stent and the aortic wall and may create an obstruction to flow. The following sections of this chapter focus on the aortic valve's anatomy, pathology and the existing surgical replacement valves available. Transcatheter aortic valve intervention (TAVI) which involves the use of percutaneous heart valves (PHV) will be discussed in Chapter 2.

1.1.1 Gross Anatomy and Location

The aortic valve consists of three semi-lunar shaped leaflets and three dilations known as the sinuses of Valsalva. It lies within the aortic root which bridges the left ventricle (LV) to the ascending aorta (Anderson 2007). The base of the valve leaflets lie just below the anatomical ventriculo-arterial junction on a virtual ring known as

the basal attachment (Piazza et al. 2008). It is this anatomical location between the ventricle and aorta that surgeons use to suture a valvular prosthesis (Sutton 1995).

The sinuses interject with the ascending aorta at a ring known as the sinotubular junction. In two of the sinuses lie the coronary ostia which give rise to the right and left coronary arteries. Thus, the sinuses are regarded as the right and left coronary sinuses respectively, and the third sinus is the non-coronary (or posterior) sinus (Thubrikar 1990). The sinuses have a scalloped or crown like border running from the basal attachment to the sinotubular junction to which the semi-lunar side of the leaflets attach, creating a hinge on which the leaflets flex. A cut-away of the heart exposing the anatomical position of the aortic valve is shown in Figure 1.1.

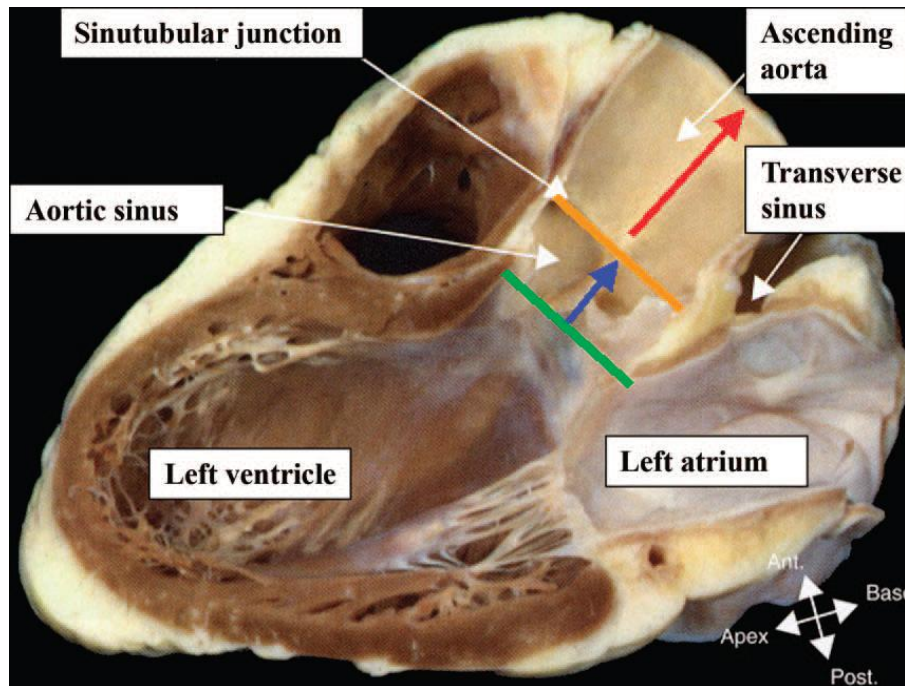


Figure 1.1 - Anatomical position of the aortic valve in relation to the left ventricle, left atrium and ascending aorta of the heart. Green line shows the basal attachment of the aortic leaflets (Piazza et al. 2008).

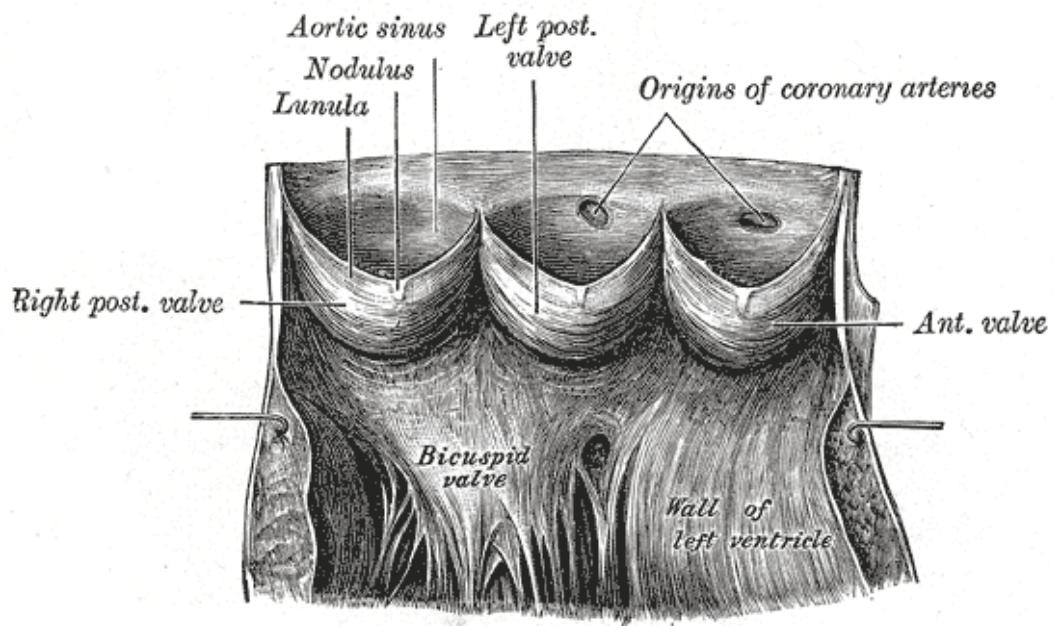


Figure 1.2 - Cut away of the aorta showing the semilunar leaflets, sinuses of Valsalva and the coronary ostia (Grays Anatomy).

Three fibrous inter-leaflet triangles form between the leaflets and the basal attachment. The inter-leaflet triangle between the posterior and left leaflet are in fibrous continuity with the anterior leaflet of the bicuspid mitral valve (Figure 1.2). Thus a low placement of the valvular prosthesis within the left ventricular outflow tract (LVOT) may result in impingement on the mitral leaflet (Piazza et al. 2008). The triangle between the right and posterior leaflet is connected to the membranous part of the ventricular septum. In congenitally deformed valves, these triangles have been observed to be inadequately formed, providing a more annular shape than normal (Anderson et al. 1991, Sutton Iii et al. 1995).

The leaflets can be considered to form part of a cylinder as they are flexed circumferentially but are flat in the radial direction. This enables them to easily reverse curvature during valve opening and closure (Thubrikar 1990). The free edges of the leaflets come together at an angle of 120° to prevent the back flow of blood (Sacks et al. 2009). The line of attachment where the leaflets come together distally is known as the commissures, which transfer the load from the leaflets to the aortic

wall. The region where the free edges overlap is known as the coaptation region or lunula, and forms due to a bend in the radial plane of the leaflets. The lunula functions to transfer the pressure load from the centre of the leaflets to the commissures (Thubrikar 1990). Fibres form a thickened nodule at the centre of the free edges known as the node of Arantius which help to ensure full coaptation.

1.1.2 Valve Dynamics

During ventricular systole, pressure in the left ventricle rises and overcomes the pressure in the aorta. This results in a rapid opening of the aortic valve with minimal resistance to blood flow. Blood reaches a peak velocity of approximately 1.35 ± 0.35 m/s in the first third of the cycle before decelerating and reversing flow (Chandran et al. 2006). Ideally, the aortic valve would be required to open rapidly with minimal resistance. In a healthy valve, it typically opens in 20-30 ms (Chandran et al. 2006). The deceleration reverses the pressure gradient, forcing the edges of the leaflets to come together and rapidly shut the valve with minimal regurgitation. The closing volume has been noted to be less than 5% of the forward flow (Chandran et al. 2006). Whilst the pressure gradient across the open valve is less than 10 mmHg in a healthy valve, typical closing pressures are 80 - 100 mmHg.

During forward flow some of the blood coils around the sinus edge, which then decelerates and forms eddy currents before returning to the mainstream flow. This action was first reported by Leonardo da Vinci in 1513 who observed vortices forming behind the leaflets of valves mounted on a glass model of the aortic root (Robicsek 1991). Similar experiments were carried out by Bellhouse and Talbot (1969) which agreed with da Vinci's findings on the role of the sinuses. The vortices keep the leaflets afloat and create a pressure gradient on the lateral aspect of the leaflets in relation to the centre, pushing them together. If the sinuses were removed, the reversal pressure gradient of the mainstream flow is alone capable of valve closure but with less speed and efficiency. During diastole, when pressures in the ventricle drop below the aorta, blood in the sinuses flows into the coronary arteries through the right and left coronary ostia.

The velocity profile of the blood flow through the aortic valve is laminar and typically flat although there is a slight skew caused by the orientation of the valve to the long axis of the LV (Chandran et al. 2006). Although the aortic valve has generally been considered to react passively to the flow of blood, it actually reacts in a complex manner to dynamic changes during the cardiac cycle. For example, the orifice has been observed to change from triangular to circular depending on the rate of flow through the valve. The base perimeter is also largest at the end of diastole and minimum at the end of systole. Additionally the leaflets are found to contract in the circumferential direction during systole to increase the orifice area and extend radially during diastole to provide full coaptation (Thubrikar 1990).

1.1.3 Structure of the Leaflets

The cellular constituents of the aortic valve can be divided into two types; the valvular endocardial cells (VEC) and the valvular interstitial cells (VIC). Together, these cells interact in a complex hemodynamic and mechanical environment to regulate the valve (Butcher and Nerem 2006). The VEC encases all the valves and serves as a non-thrombogenic barrier between the blood and leaflets. Their phenotypes have been found to be distinctly different from vascular endothelial cells. Additionally, they have been found to align perpendicular to the direction of shear stress whereas vascular endothelial cells are aligned parallel to the direction of flow (Butcher and Nerem 2006). VECs on the aortic and ventricular sides have also been reported to be intrinsically different. Calcification of the aortic valve originates from endothelial dysfunction and occurs on the aortic side of the leaflet (El-Hamamsy et al. 2010). It is possible that the greater shear stress exposed by the ventricular side increases the resistance of its VECs.

The VIC has characteristics between smooth muscle cells and fibroblasts and forms a network across the extracellular matrix of the leaflets (Filip et al. 1986, Flanagan and Pandit 2003). It has been suggested that the VIC have several phenotypes including smooth muscle cells, myofibroblasts and fibroblasts. They exhibit contractile properties as well as regulate and synthesize components of the extracellular matrix

(Chester and Taylor 2007, El-Hamamsy et al. 2010). Contractile properties have been supported by evidence of α -smooth muscle actin expression when VICs were cultured in vitro. Additionally, they are involved in the inherent repair of the valve which is subjected to damage due to the complex hemodynamic environment and their absence in prosthetic valves may be a cause for structural failure (Butcher and Nerem 2006).

Due to their thin structure, the leaflets are practically avascular and obtain their nutrients from the surrounding blood. Interestingly, they have been found to be richly innervated, particularly on the ventricular side of the leaflet, apart from the lunula. Their significance is still not clearly understood but structural changes in response to neuromodulators may suggest adaptations to mechanical properties to cope with various pathologies such as hypertension (El-Hamamsy et al. 2009).

The extracellular matrix (ECM) primarily consists of collagen, elastin and proteoglycans (PG), each accounting for 60%, 10% and 20% of the dry weight of the valve respectively (Kunzelman et al. (1993) in Flanagan and Pandit (2003)). Collagen provides the valve leaflet with much of its mechanical strength whilst the elastin provides interconnections between the fibres and helps restore the collagen to its natural crimped state (Vesely 1998). PGs are highly hydrophilic which act as shock absorbers during the dynamic changes in the valve (El-Hamamsy et al. 2010).

The leaflets of all valves are comprised of 3 layers; the fibrosa, spongiosa and ventricularis (atrioventricular valves also contain an atrialis layer which forms part of the spongiosa). These terms were first coined by Gross and Kugel in 1931 who carried out a thorough study on the topographical anatomy and histology of heart valves in an attempt to address mechanisms of valve failure. The fibrosa is the thickest layer, consisting primarily of a dense network of type I collagen fibres arranged circumferentially. It appears to be the main loading bearer and extends throughout the whole of the tissue (Sacks et al. 2009). Collagen fibres have been found to be aligned circumferentially at the commissures which become even more highly aligned in loading.

The ventricularis is a dense network of collagen and elastin fibres which face the ventricular chamber. The elastin fibres appear to be radially aligned which assists in reducing radial strains caused by fluid flow when the valve is fully open. Between the fibrosa and ventricularis is a watery connective tissue known as the spongiosa. This layer contains a high concentration of glycosaminoglycans (GAGs) and proteoglycans (PGs) which are believed to lubricate the adjacent layers as they shear and deform relative to each other during leaflet flexure and pressurization (Thubrikar 1990, Sacks et al. 1998).

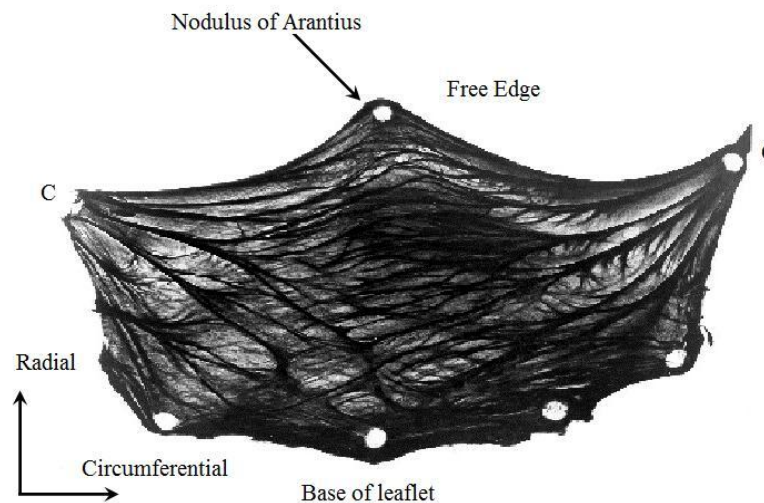


Figure 1.3 - Leaflet of an aortic valve with visible bundles of collagen fibres. C marks the commissures.

1.1.4 Mechanical Properties

Due to the circumferential and radial alignments of the collagen and elastin fibres, the valve leaflets have anisotropic and complex viscoelastic mechanical properties (Sacks 2000). The structural deformation of the aortic valve can be divided into two mechanisms; flexure and tension (Sacks and Yoganathan 2007). Flexion occurs during leaflet opening and closure whilst tension occurs during full loading from the diastolic pressures. Loading aligns and straightens out the crimped collagen fibres along the direction of the force which results in an initial toe region as the collagen straightens out followed by a rapid linear response in a stress-strain graph (Figure

1.4a). The leaflets are significantly stiffer in the circumferential direction than the radial. In a study by Kalejs et al. (2009) the elastic modulus of human aortic valve was calculated to be 15.34 ± 3.5 MPa in the circumferential direction and 1.98 ± 0.24 MPa in the radial direction.

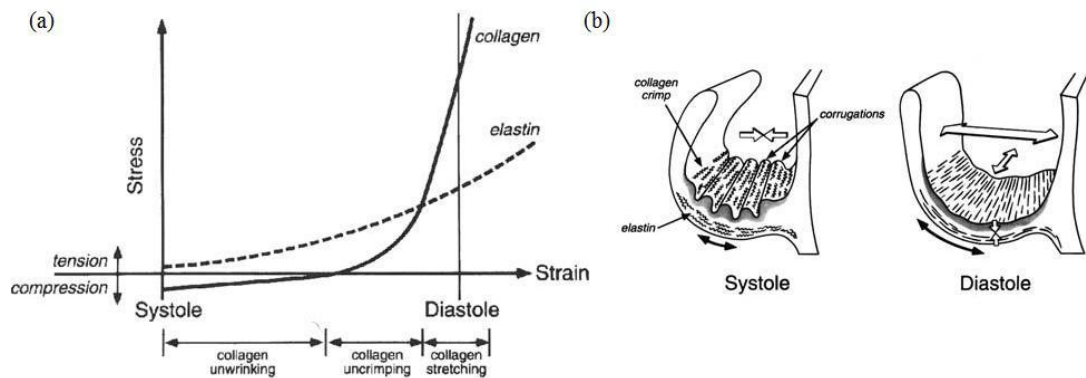


Figure 1.4 - (a) Mechanical response of collagen and elastin during the cardiac cycle and (b) schematic representation of the aortic leaflet during systole and diastole. Reprinted from (Mendelson and Schoen 2006).

The leaflets are viscoelastic, meaning that their mechanical properties exhibit both elastic and viscous characteristics. In time dependant studies, the mechanical properties of aortic leaflets were found to be independent of strain rate. They were also found to exhibit continued stress relaxation but had negligible creep over a period of three hours (Sacks et al. 2009). Materials exhibiting stress relaxation have a gradual decrease in stress at a constant strain which is beneficial during the diastolic phase of the cardiac cycle. Creep is an undesirable characteristic since it would permit the leaflets to gradually stretch with time when subjected to a fixed load which could lead to a prolapsed leaflet.

In flexion tests, the ventricularis was found to support the leaflet in tension when flexed with the curvature of the leaflets, i.e. when the valve is open. The elastin fibres arranged radially in the ventricularis enable the leaflet to extend radially for full coaptation; enabling it to handle strains of 60%. However, the elastin in the fibrosa was shown to have minimal involvement in the radial or circumferential

directions (Vesely 1998). In a study by Mirnajafi et al. (2006), the flexural stiffness at the belly region of the aortic valve was found to be three times that of the commissures. It was also found to be stiffer when the commissures were flexed in the non-physiological reverse direction and decreased with increasing flexion angle. The decrease was attributed to local tissue buckling which reduced the effective thickness of the leaflet.

1.2 VALVULAR DISEASES

Diseases of the heart valves compromise their normal function leading to other complications to the surrounding structures. They may be caused by a congenital defect, age, lifestyle habits, trauma or infection. The following sections will focus on the main valvular complications which arise from congenital deformations or due to degenerative disease.

1.2.1 Bicuspid Aortic Valves

Congenital valve defects range from a missing or complete closure of the valve as in aortic atresia, to sub-aortic or supra-valvular stenosis due to a narrowing of the LV or aortic tract respectively, to poor formation of the valve cusps. The most common congenital abnormality is the bicuspid aortic valve (BAV), where two leaflets are fused together to form one large leaflet, which occurs in 1-2% of the population and is more prevalent in males. Certain characteristics define a BAV including leaflets of different sizes, a central raphe between the largest leaflet and a smooth leaflet margin even when diseased (Ward 2000). Difference in leaflet size occurs in 92% of BAV cases and most prevalent (86%) between the right and left aortic leaflets (Sabet et al. 1999). The disease is thought to be genetic since it is highly associated with other abnormalities of the aorta such as aortic coarctation. Additionally it has been hypothesised that a lack of microfibrillar proteins during valvulogenesis may disrupt full development of the valve leaflets as well as create a weakened aortic root structure (Fedak et al. 2002).

The incidence of patients with aortic stenosis (a narrowing of the valve aperture) having a bicuspid, uni-cuspid or (rarely) quadri-cuspid valve is particularly high (Thubrikar 1990). The geometry of the valve has also been shown to play a role in leaflet calcification, thereby indicating a need to develop a valve with a native tri-leaflet design. Thubrikar (1990) noted that the greater the deviation from the normal configuration, the greater the number of valves requiring replacement and the younger the age of the patient requiring replacement.

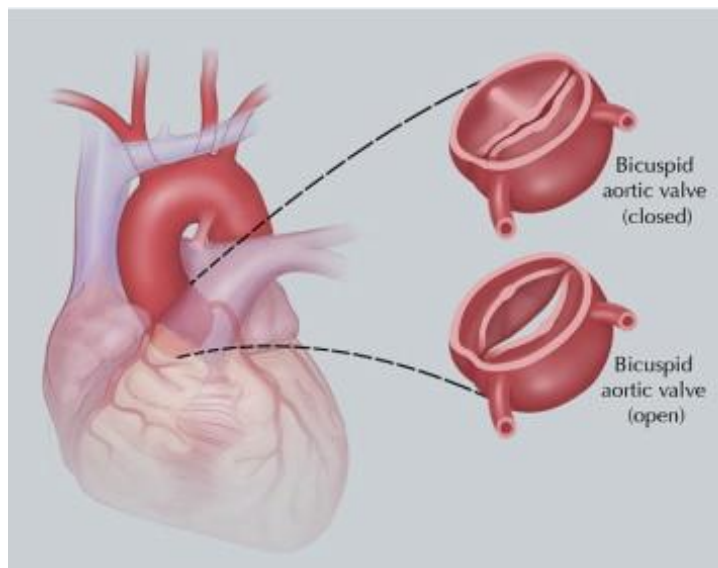


Figure 1.5 - Schematic of the bicuspid aortic valve (Siu and Silversides 2010).

As well as aortic stenosis, congenital valvular abnormalities are also associated with aortic regurgitation (AR), infective endocarditis, and aortic complications such as root dilation, aneurysms and dissection (Fedak et al. 2002). The occurrence of infective endocarditis in patients with BAV were found to range from 12% - 39% in surgical and autopsy studies (Sabet et al. 1999). Many patients with BAV have dilations of the aortic root, sinotubular junction, ascending aorta and aortic arch. These dilated structures lead to abnormal hemodynamics and shear stress, which can accelerate calcific degeneration of the valve. BAV is commonly asymptomatic from birth and the patient can function normally for 50-60 years before symptoms arise.

Symptoms detected from early childhood are generally due to severe valvular disease.

1.2.2 Aortic Stenosis

Aortic Stenosis (AS) is a narrowing of the valve aperture, reducing the aortic valve area and increasing resistance to blood flow, thereby increasing the transvalvular pressure gradient. This obstruction increases the workload of the left ventricle (LV) leading to a thickening of its walls (hypertrophy), although the ejection volume remains the same. In a population study by Nkomo et al. (2006), the mass of the LV was found to increase from 171.1 ± 70.1 g with a normal valve to 198.7 ± 80.9 g in patients with AS, suggesting ventricular hypertrophy. The most common cause of AS is calcific degeneration leading to stiffening and calcification of the tri-leaflet valve and restricting the motion of the leaflets. It can also be caused from Rheumatic fever due to inflammation of the leaflets although prevalence of this has decreased in developed countries.

Based on the results of the Euro Heart Survey on Valvular Heart Disease, AS was prevalent in 33.9% of patients with a single native heart disease, making it the most common valvular disease in Europe and America (Jung et al. 2003). In a population and community study by Nkomo et al. (2006), the prevalence of AS was observed to increase with age and can be as high as 4.6% in people ≥ 75 years. As the age of the population increases, it is likely that the prevalence of AS is onset to increase annually. It is estimated that 3.5 million people in England will have AS by 2020, amongst which 4.3% would be classified as severe (Ramaraj and Sorrell 2008).

Mechanisms of calcification in the valve seem to stem from disruption of the endocardium lining the aortic side which may be caused from increased mechanical stress or a decrease in shear stress. Additionally, the posterior leaflet is usually the first to be affected and this leaflet has a reduced shear stress compared to the left and right leaflets due to the absence of the coronary ostia (Freeman and Otto 2005). Calcific nodules form on the aortic side and at the base of leaflets and the

histological process has been likened to atherosclerosis. Lipids are seen to infiltrate through the endocardial lesion and accumulate within the sub-endocardial and fibrosa layers. Low density lipoproteins (LDLs) are oxidised and are then taken up by macrophages to produce foam cells. Additionally, inflammatory cells such as macrophages and T-cells infiltrate through the lesion, releasing cytokines which remodel the extracellular matrix. A subset of myofibroblasts in the fibrosa layer has been shown to differentiate into an osteoblast phenotype which is capable of producing calcific nodules (Figure 1.6).

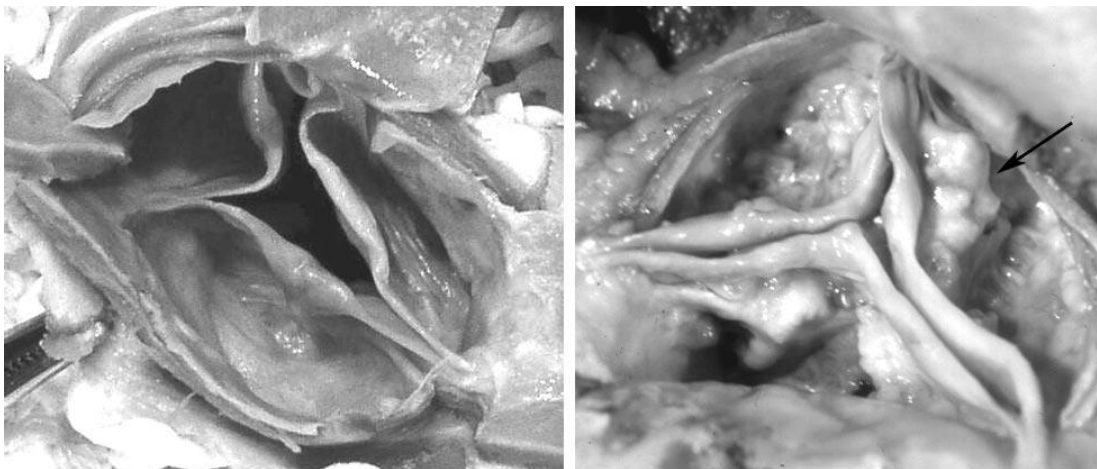


Figure 1.6 - Photograph of a minimally diseased aortic valve and a severely calcified aortic valve. Arrow points to lipo-calcific changes to the aortic side although the commissures are spared (Freeman and Otto 2005).

AS may be symptomatic; exhibiting symptoms of angina, syncope or heart failure, or be asymptomatic (Bonow et al. 2006). In symptomatic or severe cases prognosis is poor, with death occurring in 1-2 years following symptom onset and the stenosed valve would require replacement through surgical intervention. The ACC/AHA guidelines grade severe AS occurring when the orifice area is less than 1.0 cm^2 , the mean gradient is greater than 40 mm Hg or the jet velocity is greater than 4.0 ms^{-1} (Bonow et al. 2006). In milder forms of AS with areas between 1 and 1.5 cm^2 and velocities between 3 and 4 ms^{-1} , surgery is considered if calcification is significant (Otto 2006). However, approximately 30% of patients with severe AS over the age of 75 years do not undergo valve surgery due to technical complications such as a

porcelain aorta or due to patient refusal or general frailty or serious co-morbidity such as renal dysfunction (Iung et al. 2005).

1.2.3 Aortic Regurgitation

Aortic regurgitation (AR) is caused by abnormalities to the aortic leaflets or aortic root, resulting in leakage of blood from the aorta back to the LV when the valve is closed. Before anti-biotic treatment was available, the most prevalent cause of AR used to be Rheumatic fever. Nowadays, AR is more commonly caused by insufficient leaflet coaptation due to calcific degeneration, congenital defects and infective endocarditis. Other causes include trauma leading to perforations or a prolapsed leaflet. In chronic cases, the LV volume leads to ventricular hypertrophy and recruitment of sarcomeres to accommodate the increase in volume. Therefore a normal physiological stroke volume and ventricular diastolic pressure are maintained. Patients with chronic AR may be asymptomatic for decades (Bonow et al. 2008). In patients with acute AR, enlargement of the LV does not occur to accommodate the extra volume. Consequently, there is a decrease in stroke volume which leads to tachycardia to increase the cardiac output. However, usually the increase in heart rate is insufficient to cope with the demand leading to pulmonary oedema and cardiogenic shock.

1.2.4 Indications for Surgery Based on EOA

There are several approaches to determining the effective orifice area (EOA) of the stenosed valve. The most common method is the Gorlin formula which is defined as:

$$A = \frac{CO}{HR \cdot SEP \cdot 44.3 \cdot C \cdot \sqrt{\Delta P}}$$

Where A – orifice area of the valve (cm²)

CO – Cardiac output (cm³/min)

HR – Heart rate (beats/min)

SEP – Systolic ejection period (sec/beat)

44.3C – empirical constant (C is assumed to be 1.0 for the aortic valve)

ΔP – transvalvular pressure gradient (mm Hg)

Another equation which is often used is the continuity equation which states that the flow rate in the left ventricular outflow tract (LVOT) is equal to the flow in the vena contracta (VC) (Garcia and Kadem 2006). Either cardiac catheterization or Doppler echocardiography is used depending on whether the Gorlin equation or the continuity equation is used respectively. Doppler echocardiography would estimate the EOA based on the velocity time integral (VTI) at the vena contracta, which would give the smallest cross-sectional area of the stream. However, this method is likely to overestimate the severity of the AS which may lead to an unnecessary indication for valve replacement surgery. Patients with mild stenosis may be incorrectly indicated for valve replacement if they appear to have a high trans-valvular gradient. An infusion of nitroprusside or dobutamine would increase the outflow and the calculated aortic area but reduce the gradient, which would reduce the severity of the AS. In patients with severe AS, nitroprusside or dobutamine increases the gradient substantially but only mildly increases the area if at all.

Generally, there are no effective treatments for aortic stenosis or regurgitation except aortic valve replacement (Bridgewater et al. 2008). Additionally, there is no proof that medical treatment could prevent or delay valve disease (Bonow et al. 2008, Ramaraj and Sorrell 2008). Balloon valvotomy could be used as a bridge to surgery to provide temporary relief of symptoms but is not recommended as an alternative to AVR. Patients with symptomatic severe AS and those with severe AS also undergoing other heart surgery such as coronary artery bypass graft (CABG) surgery have a poor prognosis following onset of symptoms and are indicated for aortic valve replacement (Bonow et al. 2008).

1.3 AORTIC VALVE REPLACEMENT

1.3.1 Cardiac Surgery

Cardiac surgery stretches as early as 1896 when Dr. Ludwig Rehn, a surgeon from Frankfurt, Germany carried out what was considered the first successful heart operation on a 22 year old stab wound victim. It wasn't much later that the first cardiac catheterization was carried out by Dr Werner Forssmann in 1929 who at only 25 years of age delivered a catheter through to his own heart from the left elbow (Meyer 1990). Key breakthroughs in the evolution of heart surgery including the discovery of heparin, an anticoagulant by Jay McLean in 1915 and the development of the first heart and lung machine also known as cardiopulmonary bypass (CPB) by John Gibbon in 1937 enabled surgeons to carry out procedures on a bloodless heart. Heparin works by blocking thrombin which is responsible for the coagulation cascade, which was crucial to prevent thrombus formation in blood contacting external devices such as in the CPB machine.

Additionally, there is a need for a relaxed heart to enable surgery to be carried out in a bloodless and clear field. There was also a demand to protect the metabolism and function of the myocardium following ischemia (Podesser et al. 2011). Melrose and colleagues initially investigated cardioplegic properties of potassium in 1955, enabling immediate cardiac arrest and allowing short procedures to be carried out. The high concentrations used led to myocardial toxicity, and chemically induced cardioplegia was abandoned for 15 years before its revival in the 1970s. Intermittent blood cardioplegia admission was advocated in 1973, enabling surgeons to carry out procedures on a stationary and bloodless heart for several hours (Stephenson 2008). Additionally, cardioplegia was also found to protect the heart from the effects of ischemia (Podesser et al. 2011).

Initial attempts on valve repair before the introduction of the CPB machine included dilating the mitral valve through access from the atrial chamber. In 1947 Thomas Sellers used a tenotomy knife to perform a pulmonary valvulotomy through the right ventricle. The first aortic valve replacement (AVR) was carried out in the early

1950s before the use of CPB by Charles Hufnagel who developed the first ball and cage valve. Conventional heart valve replacement involves open heart surgery and placing the patient on cardiopulmonary bypass (CPB). During surgery, the aorta is cross-clamped to a CPB machine and the heart is reversibly stopped through an infusion of a cold potassium cardioplegic solution. The surgeon trims the calcified valve and a suction pump is used to remove any calcific debris from entering the blood stream. Sutures are then used to secure the replacement valve, taking care to align the commissures with the aortic sinuses if they are intact. The prosthetic valves contain an annular ring covered with a Dacron cloth which enables sewing of the valve onto the aortic annulus.

It is important to emphasize that no artificial heart valve developed can ever replace the native aortic valve in terms of its adaptability to complex hemodynamic environments. Accordingly, repair or preservation of the diseased aortic valve should be considered wherever possible. The choice of valve depends on the age and well-being of the patient. Bio-prosthetic valves have a similar hydrodynamic function to the natural aortic valve but have a limited life expectancy. Mechanical valves are more durable but require constant anti-coagulation treatment. These valves are discussed in further detail below.

1.3.2 Mechanical Valves

Mechanical heart valves typically have a longer lifespan than bioprosthetic valves; lasting approximately 25 years and so would not require frequent replacement as is the case with bioprosthetic valves. Since 1960, over 70 different mechanical heart valve designs have been developed (Vitale et al. 2004). Amongst the most common are the ball and cage valve, the tilting disc and the bi-leaflet (Figure 1.7). The ball and cage valve developed by Charles Hufnagel in the early 1950's was the first mechanical valve which functioned adequately to control blood flow. More than 200 valves were implanted in the descending thoracic aorta of patients, with some valves achieving 30 years of function with minimal wear (Gott et al. 2003). However, this valve had a high profile which was found to occlude the coronary ostia. Additionally,

excessive rubbing of the ball against the sewing ring lead to abrasion of the Dacron cloth. A similar design was developed replacing the ball with a single disc to reduce the profile of the original valve. However, high energy losses resulted from lateral flow of blood past the surfaces of the ball or disc which lead to poor hemodynamics such as high pressure drop and haemolysis.

A tilting-disc valve was developed by Bjork-Shiley in 1969 and overcame the problems with the single-disc valve. The disc freely rotates between metal struts which enable it to open by tilting at an angle of 60° . Originally this valve was made from Delrin, a poly-acetal homopolymer, but this was soon replaced with Isotropic Pyrolytic Carbon (PyC) which had excellent hemocompatibility. In 1975, Bjork-Shiley replaced the flat disc with a convexo-concaved one to enable the disc to slide by 2 mm to create a larger orifice. However, the welded struts were found to fracture, leading to a product recall in 1986 (Gott et al. 2003). The most common tilting disc valves to date were developed by Dr Karl Hall and Robert Kaster which was later known as the Medtronic Hall valve. It had a thin strut and a perforation in the middle of the disc as a guide, and an improved tilting angle of 75° in their aortic valves (Zilla et al. 2008). Early complications with this valve included friction and wear of the disc on the struts, and fracture of the struts caused by high mechanical loading during closure.

The bi-leaflet valve was developed by St. Jude Medical in 1977 and dominates the mechanical valves today. It consists of two semi-circular flaps made from PyC with the hinges close to the centre of the orifice. This creates three orifices for blood to flow through, which increases the blood contact surface area but has a higher EOA than the tilting disc or ball and cage valves. The EOA was found to increase from 1.5 - 2.1 cm^2 in the tilting disc to 2.4 - 3.2 cm^2 in the bi-leaflet valve (Zilla et al. 2008). The bi-leaflet is favourable due to its improved clinical performance, however some researchers have found the tilting disc valve to have superior hemodynamics if orientated correctly (Vitale et al. 2004).

A problem with the bi-leaflet valve was the hinge region which caused recirculation or stagnation of blood flow and elevated shear stresses which led to thrombus formation and haemolysis (Ellis et al. 1996). An interesting bi-leaflet valve which addressed this problem was the CardiaMed valve, previously known as the Jyros valve developed in Russia. This valve was designed with leaflets that continuously rotated 360° around the central axis of the valve housing with every heart beat. This enabled an even distribution of the blood flow across the prosthesis, allowing the parts to be washed to prevent thrombus formation. This feature of the valve also meant that the valve did not require orientation during the surgical procedure.

As mechanical valves are prone to thromboembolism and thrombosis, patients fitted with a mechanical heart valve would constantly require anticoagulation therapy. Failure of mechanical valves was largely caused by loading, material fatigue and cavitation. The failures lead to several design modifications such as using PyC which exhibited excellent hemocompatibility and remains the material of choice for mechanical heart valves today.

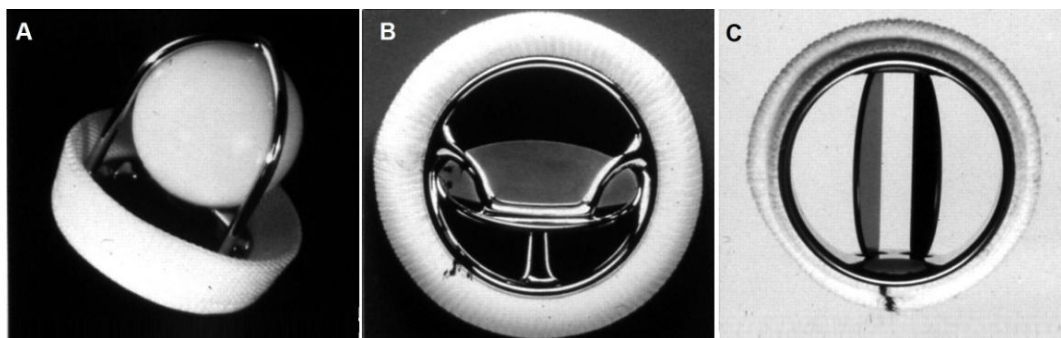


Figure 1.7 - Mechanical heart valves: A. Ball and cage valve, B. Tilting-disc valve and C. Bileaflet valve (Bloomfield 2002).

1.3.3 Bioprosthetic Valves

A bioprosthetic valve may consist of either a cadaveric valve or pericardial xenografts which suture together to form a tri-leaflet valve. The most common bioprosthetic valves are porcine aortic valves (PAV) which may be stented or

stentless, and bovine pericardium valves (BPV). A stented valve would incorporate a metal wire folded to typically form 3 prongs which serve as an attachment site for the commissures of the valve. The entire wire frame would be covered in Dacron to enable suturing of the tissue to the stent. A stentless valve is one where the valve has been excised from the animal with the conduit intact. Stentless valves have a hemodynamic advantage over stented valves as they provide a greater effective orifice area (EOA) due to the absence of the stent. The blood is also subjected to less shear stress and so the chances of haemolysis due to rupture of the blood cells is reduced. However pericardial valves are more easily mass produced as there is no problem with supply (Love 1993).

The first popular pericardial valve was the Ionescu–Shiley Pericardial Xenograft valve which was developed in 1971 and marketed in 1976. This valve was formed from bovine pericardium sutured onto a titanium stent covered with a Dacron fabric. Although having superior hemodynamic, a series of early structural failures lead to withdrawal of the valve in 1987 and almost dropping pericardium as a material of choice. It was realised that the valves had abrasive tears due to the fabric/tissue interface and due to the leaflets calcifying (Love 1993).

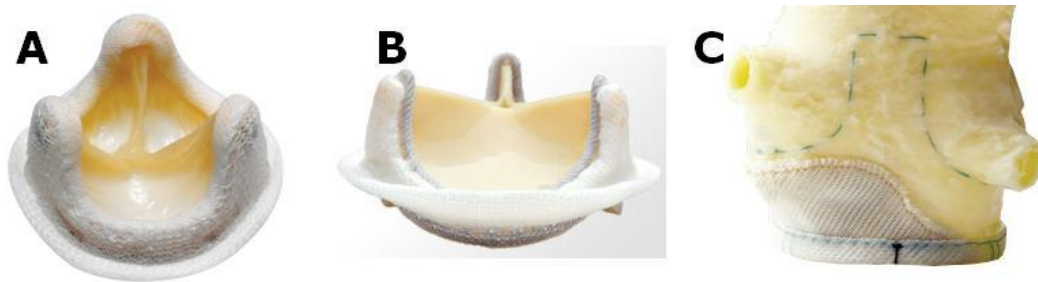


Figure 1.8 - Bioprosthetic valves: a) Medtronic Hancock II Porcine Valve, b) Edwards Pericardial Valve and c) Edwards Prima Plus Stentless Porcine Prosthesis.

Biological valve prostheses have excellent hemodynamics compared to mechanical valves due to their anatomical structure. However, they are prone to calcification and thus have a shorter life span than mechanical valves. Valves and pericardium excised from species need to be sterilized and preserved. The most common treatment

adopted for the preservation of these tissues is their fixation in glutaraldehyde, a five-carbon atom dialdehyde (Paez and Jorge-Herrero 1999). The method of fixation varies substantially. Some bioprosthetic valves are fixed at 0 mmHg or low pressures whereas others are prepared at 80-100 mmHg closing pressure. It was observed that when a high pressure fixation is adapted, the pericardium loses its natural collagen crimp structure which increases its stiffness (Thubrikar 1990). Glutaraldehyde fixation has also been found to reduce the GAG concentration in valvular leaflets during flexural fatigue, which would compromise the structure of the spongiosa layer and may contribute to tissue deterioration and calcification (Vyavahare et al. 1999).

There are two main causes of bioprosthetic valve failure; mechanical and chemical influences. Pericardium and xenografts are prone to calcification particularly in regions exposed to high stress which leads to eventual stiffening of the leaflets. However, the highest cause of failure come from mechanical stresses alone, indicating the importance of nailing valve design (Vesely 2003). Other causes of failure included stent rigidity, the level of pressure applied to glutaraldehyde fixation and anisotropy between leaflets. These design considerations are discussed in further detail in Chapter 5.

1.3.4 Tissue Engineered Valves

Tissue engineering is a field in regenerative medicine which aims to restore and maintain the function of living tissues through the applied understanding of engineering and biological sciences. They have found particular success in skin grafts for burn victims. The advantages of tissue engineered heart valves (TEHV) compared to other valve replacement options include non-thrombogenicity, infection resistance and cellular viability. It is particularly exciting in children and young adults where the possibility exists of a valve capable of growing, remodelling and repairing itself as the patient grows (Mendelson and Schoen 2006). However their design has remained challenging and their success depends on advancements in material science and culturing techniques. There have been several approaches to

TEHV including decellularization, biodegradable scaffolds, protein based, in-vivo and hybrid TEHVs.

Decellularization involves removal of the cellular contents of a native heart valve, keeping only the ECM component. This approach has the benefit of decreasing the immunogenicity response, enabling xenografts to be suitable in humans. Additionally, the matrix would have the desirable mechanical and structural integrity for use as heart valves. However, decellularizing the matrix can lead to alterations to the collagen crimp structure, GAG content and fibre structure which may influence the mechanical properties. The matrix can also be reseeded either through coating with a bioactive substance or by seeding with autologous cells, although cells have been found to leach out once implanted in vivo. The use of a decellularized matrix is also limited since it requires relatively healthy valves which would be more suited for allografts.

Biodegradable scaffolds are commonly employed in tissue engineering due to the vast availability of synthetic materials with biodegradable properties. The basic idea behind the tissue engineering approach is to create a template on which the matrix can synthesize. This requires a careful balance in controlling the rate of polymer degradation with the rate of matrix synthesis so that the cells remain seeded on a mechanically stable material. Scaffolds are seeded with mesenchymal stem cells (MSC) which should then proliferate to VECs and VICs.

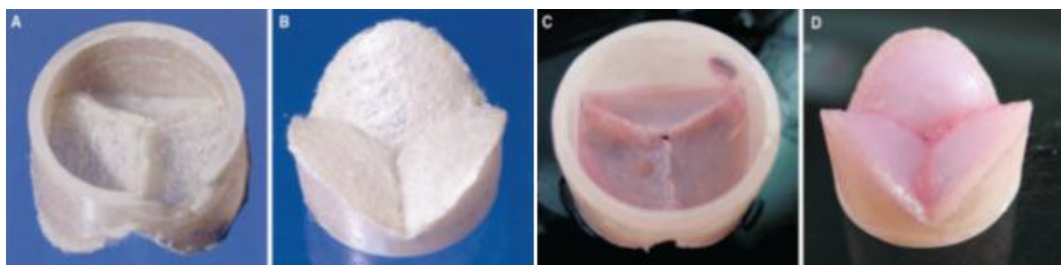


Figure 1.9 - Photographs of autologous tissue engineered valve (a) non-woven PGA scaffold coated with P4HB from the (a) aortic and (b) ventricular sides. (c) and (d) after 4 weeks of culturing. Adapted from Mol et al., (2006).

1.3.5 Polymeric Valves

Polymeric heart valves combine the durability of mechanical valves with the hydrodynamic function of bioprosthetic valves (Wheatley et al. 2000). They have a huge advantage in that they can be manufactured to various shapes and sizes (Ghanbari et al. 2009). In a comparative study of a polyurethane (PU) valve with a mechanical and bio-prosthetic valve, the PU valve was found to have superior hemodynamics compared to the bio-prosthetic valve. Additionally, incidence of thrombogenicity was lower than in the mechanical valve (Wheatley et al. 2000).

Polymeric valves have been around for over 50 years but failed to gain popularity due to their initial poor characteristics. In fact, one of the earliest prosthetic heart valves was a mitral polyurethane valve with a Teflon chordae tendineae which was implanted in a 44 year old woman in 1959 (Braunwald 1989). Many of the early polymeric valves used polymers which were prone to calcification and early degradation which prohibited their widespread use. Consequently they were only used in short term 'Bridge to Transplantation' devices such as in total artificial hearts and left ventricular assist devices. It was the introduction of polyurethane (PU), a two-phased microstructure of hard and soft segments which escalated their use as biomaterials. Biomer was the first PU stable enough to be coined as a 'biomaterial' and used to form the pump diaphragm of the Jarvic 7 total artificial hearts (Ratner et al. 2004).

Biomaterial polymers such as silicone, polytetrafluoroethylene (PTFE also known as Teflon), polyvinyl alcohol (Jiang et al. 2004, Mohammadi et al. 2009) have also been considered as alternative materials to heart valves. However, much of the focus has been on thermoplastic polyurethane (TPU) which has shown potential due to its excellent mechanical properties and bio-stability. Advanced material science has enabled development of these polymers with improved biostability and durability. Initial TPUs had polyester soft segments which were prone to hydrolysis and oxidation. The two-phase microstructure of TPU has enabled researchers to improve biostability by modifying the soft segments or through chemical substitutions to their

structure (Ghanbari et al. 2009). In 2000, Gunatilake et al. developed a polymer with silicone microdiols which gave it superior biostability in relation to other TPUs. This polymer now marketed by Aortech International Plc (Rogers, Minnesota) under the name of Elast-Eon™ and is used in the development of heart valves as well as insulation for pacemaker and defibrillator leads.

Polymeric valves have vast manufacturing possibilities including dip-coating, film casting and injection molding. They are promising in the field of percutaneous technologies due to the ability to control their thickness and create leaflets thin enough for TAVI. A UCL group developed a nanocomposite (POSS-PCU) polymeric heart valve which they aim to develop thin enough for percutaneous delivery (Kidane et al. 2009). The structure of polyurethane and its suitability as a valve material is discussed in greater detail in Chapter 6.

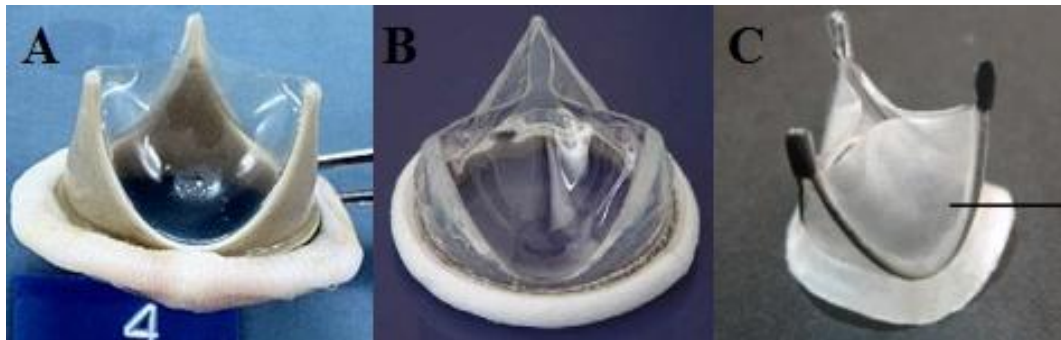


Figure 1.10 - Polymeric heart valves; (a) the Elast-Eon valve manufactured by Aortech, (b) the ADAIM Polycarbonate urethane valve and the (c) POSS-PCU valve developed at University College London.

1.3.6 Complications with AVR

AVR requires open heart surgery and placing the patient on CPB, which for many elderly patients carries a high risk. It is estimated that approximately 30% of AS patients are turned down for AVR as the procedure is deemed too risky or due to technological complications such as a porcelain aorta, where the aorta is too calcified

to allow suturing of a valve (Jung et al. 2005). The mortality rate from 2004 to 2008 for AVR alone and with CABG was estimated to be 2.8% and 5.3% respectively (Bridgewater et al. 2008). AVR is also not practical in children who need frequent replacement as they grow.

Additionally, both bio-prosthetic and mechanical valves are often unsuitable for neonates and small children due to their large size and the need for constant replacement with growth. Often a homograft is obtained from a human donor and is preferred for neonates and children as it is of an appropriate size. The Ross procedure is a heart valve replacement procedure popular by cardiac surgeons for neonates and children. It involves replacing the damaged aortic valve with the patient's own pulmonary valve (pulmonary allograft) and replaces the pulmonary valve with an aortic or pulmonary homograft. The benefits of this procedure are that the aortic valve is replaced with a valve which will grow with the patient and which will not induce an immunological response. However, two surgical procedures are performed and a highly skilled surgeon is required to perform the operation.

In 1992, Andersen et al. developed a heart valve mounted onto a stent which could be delivered to the aorta through a transcatheter intervention and placed over the native valve. These valves are known as percutaneous heart valves (PHV). The major benefit of PHVs is that the valve is deployed over the native valve via a transcatheter approach through the blood vessels without the need for open heart surgery and CPB. Since their first implantation in 2002 in a human, PHVs have enabled patients who are refused surgery due to high risk or technical complications to be candidates for transcatheter valve replacement. There are two leading valves in the market today; the Edwards SAPIEN valve by Edwards LifeSciences and the CoreValve Prosthesis by Medtronic Inc.

The current size of PHVs in their collapsed state has been shown to contribute to major vascular complications following retrograde delivery through the femoral arteries (Toggweiler et al. 2012). It is desirable to decrease the size of the delivery catheter to provide a less invasive and traumatic access vessel to the aorta. This can

be achieved by enabling delivery to a peripheral artery through a minimal or fully percutaneous incision. However this requires the valve to be collapsed into a smaller sheath and current percutaneous valves are formed from pericardial leaflets, which are too thick to enable this.

This thesis aims to address these problems by developing a reinforced polymeric leaflet, where ultra-low thicknesses can be achieved by controlling parameters of the polymer and manufacturing process. The following chapter focuses on the existing percutaneous technologies and their complications. Chapter 4 explores the properties of porcine pericardium which will be used as a comparison against the polymeric valves. The principles of polymeric valve design are discussed in Chapter 5. Chapters 6 and 7 focus on polymer-nanotube composite development and testing and the development and testing of thin nanotube reinforced polymeric valves are addressed in Chapter 8.

1.4 CHAPTER SUMMARY

1. The aortic valve consists of three leaflets and three sinuses which facilitate the one-way flow of blood with minimal regurgitation. The leaflets have a three layered structure containing a network of collagen fibres, elastin and GAGs which provide a mechanically and physically anisotropic structure capable of adapting rapidly to changes in stress.
2. It has been found that deviating away from the native tri-leaflet design of the valve leads to changes in mechanical and hemodynamic responses of the valve. This in turn leads to complications such as stenosis; highlighting the importance of designing a valve that mimics the native one.
3. The advantage with developing a polymeric heart valve is that there are vast manufacturing options possible to produce various valve designs.

Polyurethane would be a favourable synthetic material to use due to its excellent mechanical properties compared to other biostable polymers.

4. An ultra-thin synthetic leaflet material is hoped to overcome the complications related to the current femoral arterial access by enabling a lower profile delivery through a peripheral artery.

CHAPTER 2:

PERCUTANEOUS HEART VALVES

2 PERCUTANEOUS HEART VALVES

Treatment through transcatheter intervention stems back to the 1950's when a urethral catheter encasing a wire was passed through to perform a pulmonary valvulotomy. The wire was used to cut the fused commissures of the valve to free the leaflets (Rao 2012). Percutaneous technologies have since been extensively used to treat other morbidities such as using balloon dilation to perform aortic valvuloplasty, aortic coarctation, and more commonly, angioplasty to treat atherosclerotic obstructions. In fact the first percutaneous valve was developed in 1965 to treat aortic regurgitation in dogs (Davies 1965). An umbrella shaped valve was mounted on a catheter and inserted distally in the ascending aorta to allow blood to flow past but prevented reverse flow. The development of a heart valve by Andersen et al. in 1992 which is deployed percutaneously over the native leaflets has opened a window of opportunity for severe AS patients who cannot undergo surgical AVR due to comorbidities and who would have otherwise had a low chance of survival after 1-2 years following disease onset.

Since the first human implantation in 2002, there have been over 50,000 cases of transcatheter aortic valve interventions (TAVI) in over 40 countries. Two of the most widely used valves; the Medtronic CoreValve™ prosthesis and the Edwards SAPIEN valve have both received the CE Mark approval for commercial sale in Europe in 2007 (Généreux et al. 2012). Currently their use is limited to high risk older patients who have been turned down for surgical AVR. It is expected that with their continued use, younger and lower risk patients will also be referred for TAVI. From an economic viewpoint, the 12-month cost of transfemoral TAVI from the Cribier Edwards PARTNER trial was found to be comparable to AVR at \$73,219 and \$74,067 respectively (Reynolds et al. 2012). The same study found the cost effectiveness which factored patient quality of life (QoL) to be better in 70.9% of patients with transfemoral TAVI compared to AVR, although transapical TAVI was found to be least cost effective. These delivery techniques and the existing PHVs in development and clinical trials are discussed below. With increased learning and use

of a multi-disciplinary team and equipment, it is envisaged that TAVI may one day overtake surgical AVR as the gold standard treatment for aortic stenosis.

2.1 FIRST GENERATION PERCUTANEOUS HEART VALVES

2.1.1 History

Andersen et al. (1992) carried out the first study of percutaneous heart valves (PHV) on animals using a porcine aortic valve. The stent consisted of two wires folded about 15 times, with 3 of the folds higher than the rest to accommodate the commissures of the valve. The heart valve-stent assembly was then crimped onto a 3-foiled balloon dilation catheter and the entire assembly was passed through a guide wire. The catheter was then passed percutaneously through the femoral artery of the animal and passed retrograde to the descending aorta. Once the PHV was positioned over the native valve, the balloon was inflated to expand the crimped valve, flattening the native leaflets between the stent and aortic wall. Following withdrawal of the balloon, the valve immediately began to function. Wires extending from the edges of the stents allowed external fixation to the aorta.

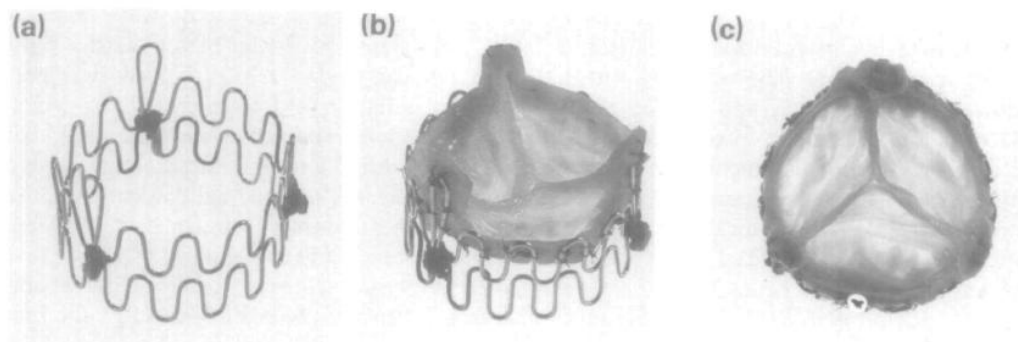


Figure 2.1 - Percutaneous valve developed by Anderson et al. (a) stent assembly, (b) porcine aortic valve sutured to stent and (c) aortic view of valve (1992).

In two of the animals, the coronary ostia were occluded, leading to left ventricular failure. A small amount of thrombus was noted on the metal stent and sutures. However, it should be noted that as this study was in its initial phase, no treatment or sterilization of the PHV was carried out prior to implantation. The authors also highlighted the limitations of their study, including problems with thrombogenicity and migration of the stent at a long-term follow-up. Long term dilation or necrosis of the aorta at the region of the implanted valve was also addressed, as they could lead to paravalvular leakage or stent migration.

In the same year, Pavcnik et al. (1992) also conducted a percutaneous heart valve replacement on dogs using a ball and cage type design. In their study, a Gianturco stainless steel stent which was self-expandable was used to form a cage which was sutured onto a ring consisting of coiled wires covered in a nylon mesh. A detachable latex balloon was used for the ball which was expanded by filling with either air or a pre-polymer which had a similar consistency to rubber when polymerized. Once the stent-ring assembly had been deployed over the native valve, the latex balloon was then inserted into the assembly and inflated to its predetermined diameter. Following deployment, the ring was found to be successfully placed below the coronary ostia in all 12 dogs and was securely anchored by barbs. However, in three of the dogs, the ball was reported to have escaped from the cage and into the aorta. Another major setback was the non-biocompatibility of the latex ball which made it susceptible to long term degradation due to the enzymes and fatty acids in circulation.

In 2002, Boudjemline and Bonhoeffer described in more detail a PHV replacement in 12 lambs, which they had previously developed. The PHV consisted of a valve from a bovine jugular vein mounted onto a platinum-iridium balloon expandable stent. To reduce the risk of coronary artery occlusion, space was made by dissecting the venous wall around the coronary orifices. They split the study into 3 groups. The first group involved creating severe aortic insufficiency and deploying the valve in the descending aorta. The second group involved deploying the valve-stent 1 cm below the aortic annulus. All the lambs in the second study group died suddenly due to an 'inappropriate placement' of the valve. In the third study group, the valve-stent

assembly was contained within another stent made from nitinol. This stent was deployed first and positioned against the ‘bottom of the native leaflets’. The balloon was then inflated to expand the valve-stent and this enabled the native leaflets to be sandwiched against the two stents. There was no stent migration reported for the last group.

The main complication with balloon catheters is that they have a fixed diameter and consequently the valve is expanded to a fixed size which may make it prone to paravalvular leakage due to an inadequate fit within the aortic annulus. Lutter et al. (2002) designed a PHV taken from porcine cadavers or pericardial tissue contained within a self-expanding stent. The stent was contained within a sheath which was unsheathed to allow the stent to expand radially within the aortic annulus. The self-expanding stent eliminates the fixed diameter issue with balloon expandable valves and enables a better fit within the aortic annulus. Despite the complications in earlier valves, these studies proved transcatheter aortic valve replacement to be feasible and paved the way for the next generation of heart valves; the Cribier Edwards valve and the CoreValve prosthesis.

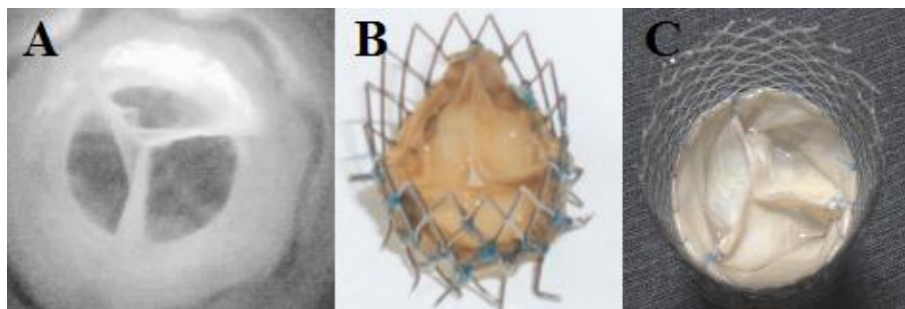


Figure 2.2 - Early percutaneous heart valves; (A) the Bonhoeffer valve, (B) Lutter valve and (C) Paniagua heart valve.

2.1.2 Cribier Edwards Valve

Professor Alain Cribier was the first to describe balloon valvuloplasty for the treatment of aortic stenosis in 1986 and also the first to implant PHV in a human in

2002. Cribier et al. (2002) implanted their balloon expandable valve into a 57 year old man. The patient was suffering from calcific aortic stenosis (AS), cardiogenic shock and severe leg ischemia and was declined conventional AVR by several surgeons. The authors gained ethical approval on compassionate grounds, and a PHV was inserted through a 24 Fr (1 mm = 3 Fr) sheath in an antegrade approach through the right femoral vein following balloon valvuloplasty of the native aortic valve. They used bovine pericardium sutured onto a short stainless steel stent which was crimped onto a balloon catheter and deployed into the native position of the aortic valve. The shorter length of the stent reduced the chance of coronary ostia occlusion, which was a problem with some of the longer stents reported by Lutter et al. (2002). Immediately after the procedure, there was improvement in the aortic pressure, the TVG (from 30 mmHg to 6 mmHg) and in the left ventricular ejection volume (14% to 17%). However, the patient died 17 weeks after PHV due to non-cardiac related complications so no long term follow-up data was available.

Following success of their first human trial, Cribier et al. implanted their stent-valve into 6 more people in 2004. Improvements were made to the stent-valve by forming the leaflets from equine pericardium (which was similar to the thickness of bovine pericardium though more compliant) and suturing them to reinforced stainless steel tubular stent. The PHV was assembled onto a 22 mm or 23 mm diameter balloon catheter using a crimping device and advanced through a 24 Fr sheath using the same antegrade approach as their previous study. Once positioned over the native valve, the balloon was inflated to expand the valve and flatten the native leaflets between the stent and aortic sinuses. Immediately, there was an improvement in the aortic orifice area, averaging 1.7 cm² and a decrease in the TVG in all but one of the patients. This patient had suffered from severe cardiogenic shock due to the native valve leaflets being disconnected from the PHV. In all valves, there was no reported regurgitation although paravalvular leakage did occur. A post mortem on a patient who had died of non-cardiac related complications revealed calcific nodules of the native valve which were responsible for an inadequate positioning of the valve leading to paravalvular leakage.

The PHV used in the studies by Cribier et al. were produced by Percutaneous Valve Technologies which was later acquired by Edwards LifeSciences (Irvine, CA) and is now known as the Cribier-Edwards valve (Brodsky 2004). The valve has since undergone a few design changes to drop down from a 24 Fr to an 18 Fr delivery profile (Figure 2.3). Initially equine pericardium was replaced with the more durable bovine pericardium to develop the Edwards-SAPIEN[®] valve. The stent has since then been modified from stainless steel to a thinner cobalt-chromium stent with fewer struts to form the Edwards SAPIEN XT[®] valve. Additionally the leaflets have a scalloped shape which overall reduced the profile of the SAPIEN XT[®] valve. A polyester skirt sutured to the stent reduces paravalvular leakage. Edwards LifeSciences have also developed two other valves currently in early clinical trials; the SAPIEN 3 and the self-expanding CENTERA valve.

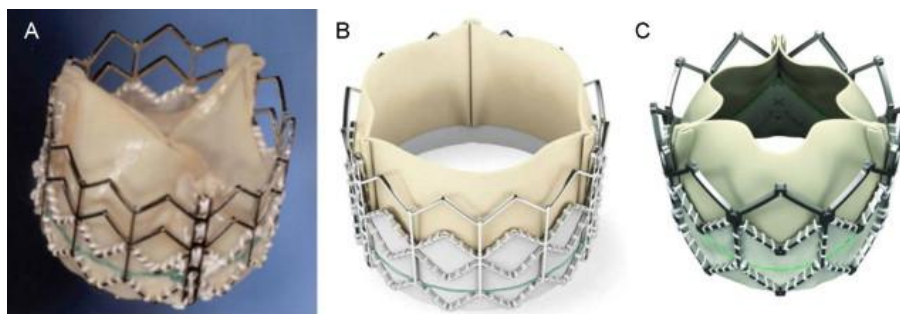


Figure 2.3 - Evolution of the Cribier Edwards valve; (A) first generation equine pericardial valve, (B) SAPIEN valve and (C) the low profile SAPIEN XT valve both with bovine pericardium (Webb and Binder 2012).

In November 2011, the Edwards SAPIEN[®] valve was the first PHV to gain FDA approval for conventional inoperable patients in the US. This followed results of the PARTNER trial which was the largest study to date comparing surgical AVR to TAVI. The results of this trial are discussed later on in this chapter. There are 4 catheter diameters, expressed in the French scale, (3 Fr = 1 mm). The 20 and 23 mm valves are housed in an 18 Fr sheath diameter and the 26 mm and 29 mm valves are housed in a 19 Fr and 22 Fr sheath respectively (Rodes-Cabau 2012). They are suitable for native annuli diameters ranging from 16-27 mm. An expandable sheath

known as the eSHEATH[®] which is currently only available in Europe and Canada enabled reduced delivery profiles of 16 Fr, 18 Fr and 20 Fr to be feasible. They expand only when the valve is passed through and collapse back to their reduced diameter, thereby reducing the time the arteries are exposed to large strains. These sheaths allow for an acceptable minimal iliofemoral arterial diameter of 6, 6.5 and 7 mm respectively (Piazza et al. 2012).

2.1.3 CoreValve Prosthesis

Grube et al. (2005) reported on a study that involved a PHV known as the CoreValve (Medtronic Inc., Minneapolis, USA), which was made from porcine pericardium sutured onto a self-expanding nitinol stent. Porcine is considerably thinner (typically 200µm thick) and stiffer than both bovine and equine pericardium. The nitinol material is a shape memory alloy of nickel and titanium which has the ability to deform at low temperatures but regain its original shape at body temperature. The CoreValve stent was designed so that the proximal end had a larger diameter than the distal end allowing secure fixation onto the ascending aorta. The middle of the stent was also slightly narrowed to prevent occlusion of the coronary ostia.

As a safety measure during the procedure, the left common artery and vein were used for hemodynamic support although rapid ventricular pacing (RVP) could have also been used (Grube et al. 2005). Patients were taken off extracorporeal support immediately after valve deployment. The overall valve stent assembly was inserted into a 24 Fr catheter sheath which was advanced through the left common iliac artery via a retrograde approach over the native aortic valve. Once the correct position was asserted, the sheath was withdrawn, deploying the self-expanding valve.

In a later study by the same group, the sheath was brought down to an 18 Fr size (Grube et al. 2005). In their study, a comparison was made between delivery of the second generation device (21 Fr) and the third generation device (18 Fr). Their results showed a significant improvement in the 18 Fr catheters compared with the 21 Fr catheters which lead to a time reduction of 148 ± 50 min compared to 188 ± 55

min respectively. 64% of patients with the 18 Fr catheters did not require extracorporeal support whereas all patients with the 21 Fr catheters did. Moreover, 42% of patients with the 18 Fr catheters did not require a surgical cut down of the access vessel and 25% of the 18 Fr catheters only needed local anaesthesia of the groin compared to none in the 21 Fr group. In a large single trial study by Grube et al. (2008) procedural success rates improved from 70.0% in the first generation valves to 91.2% in the third generation valves. The study also highlighted the high incidence of atrio-ventricular (AV) block occurring in PHV procedures compared with surgery. A higher incidence of patients fitted with a pacemaker was reported in the 18 Fr valve, although this was attributed to a change in policy to provide a 48 hour temporary pacemaker fitting. The CoreValve is available in 3 sizes; 26 mm, 29 mm and 31 mm and accommodate native annular diameters of 20-29 mm (Piazza et al. 2012).

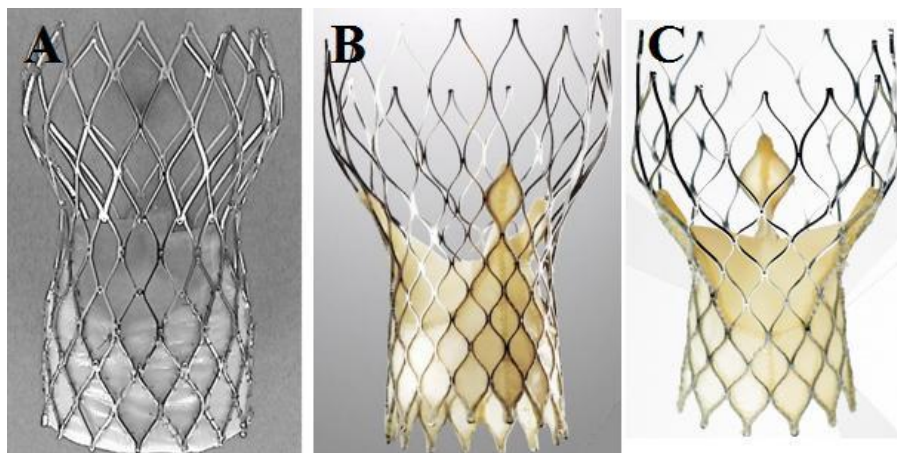


Figure 2.4 - (a) First and (b) Third generation of the CoreValve prosthesis, adapted from Grube et al. (2008) and (c) CoreValve® Evolut™ prosthesis.

2.2 TRANSCATHETER APPROACHES

2.2.1 Clinical Evaluation and Imaging

Following over 50,000 procedures, TAVI is currently recommended to be performed only in cardiology and cardiac surgery centres. This enables procedures to be quickly transferred to surgery in the case of complications. A hybrid approach consisting of a multi-disciplinary team of clinical cardiologists, interventionists, surgeons, anaesthetists and imaging specialists are involved in the technical process and pre- and post-procedural patient care and evaluation (Vahanian et al. 2012).

Two scoring systems have been used in the past to assist in determining patient eligibility and predict mortality rates for TAVI; the logistic EuroSCORE I and the Society of Thoracic Surgeons Predicted Risk of Mortality (STS PROM). However, recent outcomes from trials have highlighted the need for better predictive scoring systems which would factor frailty and comorbidities such as coronary arterial disease and congenital bicuspid valves which may contraindicate TAVI. Updated surgical risk algorithms such as the logistic EuroSCORE II and STS are expected to provide a better predictive mortality rate in high risk patients (Piazza et al. 2012). Additionally, the success of AVR in older patients depends on the skill of the surgical centre rather than age alone and therefore TAVI should be compared with results from highly skilled surgeons rather than depend on the risk scores (Antunes 2012).

As TAVI is largely non-invasive, correct imaging of the aorta, its valvular complex, the left ventricle and the arterial vasculature is of utmost importance in helping determine the route to adopt and prosthesis sizing. Additionally, the team needs to be able to visualise deployment in order to avoid complications such as stent migration or incorrect positioning. This involves a combination of echocardiography, right and left heart catheterization, left ventriculography, supra-aortic angiography, and coronary angiography (Eltchaninoff et al. 2008).

The arterial vasculature is imaged using angiography to determine the feasibility of a transfemoral approach. Tortuosity is not necessarily a contra-indication to iliofemoral arterial access since patients with healthy albeit tortuous arteries can still undergo transfemoral-TAVI whereas patients with larger but heavily sclerotic arteries may not be suitable candidates. Although there are no clinical indications as to which transcatheter approach is superior, a 'transfemoral first' decision is usually adopted before considering other methods.

Imaging of the aortic annulus has generally been performed through either the use of transthoracic (TTE) and transesophageal echocardiography (TEE). TEE in particular has been favoured for accurate imaging when performing a transapical TAVI due to the close proximity of the TEE probe to the aorta. The general shape of aortic annulus and LVOT is elliptical and two-dimensional echocardiography may not be able to correctly determine the largest annulus size. Ng et al. (2010) found 2D and 3D TEE to significantly underestimate the annular area by 16.4% and 12.9% when compared with multi-slice computed tomography MSCT. Underestimation of the EOA can lead to a patient-prosthetic mismatch (PPM) and imaging may be better suited with three-dimensional analysis using MSCT or MRI.

2.2.2 Antegrade Transseptal Approach

The antegrade transseptal approach reported by Cribier (2002; 2004) involved access through the right femoral vein, an atrial transseptal entry, through the mitral valve into the aortic annulus. Initially a stiff guide-wire is advanced from the right femoral vein through the interatrial septum to the descending aorta and externalized through the left femoral artery. A 24 Fr sheath is then inserted to advance the valve mounted balloon catheter through the guide-wire and the over the native leaflets. Rapid pacing of the right ventricle is used to decrease aortic blood flow during valve deployment. This approach enables large stent mounted catheters to be used and would also allow a more precise placement of the prosthesis as there is less motion of the large delivery system during the cardiac cycle. Additionally, the antegrade approach

enables the valve to bypass the calcific side of the native leaflets. However, this approach is technically challenging and prone to complications due to the close proximity of the mitral valve. The procedure has been largely dropped in favour of the retrograde approach through the femoral arteries.

2.2.3 Transfemoral Retrograde Approach

Panigua et al. (2005) were the first to report a clinical case in 2003 with the retrograde approach, which had a collapsed profile of 2 mm and having a 12-16 Fr introducer shield. Due to the low profile of their valve, they were able to deliver it in a 62 year old man through the right femoral artery, the abdominal aorta and the left ventricle. The TVG dropped to < 5 mmHg and cardiac output increased from 1L/min to 5 L/min. Although the patient died after 5 days due to biventricular failure and refractory hypotension, valve function was deemed satisfactory following echo-Doppler evaluation (Paniagua et al. 2005). At that time, other PHVs including the first generation CoreValve™ reported use of the transfemoral TAVI with favourable outcomes (Grube et al. 2005, Hanzel et al. 2005, Webb et al. 2006). This approach became increasingly more popular following reduction in sheath sizes of the next generation PHVs.

The general procedure for TF-TAVI involves a surgical cut down or a puncture for a fully percutaneous access to the common femoral artery. Depending on the protocol practised in the centre, the patient is given either a general or local anaesthetic and mildly sedated. TEE, fluoroscopy and aortography are commonly adopted to visualise the vasculature and provide guidance during valve deployment (Chiam and Ruiz 2009). Initially a guide wire is passed through from the femoral artery to the aorta which is then exchanged for an extra stiff 0.035" guide-wire. A balloon catheter is passed through to pre-dilate the valve. Rapid ventricular pacing of the right ventricle at approximately 200 bpm is performed to reduce aortic flow and prevent distal migration of the balloon. An introducer sheath is inserted into the femoral artery and the PHV and catheter assembly are then advanced through the sheath to the descending aorta and over the native valve. Once in the correct position, the

valve is unsheathed to enable the stent to self-expand or a balloon is used to expand the valve which begins functioning immediately. RVP is again practised in balloon expandable valves and should only be carried out once blood pressure has returned to normal following disrupted hemodynamics from previous pacing.

The introduction of steerable delivery catheters such as the Retroflex and Novaflex catheters developed by Edwards LifeSciences made the retrograde approach more feasible.

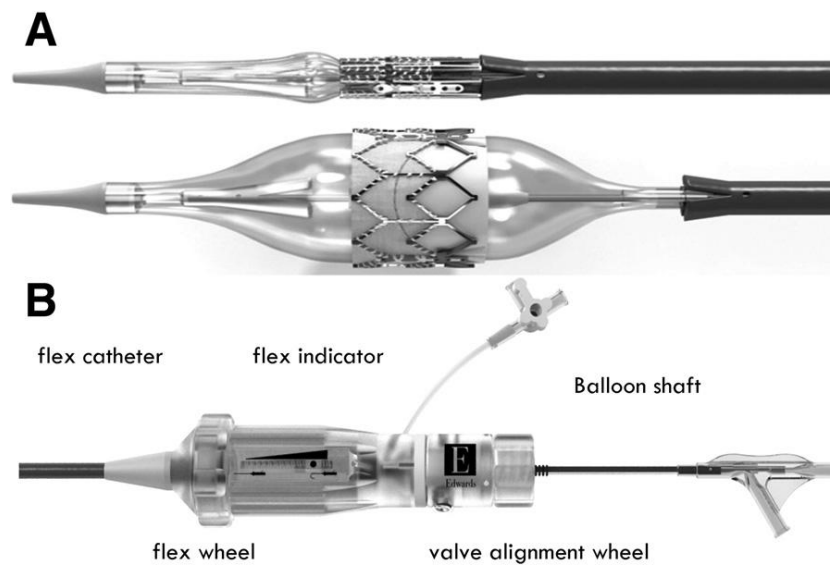


Figure 2.5 - Edwards SAPIEN XT delivery; (A) Novaflex balloon catheter in collapsed and expanded state and (B) the Novaflex handle (Willson et al. 2011).

First generation PHV required sheaths as large as 24 Fr which could lead to major vascular complications particularly in iliofemoral tortuous arteries. However with the introduction of lower 16-18 Fr delivery profiles, this complication is set to reduce. An 18 Fr catheter would enable easy delivery through femoral arteries as small as 6-7 mm compared with the 8-9mm artery diameter needed with the 21 Fr catheters. The smaller catheter size would be a suitable candidate for younger patients and females who generally have smaller femoral arteries (Sandgren et al. 1999). However the retrograde approach would still be unsuitable for patients with femoral or iliac

artery disease in which the arteries could be tortuous, making a percutaneous delivery difficult.

2.2.4 Transapical Aortic Intervention

In 2006, Lichtenstein et al. were the first to describe an approach in which the aortic valve was delivered through the apex of the left ventricle by a minimally invasive surgery but without cardiopulmonary bypass. They used a Cribier-Edwards balloon expandable valve via a 24 Fr sheath in 7 patients and reported favourable results, with an improvement in median area from 0.7 cm² to 1.8 cm² post procedure and 1.6 cm² at 1 month follow up. Paravalvular leakage was reported to be a common complication although was not considered clinically significant. The authors also noted that potential complications of this procedure could include myocardial perforation and mitral or aortic valve damage.

The transapical aortic valve intervention (TA-AVI) involves making a cut at the 5th or 6th intercostal space to expose the left ventricular apex. A superstiff guidewire is passed antegradely through a puncture in the apex, through the aortic valve and into the ascending aorta. After a pre-dilation with a balloon valvuloplasty, the sheath containing the valve is then advanced through the apex to the aortic valve using the guidewire to manipulate the valve to the correct position (Walther et al. 2011). With the Edwards Sapien valve, expansion is held for 5 seconds under RVP. Oversizing of the prosthesis and moderate over-dilating can reduce the risk of paravalvular leakage and is frequently practised. Excessive dilation can lead to regurgitation and inadequate leaflet coaptation (Lichtenstein et al. 2006).

A study was carried out on 71 patients who underwent TA-AVI with a Cribier Edwards valve having been turned down for surgical replacement and a percutaneous TF intervention. Mortality after 30 days was 16.9%, 33% of which occurred in the first 15 patients which may indicate a learning curve with this approach (Ye et al. 2010). In another study, the TA approach was evaluated in 299 patients who were

divided into an early experience (EE) and recent experience (RE) which were conducted pre- and post CE approval of TA aortic valve intervention (Kempfert et al. 2011). In their study, 30-day mortality rate was lower in the RE group compared with the EE group, also demonstrating a learning curve with the procedure. Results from the SOURCE registry have demonstrated that TA-AVI has similar procedural success rates with TF-AVI (92.7% vs. 95.2%). TF-AVI had a higher survival rate at 1 year (81.1% vs. 72.1%), however patients enrolled for a TA-AVI had more comorbidities and a higher baseline EuroSCORE (Thomas et al. 2011).

Valves designed especially for a TA-AVI approach have been developed and undergoing clinical trials. The Symetic Acuarate™ valve includes a porcine heart valve sutured to a nitinol stent with a Dacron skirt which has been found to reduce paravalvular leakage (Figure 2.6a). It is unsheathed in the ventricle through a two-step implantation procedure. This valve was tested in 90 patients with promising initial clinical results with a 30 day survival rate of 92% (Kempfert et al. 2011). The Engager™ valve has scalloped bovine pericardial leaflets sutured to a self expanding nitinol stent (Figure 2.6b). The stent has a support frame which clips over the native leaflets and a polyester skirt which seats at the base of the sinuses. The JenaValve™ consists of a porcine aortic valve sutured to a nitinol stent with a feeler to guide positioning and a clip which fits over the native leaflet (Figure 2.6c). During release of the JenaValve™, the sheath is partially retracted to release the feelers and enable correct anatomical positioning such as commissural alignment. The prosthesis then expands at the proximal end but remains connected at the distal end, enabling it to be retrieved and repositioned if necessary. This implantation procedure enables TA-AVI to be carried out without the need for RVP.

2.2.5 Other Transcatheter Approaches

Other approaches to PHV have been adopted including trans-aortic, -subclavian and -axillary, all of which enable bypass of the femoral arteries, enabling larger catheter sheaths to be used at a shorter distance. The trans-aortic approach is performed through a right or mid sternotomy and has been used with both the CoreValve and

Edwards valves. Trans-subclavian and trans-axillary require a surgical cut-down to isolate the respective arteries. The trans-subclavian can lead to serious and life threatening complications, giving the trans-axillary an advantage in that it's occlusion could be compensated through other arteries.

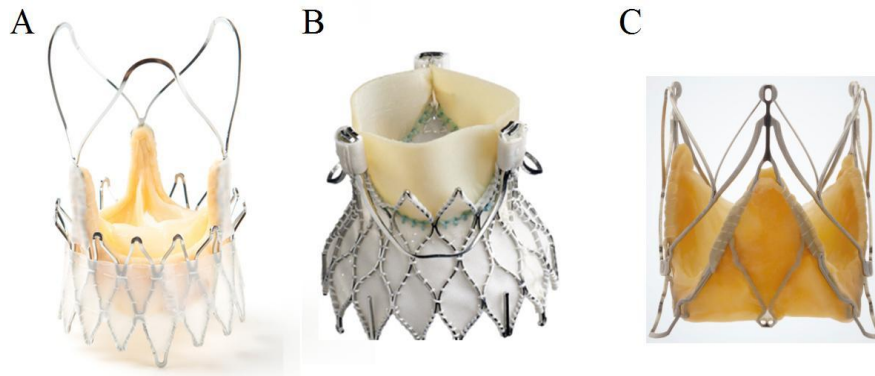


Figure 2.6 - Transapical Valves; (a) Symetis Acurate™, (b) Medtronic Engager and (c) 2nd Generation JenaValve (Sinning et al. 2012)

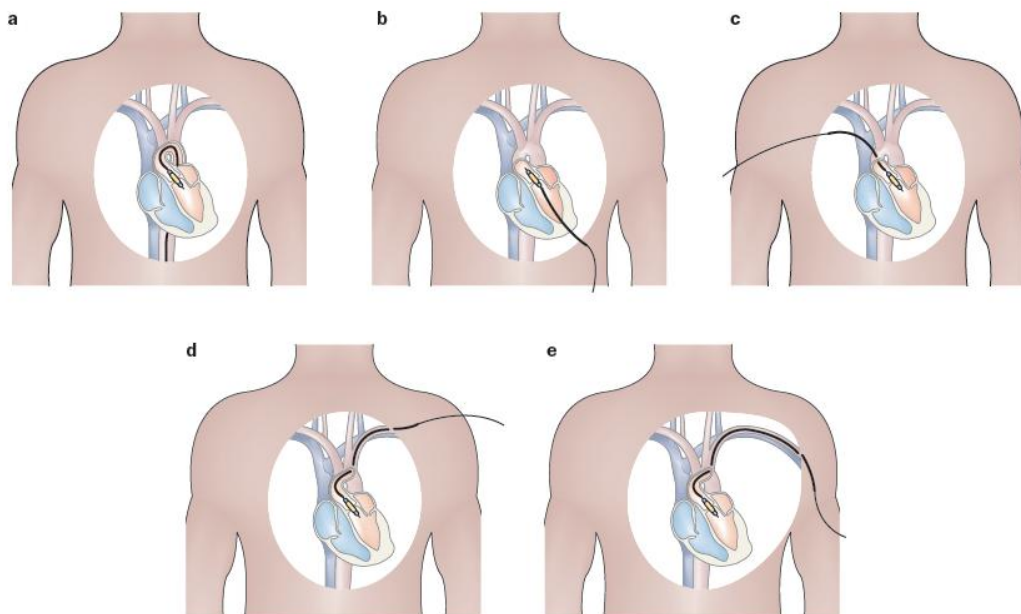


Figure 2.7 - Transcatheter approaches a) Retrograde transfemoral approach, b) Antegrade transseptal approach, (c) trans-aortic approach, (d) trans-subclavian artery and (e) trans-axillary approach (Rodes-Cabau 2012).

2.3 REPOSITIONABLE AND RETRIEVABLE PHVs

The main problem with the first generation PHV's were that once deployed they could not be repositioned or retrieved. Correct alignment and positioning of the valves has already been indicated from trial outcomes to be a necessity to reduce incidence of paravalvular leakage and obstruction of the coronary ostia. Additionally, it can lead to other complications including stent migration, fracture and mitral regurgitation. As such, it is desirable to have a valve which could be fully retrieved and repositioned in cases where a valve has been deployed in a suboptimal position.

The second and third generation CoreValve prosthesis had the ability to be fully retrievable after two thirds of the prosthesis had been deployed. However, the first fully repositionable PHV was the Sadra Medical self-expanding Lotus™ Valve prosthesis reported in a patient study by Buellesfeld et al. (2008). The valve consisted of a bovine pericardial tissue sutured onto a braided nitinol stent which had a similar design concept to the “Chinese Finger Trap” principle (Sinning et al. 2012). During delivery in a 21 Fr sheath, the stent undertook a longitudinal and narrowed shape which, when unsheathed, shrank in length and expanded radially outwards. This created a high radial force and reduced the risk of coronary ostia occlusion. The prosthesis also incorporated a self-locking mechanism, which allowed the entire valve to be retrieved and repositioned as necessary by unlocking it.

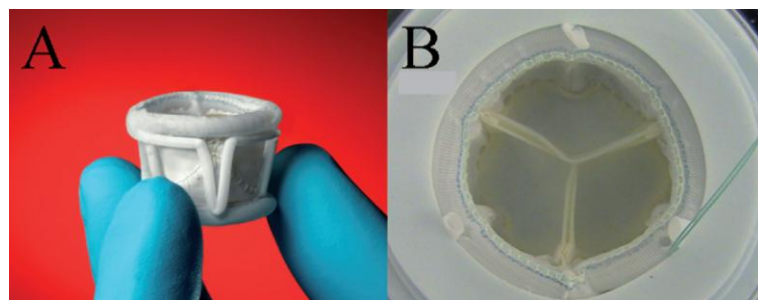


Figure 2.8 - The Direct Flow PHV; (A) Side view displaying the aortic and ventricular rings and (B) top view in a hydrodynamic testing chamber.

The Direct Flow Medical (DFM) heart valve consists of a bovine pericardial tissue tri-leaflet valve within a sheathed delivery system (Figure 2.8). The leaflets were treated with anti-calcification and sutured into inflatable Dacron cuffs which create a tight seal and reduce paravalvular leakage (Bolling et al. 2008). Once the position of the valve is determined, two cuffs, the aortic and ventricular rings can be inflated for fixation into the aortic annulus. These cuffs are inflated with either air or a contrast and saline solution which are then exchanged with a proprietary inflation medium (IM) whilst maintaining pressure to keep the valve expanded. The IM gel achieves 95% of its final hardness within hours (Bolling et al. 2008). The delivery system consisted of a 15 Fr multi-lumen catheter, and the implant was housed in the distal end which was 22 Fr in size. Three position/fill lumens (PFL's) were incorporated into the catheter which enabled the cuffs to inflate and deflate accordingly and for guiding and aligning the implant within the annulus.

Temporary placement studies of the DFM valve by Low et al. (2008) noted that the 14 mm height of the PHV was too short to accommodate the cusps of the native valve which led to a high transvalvular pressure gradient post implantation. This led to a design modification to increase the height to 16 mm and 17 mm in the 23 mm and 25 mm valves respectively, without compromising the coronary ostia. Overall, there was a drop in transvalvular gradient from a mean pressure of 87.6 mmHg pre-implantation to 17.9 mmHg post-implantation and no aortic insufficiency was evident in 7 of the patients, demonstrating excellent hemodynamics of the valve.

In another study on 16 AS patients deemed too high risk for surgery, there were improvements in mean transvalvular gradient from 50.1 mmHg to 19.6 mmHg after 30 days. Additionally, the aortic valve area increased from a baseline value of 0.57 cm² to 1.47 cm². Survival rates with the DFM valve after 1 and 2 years were 81% and 69% respectively (Bijuklic et al. 2011).

2.4 VALVE IN VALVE PROCEDURES

In 2005, a CoreValve prosthesis which was implanted in a 58 year old woman was incorrectly placed in a sub-annular position leading to severe AR through the stent struts and impingement of the anterior leaflet of the mitral valve. Due to the patient's refusal to undergo surgery, another CoreValve was deployed over the first valve in the correct position. Three year follow-up showed a reduction in a NYHA functional class reduction of IV to II. This case was the first to report the feasibility of a valve-in-valve procedure. Following this, cases of patients with degenerated bio-prosthetic valves receiving a percutaneous valve have been reported (Krumsdorf et al. 2010, Webb et al. 2010). The ability to implant a valve over an existing prosthesis creates an opportunity for patients undergoing a re-replacement with a bio-prosthetic valve to be enrolled for a PHV case (Ruiz et al. 2008). Additionally this would be most beneficial in younger patients who would have otherwise required repeat surgical AVR procedures in their lifetime.

2.5 RESULTS FROM THE PARTNER TRIAL

In 2007, Edwards Lifesciences enrolled patients for in the PARTNER (Placement of Aortic Transcatheter) trial to investigate the effectiveness and safety of TAVI using the Edwards Sapien valve. Cohort A involved 699 AS patients who were considered surgical candidates for valve replacement. They were randomly assigned to undergo either the TAVI with the Edwards Sapien valve or surgical AVR (Smith et al. 2011). Of those that underwent TAVI, the patients were divided into having a transfemoral (TF) procedure or a transapical (TA) procedure depending on whether they could accommodate the 22 Fr or 24 Fr sheaths. Cohort B consisted of 358 AS patients who were considered unsuitable for surgery were randomised into either having TAVI or non-surgical treatment (Leon et al. 2010). Of those who underwent therapy, 68% had balloon valvuloplasty.

Improvement in symptoms after 30 days was higher in the TAVI group compared to the AVR group. However, there was no significant difference between the two groups after 1 year. TAVI also had higher rates of vascular complications (11% vs. 3.2%) and major stroke (5.1% vs. 2.4%). AVR had a higher incidence of major bleeding and new onset atrial fibrillation. In the Cohort B study, the rate of death from any cause after 1 year was 30.7% in the TAVI group compared to 50.7% in the non-surgical group. However, rate of major stroke and vascular complications was higher in the TAVI group after 1 year at 5.0% vs. 1.1% and 16.2% vs. 1.1% respectively.

The major vascular complications reported with the use of the valves may be a result of the large femoral (24 Fr) sheaths that are used to access the femoral arteries. These results indicate the need for a reduced delivery profile and support frame which will enable patients with smaller iliofemoral arteries to benefit from a TAVI procedure (Leon et al. 2010). MRI studies have indicated cerebral embolism likely due to dislodged calcific debris from the aortic valve in many TAVI patients which may be the cause for the higher incidence of stroke (Kahlert et al. 2010). Other causes of stroke may be due to hypotension from rapid ventricular pacing or hemodynamic instability during the procedure (Holmes Jr et al. 2012).

2.6 COMPLICATIONS

There are several challenges still to overcome with a TAVI procedure. The rate of stroke following TAVI has been relatively high (3-9%), particularly with the CoreValve self-expandable prosthesis. AV-Block is also commonly reported in 4-8% of cases, particularly with the CoreValve due to the close proximity of the prosthesis to the AV conduction bundles. CoreValve patients are now fitted temporarily with a pacemaker to prevent atrial fibrillation although their cost effectiveness remains to be determined (Vahanian et al. 2008).

Major vascular complications are still commonly reported, having an incidence rate of 10-15% with the retrograde TAVI cases which, is largely due to the size of the introducer sheaths. In a patient population study by Toggweiler et al. (2012), arterial diameters which were smaller than the external sheath diameter were found to increase the chances of vascular complications and unplanned surgery. The study also found that when smaller 18 - 19 F sheaths were used, the prevalence of vascular complications decreased from 32% to 9%. The complications also decreased as a result of improved valvular closure techniques and percutaneous management. It is clearly evident that a reduced profile is necessary to overcome the vascular complications commonly reported. Furthermore, a reduced profile would increase the flexibility of the delivery system which would improve angular movement within the aortic root and LVOT.

As the percutaneous valve is aimed to be deployed over the calcified native valve, there holds to be a risk of emboli from the friable valve, which could cause coronary occlusion or stroke. A high incidence of this is reported in the Corevalve prosthesis which may be due to the incomplete entrapment of the friable native leaflets in the narrowed portion of the stent. Percutaneous entrapment devices to capture loose emboli have been developed and their use could reduce incidence of stroke. It is also worth noting that the calcified leaflets are pushed away from the flow boundary and as such the calcium may begin to be reabsorbed due to a lack of shear stress (Lichtenstein et al. 2006). In such an event, implant loosening or migration may occur. This would be more problematic with balloon expandable valves rather than self-expanding valves.

In FT-TAVI, rapid ventricular pacing is necessary with balloon devices to prevent migration of the balloon with pulsatile blood flow. However their use can lead to disturbances in hemodynamics which can lead to other complications. Grube et al. (2011) carried out a pivotal study which involved implanting the CoreValve prosthesis without balloon pre-dilation, thereby eliminating the need for RVP altogether. Although post-dilation was required in 10 of the 60 patients, their study demonstrated the feasibility and safety of not pre-dilating self-expanding valves and

may simplify future TAVI procedures. TAVI still remains unsuitable for patients with aortic regurgitation, particularly in cases where comorbidities such as aortic dilation and dissection exist.

2.7 FUTURE TAVI

Ten years of experience have demonstrated the feasibility of a transcatheter aortic valve replacement in patients whose chance of survival following diagnosis of severe AS would have poor prognosis after 1-2 years without surgical replacement. The procedure has also opened up an array of other opportunities such as the possibility of carrying out a simultaneous repair of mitral regurgitation or a coronary stent procedure with TAVI. Additionally, better use of imaging techniques would help reduce the incidence of patient-prosthesis mismatch (PPM) which may occur due to an incorrect determination of the annulus area.




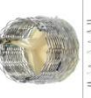
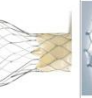

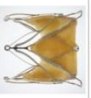

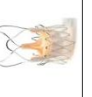
2.8 CHAPTER SUMMARY

1. Percutaneous heart valves provide a promising alternative solution to valvular replacement in patients with severe AS who cannot undergo surgery and in whom the mortality rate after 1 year is low.
2. Some of the complications of the earlier valves such as coronary ostia occlusion, paravalvular leaking and stent migration have been addressed in the next generation heart valves. However the later valve designs still have a while to go in developing a valve which will be able to survive long term implantation.
3. The next generation valves are still too large in patients with iliofemoral complications or those with smaller arteries such as children. A summary of

some of the existing percutaneous heart valves along with their advantages and disadvantages are listed in Table 2.1.

4. The following points should be considered in the design of a percutaneous heart valve. The design of a prosthetic heart valve is discussed in more detail in Chapter 5.
 - Prevention of coronary ostia occlusion, particularly from obstruction caused by native leaflets.
 - The ability to overdilate the valve to prevent paravalvular leakage but without compromising leaflet function.
 - Delivery devices which include steerable catheters and flexible sheaths to prevent aortic trauma during deployment from incorrect axial alignment.
 - Prevention of sub-annular seating too low in the LVOT which can cause compression of the His bundles and lead to AV Block.
 - Attention to the size of the deliverable technology to reduce the impact of the deployment technology on the vasculature.

Table 2.1 - Comparison of some of the current percutaneous valves.

| TRANSFEMORAL | | | | | | |
|--|---|--|--------|--|---|--|
| VALVE | PICTURE | DESCRIPTION | SHEATH | ADVANTAGES | DISADVANTAGES | REF |
| Edwards Sapien XT (Edwards LifeSciences) |  | Tri-leaflet bovine pericardial tissue with thinner cobalt-chromium stent. NovaFlex transfemoral delivery system. Product is CE Marked | 18 Fr | Thinner stent enables a lower profile delivery. Pericardial leaflets treated with the Carpenter-Edwards Thermanix process to reduce calcification. Suitable for TA-TAVI as well | Valve is not at all retrievable. Required rapid ventricular pacing (RVP) | Cribier et al. 2004 |
| CoreValve (Medtronic) |  | Tri-leaflet porcine pericardial tissue sutured onto a self-expandable nitinol stent | 18 Fr | Excellent haemodynamic and EOA (26 mm = 1.45 cm ² , 29 mm = 1.75 cm ²). Stent design prevents obstruction of the coronary ostia and slippage. Partially retrievable. | Not retrievable once fully deployed. Undersizing and inadequate positioning reported in the majority of patients | Grube et al. 2007, Suhultz et al. 2009 |
| DFM Valve (Direct Flow Medical Inc.) |  | Bovine pericardial tissue with inflatable aortic and ventricular rings | 16 Fr | Can be retrievable. Rings are inflated with a saline solution which can be replaced with a hardener to provide a rigid stent. DISCOVER Trial results show minimal regurgitation | Annular ring reduces the EOA of the valve. | Bijakic et al. 2011 |
| Sadra Medical Lotus™ Valve (Boston Scientific) |  | Bovine pericardial leaflets sutured to a braided nitinol stent. Stent is designed to elongate in collapsed state and shorten when expanded | 18 Fr | Ability to shorten and expand with high radial force. Short stent reduces coronary ostia obstruction. Flexible seal membrane (Adaptive Seal™) seals potential gaps between native aortic valve and prosthesis. No obstruction to flow during implantation. | No long term follow-up study yet | Simming et al. 2012 |
| Portico™ (St. Jude Medical) |  | Bovine pericardial leaflets sutured to a nitinol stent | 18 Fr | Low positioning of leaflets in stent reduce stent protrusion into the LVOT thereby minimising conduction interference. Can be completely retrieved and repositioned. Suitable for TA-TAVI | Rather low EOA at 1.3 cm ² . Degree of eccentricity and underexpansion at the inflow commonly reported | Wilson et al. 2012 |
| The Colibri Heart Valve (Colibri) |  | Dry packaged porcine pericardial membrane | 14 Fr | Low profile delivery. Thin pericardium material has a high strength and durability. Large EOA and < 200 sutures used | No long term follow-up study yet | www.colibrihv.com |
| TRANSAPICAL | | | | | | |
| DEVICE | PICTURE | DESCRIPTION | SHEATH | ADVANTAGES | DISADVANTAGES | REF |
| Jena Valve (Jena Technology) |  | Nitinol self-expanding stent with clip design. Pericardial leaflets | 32 Fr | Clip sandwiches native leaflets and offers support from stent migration. No RVP required. Fully repositionable and retrievable. Good initial clinical results with a 30 day survival rate of 92% | No long term follow-up study yet | Simming et al. 2012 |
| Engager (Medtronic) |  | Nitinol self-expanding stent with a support frame. Bovine pericardium | 30 Fr | Second generation have reduced paravalvular leakage | High rate of AV-Block due to compression of stent on Bundle of His fibres | Falk et al. 2011 |
| Symetic Acurate TA™ (Symetis) |  | Nitinol self-expanding stent with a support frame. Porcine aortic valve | 30 Fr | Dacron skirt prevents paravalvular leakage. Stabilising arches help self-position valve axially | High rate (9%) of AV-Block due to compression of stent on Bundle of His fibres | Kempfer et al. 2011 |

CHAPTER 3:

THESIS AIMS AND OBJECTIVES

3 THESIS AIMS AND OBJECTIVES

Transcatheter aortic valve interventions are a rapidly growing field in cardiac research with promising outcomes following 10 years' clinical experience. It is envisaged that, with improvement in technology, they will benefit a wider patient population, for example younger patients or those with a low risk from conventional surgery (Chiam and Ruiz 2009, Rodes-Cabau 2012). Additionally their cost effectiveness has been shown to be lower than that for AVR and that is set to increase with improvement and experience in TAVI management (Reynolds et al. 2012). Major vascular complications are common in transfemoral procedures and have been largely due to the large size of the introducer sheaths in relation to the patient's arterial dimensions. In some cases, access still requires a surgical cut down which can lead to complications such as infection and post-procedural hematoma. The transapical approach has a far less restriction on the delivery profile size but it is still an invasive procedure, requiring thoracotomy and exposure of the LV apex. Larger vessels such as the femoral arteries are also often atheromatous or tortuous, making delivery difficult. It is more desirable to utilise a smaller, upper limb artery where such complications are less common.

All currently CE-marketed valves incorporate chemically fixed pericardium or porcine valves to form the leaflets of the valve which are prone to calcification. Moreover, tissue prosthesis typically require over 1000 sutures to attach to the stent which causes regions of stress concentration and void spaces which can initiate calcification. Pericardial tissue, having thicknesses ranging from 200-400 μm are also much too thick to enable a reduced delivery profile. For this reason, a desire to steer away from pericardial tissue and adopt synthetic materials has been considered in the design of a valve. Synthetic materials like polyurethane have unlimited availability, vast manufacturing options and advancements in technology have given them superior biostability, making them favourable candidates in the design of a PHV. Additionally they can be incorporated with additives such as reinforcing fillers or radiopacifiers to enhance their properties.

As the natural leaflets are naturally reinforced with collagen and elastin, the desire to develop a reinforced synthetic leaflet structure is not novel. However, previous approaches have used large fibres which may compromise the flexibility of the leaflets, decreasing the rate of valve opening and closure and leading to high energy losses. Additionally, durability tests have shown large reinforced meshes to be prone to ‘blow outs’ in the unreinforced regions (Gallocher 2007). It would be more desirable to reduce the diameters of the fibres which would increase their surface area to volume ratio as well as improve leaflet flexibility. A random alignment of nano-sized particles with high aspect ratios is envisaged to enable thin synthetic leaflets to be developed without compromising their mechanical integrity.

The aim of this thesis is therefore **to develop an ultrathin reinforced synthetic heart valve for delivery through a super-peripheral access site such as the brachial or radial arteries**. This will be achieved through the following objectives:

1. TO EXPLORE THE MECHANICAL PROPERTIES OF PORCINE PERICARDIUM

Pericardium is the gold standard material of choice in bio-prosthetic valves and almost all percutaneous heart valves incorporate pericardium. The first stage of the project will be involved in determining the mechanical properties of porcine pericardium which will be used to determine the requirements for the development of a synthetic reinforced leaflet.

2. TO DEVELOP A SYNTHETIC MATERIAL WHICH WOULD BE REINFORCED WITH CARBON NANOTUBES

It is believed that a thin and durable synthetic material can be achieved through reinforcement with carbon nanotubes. The second stage of the project will involve creating an array of thin film composites using polyurethane with varying nanotube content which will be mechanically tested alongside a non-reinforced polymer to determine the best nanotube content to achieve optimal properties.

3. TO PRODUCE A COMPOSITE TRI-LEAFLET HEART VALVE WHICH WILL BE DURABILITY TESTED

The final stage of this project will be to develop tri-leaflet artificial heart valves by dip coating a former and stent with the optimal polymer-nanotube solution. The valves will be tested using the ViVitro Hi-Cycle accelerated fatigue tester to determine their durability. A series of different leaflet thicknesses will be developed through varying the number of dip coats to determine the influence leaflet thickness has on the durability of the valve.

CHAPTER 4:
PERICARDIAL TESTING

4 PERICARDIAL HEART VALVES

4.1 INTRODUCTION

The gold standard material of choice for bioprosthetic valves is pericardium; a dual layered sac which encloses the heart and functions to protect the heart from external infections or shocks. Porcine (PP) and bovine (BP) pericardium are the most common heterograft sources although other species such as canine and equine have also been used. Being heterografts, they have an advantage in that there are no restrictions to the valve leaflet geometry (Mirnajafi et al. 2005). However, their use as biomaterials requires them to be treated chemically or physically to reduce the immunogenic response, prevent chemical degradation and to sterilize the tissue (Chachra et al. 1996).

Several studies have been carried out to investigate the mechanical properties of pericardium to determine its suitability for bioprosthetic heart valves (Zioupos 1989, Zioupos et al. 1992, Paez and Jorge-Herrero 1999, Mirnajafi et al. 2005). These studies have shown pericardium to be anisotropic, meaning that the alignment of the fibres differs in all directions. This has shown the tissue to be least extensible in the circumferential direction and most extensible in the root to apex direction. However, the fibre orientation and mechanical properties are rarely taken into account when forming the leaflets for pericardial valves despite the fact that this may have detrimental effects to the durability of the valves. Additionally the age of the animal, the selection site and the species impact upon its structural content, may affect its mechanical properties (Paez and Jorge-Herrero 1999, Shabetai 2004). Furthermore, the type of chemical or physical treatment used, such as glutaraldehyde (GA), affects the structural and mechanical properties of pericardium. In this chapter, the uni-axial mechanical properties of porcine pericardium will be assessed and used for future comparison in the development of polymeric valves.

4.2 STRUCTURE AND BIOCHEMISTRY OF PERICARDIUM

The pericardial tissue essentially consists of two interconnected layers; a serous layer and an outer fibrous layer (Figure 4.1). The serous layer is lined by a single layer of mesothelial cells and is divided into two layers; the visceral and parietal pericardium. The inner visceral pericardium closely attaches to the epicardium which is the outer layer of the heart wall (myocardium). It folds back to create the inner layer of parietal pericardium (Chinchoy et al. 2005). The pericardial cavity lies between these two layers and holds about 15-35 ml of pericardial fluid, which acts as a lubricant to reduce the friction between the sliding surfaces of the pericardium and the heart as the heart beats (Spodick 1997).

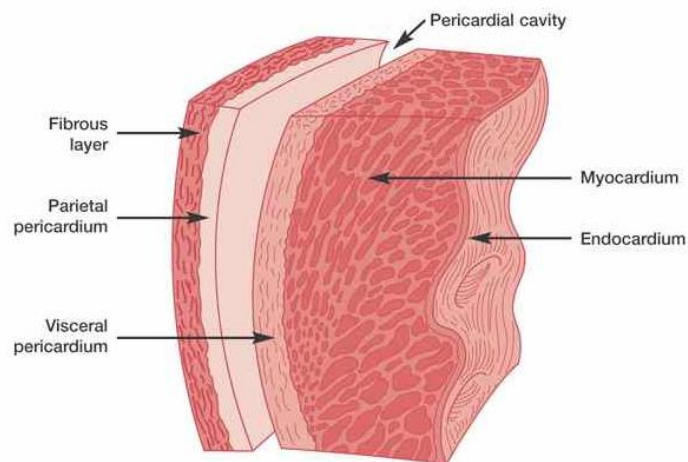


Figure 4.1 - Schematic representation of the layers of pericardium (taken from mediconweb.com).

Pericardium used in the design of prosthetic valves are devoid of the mesothelial cell layer and are arranged such that the rough surface of the epicardium faces the inflow and the smooth serosal layer faces the outflow (Ishihara et al. 1981). The extracellular constituents of pericardium include collagen, elastin and glycosaminoglycans. Collagen and elastin have been found to be orientated together and the orientation of these fibres is seen to change through the layers which has led some to believe that it is an isotropic material rather than anisotropic.

4.3 MECHANICAL ANISOTROPY

Pericardium is now widely regarded to be mechanically anisotropic (Zioupos et al. 1992, Sacks 2000), meaning its mechanical behaviour is dependent on the direction of the collagen and elastin fibres (Paez and Jorge-Herrero 1999). Although tissue anisotropy is also present in native valve leaflets, in which the fibres are aligned parallel to the free edge of the leaflet (Paez and Jorge-Herrero 1999) there is no evidence in literature supporting pericardium being aligned to optimise valve function. Accordingly, this has led to extensive interest in determining its suitability as a material in bioprosthetic valves. Various methods have been adopted to measure the mechanical properties of pericardium, including uniaxial (Zioupos et al. 1994) and biaxial tensile (García Páez et al. 2002), inflation (Zioupos et al. 1992) and flexure tests (Mirnajafi et al. 2005).

Zioupos (1989, 1992) used a method of inflation to consider the anisotropy of bovine pericardium. This involved clamping the pericardial sheet to an annulus ring and applying air pressure to deform it in a shape decided by the central aperture of the inflation apparatus. It was observed from the inflation tests, that the pericardium deformed into an oval shape, ruling out axi-symmetry and suggesting that the tissue exhibited some orthotropic symmetry. However, uni-axial tensile tests carried out in the circumferential and root-to-apex directions indicated that bovine pericardium was anisotropic. The mean (SEM) terminal tensile modulus was 46 (2.2) MPa for the circumferential strips compared with 14 (1.0) MPa for the root-to-apex strips. They also reported a significant difference in the tensile strength of circumferential and root-to-apex strips of 18 (0.4) MPa and 2.5 (0.3) MPa respectively.

In a later study by Zioupos et al. (1994), the mechanical anisotropy of bovine pericardium was apparent by looking at the modulus of the initial curvature of a stress-strain graph. It was noted that the initial modulus of fixed BP was significantly higher in the circumferential direction compared to the root to apex direction and was 10 times greater than that of fresh BP. They concluded that the anisotropy can be used to align the fibres along the circumferential direction of the valve leaflets as

well as enable the radial direction to be more extensible which would facilitate coaptation.

GA cross-linking is currently the standard treatment for pericardium and is necessary in order to reduce the immunological response and degradation of the tissue. However, the degree of cross-linking has been known to affect the structural and mechanical properties of pericardium as well as accelerate calcification. Other treatments such as photo-oxidization (Bianco et al. 1996, Verbrugghe et al. 2009) or decellularization techniques have been considered as an alternative to GA. However, long term information on the impact that these treatments have on the structural and mechanical properties of the tissue still needs to be determined (Mirnajafi et al. 2005, Rémi et al. 2011). The mechanical properties of the porcine pericardium were obtained by conducting a uni-axial tensile test using a universal testing machine.

4.4 SAMPLE PREPARATION

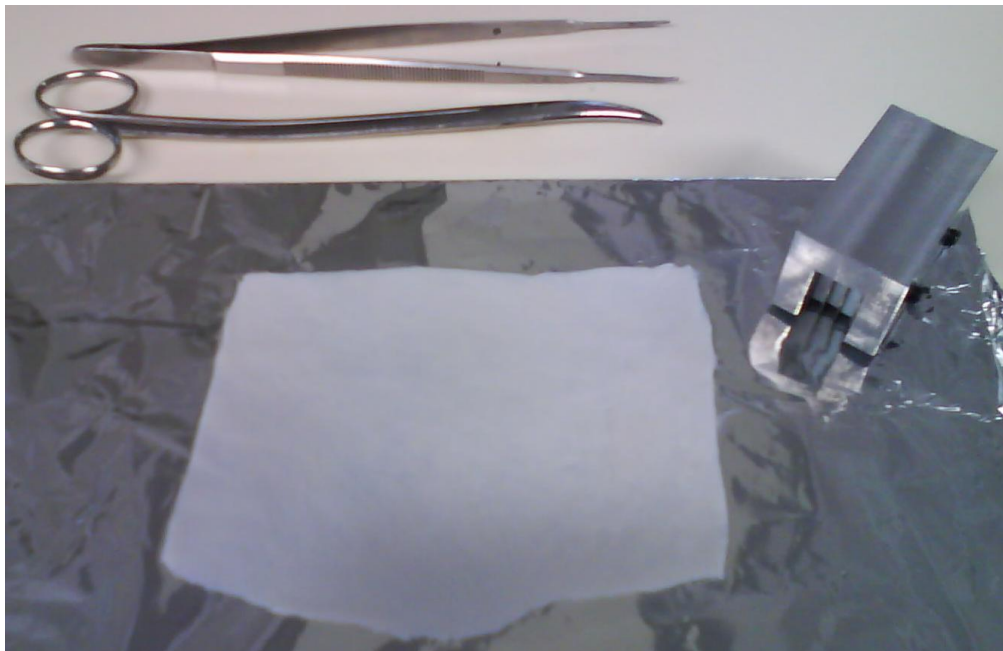


Figure 4.2 - Photograph of fresh porcine pericardium and the parallel blade cutter used to cut the strips.

Fresh and fixed (treated in GA at zero pressure) sheets of porcine pericardium (PP) were obtained from Vascutek Ltd. (Vascutek Porcine Pericardial Patch, Glasgow, UK). The fresh PP was contained in phosphate buffered saline (PBS) solution and the GA fixed PP in ethanol. The fresh PP was whitish in colour and easily compressible compared to the GA treated PP which was tougher and had a yellowish colour. Figures 4.5 and 4.6 show images of the layers of the fresh and fixed porcine pericardium respectively which were viewed under a polarized microscope (Axio Lab.A1, Carl Zeiss MicroImaging, LLC, North America). The fibres appear to be loosely bound in the fresh pericardium compared to the fixed tissue which has a tighter crimp due to the GA treatment. In both the fresh and fixed pericardium, the orientation of the collagen fibres was seen to change as the microscope progresses through the layers.

A scalpel was used to carefully strip the underlying layers of a section of the pericardium and viewed using an optical light microscope to determine the predominant direction of the collagen fibres. Once an alignment had been established, strips of pericardium measuring 3 x 30 mm were cut at 0° and 90° to the fibres using a parallel blade cutter and a hammer (Figure 4.3). The strips were then kept in fresh PBS and stored at 4°C until needed for testing. A detailed description of the sample sets is described in Table 4.1.

Table 4.1 – Description of the testing samples

| Set Number | Treatment | Fibre Orientation |
|-------------------|--|--------------------------|
| 1. | Fixed at 0 mmHg in glutaraldehyde | 0° |
| 2. | Fixed at 0 mmHg in glutaraldehyde | 90° |
| 3. | Fresh (formally treated with formaldehyde) | 0° |
| 4. | Fresh (formally treated with formaldehyde) | 90° |

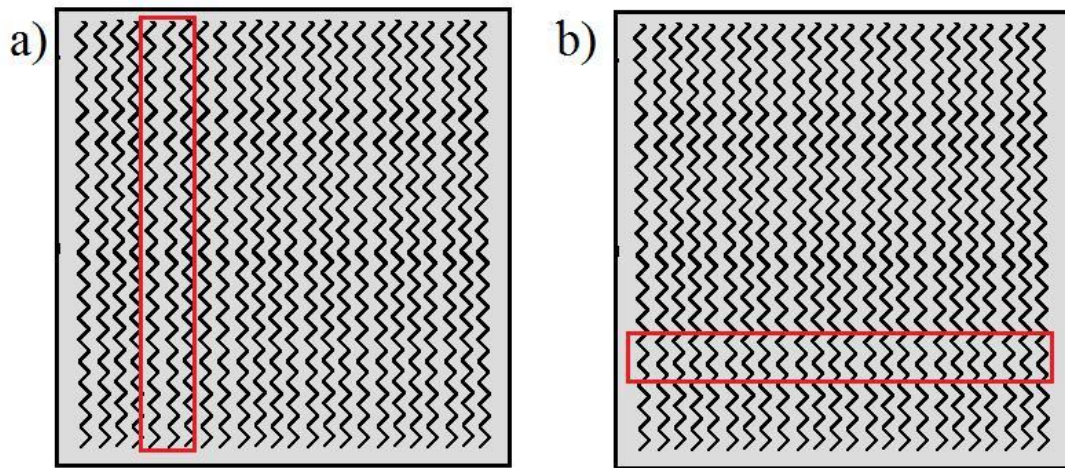


Figure 4.3 – Strips cut from a sheet of pericardium aligned at (a) 0° and (b) 90° to the direction of the fibres.

The thickness of the pericardial strips was measured immediately before testing using a vernier calliper with a precision of 0.01 mm by sandwiching the strips between two glass slides and taking readings from 4 equal points along the strip. The strips were then mounted between square frames of waterproof sandpaper and fixed in place using a biological adhesive. The mounted specimens were kept in their solution at room temperature to prevent them from drying out until they were ready for testing.

4.5 TENSILE TESTING

A 100 N load cell was used for all of the tests. The specimens were mounted between the grips of the Instron machine and a gauge length of 10 mm was set. Once fixed in place, the sides of the sandpaper were carefully cut away. Like native valve leaflets, pericardium is also viscoelastic and its properties are time dependant (Lee et al. 1994). Preconditioning is necessary to reduce hysteresis caused by fibre re-alignment. All strips were initially preconditioned between 0.5 and 2.5 N for 20 cycles at a rate of 1 N/s. However, it was preferred to reduce the preconditioning to a maximum of 2.0 N for the fresh samples. Three strips from each set were then stress

relaxed by fixing the crosshead extension at 2.5 mm and holding for 120 seconds. All strips were then uni-axially stretched to failure at a rate of 10 mm/min. An ANOVA one-way statistical analysis was carried out on the data at a 95% confidence interval.

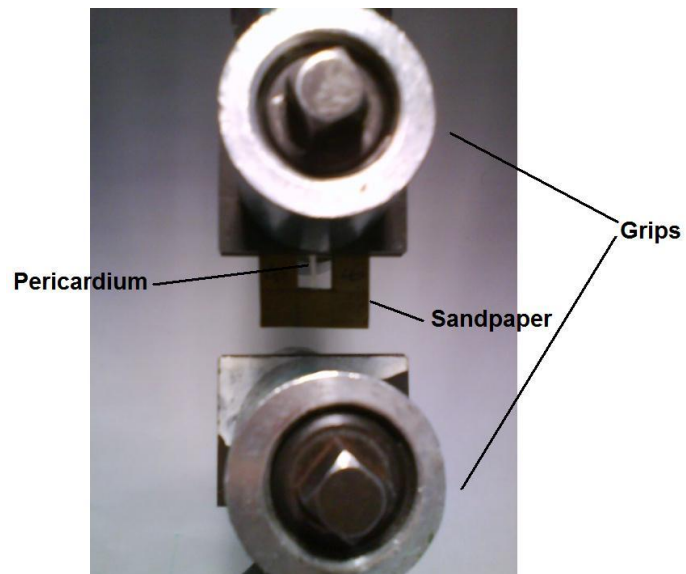


Figure 4.4 - Porcine pericardium strip sandwiched between frames of sandpaper and clamped on to the Instron grips.

4.6 RESULTS

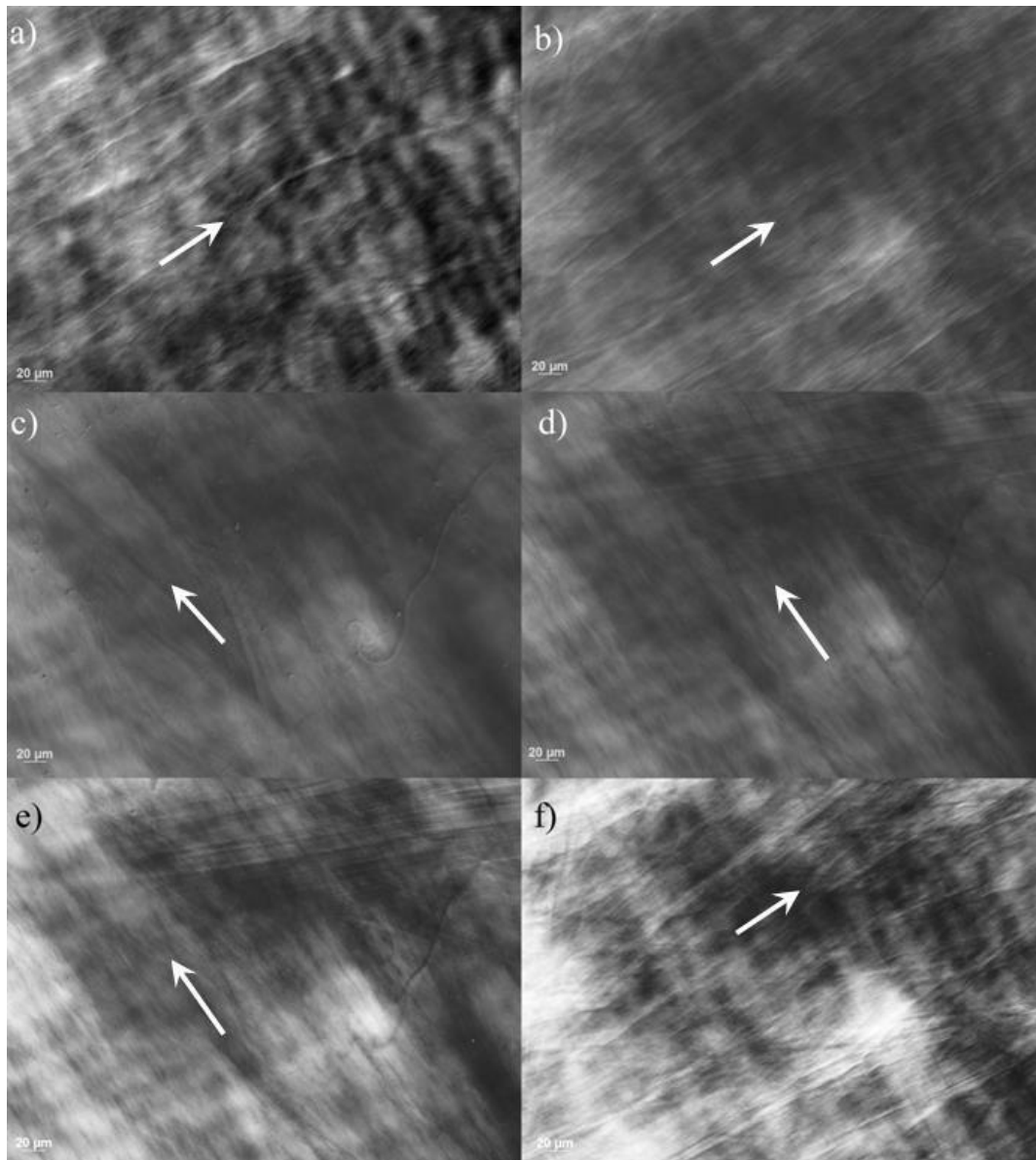


Figure 4.5 – Images from microscope taken of fresh porcine pericardium, descending through its layers (a)-(f). Arrows indicate predominate direction of fibres. Note the change of direction of fibres from (b) to (c). The bundles of fibres appear to be loosely bound.

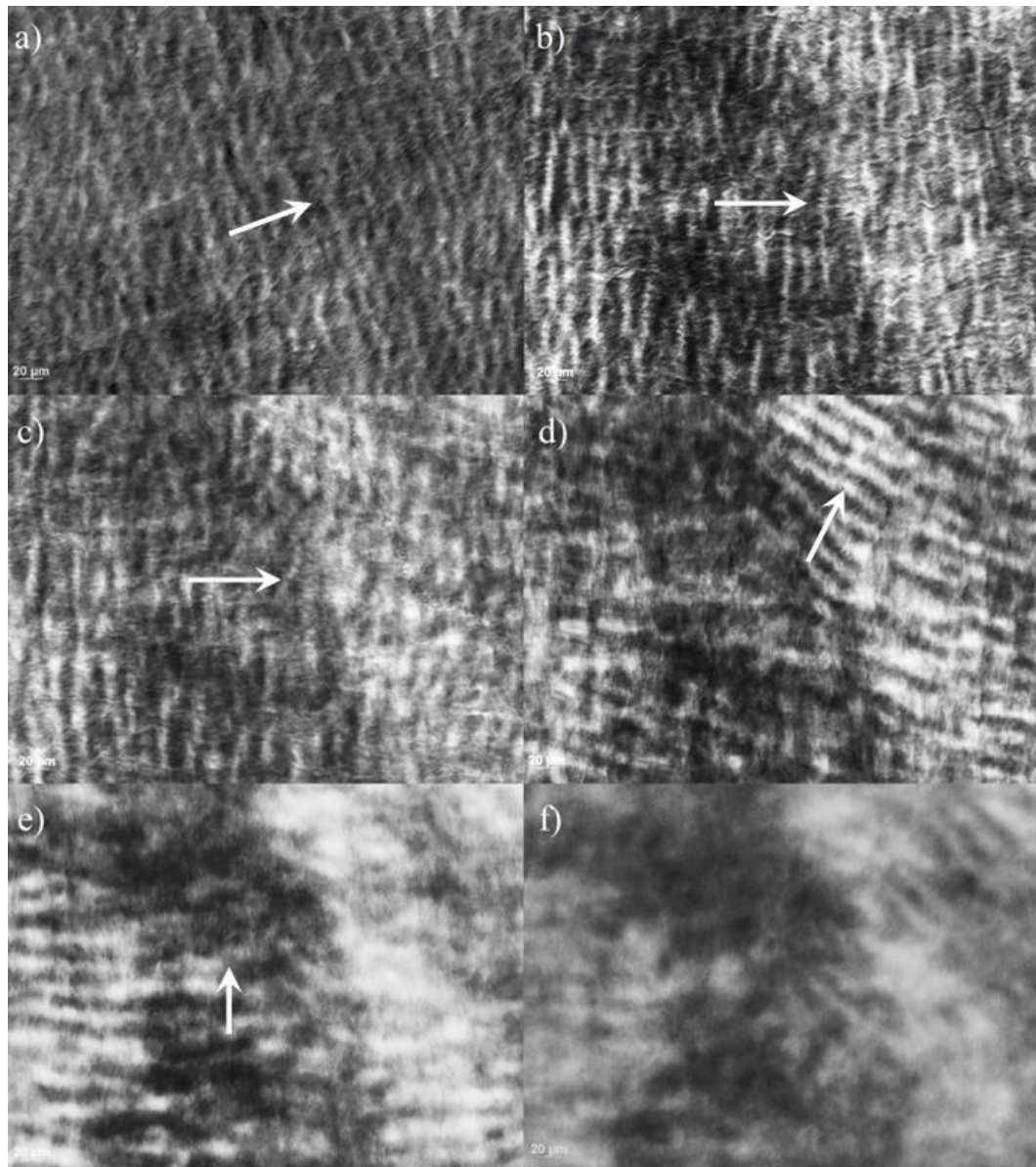


Figure 4.6 - Images from microscope of fixed pericardium descending through the various layers (a)-(f). Arrows indicate predominant direction of fibres. A tighter crimp formation in comparison to the fresh pericardium is apparent by the increased amplitude of the ridges. The resolution decreases as the depth of the images increases.

The results of the tensile properties of porcine pericardium are shown in Table 4.2. The overall thickness of the pericardial strips ranged from 170 to 292.5 μm for the fixed samples and 85 to 125 μm for the fresh samples. The mean (\pm SEM) thickness for the fixed and fresh pericardium was statistically significant ($p < 0.05$) at $210.4 \pm 9.8 \mu\text{m}$ and $102.4 \pm 2.9 \mu\text{m}$ respectively. The fresh pericardium is considerably softer than the fixed tissue and the possibility of there being some degree of tissue

compression should not be ruled out. Therefore another set of strips of fresh pericardium were prepared and measured after 5 seconds of contact was established between glass slides. The mean (\pm SEM) thickness for the first 6 samples was $124.2 \pm 5.7 \mu\text{m}$ and when less compression was applied the thickness was $150.6 \pm 7.0 \mu\text{m}$ for the second 6 samples.

For both the fixed and fresh pericardium, the elastic modulus was higher in the 0° direction compared to the 90° direction. This was significant ($P < 0.05$) in the fixed pericardium but not the fresh tissues. The elastic modulus ranged from 49.6 to 169.2 MPa and 90.9 to 267.6 MPa for the fixed and fresh pericardium respectively and was overall higher for the fresh pericardium although the difference between the fresh and fixed PP was not significant in the 0° direction. The ultimate tensile strength (UTS) was observed to be twice as high for both fixed and fresh pericardium when the fibres were aligned parallel (0°) to the direction of the tensile force.

The modulus of the initial slope for the fixed samples at 0° and 90° to the direction of the fibres were 6.8 ± 0.2 MPa and 1.0 ± 0.2 MPa respectively. The initial slope of the fresh samples was considerably shorter and therefore was difficult to determine accurately. The fixed samples were observed to have an overall higher strain at failure compared to the fresh samples. For the fixed pericardium, the strain at failure was significantly different ($p < 0.05$) in the 0° and 90° fibre orientations, having a strain of $21.9 \pm 0.9\%$ and $32.8 \pm 1.1\%$ respectively. The percentage stress relaxation was also higher for the 0° tissue and overall higher for the fresh pericardium.

Table 4.2 – Summary of results (mean \pm SEM) from the tensile testing for each set group.

| Set Number | N | Thickness (μm) | E. Modulus (MPa) | UTS (MPa) | % Strain at Failure | % Stress Relaxation |
|---------------------------------------|---|--------------------------------|-----------------------|----------------|------------------------|------------------------|
| 1. Fixed 0° | 6 | 184.6 ± 2.9 | 140.5 ± 10.8 | 15.1 ± 1.1 | 21.9 ± 0.9 | 12.1 ± 1.0 |
| 2. Fixed 90° | 6 | 240.4 ± 12.5 | $57.1 \pm 2.5^*$ | 6.7 ± 0.5 | 32.8 ± 1.1 | 9.5 ± 1.9 |
| 3. Fresh 0° | 9 | 106.0 ± 4.4 | 184.7 ± 19.3 | 18.0 ± 1.7 | 18.5 ± 1.1 | 37.5 ± 2.9 |
| 4. Fresh 90° | 7 | 99.1 ± 3.6 | $137.3 \pm 22.3^{**}$ | 8.3 ± 1.0 | 15.2 ± 1.6 | 21.0 ± 2.6 |

*Significant difference ($P < 0.05$) compared to fixed 0° PP.

** Significant difference ($P < 0.05$) compared with fixed 90° PP.

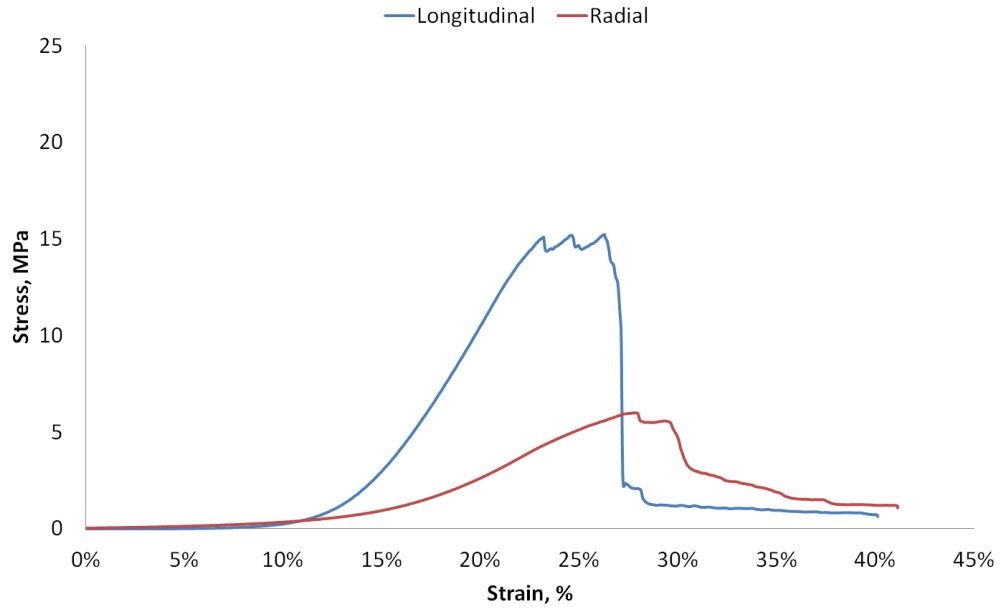


Figure 4.7 – Graph of the stress-strain relationship for a fixed pericardium strip in the longitudinal and transverse directions.

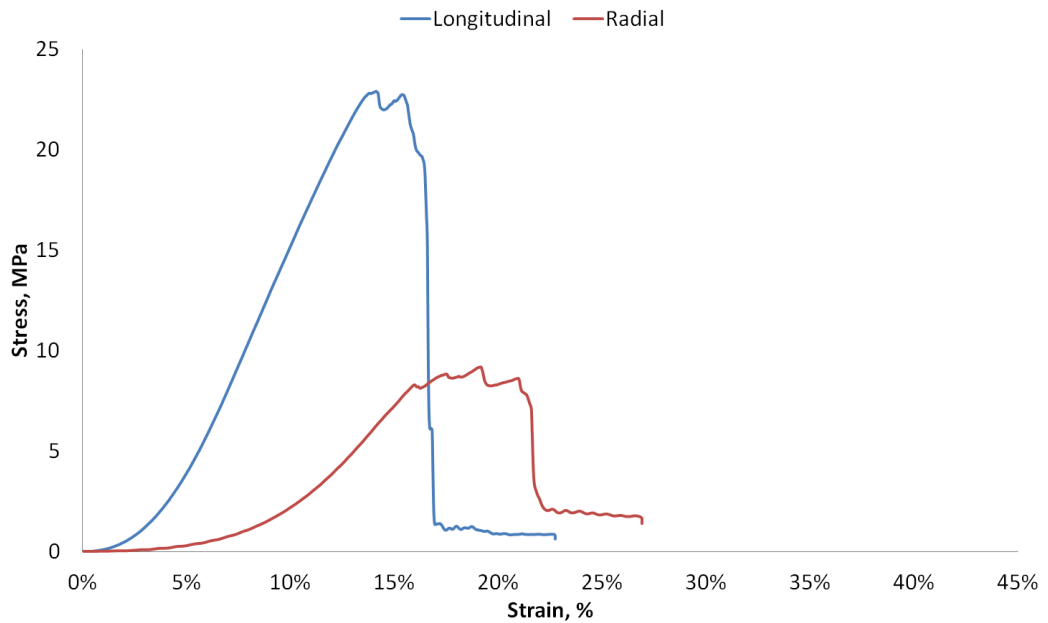


Figure 4.8 – Graph of the stress-strain relationship for a fresh pericardium in the longitudinal and transverse directions.

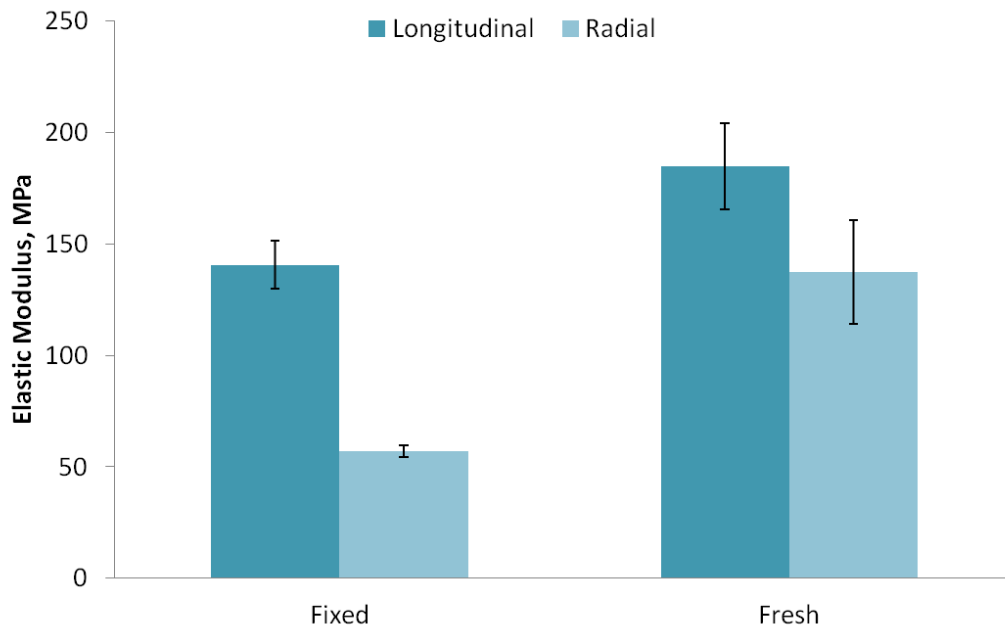


Figure 4.9 - Mean (\pm SEM) of the Elastic modulus in MPa of fixed and fresh porcine pericardium (n = 6 for the fixed PP, n = 9 fresh 0° PP and, n = 7 fresh 90° PP).

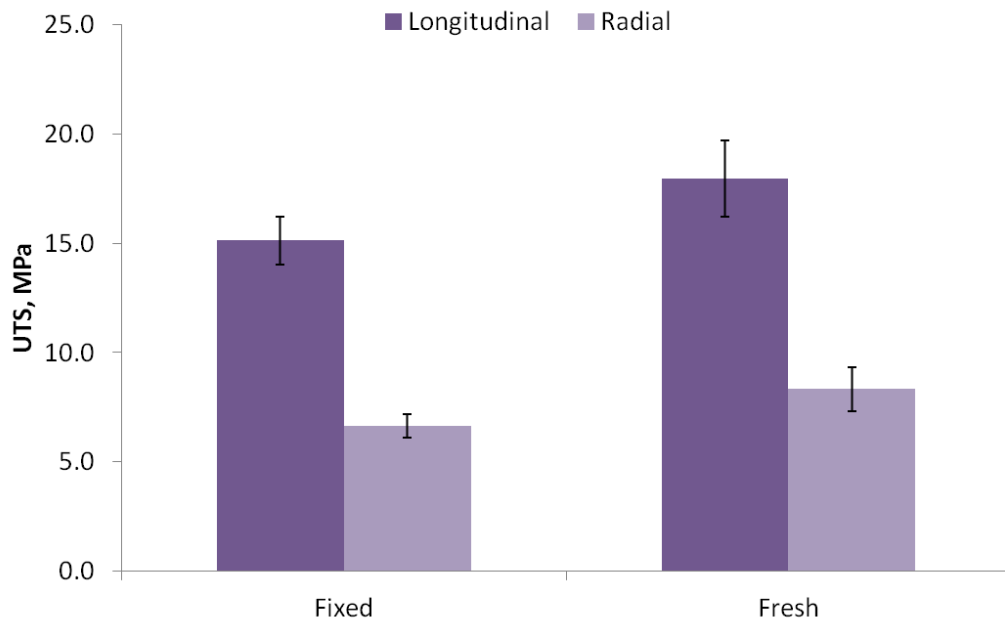


Figure 4.10 - Mean (\pm SEM) of the Ultimate tensile strength in MPa of fixed and fresh porcine pericardium (n = 6 for the fixed PP, n = 9 fresh 0° PP and, n = 7 fresh 90° PP).

4.7 DISCUSSION

Bovine pericardium (BP) is more commonly used in pericardial prosthesis compared to porcine pericardium (PP). However, PP is substantially thinner ($200 \pm 10 \mu\text{m}$ compared to $420 \pm 10 \mu\text{m}$) and stiffer than BP (Naimark et al. 1992, Lee et al. 1994). The increased stiffness of PP is attributed to a higher degree of cross-linking and an increase in collagen type III although the total collagen content is not different between PP and BP. The modulus and UTS values of the fixed porcine pericardium from this study were found to be similar to the results reported by Gauvin et al. (2012) who treated Vascutek porcine pericardial patches in 0.5% GA for 24 hours. However, they reported a higher modulus and UTS with the bovine tissue.

The measured thickness of the fixed pericardium was observed to be twice that of the fresh pericardium. Langdon et al. (1999) found unconstrained GA fixed bovine pericardium to be significantly thicker than the fresh pericardium, whereas tissue that was cross-linked under a constraint had a thickness similar to the fresh tissue. The increase in tissue thickness following unconstrained GA fixation was attributed to planar shrinkage of the tissue and a decreased collagen crimp wavelength. In the present thesis, the pericardium was fixed at 0 mmHg, which agrees with the findings by Langdon et al. Arbeiter et al. (2012) also found fresh porcine pericardium to be much thinner than GA-fixed tissue, having a thickness of $130 \pm 11 \mu\text{m}$ compared to $220 \pm 20 \mu\text{m}$. These findings can help conclude that thickness measurement of fresh pericardium can induce compression and that fresh pericardium is still found to be thinner than GA fixed pericardium.

There are many other methods that could also be used to measure the thickness of soft tissues without inducing compression, including a Hall probe, a travelling microscope or ultrasound. Lee and Langdon (1996) examined 5 methods of bovine pericardium thickness measurement which they normalized against their thickness measured in a frozen state. They reported similar findings between a non-rotating thickness gauge and an instrumented thickness gauge and concluded that the non-rotating gauge was the most convenient of the methods tested due to its portability

and simplicity. This method was also adopted by Hiester and Sacks (1998) to obtain the thicknesses of bovine pericardial sacs. Therefore it would seem that a non-rotating thickness gauge would be sufficiently effective in measuring pericardial tissue and their thicknesses in a frozen state should also be determined to eliminate compression errors.

The elastic modulus of both the fresh and fixed pericardium aligned parallel to the direction of the collagen fibres was higher than in the perpendicular direction. This anisotropy was more pronounced in the fixed than the fresh PP. The fresh pericardium also had a higher elastic modulus compared to the fixed pericardium. Variation in the cross-sectional area associated with tissue compression may induce an error in these measurements. However, the stiffness of the fixed PP was not significantly different ($p>0.05$) to the stiffness of the fresh PP when the fibres were aligned parallel to the direction of the load. If the error due to compression was accounted for, this difference would be even less. These findings agree with those found by Liao et al. (2005) who, were reportedly the first to observe that glutaraldehyde fixation did not change the intrinsic collagen molecular stiffness of the pericardium.

The initial slope region was found to be a better determinant of mechanical anisotropy and effects of GA fixation (Zioupos et al. 1994). From the stress-strain graphs shown in Figures 4.7 and 4.8, it is clear that the initial slope region is larger in the fixed samples than the fresh. This may be due to the increased amplitude of the crimp pattern of the collagen which would need to extend further to straighten upon contact with the load. Additionally, there appears to be a shift to the right in GA fixed pericardium compared to the fresh PP. This shift correlates with the increased extensibility of GA fixed PP and was also noted in others work (Lee et al. 1994, Hulsmann et al. 2012). The fixed samples had a higher overall strain at failure than the fresh pericardium which suggested that the GA fixation increased the extensibility of the sample; this is possibly attributed to the higher degree of cross-linking in the tissue.

The percentage stress relaxation is markedly greater in fresh tissue, being three times higher than fixed porcine pericardium. Dynamically fixed porcine valves in 0.05% GA had a higher stress relaxation than statically fixed valves in 0.5% GA and stress relaxation that was comparable to the fresh tissue (Duncan et al. 1997). The UTS of fresh pericardium aligned parallel to the direction of the fibres was 18.0 MPa. This value compared well with the findings by García Páez et al. (2002) who determined the uni-axial UTS values to be between 19.66 and 23.34 MPa in the root to apex direction.

It was seen from the microscopic images shown in Figures 4.5 and 4.6 that the fibre orientation differed through the depth of the tissue. Alavi et al. (2012) looked at the fibre orientation of bovine pericardium as they descend through the tissues layers following uni-axial longitudinal (90° to the direction of the fibres) and transverse stresses (0°) and biaxial stresses. Uni-axial longitudinal tests were found to align the fibres perpendicular to the direction of the load at the surface and parallel to the load in the deeper layers. They reported similar findings with transversely loaded samples, which oriented 60° to the direction of the load at the surface and parallel to the load in the deeper layers. These findings suggest that pericardium can be aligned so that the longitudinal loading is in the radial direction of shear stress which can dampen the shear stresses the leaflet would be exposed to during blood flow.

There was harmony in the results from the data in this thesis in relation to the mechanical properties of PP reported by other research groups. However, there are elements of valuable characteristics that were not determined in this present work. These properties are well defined in literature and include the issues of biaxial testing, calcification and method of treatment. The UTS values following biaxial tests of porcine pericardium were significantly higher ($P < 0.001$) ranging between 61.15 and 67.12 MPa, compared to uni-axial results (García Páez et al. 2002). Biaxial testing provides a more accurate measurement of the mechanical properties of soft tissues since the stresses are applied in two directions such as is the case for a valve leaflet which is exposed to circumferential and radial stresses.

The method of treatment of pericardium has detrimental effects to its mechanical properties and potential to accelerate calcification. Calcification increased in both porcine and bovine pericardium with increased concentration of GA fixation and decreased with increasing fixation time in the porcine but not bovine pericardium. This was attributed to the different cellular contents and composition of the ECM between PP and BP (Sinha et al. 2012). Additionally, the long term effects of collagen structure due to crimping need to be known. Stent imprinting and histological damage to the collagen fibres of stented bovine pericardial leaflets were evident following balloon expansion (de Buhr et al. 2012). Some work has focused on alternative materials to overcome these complications. For example, donkey pericardium is thinner than bovine pericardium, stiffer (81.67 MPa vs 21.67 MPa) and has a significantly reduced calcium content following 4 and 8 weeks implantation (Chen et al. 2013).

4.8 COMPARISON WITH POLYMERIC LEAFLETS

The elastic response of pericardium is very different to the elastic response of polyurethane (Figure 4.11). Polyurethane has an initial stiff linear region followed by a decrease in stiffness with increasing strain. However, as can be seen from Figures 4.7 and 4.8 the stiffness of pericardium is very low at low strains and increases at higher strains. This may facilitate coaptation by enabling large deformations in the radial direction if fibres are aligned perpendicular to the direction of flow. With polyurethane, having a higher stiffness at low levels of strains may prevent plastic deformation and creep when the valve is closed and exposed to diastolic loads.

As a comparison, the ultimate tensile strength would be a better indicator of a tear threshold. The UTS of the PP samples differed considerably depending on the orientation of the fibres. Polymeric leaflets that are either unreinforced or reinforced with random fibres would be isotropic, meaning that their properties are the same in all directions. It would therefore be appropriate to compare their UTS with that of the PP aligned parallel to the direction of the load.

Since the loading response of polyurethane differs from that of pericardium, the requirements in the design of a polymeric valve will be very different to that of a bioprosthetic valve. These are discussed in further detail in the following chapter.

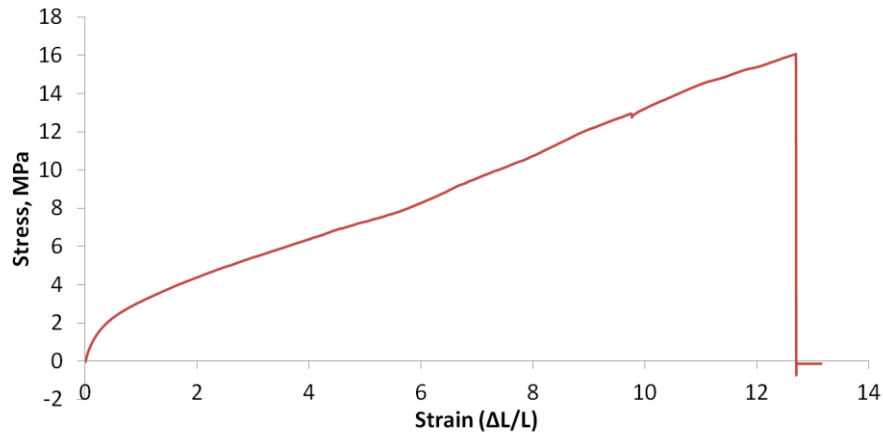


Figure 4.11 – Load – deformation response of polyurethane.

4.9 CHAPTER SUMMARY

1. Glutaraldehyde fixation increases the thickness and decreases the percentage stress relaxation of porcine pericardium.
2. The properties of GA fixation reported in this work with porcine pericardium have also been reported in other literature with bovine pericardium.
3. These findings have shown that the load-deformation response of pericardium varies greatly to that of polyurethane and therefore the design requirements of a polymeric valve will be different to that of a pericardial one.

CHAPTER 5:

PRINCIPLES OF VALVE DESIGN

5 PRINCIPLES OF VALVE DESIGN

5.1 INTRODUCTION

The function of the heart valve is to allow a one way flow of blood with minimal regurgitation. In flexible prosthetic heart valves such as bioprosthetic and polymeric valves, the leaflets would be required to flex rapidly under high stresses during the cardiac cycle without tearing or causing obstruction to flow. Over the years, prosthetic valves have undergone several design modifications to improve their performance, durability and aesthetics. In some instances, these modifications can lead to catastrophic consequences if thorough testing is not carried out. In other instances, a valve may have been subjected to rigorous in vitro or animal studies and still be found to fail when implanted in a human. These past experiences have demonstrated the difficulty in developing a functional heart valve with minimal complications but it is through these experiences that successful designs have been possible.

One example of this is the Ionescu-Shiley bovine pericardial valve which endured a period of success before a series of failures lead to their withdrawal. Stent rigidity, leaflet abrasion and commissural sutures were found to be the cause and introduction of a low profile flexible stent reduced the incidence of failure. Additionally low pressure glutaraldehyde fixation and leaflets that were sutured to the Dacron cloth rather than around it overall improved the performance of the next generation pericardial prosthesis. As with pericardial valves, polymeric valves have also undergone several design changes. Earlier polymers used for valve leaflets had poor durability, lasting only a few million cycles in accelerated fatigue tests. Improvements in polymer development such as increased biostability have enabled polymeric valves to last up to 800 million cycles (Bernacca et al. 1997).

The native aortic valve undergoes several structural deformations in response to the pressure changes during the cardiac cycle. One pronounced difference between native and synthetic leaflets is the inability of the synthetic material to adapt to the

large structural deformations with time. On one side, this can simplify design since the leaflets of a rigid valve do not need to adjust to a changing orifice. However on the other end, the leaflets of a synthetic valve will be subjected to higher stresses. This indicates the challenges faced in developing a synthetic material capable of handling the stresses induced during the complex dynamics of the cardiac cycle. An ideal valve should factor the following design constraints:

1. Be biocompatible
2. Be hemocompatible; i.e. non-thrombogenic
3. Have no obstruction to flow i.e. have minimal transvalvular pressure gradient
4. Minimal leakage and para- or peri- regurgitant flow
5. Minimal valve opening and closure times
6. Minimal shear stress to blood
7. Be technically feasible to implant
8. Be durable to prevent structural changes with time
9. Have an acceptable shelf life after sterilization

Additionally, percutaneous heart valves for TAVI should also have:

10. No obstruction to the coronary ostia
11. No stent migration
12. Minimal damage to leaflets in a collapsed state
13. Feasibility in mounting onto a catheter
14. Ability to be crimped down to a reduced profile
15. A stent with a radial force greater than that of the aortic wall

The design considerations for a polymeric aortic valve are symbiotic; for example the degree of leaflet flexion will depend on the material extensibility, leaflet thickness and curvature, leaflet-stent interface and stent flexibility. Similarly, the effective orifice area will depend on the degree of leaflet curvature and flexion and the shape in the unloaded state. These features will be discussed in more detail in the following sections.

5.2 THE DIMENSIONS OF THE NATIVE AORTIC VALVE

A comprehensive understanding of the anatomy of the aortic valve is essential when developing a heart valve. For example, it is imperative to design a flexible valve which mimics the native tri-leaflet shape as steering away from this structure has been shown to lead to complications like those described with congenital bicuspid valves in Chapter 1. Additionally, the distance of the free edges of the leaflets in a tri-leaflet valve total to approximate the circumference of a circle. A two- or four-leaflet valve would have total edges that are either less than or greater than the valve circumference, creating leaflets with large strains or excessive buckling (Thubrikar 1990).

The gross structure of the aortic valve has already been discussed in Chapter 1, and it is well known that the dimensions of the valve alter throughout the cardiac cycle. Thubrikar et al. (1981) studied the aortic dimensions of dogs in vivo during mid-diastole and highlighted 4 fundamental design parameters; the radius of the base R_b , radius of the commissures R_c , free edge angle ϕ , and leaflet base angle α (Figure 5.1). These parameters are interdependent and changing one dimension will affect the valve's functionality. For example, the ratio of R_b to R_c was determined to be 1.2, suggesting a slight tilt of the leaflets towards the ventricles. A reduced $R_b : R_c$ ratio of 1.0 would result in a tall valve; conversely a greater ratio would create a valve with commissures that projected far into the bloodstream. The height of the commissures, H_s , also needs to be factored in; if H_s is 0, then the valve would have to be very tall in order to coapt. If it is too large, then the valve would have incomplete coaptation (Thubrikar 1990).

During the cardiac cycle, the base of the leaflets due to the LVOT is at a maximum during diastole and decreases by 9-22% in systole. Similarly, the commissures expand outwardly by 12% during systole and are smallest in diastole. Therefore during diastole, the decrease in pressure in the aorta causes the angle of the leaflets to the commissures, ϕ to be at its maximum and the angle of the leaflets to the base to be at its minimum. In systole, the radius of the commissures increases; decreasing ϕ

and increasing α so that the leaflets move outwards. This creates a cylindrical flow conduit which maximises the flow (Thubrikar 1990).

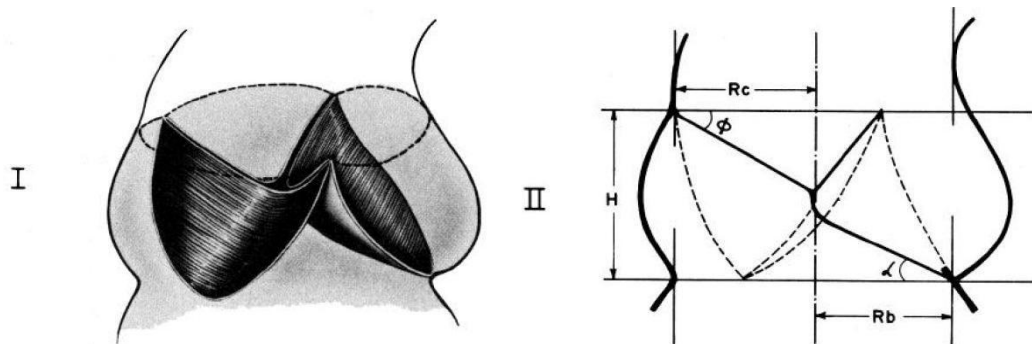


Figure 5.1 - The aortic valve (I) schematic and (II) valve parameters; H – height, R_b – Radius of base, R_c – radius of commissures, ϕ – angle from free edge to plane of commissures, α – angle of base of leaflets to a plane through the commissures (Thubrikar et al. 1981).

Swanson and Clark (1974) studied the dimensions of human aortic valves from silicone rubber casts which were formed at pressures varying from 20-120 mmHg. Thubrikar et al. (1981) compared their findings on dogs with those reported by Swanson and Clark and found little difference between the ratios of parameters in different species. This finding demonstrates that the aortic valve has similar characteristics irrespective of species and, from a design point of view argues for the use of bioprosthetic xenografts in humans.

5.3 LEAFLET GEOMETRY

5.3.1 Polymeric Valve Geometries

The leaflets of the native valve are only curved in the circumferential direction and not the radial direction, meaning that they have a cylindrical rather than spherical curvature. This enables a reversal of curvature with less stress than would be needed with a spherical surface. However, the leaflet geometry of polymeric valves has been

described over the years as cylindrical, spherical, hyperbolic, elliptical, or a superposition of wave functions. Additionally, their configuration in the unloaded state has varied from open to semi-open to a fully closed position to optimise leaflet opening, coaptation, minimise stresses or thrombolytic propensity. A valve manufactured in an open cylindrical configuration would have an opening angle of 0° which, although would create a large orifice area, would lead to incomplete coaptation due to an insufficient leaflet surface area. Therefore if the valve were to be developed in an open configuration, the opening angle β would need to be greater than zero. Most polymeric valve designs have been developed in a semi-open or closed position. This reduces the orifice area but produces a valve with minimal stresses during diastole than if the leaflets were designed in an open configuration.

Some polymeric valve designs are shown in Figure 5.2, having semi-open or fully closed leaflets as their natural unloaded states. Other valves are shown with gaps in the commissural region to prevent flow stagnation points which can lead to thrombosis. Cai et al. (2003) claimed that the leaflets of the valve should be developed in an intermediate position to increase the lumen area to 50-80% of the fully open lumen. The ADIAM aortic valve was developed in a semi-open configuration, with leaflets that are flat in the radial plane and a stent that was fairly flexible. This created a valve with an almost circular opening, minimised leaflet buckling and the flexibility of the stents enabled coaptation (Daebritz et al. 2004). Aortech have patented a polymeric valve (US8216631) with leaflets formed in a semi-open configuration that can be either symmetric or asymmetric about the flow axis (O'Connor et al. 2012). The asymmetrical design concept was believed to enable a curve with a greater radius than is possible with a symmetric leaflet to be developed which can reduce the energy required to open the valve. Additionally, they believed that asymmetry produces a helical flow profile which is similar to that of the native flow through the aorta.

Leaflet curvature has often been defined using mathematical shapes or by imposing one wave over another. Mohammadi and Mequanint (2011) developed a polymeric leaflet formed by a Bezier curve which helped define the leaflet-stent interface more

accurately since the boundaries of the stent could be taken into account. Leat and Fisher (1994) developed a synthetic polymer valve which was defined as an alpha-parabola; having a parabolic radial and spherical circumferential curvature so that the radius of the curve in the circumferential direction increased from the edge of the leaflets to the base. The valve displayed better hemodynamics than both a spherical valve and a bioprosthetic valve. Wheatley et al. (1998) developed a valve with a truncated spherical surface near the free edge joined tangentially to a truncated conical surface near the base. A valve defined as hyperbolic in the circumferential direction and elliptical in the radial direction has shown excellent durability, surviving 527 million cycles (Mackay et al. 1996).

The impact that leaflet geometry has on valve performance is evident. Innovia LLC (Miami, FL) developed a polymeric valve using poly(styrene-block-isobutylene-block-styrene) (SIBS) reinforced with Dacron (Yin et al. 2005). The authors modified the valve by increasing the stent profile and changing from a spherical to a cylindrical leaflet structure (Claiborne et al. 2011). This produced a drop in transvalvular pressure gradient from 42.85 to 25.73 mmHg, a drop in mean regurgitant fraction from 7.34% to 1.01% and an increase in EOA from 0.8 to 1.09 cm². In another comparative study, Lim et al. (2004) looked at the stresses in flat leaflets with those in three dimensional leaflets in solid models of the aortic root. The study assumed linear isotropic mechanical properties for pericardial leaflets and the aortic root, and found a reduction in stress at the commissures in the curved leaflets compared to the flat which was attributed to a greater leaflet length and coaptation area. A leaflet which is flat circumferentially would have a short free edge length that would need to endure greater strains to coapt compared to a leaflet that is curved.

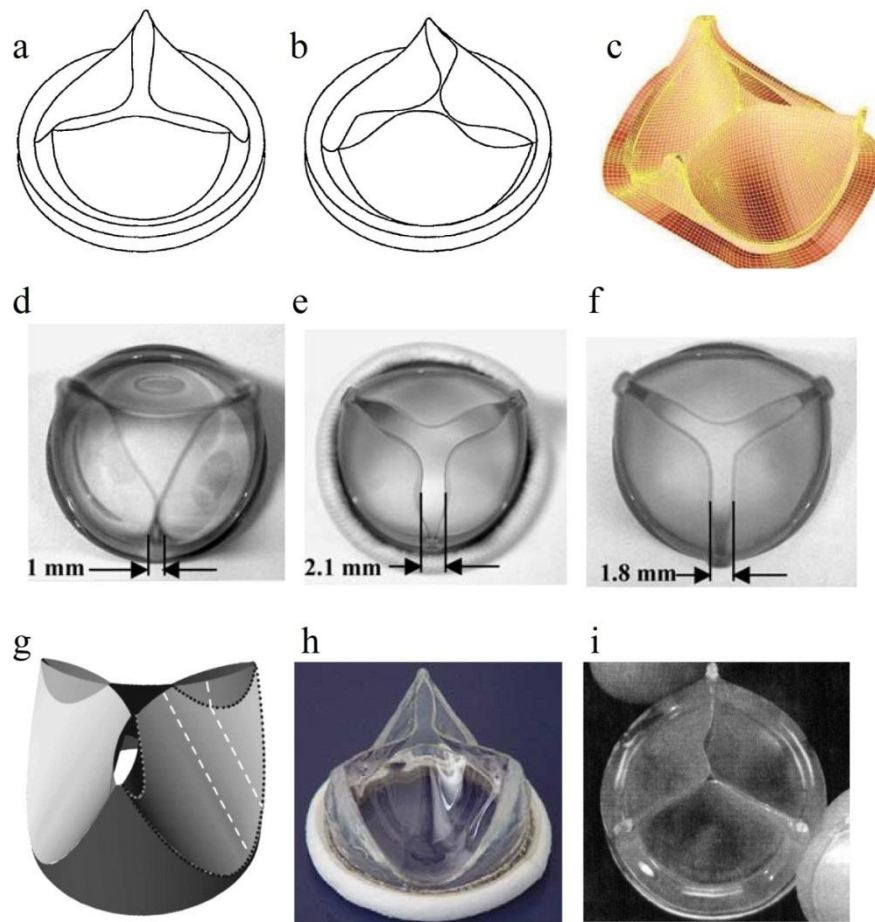


Figure 5.2 - Various design concepts; (a) symmetric and (b) asymmetric valve design by Aortech in a semi-open positions, (c) Bezier surface valve by Mohammadi et al. (2011), (d)-(f) different commissural opening; closed, open and semi-open with flat leaflets, (g) Burrisci valve with open coaptation regions and a flat surface, (h) ADIAM valve mid open position and (i) Mackay valve.

5.3.2 The Valve Design

The fabrication of the polymeric tri-leaflet valves developed in this thesis was achieved by dip-coating a stent mounted onto a 22 mm diameter highly polished stainless steel former. This former is similar to the one developed by Mackay et al. (1996) which had three scalloped surfaces at the top which came together at an angle of 120° to create the valve leaflets (Figure 5.3a). The curvature of the scallops was defined by an ellipse in the radial direction (along the direction of the blood flow) and by a continuous series of hyperbolae in the circumferential direction. Three fins,

having a thickness of 0.4 mm formed the commissures, enabling a fully closed valve design.

A hyperbola is defined by:

$$\left(\frac{x-h}{H_{major}}\right)^2 - \left(\frac{y-k}{H_{minor}}\right)^2 = 1$$

Where; h is the x axis off-set, k is the y-axis offset and H_{major} and H_{minor} are the major and minor axis of the hyperbola. The Mackay former has an x-axis offset H_o and no y-axis offset. Thus the equation becomes:

$$\left(\frac{x-H_o}{H_{major}}\right)^2 - \left(\frac{y}{H_{minor}}\right)^2 = 1$$

The ellipse in the radial direction is defined by:

$$\left(\frac{x-E_o}{E_{major}}\right)^2 + \left(\frac{z}{E_{minor}}\right)^2 = 1$$

Where E_{major} and E_{minor} are the major and minor axis of the ellipse and E_o is the ellipse x-axis off-set. H_{major} spans from the mid-leaflet ellipse to the x-axis off-set so it increases continuously from the free edge to the leaflet base (Mackay et al. 1996):

$$H_{major} = E_o - \left(E_{major} \left(1 - \frac{z}{E_{minor}}\right)^2\right)^{\frac{1}{2}} - H_o$$

For a 22.4 mm inner diameter valve, these parameters are defined as:

$$E_{major} = 22.032 \text{ mm}$$

$$E_{minor} = 15.574 \text{ mm}$$

$$E_o = 22.332 \text{ mm}$$

$$H_o = 0.23 \text{ mm}$$

Thus at the base of the leaflets, the mid-line of the ellipse would have a co-ordinate of $x = 11.2 \text{ mm}$, $y = 0$ and $z = 0 \text{ mm}$. The free edge at the mid line of the ellipse would lie on the co-ordinates $x = 0.23 \text{ mm}$, $y = 0$, $z = 13.279 \text{ mm}$.

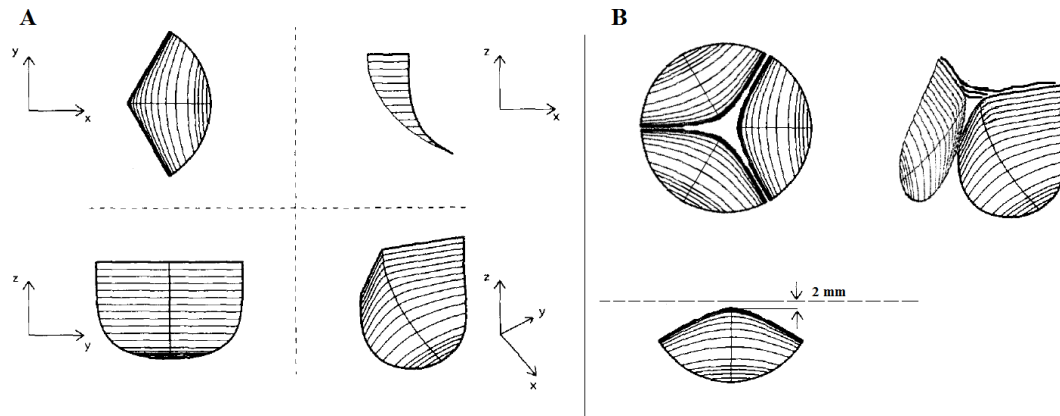


Figure 5.3 - Leaflet design (a) Hyperbolic in the circumferential direction and elliptical in the radial direction (Mackay et al. 1996). (b) Major axis of hyperbole increased.

H_{major} was increased to provide a 2 mm gap between the radial axis and the mid region of the free edges when closed (Figure 5.3b). This allowed a smoother leaflet curvature and reduced leaflet buckling when the valve was open. The top of the former which forms the free edges was extruded 10 mm along the z axis to allow the polymer to run down during the dipping procedure when inverted and be trimmed off when dry so that thin free edges were achievable. A photograph of the former is shown in Figure 5.4.

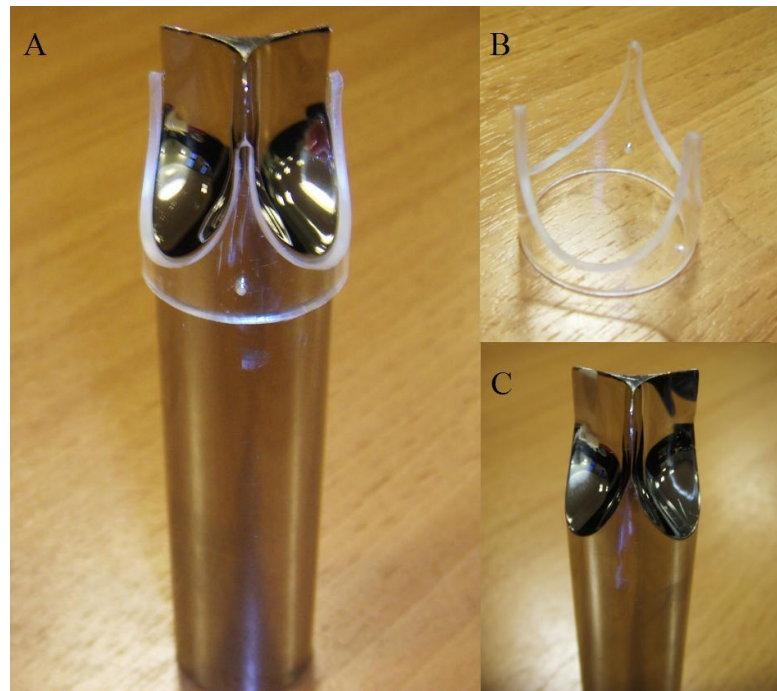


Figure 5.4 - Photograph of (a) the assembled stent and former used and separate photographs of the (b) polycarbonate stent and (c) stainless steel former.

5.4 MATERIAL CONSIDERATIONS

The material properties of the polymeric valve play a major role in the hemodynamic and durability performances of the valve. The valve needs to handle pressures as high as 100 mmHg during diastole and be able to transmit the load from the central portion of the leaflet to the aortic wall (Thubrikar 1990). Over the years, silicone, Teflon, Dacron, PVA and polyurethane have all been considered candidates for heart valve leaflet material. However thermoplastic polyurethane (TPU) has been found to have superior mechanical properties compared to most polymers, due to its soft and hard segmented nature. Early polyurethanes had polyester and polyether soft segments which were prone to hydrolysis and oxidation. The use of polycarbonate urethanes and other modifications to the soft segment has enabled increased hydrolytic and oxidative resistance.

The following sections focus on some of the material aspects that should be considered when designing a polymeric heart valve.

5.4.1 Mechanical Properties

A low stiffness polymer would have high flexibility but would endure high strains and creep at low stresses. Conversely, a polymer with a higher stiffness would endure higher stresses at low strains but may not have adequate flexibility which would compromise the hydrodynamic properties of the valve. The governing rule for elastic materials is Hooke's law which describes the linearity between the stress applied to a material and the resultant strain when subjected to a uniaxial force. The ratio of stress, σ to strain, ϵ is known as the Young's Modulus (or stiffness):

$$\text{Young's Modulus, } E = \frac{\sigma}{\epsilon}$$

Where

$$\sigma = \frac{\text{Force, } F}{\text{Cross-sectional area, } A}$$

And,

$$\epsilon = \frac{\text{Change in length, } \Delta l}{\text{Original length, } l}$$

In a fully viscous material, the shear stress, τ is directly proportional to the rate of deformation, $\dot{\gamma}$:

$$\tau = \mu \frac{d\gamma}{dt} = \mu \dot{\gamma}$$

Where, μ is a constant known as the viscosity of the material.

Viscoelastic materials such as tissues and thermoplastic polyurethanes have mechanical properties that include both viscous and elastic components and are therefore time, temperature and strain rate dependant (Crawford 1998). Therefore body temperature at 37 °C will influence the hydrodynamic performance of the

polymer in comparison to its behaviour at room temperature. Two phenomena specific to viscoelastic materials are creep and stress relaxation. In creep (Figure 5.5), a material subjected to a fixed load continues to strain and can lead to permanent plastic deformation prior to failure. Leaflets of the aortic native valve have been found to not creep (Sacks et al. 2009). However, polymeric materials all exhibit creep which may be detrimental to leaflets in diastole when they are exposed to high loads for a period of time. In stress relaxation (Figure 5.6), the stress in a material subjected to a fixed strain continues to decrease, initially rapidly and then progressively. This enables a material to cope well under the strains it is subjected to during diastole.

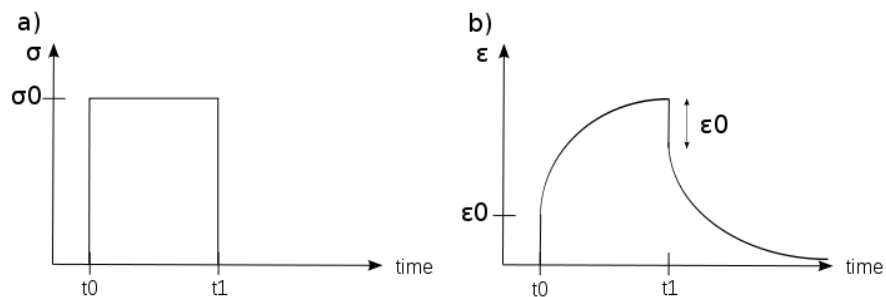


Figure 5.5 - Creep properties (a) constant stress applied between t_0 and t_1 and (b) strain response.

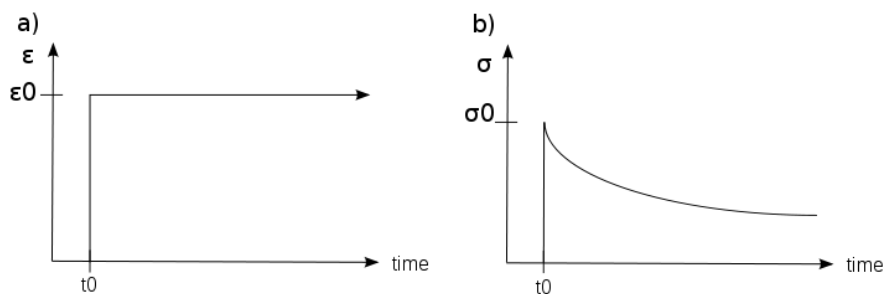


Figure 5.6 - Stress relaxation properties (a) constant strain applied at t_0 for a length of time and (b) stress response.

Determining the stiffness of polyurethanes is not as straightforward as with elastic materials mainly due to the time dependency and environmental factors which affect the elastic modulus measured. Unlike tissues such as the native leaflets which

increase in stiffness following increased strain due to collagen fibre unfolding and alignment, the stiffness of TPU decreases with strain. It is better to assume a ‘short term’ modulus with polyurethane, which can be used to compare against other TPUs tested under the same conditions. A ‘secant modulus’ could also be used instead, which is determined from the gradient of a straight line in a stress-strain curve at a known point (Figure 5.7). However, these values should not be used as absolute unless they have been repeatedly tested in the environment in which they are set out to be in.

Viscoelastic materials generally have a higher stiffness at very high strain rates. This is due to the polymeric chains having insufficient time to rearrange themselves when strained, which causes the material to remain rigid. Temperature has an opposite effect; an increase in temperature allows the chains to slide past each other easily which reduces the stiffness.

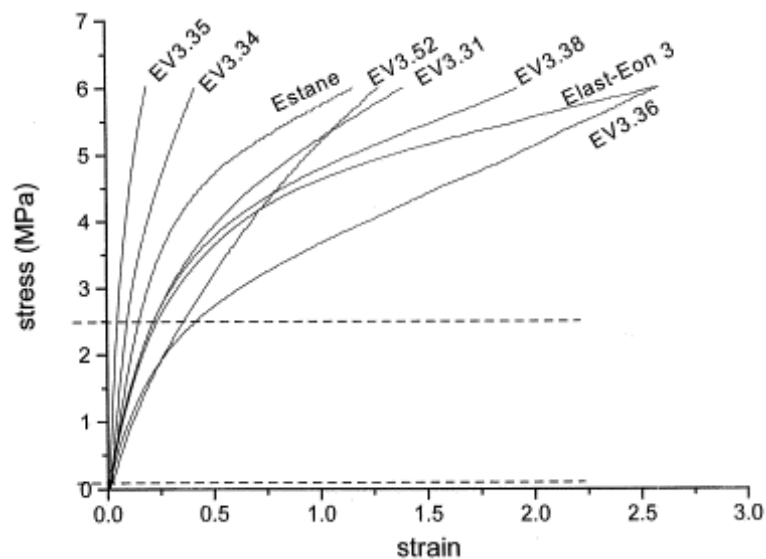


Figure 5.7 - The stress-strain relationship of several polyurethane elastomers (Bernacca et al. 2002).

Dynamic mechanical analysis (DMA) is often used to characterise viscoelastic materials. During DMA testing, the material is cycled at altering temperatures or frequencies and the stress and the corresponding strain are plotted. Due to the viscous component of the material, a phase lag is observed between the applied

sinusoidal stress and the corresponding strain. This phase lag, ϕ is used to determine the storage and loss modulus of the material which corresponds to the elastic and viscous components respectively.

If the strain applied is:

$$\varepsilon = \varepsilon_0 \sin(t\omega)$$

Then the corresponding stress would be:

$$\sigma = \sigma_0 \sin(t\omega + \phi)$$

The storage modulus, E' is calculated as:

$$E' = \frac{\sigma_0}{\varepsilon_0} \cos\phi$$

And the loss modulus is:

$$E'' = \frac{\sigma_0}{\varepsilon_0} \sin\phi$$

Due to the phase lag, the storage modulus calculated is typically less than the elastic modulus. From altering the frequency of the cycles or the temperature, a curve can be obtained which can be used to determine the glass transition temperature, T_g of materials. This value is useful in characterizing whether a material is crystalline or amorphous at room or body temperature which has a significant impact on its mechanical behaviour.

5.4.2 Leaflet Thickness

In a study by Bernacca et al. (2002), the hydrodynamic properties of the valve were found to be significantly correlated with the thickness of the leaflets, more so than the stiffness of the leaflets. Only when the polymeric leaflets had a high stiffness of 63.6 MPa, was a large pressure gradient apparent. The thickness variation along the

leaflets is also a major determining factor of the hydrodynamic properties. The free edge of the leaflets need to be sufficiently stiff to enable coaptation but flexible enough to allow the valve to open rapidly. A thick belly region would likely require a higher force to open the valves due to its reduction in flexure. A thinner belly region would flex easily but would increase the risk of rupture due to its reduced tear strength.

It is not necessary to achieve an even thickness across the leaflet since the native leaflets themselves have an uneven thickness distribution. Barsanti (1998) compared the stresses in a model of an even thickness leaflet and an uneven one and found an uneven thickness to provide a greater leaflet deflection, reduced principal stresses and a 25% reduction in the obstruction to the flow. This was attributed to the uneven leaflet having a thinner belly region compared to the thickness of the uniform leaflet. This may imply that a thinner uniform leaflet would therefore create a better performing valve than an uneven or a thick uniform leaflet. However, durability can be compromised with very thin leaflets in which case an uneven but relatively thin leaflet would be the best solution. This gives dip coating an advantage since leaflets are likely to be created with an uneven thickness. However, variation in thickness should have a smooth transition since large differences are likely to cause stress concentrations or weak points leading to tears.

One of the main objectives of this thesis is to develop a reinforced ultra-thin leaflet to minimize the size of the delivery catheter. The minimum cross sectional area taken up by the leaflets equates to the product of the leaflet perimeter and the leaflet thickness. A model was developed by Li and Sun (2010) to estimate the size of the leaflets in relation to the delivery catheter (Figure 5.8). Therefore, assuming the thickness of the stent, guide wire and balloon remain unchanged; the diameter of the catheter can be estimated from the leaflet thickness. A leaflet thickness of 200 μm would require a minimum catheter size of 18 Fr. Conversely, in order to reduce the catheter dimensions to 15 Fr, the leaflets need to be 100 μm thick at most (Figure 5.9).

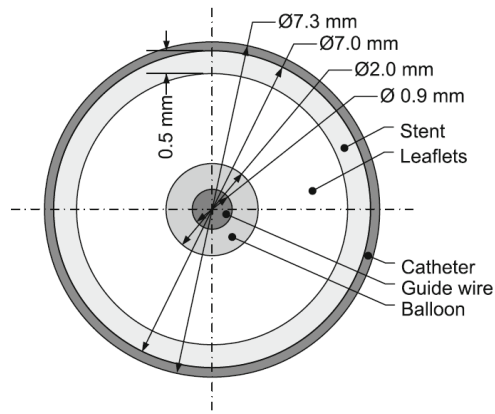


Figure 5.8 - Cross sectional view of a crimped percutaneous valve and catheter assembly (Li and Sun 2010).

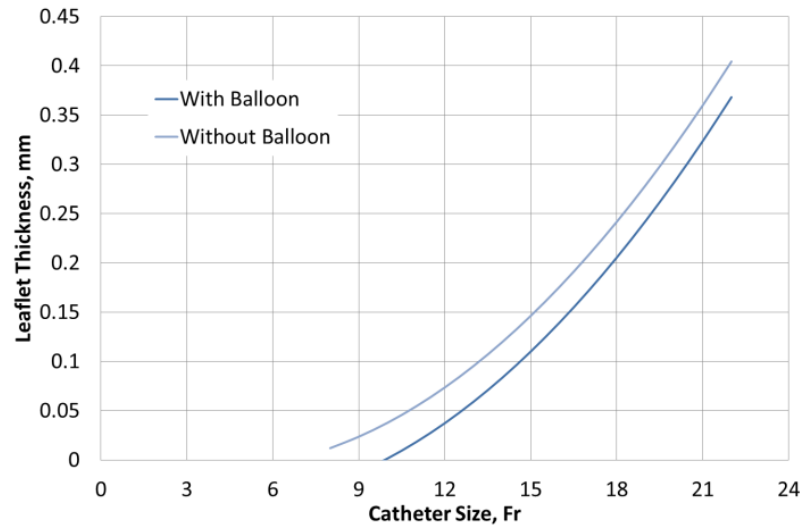


Figure 5.9 - Minimum catheter size needed in relation to thickness of valve leaflet with and without a balloon expandable stent based on the model by Li and Sun (2010).

5.4.3 Fibre Composite Valves

The idea of reinforcing a polymer valve with a fibre or particle stems from the idea that collagen fibres of the natural valve help to reduce its stresses. However the geometry of the valve, the leaflet material and composite material, composite size and shape and composite-matrix interface all affect the overall reduction in stress. From previous failures, it has been evident that the commissural region is most

susceptible to high stresses and models of reinforced heart valves have shown evidence of stress reduction in those areas.

De Hart et al. (1998) modelled a rubber valve with 10 or 20 fibres running circumferentially or sinusoidally between the aortic and ventricular layers. They found the greatest homogenous stress distribution to be achieved when 20 sinusoidal fibres were used. A stress reduction of up to 60% was achieved on the aortic side with the uni-direction fibres arranged circumferentially compared to the unreinforced valve. Liu et al. (2007) modelled the Quartomer polymeric leaflet with 25 μm polypropylene fibres running along the geodesic lines at various angles. Single ply fibres were found to reduce the principal stresses by as much as 64% whereas a reduction of more than 86% was achieved through double ply fibres. These optimal values were achieved when fibres ran almost perpendicularly to the stent edge at 30° in the single ply and at an angle of 45° in the double ply (which crossed at 90° to each other).

In this study, polyurethane will be reinforced with carbon nanotubes to improve its mechanical properties. Carbon nanotubes are rolled up sheets of graphene having single or multi-layer walls. They have diameters in the nanometer range and micrometer lengths, giving them very high aspect ratios which can improve fibre-matrix interface. Additionally, their mechanical stiffness has been measured to be as high as 1 TPa which is much greater than that of polyurethane which usually has a modulus of less than 100 MPa. The properties of polymer-nanotube composites are discussed in more depth in Chapter 6.

5.4.4 Leaflet Manufacturing

The advantage that polymeric heart valves have over bioprosthetic and mechanical heart valves is that they have more variety in manufacturing options. Common techniques include dip coating (Jansen et al. 1992, Mackay et al. 1996), injection moulding (Mackay et al. 1996), compression moulding, vacuum forming and solvent casting (Gallocher et al. 2007). Other novel methods include electrospinning in tissue

engineered scaffolds (Del Gaudio et al. 2008, Chen et al. 2009) and droplet deposition (Daebritz et al. 2004). Material processing plays a crucial role in valve performance since the material stiffness, leaflet thickness and stent-leaflet adhesion are all influenced by the manufacturing process. Pellets of polyurethane can be dissolved in a solvent to produce a solution which can be poured over a desired surface and the solvent evaporated to leave behind a polymeric film. Polymeric solutions are handy in dip coating, solvent casting and electrospinning processes.

Dip coating is achieved with a mandrel or former having an end which replicates the contact areas of the ventricular side of the valve to which a stent is fitted over. Mackay (1992) experimented with rotation of the mandrel whilst drying but found the polymer to run into the stent, forming a thicker leaflet at the stent-leaflet interface. An even thickness is difficult to achieve with a dip coated valve; the leaflet will be thicker at either the base or the free edges depending on whether the mandrel is positioned in an upright or inverted position respectively. In injection moulding, pellets of polymer are melted as they are injected into a cavity which forms the shape of the valve and stent. The benefit of this method is that the leaflets can be formed with a uniform thickness and repeatability. However, small cavities can be difficult to fill completely with viscous solutions and gaps or bubbles may arise. Electrospinning forms woven fibres with nano- to micrometer diameters which would be suitable for the formation of biodegradable scaffolds in tissue engineered heart valves. However their porosity does not make them ideal for polymeric heart valves.

Leat and Fisher (1995) examined the properties of dip coated and thermal formed polymeric heart valves and found that whilst hydrodynamic function was slightly different for both valves, the dip coated valves had superior durability. This is likely due to the dip coated valves having a continuous leaflet-stent interface whereas the thermally formed valves suffered leaflet debonding. Additionally, whilst the latter valves had a slightly better effective orifice area, they also had higher leakage due to the gaps at the commissures. These findings support dip coating as a suitable manufacturing process to provide functional and durable polymeric valves.

5.4.5 Leaflet Calcification and Thrombosis

Both the choice of polymer and the geometry of the valve affect calcification and thrombosis. Calcification has been a common cause of failure in polyurethane heart valves causing leaflet stiffening, thrombi formation and tears. Polymer surface and chemistry can influence the degree and rate of calcification. Polymers that do not have a high degree of biostability are prone to degradation which allows for extrinsic calcification (Wheatley et al. 2000). The calcific nodules appear to occur in high stress regions although the course of the mechanism is still relatively unclear. Some speculate that tears in polyurethane create sites for calcium ions to bind to, although the tears may have also occurred from a weakening due to a build-up of calcium on the leaflets. Another theory based on a calcification study of polymeric jellyfish valves suggested that polymer membrane stretching with time create microgaps which are soon filled with calcium and eventually phosphorous ions (Imachi et al. 2001).

Calcification is likely to be influenced by the polymers degree of hydrophobicity and studies on surface modification have been found to reduce calcification. A study by Park et al. (2001) found polyurethane to exhibit less calcification than PTFE and silicone, which they attributed to the smoother surface of the TPU. Calcium permeation was found to decrease when biophosphonate was covalently bound to polyurethane (Joshi et al. 1994). Dabagh et al. (2005) found calcification to decrease in polyurethane grafted with silicone, which increased its surface hydrophobicity, although platelet activation did not change. A nanocomposite polymeric material developed by a team at University College London, was found to have a more hydrophobic surface and lower levels of calcification compared to a control TPU and bovine pericardium (Ghanbari et al. 2010).

Mechanical valves are long known to be thrombogenic and one benefit of polymeric valves is that thrombogenicity may be low enough to not require anticoagulation. Wheatley et al. (2000) compared their polyurethane dip moulded valves with a bioprosthesis and a mechanical valve implanted in the mitral position of sheep. They

found a comparable detection of high intensity transient signals (HITs) from microemboli with the bioprosthetic valve and a lower count than the mechanical valve. The Innovia polymer valve was also found to have similar thrombogenicity to bioprosthetic valves. Following design changes, the platelet activation rate was found to be significantly less than that for the Carpenter Edwards bioprosthetic valve (Claiborne et al. 2011).

5.5 CHAPTER SUMMARY

The principles of valve design can be separated into two aspects; material considerations and valve geometry:

1. Material considerations include optimising stiffness, stress relaxation and creep to enable a leaflet to be stiff enough to withstand high loading deformations during diastole whilst maintaining good flexibility to prevent obstruction to flow and enable full coaptation.
2. The choice of polymer will not only influence the material properties, but also the tendency for calcification and platelet formation. It is believed a more hydrophobic surface is ideal to improve valve biostability and durability.
3. Valve geometry includes optimising leaflet curvature to increase flexibility and prevent obstruction to flow whilst enabling full coaptation. Additionally, there needs to be a good interface between the stent and leaflet material to enable stress transfer and prevent deflection of the stent posts due to the high stresses at the commissures.
4. An uneven leaflet thickness is believed to improve flexibility and reduce stresses which can be achieved through dip-coating.

5. Nano-reinforcement of leaflets is envisaged to produce ultra-thin leaflets without compromising their mechanical integrity.

CHAPTER 6:

POLYMERIC VALVE COMPOSITES

6 POLYMERIC VALVE COMPOSITES

6.1 REINFORCEMENT OF HEART VALVES

A composite is a material formed from two or more materials; usually consisting of a discontinuous phase known as the reinforcement embedded in a continuous phase known as the matrix (Migliaresi 2013). Often the matrix is of a softer material and the reinforcement is significantly stiffer, consisting of particles or fibres. For example, the extracellular matrix in the native heart valve is reinforced with collagen and elastin fibres. The main purpose of reinforcement is to transfer the stress from the matrix material to the stiffer reinforcing component to reduce the overall stress in the leaflet. Additionally, fibre reinforcement can prevent crack propagation along the matrix when it encounters the stiffer fibre. The resultant composite depends on many factors including the fibre or particle aspect ratio, matrix-reinforcement interface, concentration and fibre orientation. It is essential to get the interface right: a poor interface can result in a composite material with weaker properties than the matrix alone. This is due to the reinforcement fillers acting as defects rather than transferring the load from the matrix to the filler. Additionally, a poor bond could result in fibre pull-out from the matrix leading to premature failure.

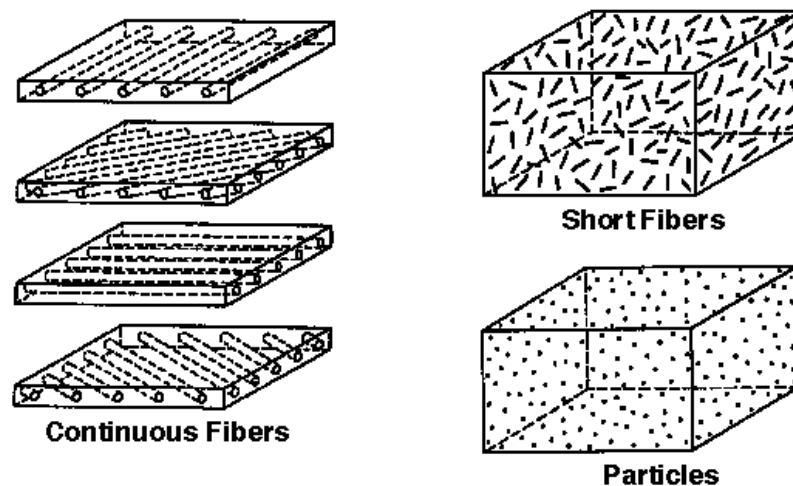


Figure 6.1 - Types of composite reinforcements (Mathworld)

The aspect ratio of fibres is the ratio of their length to their diameter. Thus long continuous fibres are considered to have larger aspect ratios than short discontinuous fibres. Nanotubes are discontinuous fibres with diameters that are significantly smaller than their lengths, giving them very high aspect ratios. It is worth noting that as we approach nanoscale reinforcement and as the aspect ratio increases, it is more difficult to predict the material properties (Migliaresi 2013). This is due to the increased attraction between the fibres which makes it difficult to separate into individual fibres in the matrix.

Two other groups have previously developed reinforced polymeric heart valves using macroscopic fibres which run along the entire surface of the leaflet. Cacciola (1998) developed a fibre reinforced stented and stentless heart valve using ethylene propylene-diene-monomer rubber matrix (EPDM) reinforced with high-performance polyethylene (HP-PE) fibres (Figure 6.2a-c). The matrix had an elastic modulus of 1.5 MPa and the fibres had a diameter of 0.06 mm and an elastic modulus of 30 GPa arranged in both uni- and sinusoidal directions. Opening times took approximately 22-38% of the cardiac cycle time which the author attributed to the delay of the third leaflet from opening since the other two leaflets opened in a lesser time. However, even the opening of the first two leaflets appeared to be slightly delayed (~60 ms), perhaps due to the leaflets being too stiff. Valves remain open for longer than usual and shut for a shorter duration compared to a tissue stented valve. Additionally, regurgitation was reportedly high particularly in the stentless valve, possibly due to the valve being manufactured in the open configuration.

Gallocher (2007) attempted several methods of reinforcement; initially aligning polypropylene (PP) fibres circumferentially in a SIBS polymeric matrix. The reinforcing material was replaced with a LARS mesh (Figure 6.2d) to provide repeatable valve design which was found to enable transfer of the maximum curvature between the basal region and the free edge during motion. During accelerated fatigue testing, polymer blowout was observed in the leaflet with the LARS mesh due to the inability of the unreinforced regions to support the high load. The mesh was then replaced with a Dacron fabric (Figure 6.2e) which was aligned so

that the long axis was parallel to the circumferential direction. However, holes were formed due to the high stresses the leaflet had experienced in the circumferential direction. Finally changes to the design lead to the development of the Innovia valve which had a SIBS polymer matrix reinforced with a high density Dacron fabric (Claiborne 2011).

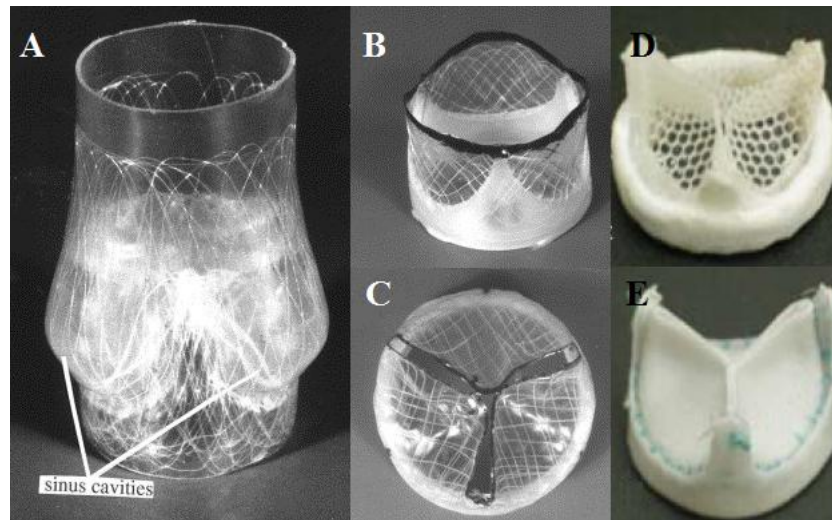


Figure 6.2 - Reinforced polymeric heart valves; (a) stentless reinforced valve, (b) side and (c) top view of a stented reinforced valve, (d) LARS mesh reinforced and (e) Dacron reinforced valve.

The use of carbon nanotube reinforcement in heart valve leaflets has never been reported. The advantages with carbon nanotube reinforcement (as compared with larger, macroscopic fibres such as illustrated above) are that they have a low density and nanometre dimensions, enabling thin leaflets to be developed without compromising flexibility. Additionally, they can be mixed into a polymeric solution for random alignment so the need for manual and arduous fibre placement is eliminated. The following sections discuss the properties of carbon nanotubes and composite development in further detail.

6.2 INTRODUCTION TO POLYURETHANE ELASTOMERS

Thermoplastic polyurethane elastomers (TPU) are a class of polymers with hard crystalline segments (HS) and soft elastomeric segments (SS). They have been extensively used in medical applications due to their excellent mechanical properties as well as relatively good biostability (Gunatillake et al. 2000, Ghanbari et al. 2009). The hard segments have a glass temperature, T_g above ambient temperatures and are formed by the reaction of a diisocyanate such as 4,4'-methylene diphenyl diisocyanate (MDI) with a short chain extender such as 1,4-butanediol (BDO). The soft segments have a T_g below ambient temperature and are formed by the reaction of the diisocyanate with a higher molecular weight polyol (Ghanbari et al. 2009). This polyol tends to be ester, ether or carbonate based. The two segments are joined end to end through covalent bonding of urethane linkages (Crawford et al. 1998).

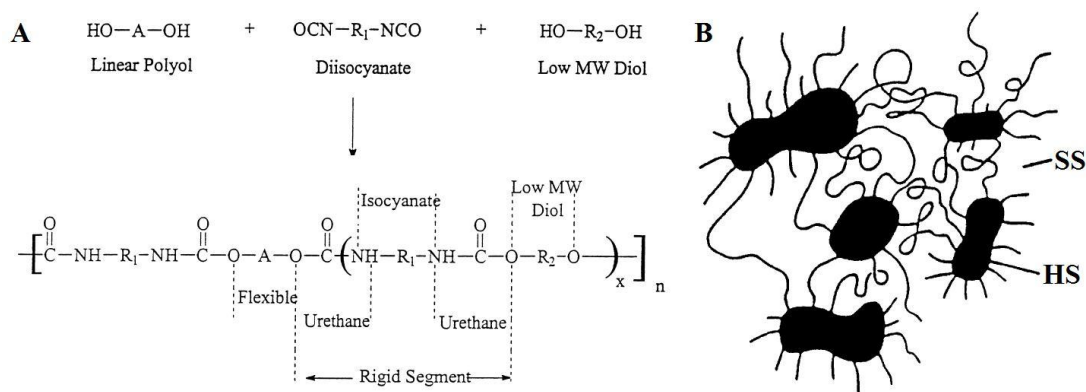


Figure 6.3 - (a) Formation of a polyurethane segment and (b) schematic of the segmented structure. SS – soft segment. HS – hard segment. Adapted from Crawford et al. (1998).

The thermodynamic incompatibility between the HS and SS components leads to a phase separation; the greater the distance between the hard segments, the larger the phase separation. The degree of phase separation and the ratio of hard to soft segments affect the hardness of the polyurethane. One method of determining the hardness is by a Shore durometer which measures the indentation caused to the

material relative to a scale. The most common durometer scales are the ASTM D2240 (or ISO 7619) Shore A and D scales; Shore A is used for softer plastics and Shore D is for harder plastics.

An increase in hard segments will lead to an increase in hardness and stiffness of the polymer although this increase is not linearly related. For example, Pellethane 2363 80A and 55D have very different mechanical properties; 55D is significantly stiffer and more biostable although the former only has 11% more polyether macrodiol (Taylor et al. 2006). Martin et al. (1999) suggested a HS composition threshold of 52 wt% above which a transition from discrete to interconnecting hard segments occurs. They also proposed that the interconnecting hard segments may reduce the stress exposed to the softer segments and prevent oxidative matter from passing through the polymer.

Production of TPUs can be a one-pot procedure which is industrially more economical and efficient or by the production of a pre-polymer reaction with the chain extender. It can be aromatic or aliphatic depending on the structure of the isocyanate. Polymers with MDI or TDI (toluene diisocyanate) tend to be aromatic whereas polymers with isocyanates such as HDI (hexamethylene diisocyanate) are aliphatic. Aromatic TPUs have been found to generally have better mechanical properties and resistance to biodegradation than aliphatic polymers. However, they are also prone to yellowing when exposed to sunlight, although this feature is cosmetic and does not affect the physical properties of the material (Pinchuk 1994).

The first TPUs had polyester soft segments but were found to be prone to hydrolysis following long-term implantation. The more porous the surface, the faster the polymer degrades due to hydrolysis (Pinchuk 1994). Polyether polyurethanes (PEU) replaced the polyester soft segment of TPUs with a polyether macrodiol such as polytetramethylene oxide (PTMO), which had improved biostability compared to PEU. However, they were also prone to in vivo oxidative degradation. A newer class of polyurethanes are polycarbonate urethanes (PCU) which were suggested to have better resistance to hydrolysis and oxidative degradation than PEUs (Chen et al.

2007). In a comparative study by (Christenson et al. 2004), PCUs were found to have a higher elastic modulus compared to PEU. This was attributed to the PCU having a better phase separation of the hard and soft segments than the PEU despite both polymers having a shore hardness of 80A. However, the study also found chemical and physical degradation of PCU to not be significantly different to the PEU polymer.

In 2000, a biomaterial was developed which combined the biostable silicone with the biocompatible polyurethane (Gunatillake et al. 2000, Martin et al. 2000, Simmons et al. 2004, Smart et al. 2006). The soft segment of the TPU consisted of poly(hexamethylene oxide) (PHMO) and poly(dimethylsiloxane) (PDMS) macrodiols in a ratio of 20:80. The incorporation of silicone, which has excellent biostability, into polyurethane has been found to increase its oxidative stability. The polymer is now marketed by AorTech International under a family of polymers known as Elast-EonTM and has been used in polymeric heart valves as well as other long term implantation products and as coatings for medical devices such as pacing wires. Another biostable polymer was a nanocomposite developed by a research team at University College London (UCL) consisting of poly(carbonate) urethane and polyhedral oligomeric silsesquioxane (POSS) nanoparticles. This polymer was found to exhibit excellent mechanical properties, biostability and non-thrombogenicity compared to neat PCU and its in vivo performance is currently being tested (Kidane et al. 2009).

Polyurethane behaves as a viscoelastic material due to the varying soft and hard segments and exhibits different mechanical properties depending on strain rate. In this present study, preliminary work was conducted on a PEU known as Estane® which exhibited tackiness making film casting difficult. An attempt to reduce the stickiness by the addition of a filler had little significant effect. Consequently further testing was carried out with two different grades of Carbothane®, a PCU by the Lubrizol Corporation (Ohio, USA) and Elast-EonTM. This is discussed further in Chapter 7.

6.3 STRUCTURE OF NANOTUBES

Graphite and diamond have long been known to be allotropes of carbon. In recent years, other allotropes of carbon having nanometer dimensions and superior mechanical properties have been discovered. Sir Harold Kroto and Richard Smalley (Kroto et al. 1985) accidentally discovered a ‘football’ like polygonal structure consisting of 60 carbon atoms with 12 pentagonal and 20 hexagonal faces (Kroto et al. 1985). The structure was named the C₆₀ buckminsterfullerene after the geodesic dome architect R. Buckminster Fuller (Thostenson et al. 2001). Fullerenes are defined as any geometric cage-like molecule consisting of pentagons and hexagons of carbon (Vaisman et al. 2006). Spherical structures are known as ‘buckyballs’ and cylindrical structures are known as ‘nanotubes’. Carbon nanotubes have also been dated back to the 17th century when they were discovered on the surface of ancient Damascus steel blades (Reibold et al. 2006). However, it wasn’t until they were reported by Iijima in 1991 that interest in carbon nanotubes rapidly increased.

Iijima (1991) observed graphitic carbon needles ranging from 4 to 30 nm in diameter and up to 1 μm in length growing on an electrode during an arc-discharge evaporation of carbon. The needles observed consisted of rolled up layers of graphene sheets ranging from 2 to about 50 layers were known as multi-walled nanotubes (MWNT). Less than 2 years later, the synthesis of single-walled nanotubes (SWNT) was reported (Iijima and Ichihashi 1993). In addition to single- and multi-wall, nanotubes can also be double walled (DWNT) or have buckyballs attached to their surfaces. The arrangement of the carbon atoms on its wall determines whether the nanotube has an “armchair”, “zig-zag” or helical structure. The ‘chirality’ of the nanotubes determines whether they are semi-conducting or metallic. The chiral vector, \vec{C}_h defines the tube chirality by:

$$\vec{C}_h = n\vec{a}_1 + m\vec{a}_2$$

Where the integers n and m are the number of steps along the ‘zig-zag’ bonds of the hexagonal lattice and \vec{a}_1 and \vec{a}_2 are unit vectors’. If $2n+m=3q$ where q is an integer, then the nanotube is metallic, in all other cases the nanotube is semi-conducting (Figure 6.5).

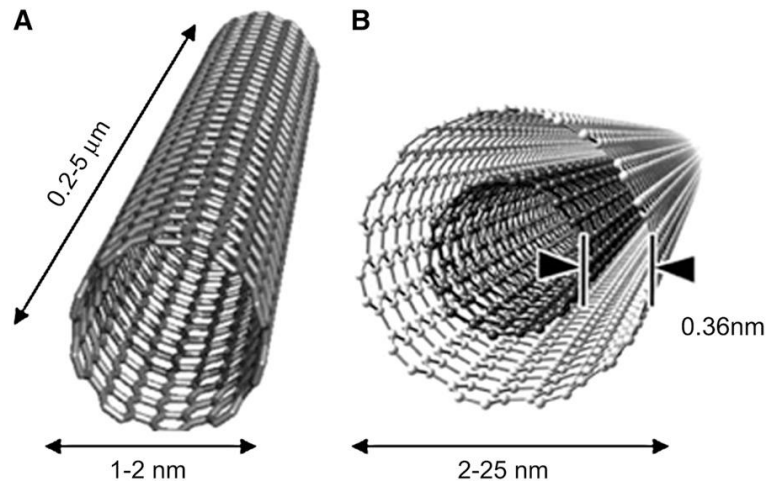


Figure 6.4 - Conceptual diagrams of (a) single and (b) multi-walled carbon nanotubes and their typical dimensions (Reilly 2007).

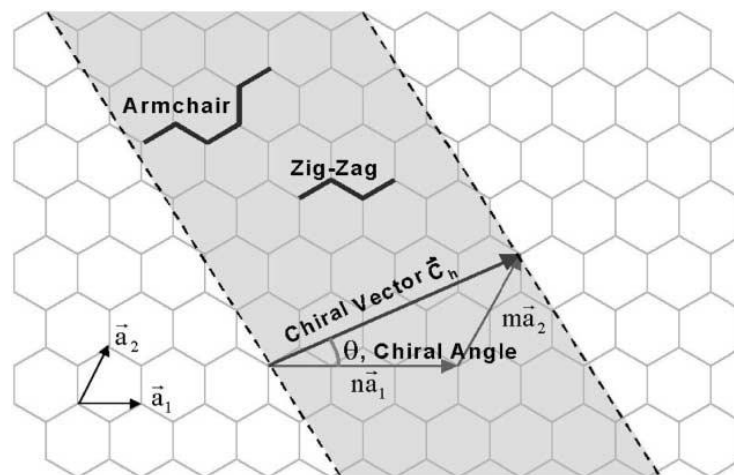


Figure 6.5 - Schematic of the hexagonal lattice of the nanotube (Thostenson et al. 2001).

Carbon nanotubes can be produced through a wide range of processes. Commercially, the two most common types are the arc-discharge method and the chemical vapour discharge (CVD) method. The arc-discharge method involves

applying a DC current to two graphite electrodes in the presence of an inert gas at very high temperatures. Carbon soot containing CNTs are deposited onto the cathode. Adding a metal catalyst onto the graphite rod enables SWNTs to be produced (Khare and Bose 2005). The arc-discharge method produces a higher quality of CNT's but the quantity is low and hence the process is expensive.

CVD on the other hand is inexpensive to run and thus can be used to commercially produce large quantities of the nanotubes. It involves incorporating hydrocarbon gas, such as acetylene, ethylene or methane with a process gas such as ammonia, nitrogen or hydrogen. A substrate with metal catalyst particles enables nanotube growth and their final size is determined by the size of the particles. However, the nanotubes tend to have greater structural defects which compromise their mechanical integrity. A large amount of nanoparticles and open shells are also produced which would need to be filtered out to obtain a purified sample of nanotubes. The purification of nanotubes is discussed in further detail in Section 6.5.

CNTs could be ideal fillers for polyurethane heart valves since they wouldn't compromise leaflet flexibility due to their nanoscale dimensions. Additionally, they can be incorporated into polymeric solutions, which is useful in the dip coating process. Some of the properties of CNTs are discussed in the following section.

6.4 PROPERTIES OF NANOTUBES

6.4.1 Mechanical Properties

Graphite is known to have an in-plane modulus of approximately 1 TPa (Yu et al. 2000, Coleman et al. 2006, Spitalsky et al. 2010). For this reason, carbon nanotubes have been predicted to have extremely high tensile strengths despite their high flexibility, low mass density and large aspect ratios (Moniruzzaman and Winey 2006, Spitalsky et al. 2010). Following these predictions, several methods were used to determine the tensile modulus of CNT's including mathematical modelling,

transmission electron microscopy (TEM) and atomic force microscopy (AFM). Yu et al. (2000) carried out a tensile test on MWNT's using scanning electron microscopy (SEM). The ends of the nanotubes were attached to the tips of AFM cantilever probes which acted as force sensors by imaging their deflection. They reported a Young's modulus of 0.27 to 0.95 TPa and as high as 12% for the percentage strain at failure. The mechanical properties of SWNTs are more difficult to obtain predominantly due to the attractive van der Waal forces between the tubes causing them to cluster. Yu et al. (2000) measured the mechanical properties of single-walled nanotubes using a similar method to the MWNT's. However, as individual SWNTs are difficult to isolate, they tested the free ends of the nanotubes in an SWNT rope. They found the strength of the SWNTs to range from 13 to 52 GPa and the elastic modulus to range from 320 to 1470 GPa.

There has been a vastly increasing interest in using the high strengths of CNTs to reinforce materials since they have superior mechanical properties and higher aspect ratios compared to conventional fillers such as carbon nanofibres, silica and clay. CNTs have been incorporated into metals for the reinforcement of vehicles and in the aviation and space industry. Their discovery has even enabled the concept of a space elevator to be considered possible due to their high strength to density ratio (Pugno 2013). More commonly, CNTs have found favour as reinforcing fillers in polymers to improve their mechanical integrity without compromising their flexibility. They also overcome problems faced with conventional fillers. For example, carbon nanofibres would have been too large to incorporate into the plastic for processing by injection moulding, whereas CNT's would be small enough. Additionally, larger fibres would compromise the flexibility of the leaflets which would increase the valve opening and closing times.

6.4.2 Electrical and Thermal Conductivity

Due to the nanoscale diameters of nanotubes, electrons and phonons can propagate along the nanotube length without scattering (Baughman et al. 2002). This 'ballistic transport' of electrons in nanotubes enables them to have an electrical conductivity

that is several times that of copper with minimal heat. Nanotubes are also thermally conductive and have even been used in the development of a cloaking device by creating a steep thermal gradient to reflect light off a surface of an object (Campbell 2011). These properties are beyond the scope of this thesis, and will not be covered in further detail. However it is worth noting that the thermal conductivity of nanotubes should increase the glass transition temperature and the crystallinity of the polymer composite (Xie et al. 2005), making them favourable properties when exposed to body temperature.

6.4.3 Biocompatibility

Based on Williams' definition, the term 'biocompatibility' is used to mean 'the ability of a material to perform with an appropriate host response in a specific application' (Williams 1999). Carbon has long been used in biomaterials; Pyrolytic carbon is the ideal material of choice in mechanical heart valves and diamond-like carbon (DLC) has been used in stent coatings. These carbon biomaterials as well as others have demonstrated good stability and no immunological response in the biological environment (Smart et al. 2006). A quantitative assessment on CNT toxicology is difficult to determine due to their variable morphology and their tendency to form clusters. Agglomerates would increase the surface contact area, which increases the capacity for toxicological substances to be absorbed and transported (Smart et al. 2006). Consequently, the toxicity of CNTs in its powder form has received mixed responses in literature.

Several toxicology studies on the effect of inhaling or instilling CNTs in rats have demonstrated pulmonary inflammation and oxidative stress (Lam et al. 2004, Shvedova et al. 2008). More recently however, Kagan et al. (2010) discovered that short cut nanotubes biodegraded with time when incubated with human myeloperoxidase (hMPO) and hydrogen peroxide (H₂O₂). They reported no sign of tissue granulomas when the biodegraded nanotubes were aspirated into the lungs of mice. Additionally, there have been several promising cellular studies with CNT composites, particularly in bone matrix where osteoblast adhesion was seen to

increase and in neural cells (Smart et al. 2006). In a study by Webster et al. (2004), the adhesion of osteoblasts (bone forming cells) and neural cells were seen to increase with increasing nanotube loading on a poly(carbonate urethane) matrix. Additionally they observed a decrease in adhesion of fibroblasts and astrocytes, which are undesirable cells responsible for scar-tissue around bone and neural implants respectively.

Several papers have also noted an improvement in blood - nanotube composite interactions. Meng et al. (2005) looked at the effect that MWNTs would have on platelet interactions with polyurethane. In their study, they observed that the morphology of the platelets on PU alone had a spread, fully spread or non-viable state compared with the PU/MWNT composites which had dendritic platelets, indicating lower levels of activity (Figure 6.6). In a later study by the same authors, electrospun MWNT/PU composites were found to vastly increase cell proliferation of fibroblasts compared to control tests of pure PU and smooth composite films (Meng et al. 2009). They also found cell migration to be more profound when smooth PU films were placed alongside the woven composite. Good results have also been seen with bovine aortic endothelial cells which attached well to chitosan-CNT composite films (Takahashi et al. 2009). The authors also noted that platelet adhesion and activation were inhibited at larger concentrations of CNT.

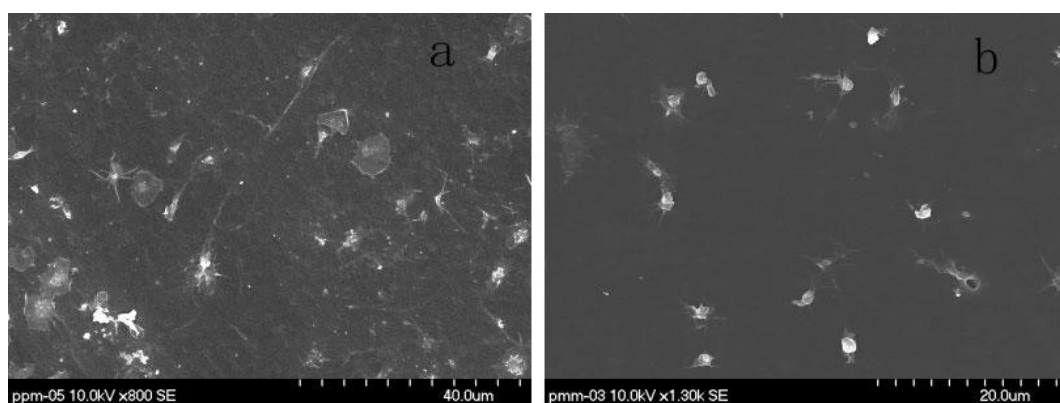


Figure 6.6 - SEM images of platelets adhered on (a) PU or (b) MWNT-PU surface (Meng et al. 2005).

In this work, CNTs are treated as toxic in their powdered forms and therefore only handled wearing full laboratory gear (gloves, goggles, lab coat), as well as a dust mask to prevent inhalation. Work is also carried out inside a fume hood, with the air switched off temporarily to prevent the low density nanotubes from blowing away. Once the nanotubes are incorporated into the polymer matrix, the risk of toxicity is vastly reduced since the nanotubes would be encapsulated within the polymer, making inhalation difficult and creating a barrier from skin irritation. In the following chapter, the effect of gamma sterilization on the mechanical properties of nanotube composite samples will be investigated.

6.5 PURIFICATION OF NANOTUBES

The impurities left in the crude mixture of nanotubes depend on the synthesis method used. Carbon nanotubes produced by CVD method leave carbonaceous products such as amorphous, polyhedral and aromatic carbons and metal impurities. SWNTs produced by the arc-discharge or laser ablation method leave metallic particles enclosed in carbonaceous products (Hou et al. 2008). Several papers have reported methods of purifying the samples of carbon nanotubes from the remaining carbon soot including chemical and oxidative treatments, filtration and centrifugation. As the impurities depend on the synthesis of the nanotubes, the purification procedures reported in literature is widely variable. Purification steps can involve chemical oxidation, physical techniques or a combination of both.

Chemically treating the crude mixture with acid has been shown to be effective in dissolving the metallic impurities but can be destructive to the nanotube structure which can compromise its mechanical and electrical properties. Physical methods such as filtration are less destructive but cannot remove the metallic particles. Bonard et al. (1997) developed an effective and non-destructive method of purifying MWNTs produced by the arc-discharge method. They began by centrifuging the crude mixture to allow large particles to sediment and then filtering the decanted

mixture to separate the nanotubes from the liquid. The final mixture had a yield as high as 90% without damaging the structure of the MWNTs.

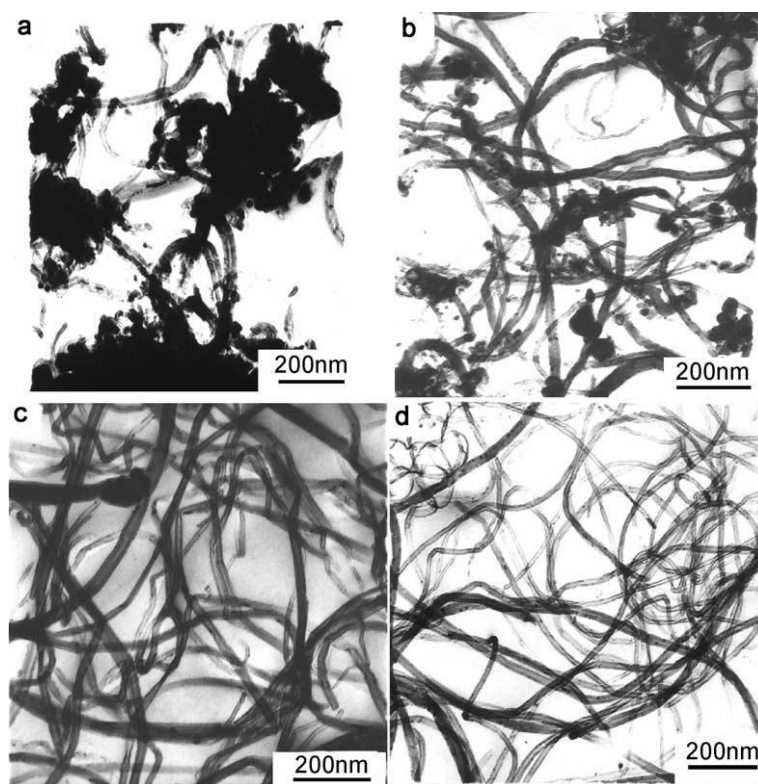


Figure 6.7 - TEM images of: (a) as-produced crude materials, (b) material that was refluxed for 24 h in 3 M HNO₃, (c) material produced by treating the HNO₃-treated sample in 5 M HCl for 6 h, (d) purified MWNTs produced by oxidizing the acid-treated sample for 60 min in air at 510 °C (Chen et al. 2002).

Carbon nanotubes synthesized by methods other than the arc-discharge method produce metallic catalysts which could be removed through acidic treatment (Hou et al. 2008). Acids such as nitric acid, sulphuric acid and hydrochloric acid are commonly employed to dissolve metallic particles and oxides in as-synthesized carbon nanotubes. However, acidic treatments create defects within the carbon framework which compromise their mechanical, electrical and thermal properties. Acidic treatments also create excessive amorphous carbon due to the shortening of the nanotubes. The carbonaceous compounds would need to be removed by thermal oxidation under an oxidizing atmosphere such as air, which is most commonly used

or under a mixture of oxidants. Carbon nanotubes are more resistant to oxidation than graphite and amorphous carbon due to the sp^2 hybridization bond in the carbon atoms (Chen et al. 2002). The oxidative resistance to the carbon impurities can also be reduced by introducing intercalated atoms within the graphitic structure, creating reactive sites due to the structural defects (Hou et al. 2008).

The reactivity of fullerenes and nanotubes to addition reactions strongly depends on the curvature of their carbon ‘framework’ (Chen et al. 2003). A higher degree of curvature, would mean a greater strain on the bonds which would increase its reactivity (Rosca et al. 2005). Therefore smaller diameter nanotubes would respond to oxidation at a faster rate than larger nanotubes. A simple non-destructive method for purifying MWNT’s produced by CVD was reported by Chen et al. (2002), the results of which are shown in Figure 6.7. Initially the crude mixture of MWNT’s were heated in nitric acid for 24 hours and then heated at a higher temperature in hydrochloric acid. The mixture was finally left to cinerate in air at 510°C; beyond this temperature the weight dropped significantly, indicating destruction of the nanotubes. This method produced MWNT samples with a purity of 96% and was adopted in this thesis’ work, details of which are mentioned in the next chapter.

6.6 POLYMER NANOTUBE COMPOSITES

6.6.1 Dispersion Techniques in Polymer

Progress with nanotube composites has been mainly hindered by their inability to be adequately dispersed within the composite matrix. The properties of the nano-composite material depends on the dispersion quality, the final aspect ratio after treatment and the integrity of the CNT/matrix interface (Vaisman et al. 2006). Nanotubes, in particular SWNT’s as they have a larger aspect ratio, have a large tendency to aggregate into bundles due to the high attractive van der Waal forces between the walls. Various techniques have been adopted to homogenously disperse the nanotubes. The main ones can be divided into mechanical or chemical methods.

6.6.1.1 Mechanical Dispersion

Ultrasonication has been a popular and effective method used to disperse the nanotubes. An ultrasonic probe at 40 Hz or bath at 25 Hz produces micro-bubbles in the nanotube/solvent solution which when collapse create a vacuum space dispersing the particles. It is vital to determine an optimal sonication period to provide adequate dispersion. Prolonged sonication has been found to open the end caps and shorten the nanotubes which would reduce their aspect ratio. The solvent choice is important as it influences the solubility of the nanotube and the period that the nanotube remains dispersed following mechanical mixing. For example, Foster et al. (2005) found that nanotube/polymer suspensions in toluene and chloroform showed sedimentation of SWNTs after a few minutes whereas tetrahydrofuran (THF) and 1-methyl-2-pyrrolidinone (NMP) had nanotube stability lasting several months. In another study, PDMS was found to have a high affinity to nanotubes (Barber et al. 2004); this would suggest that Elast-Eon™ (which has a PDMS soft segment) should have a high affinity to nanotubes.

Re-agglomeration can also happen during the polymer curing period due to the attractive van der Waal forces. One way to avoid this could be to increase the viscosity of the solution by evaporating the solvent at a high rate. Another method could be to cure the composite below the T_g in order to ‘freeze’ the nanotubes (Ciselli 2007). However, polyurethane and the solvent it is dissolved in are hygroscopic and humidity would affect their film formation; this requires curing the composite at a high temperature to evaporate any water present in the solvent. Therefore the former technique would be more feasible to implement by curing at high temperatures to increase the viscosity and evaporate any absorbed water from the composite.

6.6.1.2 Chemical Functionalization

Nanotubes can be covalently or non-covalently functionalized to enhance their wettability within the polymer matrix. Non-covalent treatment involves polymer adhesion and wrapping or the use of surfactants. The benefits of non-covalent treatment are that the π -bonding remains unaffected and the surfaces are free from structural damage. Nanotubes have been effectively dispersed in aqueous solutions with the aid of surfactants such as sodium dodecyl sulphate (SDS) and TritonTM X-100. The molecules adsorb onto the hydrophobic nanotube surface and provide a hydrophilic surface to enhance wetting in aqueous solutions. These techniques have created nanotube suspensions which remain stable over a long period of time. CNTs have been known to be soluble in some solvents such as DMAc, however in other less soluble solvents; a non-ionic surfactant can be used (Vaisman et al. 2006). Co-solvents have also been used to effectively disperse nanotubes. For example, Chen et al. (2007) used a co-solvent of trifluoroacetic acid (TFA) and dimethylformamide (DMF) to disperse MWNTs in poly(methyl methacrylate) (PMMA).

Covalent surface treatment involves the addition of surface reactants onto the nanotube structure to enhance the wettability of the nanotube with the matrix. The functional groups can be grafted to or from the nanotube surface. The acidic and oxidative treatments of CNTs following purification introduce functional groups such as carboxylic acid (COOH^-) onto the sides and endcaps of the nanotubes. These functional groups create a repulsive force between the nanotubes and enable the attachment of molecular and biological moieties (Banerjee et al. 2005).

6.6.2 Alignment of Carbon Nanotubes

Alignment can create an anisotropic structure with properties superior parallel to the fibre direction. This can be beneficial by reinforcing the leaflet along the circumferential direction to reduce the stresses at the commissures. Several methods can be used to align nanotubes including mechanical extraction, electromagnetism

and fibre spinning. An attempt was made in this study to align an Estane/MWNT composite solution through spin coating. The procedure involved adding a droplet of the composite solution onto a microscope cover slide which was then spun at two very high speeds (1000-2000 rpm). The first speed enabled a very thin film ($< 15\mu\text{m}$) to be developed and the second speed allowed evaporation of the solvent. The final film thickness depends on the viscosity of the solution, the temperature, solvent volatility, the rotation speed and time.

The high angular velocity enables nanotubes to be aligned radially as shown in Figure 6.8. This technique has advantages, namely creating an ultra-thin film with aligned nanotubes with a controllable thickness. However, bubbles were apparent in all substrates spin coated and a suction effect was noticeable, creating a ring of carbon nanotubes at the region of the vacuum chuck. Additionally, film casting polymeric valves have been known to have poor bonding to the stent which compromises their durability (Leat and Fisher 1995, Gallocher 2007). Therefore it was decided to develop dip coated valves with randomly aligned nanotubes which were likely to be more durable than valves with leaflets thermally bonded to the stent.

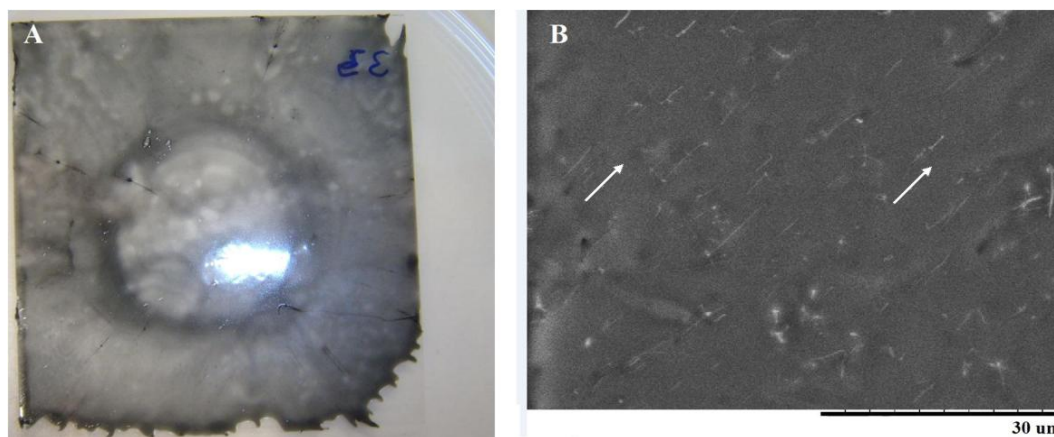


Figure 6.8 - Carbon nanotube in Estane polymer (a) spin coated on a substrate and (b) SEM photograph of aligned fibres (arrows highlighting direction of fibres).

6.6.3 Mechanical Properties

Literature on the mechanical properties of nanotube composites is contradictory and diverse since there are many variables which influence the measured property. For example, the dispersion methods used can vary. Even if an ultrasonic bath was adopted in all cases, the solvent choice, sonication time and type of nanotube would all influence the final dispersion state. Additionally, there is the difference in mechanical property testing; testing rate, sample size and temperature and room conditions would all be difficult to compare.

Generally, there is an agreement in the literature that the incorporation of nanotubes into a polymeric matrix has led to an improved elastic modulus and tensile strength. Additionally, the majority of studies reportedly find that the strain at failure decreases with increasing nanotube content. Safadi et al. (2002) determined the modulus of spin coated and cast polystyrene reinforced with up to 2.5% MWNTs and found improvement in the elastic modulus (from 1150 MPa to 3400 MPa). However no significant difference was observed in the mechanical properties of the 40 μm spin coated with aligned nanotubes and the 400 μm drop cast composite film.

In Chapter 7, the methods used to create carbon nanotube composite films using several different types of polyurethane will be discussed. The composites will be tested to determine changes to the mechanical properties with regards to nanotube concentration, water absorption, sterilization, strain rate and immersion at 37 °C.

6.6.4 Fatigue Life

The idea that nanotubes can enhance fatigue life of carbon nanotube composites has been debateable. Some authors have found improvement in the fatigue life whereas others have found the fatigue life to be compromised. Loos et al. (2012) found the durability of polyurethane reinforced with carbon nanotubes to increase in high stress amplitude, low cycle regimes. However, the durability of polyurethane was greater in

the low stress high cycle regime. Kuronuma et al. (2011) studied the crack growth resistance of MWNT reinforced thermoplastics and found the resistance to cracking to increase with the inclusion of MWNTs at room temperature but not at cryogenic temperatures due to the defects in the matrix when cooled. Thus it appears that warmer temperatures improve the fatigue properties of polymer-nanotube composites which come in favour for nanotube reinforced heart valves at 37°C.

6.7 CHAPTER SUMMARY

1. Composite leaflets can reduce the leaflet stresses and improve mechanical properties compared to neat polymeric leaflets. Particular interest lies in improving the fatigue and thermal properties of polymeric leaflets.
2. Polycarbonate urethane has been shown to have improved biostability and mechanical properties compared to polyester and polyether based urethanes.
3. Carbon nanotubes can be dispersed efficiently into a polyurethane solution through the aid of an ultrasonic bath to allow repeatable dip coated composite heart valves to be developed.
4. Carbon nanotube composites have been shown in studies to reduce platelet adhesion and promote aortic endothelial cell attachment which demonstrates good hemocompatibility.
5. The dispersion and relative volume of the nanotubes influences the mechanical characteristics of the composite.

Ideally, a polyurethane heart valve would be reinforced with carbon nanotubes that are well dispersed such that the bundles are separated into individual fibres surrounded by matrix. This would provide an effective transfer of load from the matrix to the nanotube. Additionally, the ideal composite leaflet material would

improve the fatigue life by bridging cracks that may develop in the matrix to prevent crack propagation and tears.

CHAPTER 7:

COMPOSITE MATERIALS TESTING

7 COMPOSITE MATERIALS TESTING

7.1 PREPARATION OF MATERIALS

7.1.1 Materials

Two different sized CVD synthesized multi-walled carbon nanotubes (MWNTs), one having a length to diameter aspect ratio of ~50 and the other having an aspect ratio of ~400, were obtained from Sigma-Aldrich (Dorset, UK). The former has a diameter of 110-170 nm and a length of 5-9 μm with an aspect ratio of ~50, and the latter has a diameter of 10-15 nm and a length of 0.1-10 μm with an aspect ratio of ~400. All throughout the remainder of this thesis, the MWNTs will be referred to as 'thick' and 'thin' fibres respectively.

All polyurethanes used in this work were obtained in their pellet forms. Estane[®] 5702 F2, a polyether urethane having a shore hardness of 65A was obtained from the Lubrizol Corporation (Cleveland, Ohio). Carbothane[®] PC3585A and PC3595A are clear aliphatic polycarbonate urethanes having shore hardnesses of 85A and 94A respectively also obtained from Lubrizol. Elast-Eon[™] E5-325, with a shore hardness of 82A was obtained from Aortech International Plc (Rogers, Minnesota). The solvents used to dissolve the polyurethanes were dimethylacetamide (DMAc) and tetrahydrofuran (THF) both obtained from Sigma-Aldrich (Dorset, UK).

7.1.2 Purification of Carbon Nanotubes

The raw materials had a purity of 90% and were further purified and functionalized following the three step procedure outlined by Chen et al. (2002) as it was simple and applicable to fibres synthesised by CVD. Initially the MWNTs were treated in 3M of nitric acid at 60 °C for 24 hours followed by 5M of hydrochloric acid treatment at 120 °C for 6 hours (Figure 7.1). This allowed the metallic impurities left behind from the synthesis process to dissolve. The solution was continually stirred with the aid of a magnetic stirrer. Between each step, the nanotubes were filtered

through filter paper on a funnel and rinsed in distilled water to wash away the acid. The refluxed material was then dried and weighed to determine the yield.

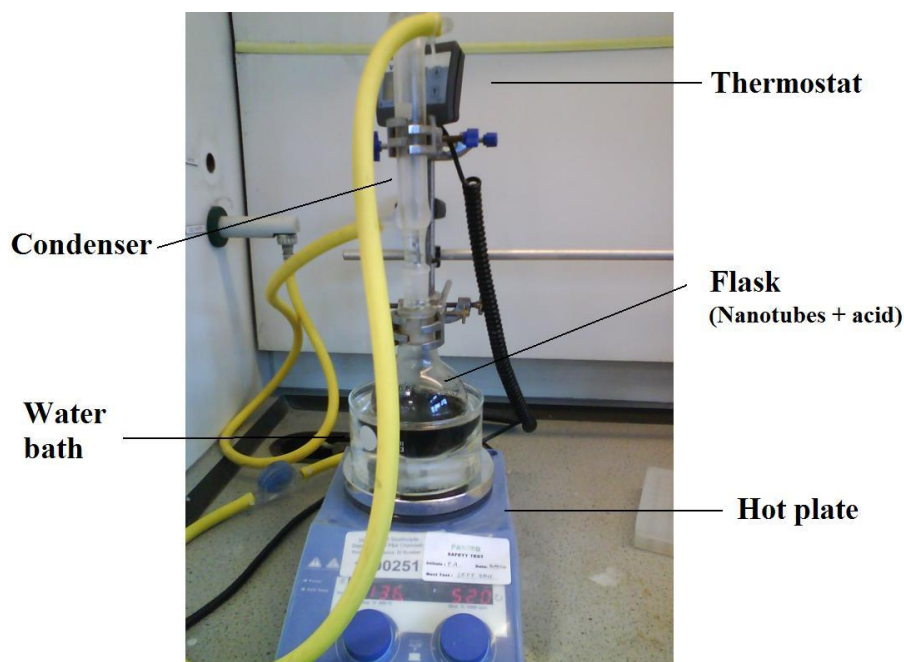


Figure 7.1 - Acid refluxing process of the carbon nanotubes

The final step was to calcine the MWNTs in static air at 510 °C for 60 minutes to allow oxidized groups such as carboxylic acid to attach onto the opened ends. Scanning electron microscopy (SEM) and Raman Spectroscopy images of the MWNT's were taken to determine any structural changes to the nanotubes following treatment.

7.2 DETERMINATION OF THE TENSILE PROPERTIES OF MWNT COMPOSITES

7.2.1 Estane[®] with Impure Thick MWNTs

Preliminary composite development was carried out with Estane and the thick MWNTs in their raw states without purification. Pellets of Estane were dissolved in THF solvent to make up 15% w/v polymeric solutions. Initial attempts to dissolve

the polymer in DMAc created solutions with cloudy precipitates that were difficult to filter out. The MWNTs were weighed in a fume hood with the air switched off to prevent the nanotubes from being blown away. From literature, low concentrations of carbon nanotubes have been shown to improve the stiffness of polymers (Qian et al. 2000, Safadi et al. 2002, Loos et al. 2012). Therefore, 1%, 2%, 3% and 4% w/w of MWNTs were added directly to the polymeric solution and dispersed for an hour in an ultrasonic bath at 37 kHz. The composite solutions were then poured into glass Petri dishes to form films with a thickness of 80-100 μm and left overnight for complete solvent evaporation. As THF is highly volatile, the dishes were covered with foil to allow an even thickness to develop prior to solvent evaporation. The dry composite films were then easily peeled off the glass with the aid of water.

Strips of the composite film measuring 3.5 x 30 mm were cut using a parallel blade cutter and sandwiched between two glass slides to obtain their mean thickness at 4 equal distances apart using a micrometer with a resolution of ± 0.001 mm. The strips were then mounted between pneumatic grips of an Instron[®] universal testing machine (Series 4500) and subjected to a tensile strain at 10 mm/min until rupture. The mechanical properties of the 3% and 4% composite were obtained after 30 mins and 1 hour of sonication to determine the effect that dispersion time has on their properties. The samples were tested to a strain of 1500% regardless of whether rupture happened to occur and the ultimate tensile stress (UTS) and strain were recorded for the samples that did rupture.

7.2.2 Carbothane[®] and Elast-Eon[™] MWNT Composites

Pellets of Carbothane and Elast-Eon were dissolved in dimethylacetamide (DMAc) solvent to make up a 15% w/v polymer solution. 1% w/w mass (to 7.5 g polymer) of thick and thin MWNTs before and after purification were added to 10 ml of DMAc solvent. The nanotubes were dispersed by sonicating in an ultrasonic bath with a frequency of 37 kHz for 1 hour. 10 ml of the polymer solution was then added to each of the nanotube/DMAc solutions to make up 7.5% w/v polymeric composite

solutions which were further sonicated until no visible clumps of the nanotubes were apparent (Figure 7.2).

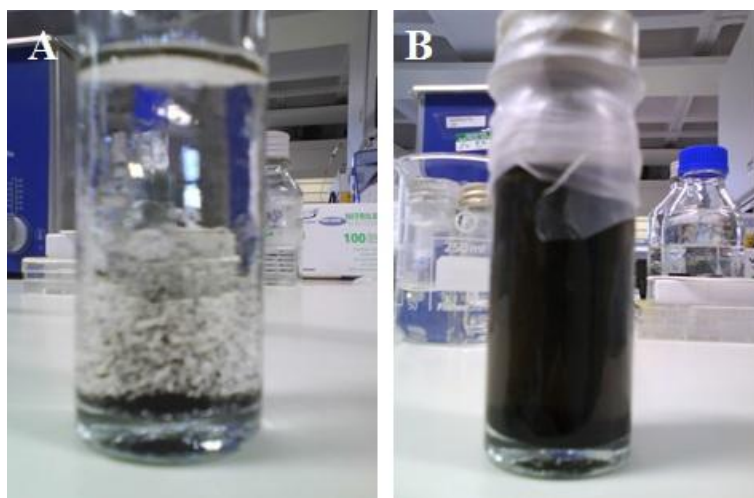


Figure 7.2 - Nanotubes dispersed in DMAc solvent (a) before and (b) after sonication

Films of MWNT/TPU having thicknesses of approximately 50 μm were formed by casting approximately 5 ml of the composite solution into 10 mm glass Petri dishes and curing on a hot plate at 50°C for an hour then left overnight in a fume hood for complete solvent evaporation. Images of the composite were also taken with an optical microscope to determine the particle size of the clusters. As the nanotubes were embedded beneath the surface of the polymer, SEM imaging of the nanotubes within the composites was not possible.

Strips measuring 3.5 mm x 30 mm were cut from the cast films using a parallel blade cutter. In all the following mechanical tests, tensile testing was conducted using the Bose EnduraTech Electroforce (ELF) 3200 universal tester (Bose Corporation, Framingham, USA) with either a 22 N load cell or a 1000 g load cell. A gauge length of 11 mm was set. This value was solely selected to remain consistent with an initial set-up which had been used in preliminary test results. A gauge length of 10 mm would have been just as sufficient. The following tests were performed:

1. *Stiffness and Stress Relaxation* - the crosshead was displaced at a rate of 1 mm/sec to 5 mm and held at that displacement for 30 seconds whilst the stress was recorded.
2. *Creep* - the stress of the samples was held after a 3 mm extension and the displacement of the crosshead was measured for 30 seconds. This is known as a displacement controlled creep test. A load controlled test, which would have been ideal, was difficult to set up since the system was unable to settle on a fixed load.
3. *Tear Testing* - a cutter was developed to allow trouser specimens to be prepared for tear testing. A leg of the sample was attached to the top grip and the other leg to the bottom grip and the extensometer was displaced at a rate of 50 mm/min until the sample tore. If the tear force was uniform along the test, the average tear force was taken, otherwise if the tear force increased with increasing displacement, the maximum tear force was taken.

7.2.3 Carbothane PC3595A with Thick Impure MWNTs

From the preliminary data, presented later on in this chapter, Carbothane PC3595A appeared to have the best tensile properties with the thick impure MWNTs. Further testing was therefore conducted with this composite (referred to as 95A-MWNT) to determine the influence that certain conditions have on its tensile properties. For the dip coating process, (discussed in Chapter 8) 0.125%, 0.25%, 0.5%, and 1.0% 95A-MWNT solutions were prepared in larger diameter bottles without initially diluting in DMAc solvent. Approximately 5 ml of the solutions were cast into glass Petri dishes to form films having an average thickness of 40 μm . In the following tests, the samples were preconditioned between 0 and 1 mm for 10 cycles at 1 Hz prior to determining the stiffness and stress relaxation as described before.

7.2.3.1 Effect of Sonication Times on Dispersion

Both the change in rheological properties and the bottle size would affect the efficiency of ultrasonic dispersion. The ideal dispersion rate was determined from the tensile properties of 0.5% and 1.0% 95A-MWNT composites after 1, 2, 2.5, 5 and 7 hours of dispersion in an ultrasonic bath at 37 Hz with the temperature of the water raised to 50 °C to reduce the solution viscosity. The samples were also cycled between 0 and 0.5 mm at 20 Hz to determine the storage modulus.

7.2.3.2 Immersion in Distilled Water

Strips of 0% and 1% 95A-MWNT composites were left in water over several months to determine the influence that water absorption (if any) would have on the thickness and stiffness of the composites. The samples were contained in distilled water which was filtered through with a 0.45 µm PDVF membrane filter under a laminar flow hood and kept at room temperature. They were taken from the water and tested intermittently for 9 months, dried on a paper towel and left at 23 ± 1 °C for a few minutes prior to testing. The thickness of the samples was measured prior to each test and the stiffness and stress-relaxation properties were determined as previously detailed in Section 7.2.2. The water was changed after every test to reduce the risk of sample contamination.

7.2.3.3 Effect of Temperature on Composites

A water bath was set up on the ELF tester (Figure 7.3) to allow 0%, 0.5% and 1.0% composites to be tensile tested at 37°C. The samples were mounted as before, this time using a 250 g submersible load cell. The neat polymeric samples had difficulty being mounted due to their transparency which made them difficult to observe when immersed. Therefore not many samples of the neat polymer were tested.

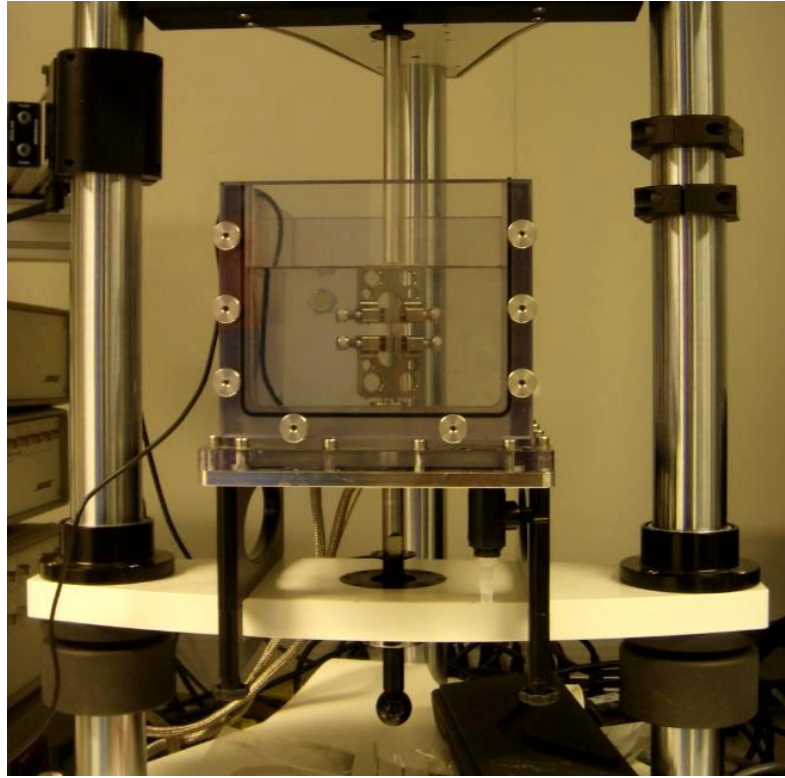


Figure 7.3 - Water bath testing on BOSE ELF system.

7.2.3.4 Tension – Tension Fatigue

Composite strips that had been used in the previous mechanical tests were subjected to cyclic tensile strains to determine their comparable fatigue life. The strips were cycled between 0% and 70% at a frequency of 20 Hz until failure. Failure was defined as the number of cycles taken for complete rupture of the polymer. Whilst the crosshead of the ELF tester can achieve frequencies of up to 200 Hz, it was decided to keep the frequency low to avoid overheating the polymer. The room temperature was maintained at 23 ± 1 °C to reduce influence of temperature on sample failure.



Figure 7.4 - Fatigue testing polymer samples between grips of the Bose ELF Tester.

7.2.3.5 Strain Rate Dependence

It was suggested that higher nanotube concentrations could lead to difficulty providing an effective dispersion. Therefore 0.125% and 0.25% were developed alongside 0.5% and 1.0% 95A-MWNTs. Strips of these composites were tested at strain rates of 1, 2, 5 and 10 mm/sec to 45% strain and stress relaxed. The 1 mm/sec was used as a control and derived from old testing data whereas the other strain rates were applied consecutively by loading the sample and returning the crosshead to its default position before loading the next strain rate. It was hypothesized that there would be an increase in stiffness with increasing strain rate as the chains would not have time to slide over each other.

7.2.3.6 Effect of Gamma Sterilization

Although medical grade polyurethanes are suitable for sterilization, there can be changes to the physical and mechanical properties which depend on the dosage and sterilization method used. It would be desirable to determine if the incorporation of

MWNTs has any effect on the mechanical properties following sterilization. 0% and 1% composite strips were paired and divided as a control and sterilized batch. The sterilized batch were subjected to a gamma radiation dose of 32.5 kGy and their tensile properties were determined at 2 days, 2 weeks and 6 weeks post sterilization.

7.2.3.7 Effect of Crimping

As percutaneous leaflets are subjected to crimping, it is desirable to know the influence that these creases may have to the mechanical properties of the composites. Strips of 0%, 0.5% and 1% 95A-MWNTs were prepared in pairs and divided into control and crimped specimens. The crimped samples were folded in half twice to create three folds in the material and a 1 kg load was left on these samples overnight. The samples were then unfolded and loaded to tension to determine their elastic modulus. Care was taken to ensure the mid fold was placed midway between the grips of the tester.

7.3 RESULTS

7.3.1 SEM and Raman Imaging

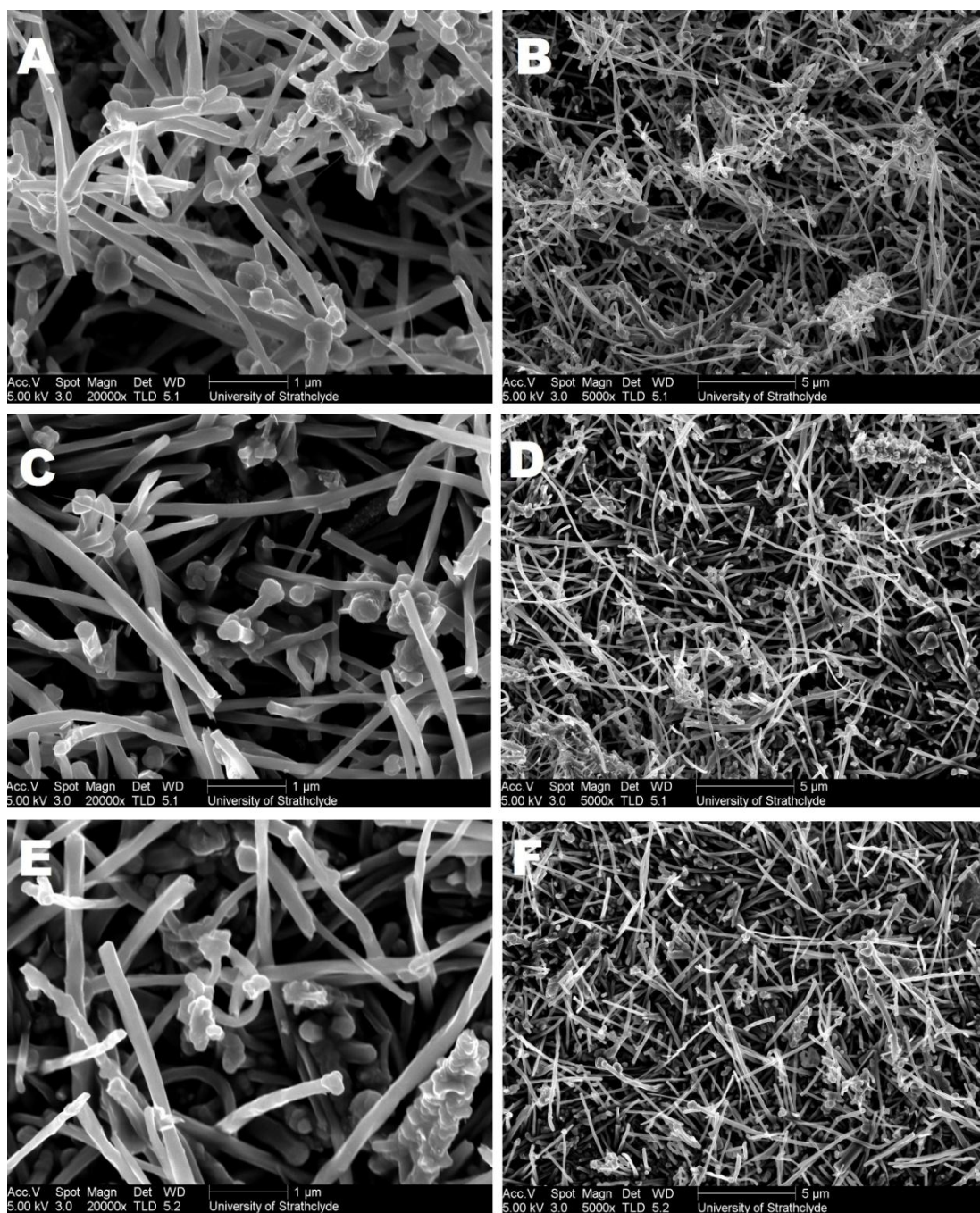


Figure 7.5 - SEM at two different magnifications of thick MWNTs; A & B – Raw form, C & D after acid treatment and E & F following calcination in static air.

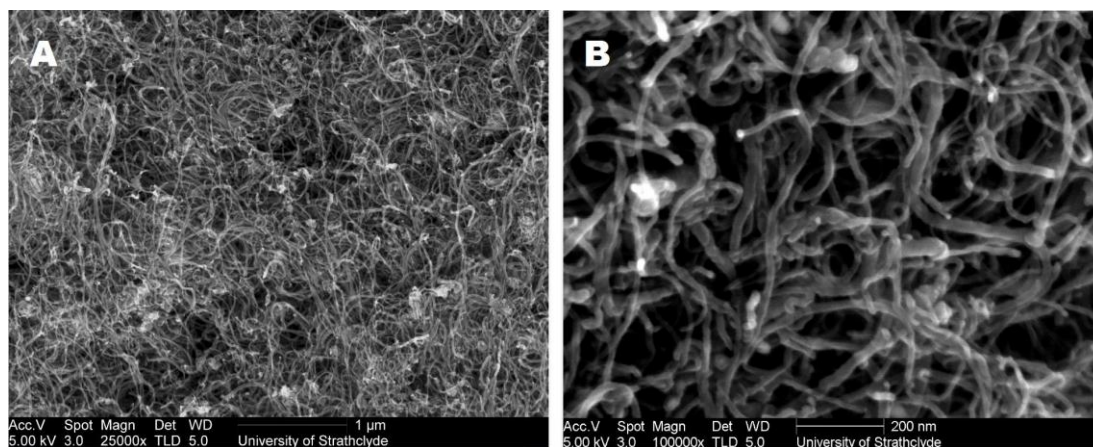


Figure 7.6 - SEM images of thin MWNTs at two different magnifications; A & B – Raw form

The SEM photographs of thick and thin MWNTs are shown in Figures 7.5 and 7.6 respectively. At the time the images were taken, the purification of the thin MWNTs had not yet been carried out. The thin MWNTs are seen to be highly interwoven due to their higher aspect ratios and flexibility. Therefore it is apparent that they would be more susceptible to agglomeration compared to the more rigid thick MWNTs. A higher concentration of impurities is apparent in the raw MWNTs, however little difference was observed between the acid refluxed and the calcined MWNTs.

Raman spectroscopy was carried out using a WITec Alpha 300R confocal Raman microscope for all spectral acquisitions at an excitation wavelength of 532 nm. Spectra were collected using an olympus MPLanFL N 100×/NA 0.9 objective lens and the data was analysed using WITec Project software, version 2.02. There are three major peaks apparent from the Raman spectroscopy at approximately 1350, 1580 and 2700 cm^{-1} , representing the D, G and G' bands respectively. A peak at approximately 75-300 cm^{-1} is referred to as the Radial Breathing Mode (RBM) often visible with SWNTs which can be used to estimate their diameters. However, this peak is too weak to show up with larger diameter MWNTs (Datsyuk et al. 2008). The G band is a representation of the stretching mode of the carbon-carbon bonds in the graphene plane and the D band represents the disorder in carbon bonds. A ratio of the D/G band can be used to determine the purity of the nanotube. The thick MWNTs had significantly smaller ratios than the thin MWNTs, suggesting a higher level of purity. Additionally, there is a drop in the D/G ratio in the thick MWNTs from their

raw state of 0.17 to 0.12 in their pure state. The thin MWNTs showed an increase in purity once refluxed but this decreased again after calcination.

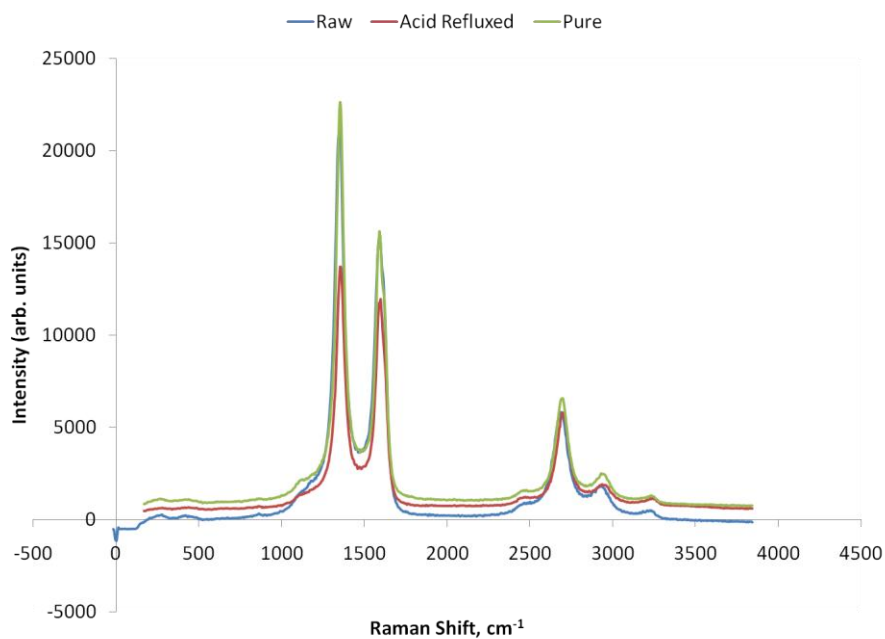


Figure 7.7 - Raman spectroscopy of the thin (10-15 nm) MWNTs in their raw, acid treated and pure states.

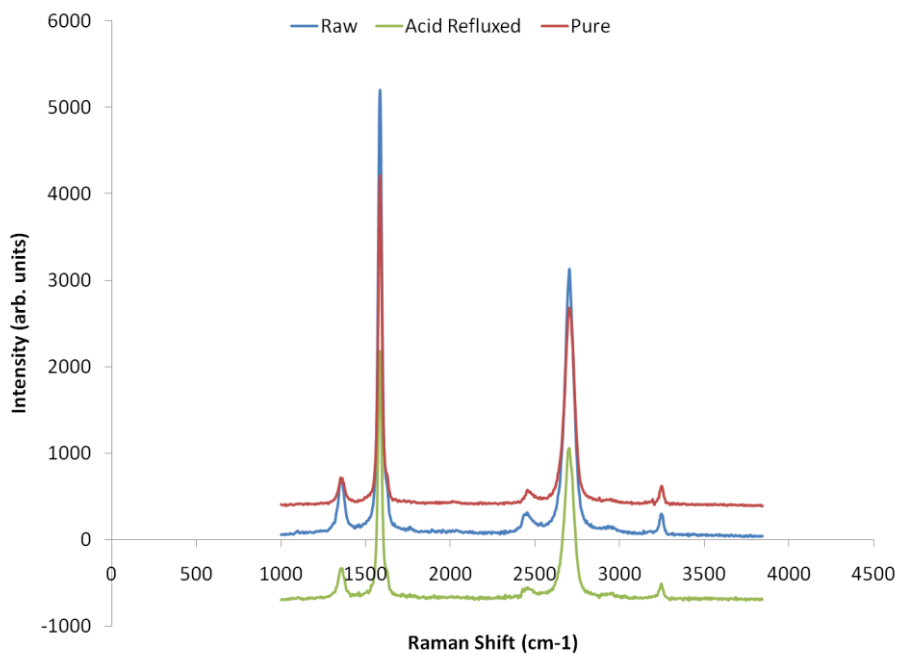


Figure 7.8 - Raman spectroscopy of the thick (110-170 nm) MWNTs in their raw, acid treated and pure states.

Table 7.1 - Ratio of intensity bands for thin (high aspect ratio) MWNTs in their raw, refluxed and pure states (n=3).

| <i>MWNT</i> | <i>ID/IG</i> | <i>ID/IG'</i> | <i>IG/IG'</i> |
|----------------------|--------------|---------------|---------------|
| Raw | 1.32±0.02 | 2.45±0.40 | 1.85±0.28 |
| Acid Refluxed | 1.15±0.00 | 2.28±0.19* | 1.99±0.17 |
| Pure | 1.33±0.07 | 2.62±0.45 | 1.94±0.23 |

*p<0.05 compared to raw samples based on a one-way ANOVA study.

Table 7.2 - Average ratio of intensity bands (\pm S.E.) for thick MWNTs in their raw, refluxed and pure states (n=3).

| <i>MWNT</i> | <i>ID/IG</i> | <i>ID/IG'</i> | <i>IG/IG'</i> |
|----------------------|--------------|---------------|---------------|
| Raw | 0.17±0.04 | 0.28±0.05 | 1.64±0.04 |
| Acid Refluxed | 0.13±0.00 | 0.21±0.00 | 1.63±0.03 |
| Pure | 0.12±0.03 | 0.19±0.04 | 1.58±0.01 |

7.3.2 Estane with thick impure MWNT Composites

All samples exhibited an initial stiff region, followed by a decrease in stiffness with increasing strain, before rapid stiffening prior to rupture. A summary of the results of Estane with varying nanotube content is shown in Table 7.3. Initial results with the MWNTs showed increasing elastic modulus with increasing nanotube content (Figure 7.9). However, when the results were repeated with the 2% MWNT content, there was a significant drop in elastic modulus and UTS despite the strain at failure remaining the same. The 3% and 4% Estane-MWNT were initially sonicated for 30 minutes and then a further 30 minutes. A drop in elastic modulus was noted when they were sonicated for a further 30 minutes which may indicate a threshold sonication period after which the stiffness of the composites is compromised.

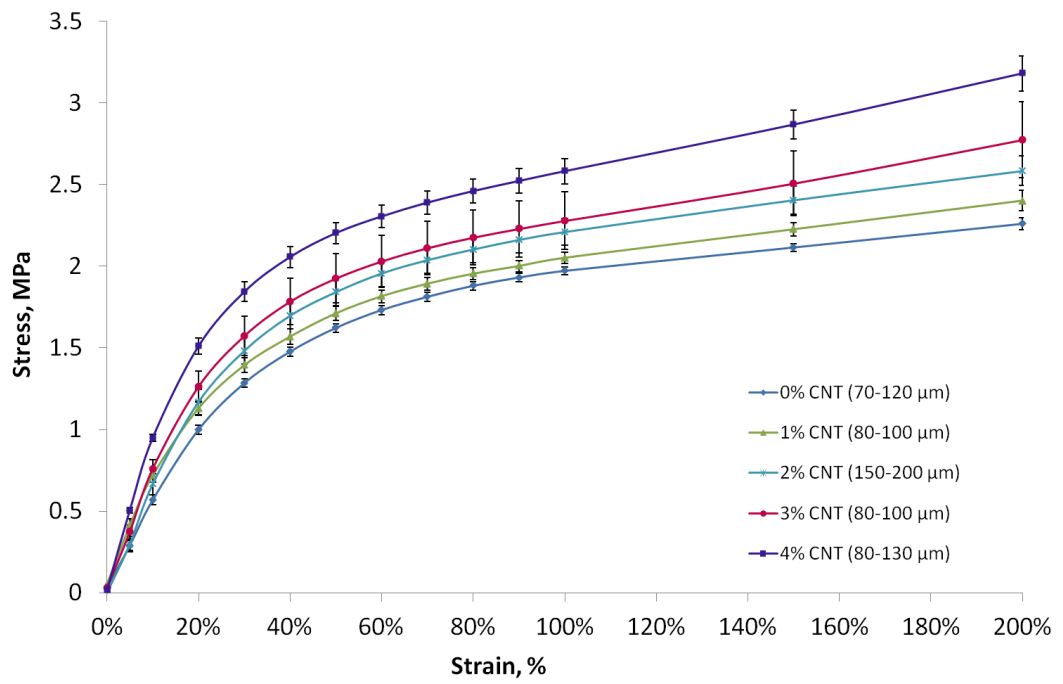


Figure 7.9 - Stress-strain relationship of Estane with up to 4% MWNTs.

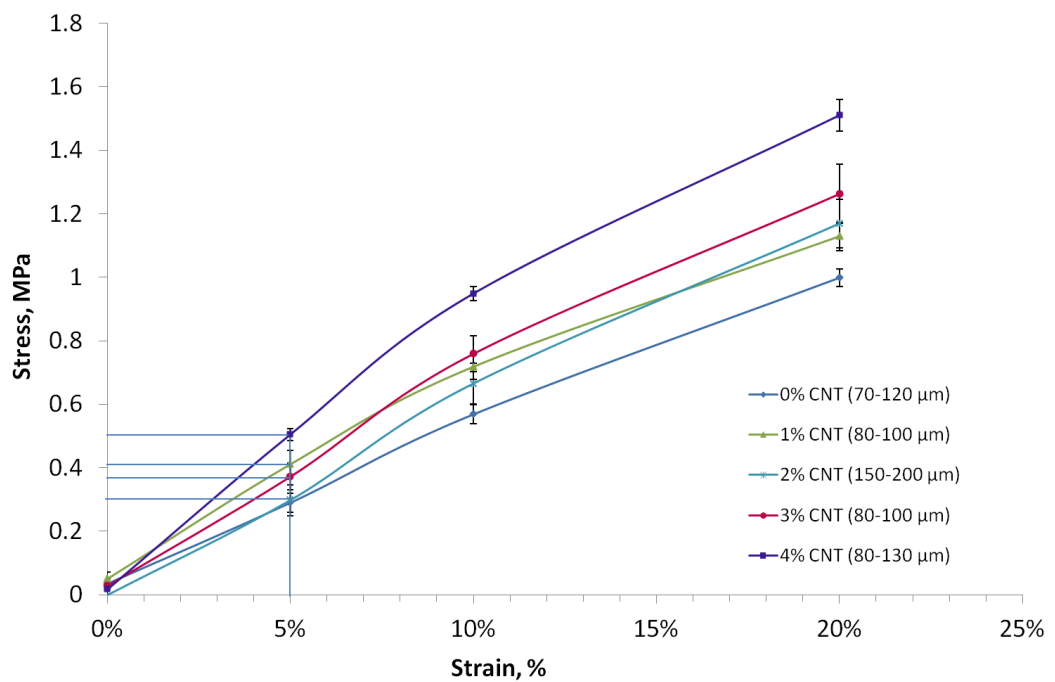


Figure 7.10 – Close up of Figure 7.9. Secant modulus is derived from dividing the stress at 5% strain by 0.05.

Table 7.3 - Average (\pm SEM) of the tensile properties of Estane with 1-4% thick and impure MWNTs (n=7-10).

| <i>Composite (n)</i> | <i>Thickness, μm</i> | <i>5% Secant Mod, MPa</i> | <i>UTS, MPa</i> | <i>Strain at Failure ($\Delta l/l_0$)</i> |
|-----------------------------|--|---------------------------|-----------------|--|
| Pure TPU (9) | 75.7 \pm 5.1 | 6.2 \pm 0.4 | 22.3 \pm 1.6 | 11.8 \pm 0.7 |
| 1% CNT (10) ^b | 83.8 \pm 3.2 | 8.0 \pm 0.8* | 20.8 \pm 0.3 | 12.7 \pm 1.0 |
| 2% CNT (8) -1 ^b | 170.2 \pm 5.1 | 6.6 \pm 0.7 | 12.3 \pm 0.8 | 12.1 \pm 0.7 |
| 2% CNT (10) -2 | 90.4 \pm 2.1 | 5.9 \pm 0.4 | 20.7 \pm 2.2 | 13.4 \pm 0.2 |
| 3% CNT (7) -1 ^a | 149.1 \pm 16.2 | 7.1 \pm 0.8 | 16.4 \pm 1.8 | 13.0 \pm 0.7 |
| 3% CNT (10) -2 ^b | 63.7 \pm 2.2 | 5.8 \pm 0.6 | 24.4 \pm 0.6 | 12.7 \pm 0.5 |
| 4% CNT (8) -1 ^a | 99.7 \pm 6.5 | 10.1 \pm 0.4* | 25.8 | 13.7 |
| 4% CNT (10) -2 ^b | 85.5 \pm 6.9 | 7.3 \pm 0.5** | 16.6 \pm 3.8 | 11.8 \pm 0.7 |

^a 30 min sonication

^b 1 hr sonication

* Significant increase in modulus ($p < 0.05$) compared to control

** Significant drop in modulus ($p < 0.05$) following further sonication.

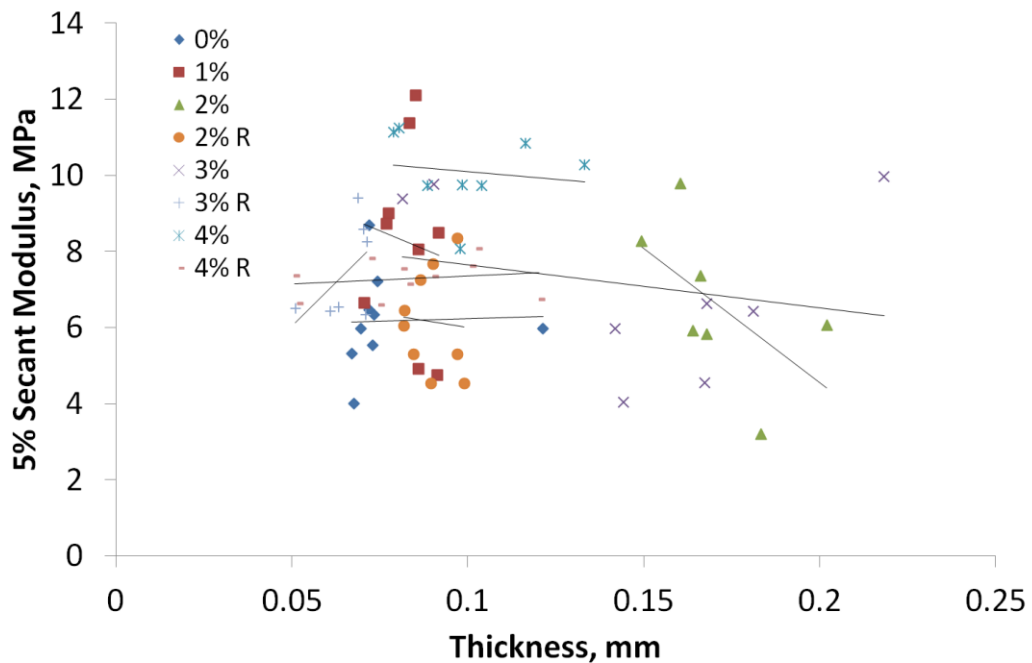


Figure 7.11 – Relationship between the secant modulus and the thickness of the samples showing no correlation. R – Repeat composite.

No correlation was observed between the thickness of the composites and their stiffness. The composites with 1% MWNT content showed a substantial increase of 29% in elastic modulus despite its low concentration. It is hypothesised that dispersion for 1 hour in an ultrasonic bath would have been more effective with lower nanotube concentrations as there would be more space within the matrix to allow for an efficient dispersion. Since a 1% MWNT addition was shown to have an effective reinforcement, it was decided to use this concentration to determine the mechanical properties of the Carbothane and Elast-Eon TPUs. A comparison of the mechanical properties of the different TPUs in their neat form is shown in Figure 7.12. Carbothane 95A is shown to have the stiffest properties, followed shortly by Elast-Eon. Estane appears to be the least stiff. Additionally, it is a PEU and its structure is prone to hydrolysis. Consequently further testing with Estane was dropped.

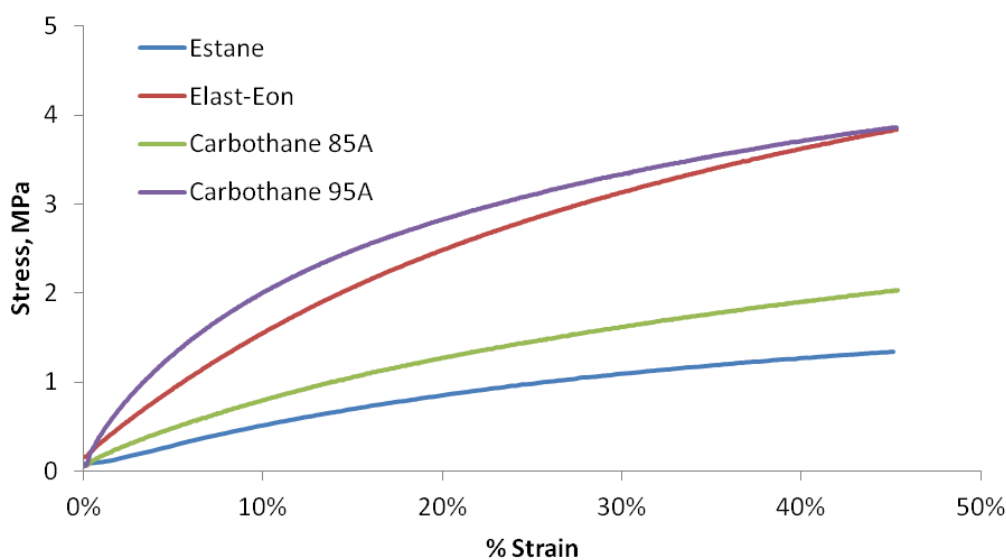


Figure 7.12 - Comparison of the typical mechanical properties of polyurethanes up to 45% strain.

7.3.3 Carbothane / and Elast-Eon / MWNT Composites

The secant modulus at 5% strain and the creep modulus of the polyurethane composites are shown in Figures 7.13 and 7.16 respectively. Carbothane 85A with impure thick MWNTs was shown to have the highest improvement in the elastic modulus, showing a 49.4% increase compared to the control. Carbothane 95A with the impure thick MWNTs had the highest elastic modulus and tear strength overall at 39.4 MPa and 21.2 N/m respectively. A significant improvement ($p < 0.05$) was noted in both impure and pure thick MWNTs in Carbothane 95A compared to its neat form. In all cases, there was no significant difference between pure and impure MWNTs with the exception of the thin MWNTs in Carbothane 85A. No improvement was found to be significant with the thin MWNTs in all cases at a 95% confidence interval.

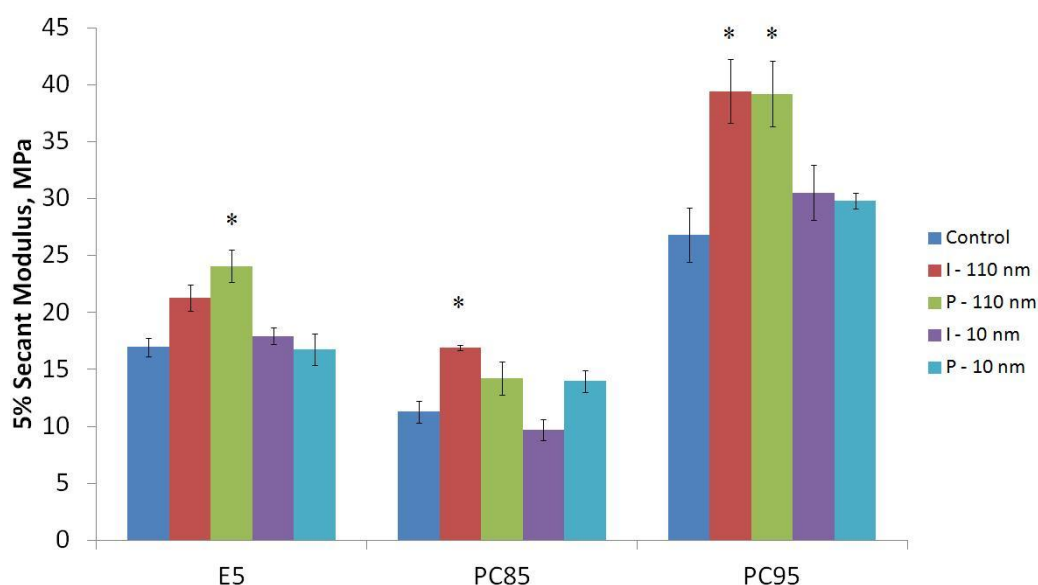


Figure 7.13 - The average (\pm S.E.M) secant modulus at 5% strain of 1% of MWNT composites having 110 nm and 10 nm diameters. I – Impure nanotubes, P – Pure nanotubes. E5 –Elast-Eon, PC85 and PC95 – Carbothane PC3585A and PC3595A respectively ($n=5$, * indicates significance difference from neat polymer, $p < 0.05$ based on a one-way ANOVA test).

Creep was carried out over displacement control at 3 mm, since load control was difficult to achieve (Figures 7.14 and 7.15). For this reason, the creep modulus was used, which is defined as the stress over the displacement after 30 seconds of creep deformation. The incorporation of the thick impure MWNTs was seen to improve the creep modulus of all the composites. Elast-Eon exhibited the greatest improvement in creep modulus with a 14.5 % and 11.5 % increase with the pure and impure thick MWNTs respectively (Figure 7.16).

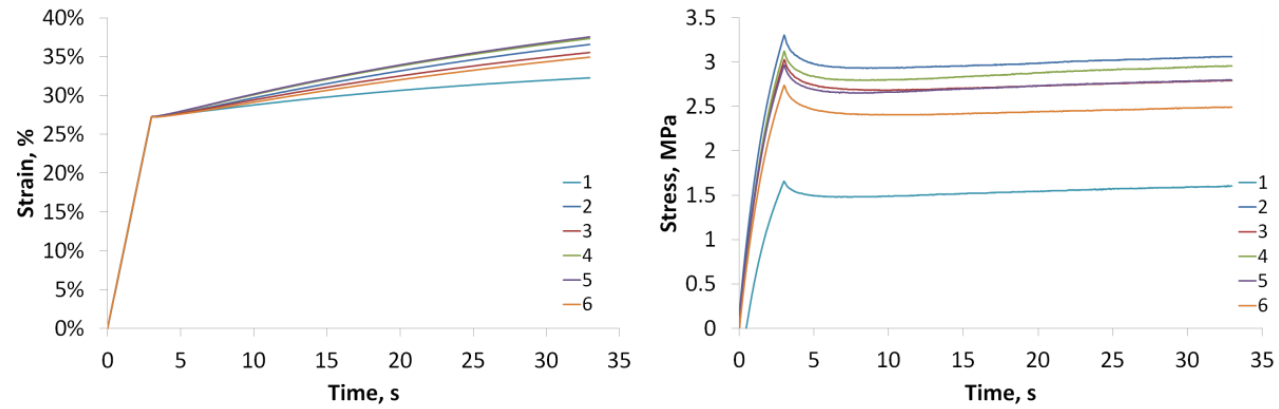


Figure 7.14 – Stress and strain relationships with time using displacement controlled creep for neat Elast-Eon. Variability in stress at a fixed strain is noticeable. Sample 1 has a reduced stress due to initial tuning of the testing system.

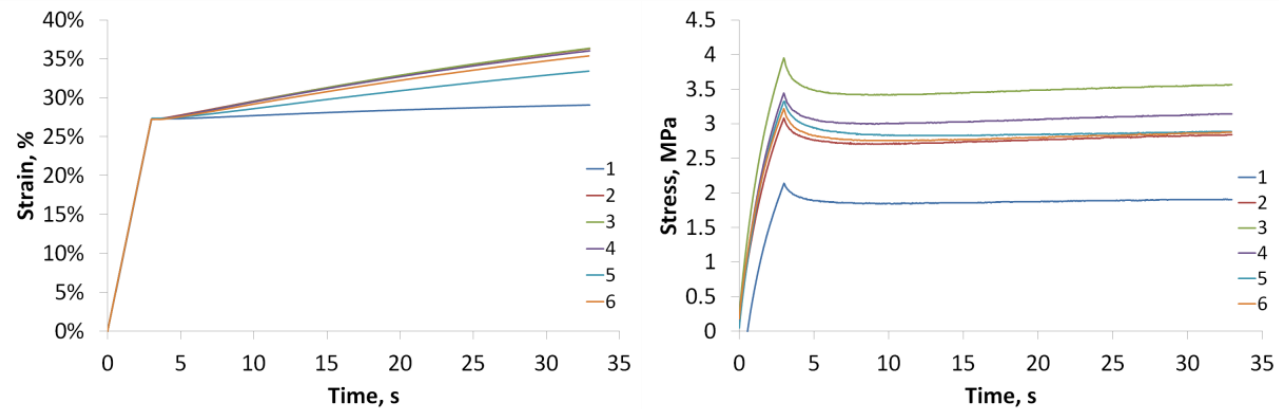


Figure 7.15 – Stress and strain relationships with time using displacement controlled creep for Elast-Eon with impure 110 nm MWNTs. Sample 1 has a reduced stress value due to initial tuning of the test system.

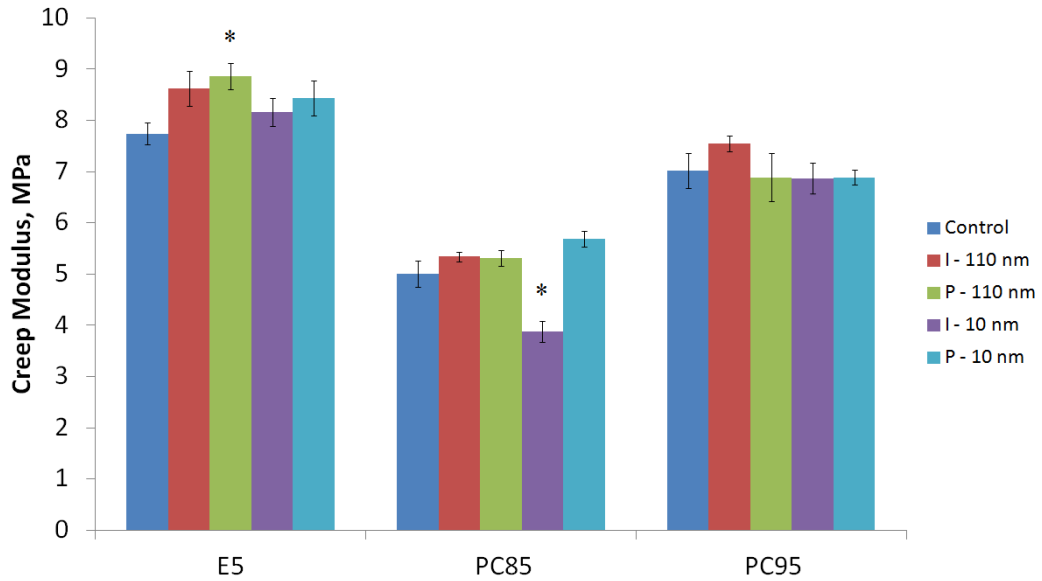


Figure 7.16 - Creep modulus of 1% MWNT composites after 30 seconds. I - Impure nanotubes. P - Pure nanotubes. (n=5 except for PC85-P-110 nm, * indicates significance difference from neat polymer, p<0.05 based on a one-way ANOVA test).

The percentage stress relaxation (% SR) after 30 seconds of fixed strain is shown in Table 7.4 for all composites. Carbothane PC3595A had the highest reduction in stress although little difference was noted with the incorporation of the MWNTs. Both the impure and pure thick MWNTs were found to increase the % SR of the other polymeric composites. However, only the thin MWNTs improved the % SR of the Elast-Eon polymer. This may be attributed to a better adhesion between the fibres and the polymer matrix of Elast-Eon.

Table 7.4 – Percentage stress relaxation (%) in composites (n=5).

| <i>Polymer</i> | <i>Control</i> | <i>Wide (110 - 170 nm)</i> | | <i>Thin (10 - 15 nm)</i> | |
|----------------|----------------|----------------------------|---------------|--------------------------|---------------|
| | | <i>Impure</i> | <i>Pure</i> | <i>Impure</i> | <i>Pure</i> |
| E5-325 | 25.40 ± 0.58 | 28.70 ± 0.86* | 30.29 ± 0.93* | 27.69 ± 0.49* | 27.17 ± 0.77 |
| PC3585A | 31.59 ± 0.10 | 33.41 ± 0.63* | 32.77 ± 0.40* | 32.20 ± 0.16* | 32.06 ± 0.32 |
| PC3595A | 47.35 ± 0.16 | 46.41 ± 0.11* | 45.78 ± 0.39* | 46.94 ± 0.19 | 48.66 ± 0.04* |

*Significant difference (p<0.05) compared to neat polymer based on a one-way ANOVA study.

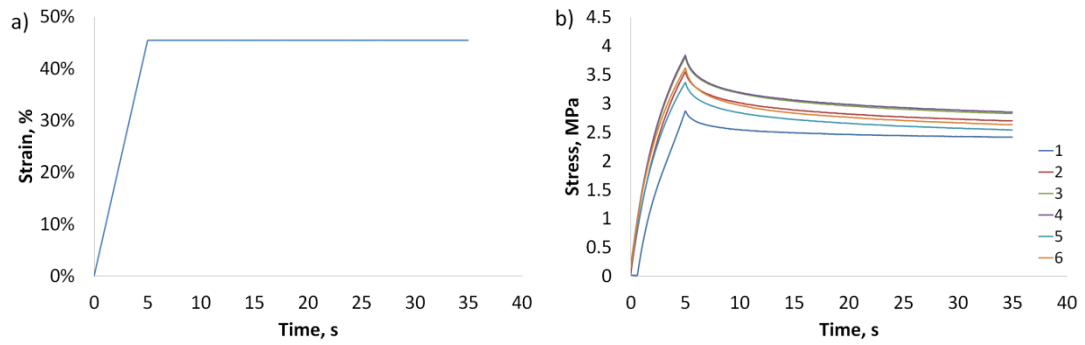


Figure 7.17 – a) ramp graph of strain against time and b) stress response for samples of neat Elast-Eon.

The tear strength of the composites is shown in Table 7.5. Carbothane PC3595A had the highest tear strength overall though little or no improvement was noted with the incorporation of the thick MWNTs. The tear strength of Elast-Eon and the softer grade Carbothane (PC3585A) were similar. Incorporation of the thinner MWNTs was found to reduce the tear strength of the composites in all cases.

Table 7.5 – Tear strength (N/mm) of composites (n = 3)

| <i>Polymer</i> | <i>Control</i> [†] | <i>Wide (110 - 170 nm)</i> | | <i>Thin (10 - 15 nm)</i> | |
|----------------|-----------------------------|----------------------------|--------------|--------------------------|---------------|
| | | <i>Impure</i> | <i>Pure</i> | <i>Impure</i> | <i>Pure</i> |
| E5-325 | 12.94±0.44 | 13.06 ± 2.33 | 14.56* | 10.17 ± 0.69** | 9.45 ± 1.88** |
| PC3585A | 14.18±1.16 | 15.58 ± 0.57 | 13.05 ± 0.74 | 10.99 ± 0.65 | 13.05 ± 0.98 |
| PC3595A | 20.10 ± 1.44 | 21.23 ± 0.80 | 17.28 ± 1.02 | 10.58 ± 1.08** | 18.75 ± 0.96 |

[†]n=5-7

* n=1

** Significant difference (p<0.05) compared to neat polymer based on a one-way ANOVA study.

7.3.4 Carbothane 95A with Thick Impure MWNTs

7.3.4.1 Effect of Sonication Times on Dispersion

In the dispersion rate study, the elastic modulus (Figure 7.18) was highest after 1 hour for both composites, with the 0.5% and 1% fibres having a stiffness of 44.2 MPa and 44.1 MPa respectively compared to an average stiffness of 34 MPa for the neat polymer. Stiffness remained higher than the neat polymer after 2 hours but rapidly declined after 5 hours which may imply degradation of the nanotubes or of the polymer solution. Conversely, the % SR increased slightly with increasing dispersion times. Optical microscopy images appear to show complete dispersion after 5 hours (Figure 7.20).

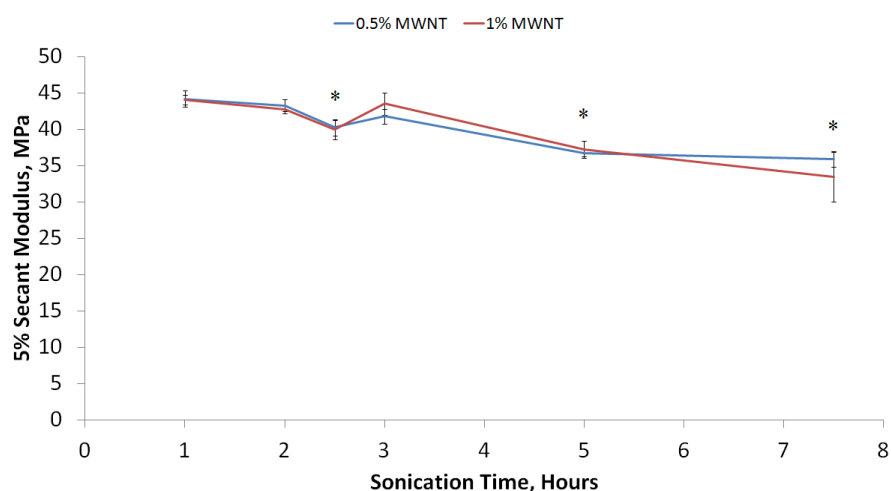


Figure 7.18 - Mean (\pm S.E.M) stiffness against dispersion time (hours) in an ultrasonic bath for 0.5% and 1% fibres. N=5, * represents significant difference ($p < 0.05$) compared to composite at 1 hour sonication time, based on a one-way ANOVA study.

The storage modulus, E' in relation to the sonication time is shown in Figure 7.19. E' is seen to vary widely from 1 - 3 hours of sonication. After 2 hours of sonicating the 1% composites had a maximum E' of 18.6 ± 0.38 MPa which was slightly higher than the neat polymer which had a storage modulus of 18.4 ± 0.36 MPa. For both the

0.5% and 1% fibres, there was a significant difference in E' at 3 hours compared to 1 hour and E' was found to be similar beyond 3 hours of sonication. It is interesting to note that E' did not significantly decrease after 5 hours as was the case with the secant modulus of the composites. From this data, it was decided that a period of 2 hours is sufficient for dispersion of the composite solutions using an ultrasonic bath.

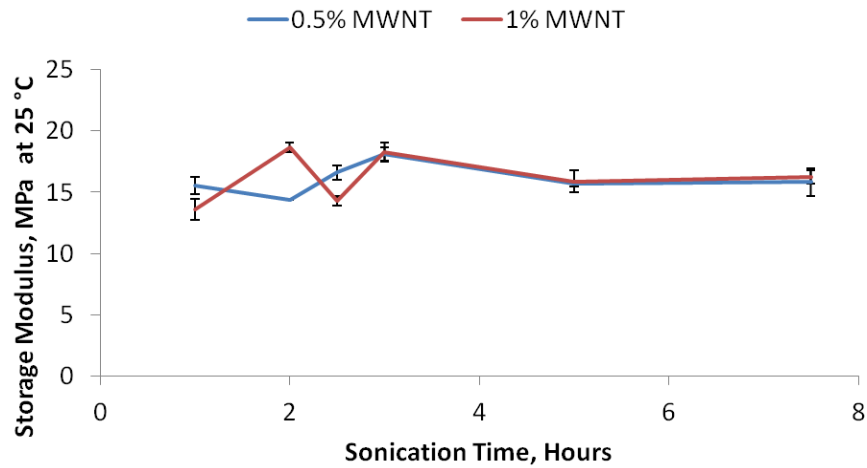


Figure 7.19 - Mean (\pm S.E.M) storage modulus of the 0.5% and 1% fibres after 1 hour and 7.5 hours dispersion time (n=6).

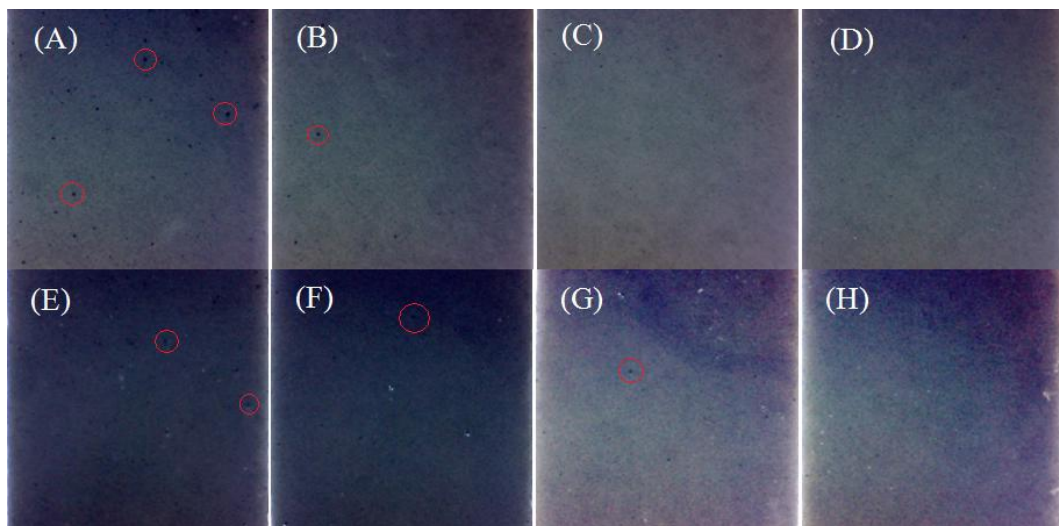


Figure 7.20 - Optical microscope images of the 0.5% (a-d) and 1% (e-h) MWNT composites following 1 (a, e), 3 (b, f), 5 (c, g) and 7.5 hours (d, h) dispersion in an ultrasonic bath (35x magnification). Red circles highlight some of the clusters in the matrix.

7.3.4.2 Strain Rate Dependence

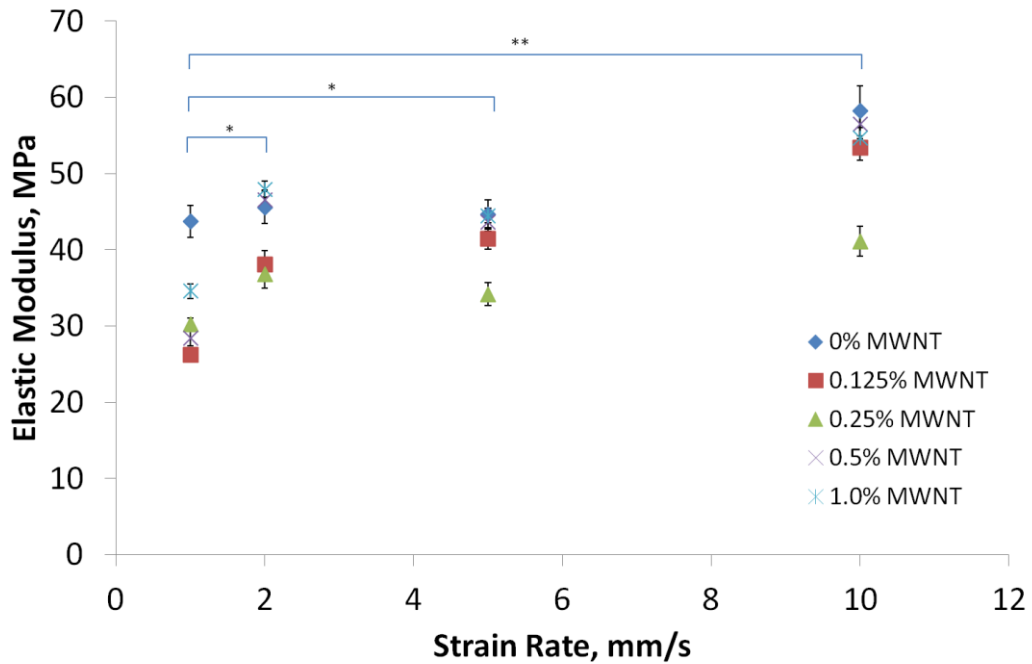


Figure 7.21 - Elastic modulus between 0.5 and 1.0 MPa stress with increasing strain rate and nanotube content. $N > 4$, * represents significance, $P < 0.05$, in composite samples only. ** represents significance, $P < 0.01$ in all samples based on a one-way ANOVA study.

The stiffness of the composites was determined from the linear region of the graph between 0.5 MPa and 1.0 MPa for varying nanotube contents at 1, 2, 5 and 10 mm/second strain rate. An attempt was initially made to derive the secant modulus but readings were inaccurate due to the slack in the samples prior to the next loading step. Only the 0.5% and 1.0% composites showed a significant difference in modulus between the 2 mm/s and 5 mm/s strain rates. The stiffness of the composites significantly increased ($p < 0.05$) with increasing strain rate. However, the stiffness of the neat polymer did not significantly increase until a strain rate of 10 mm/s was applied. The stiffness of the neat PU remained higher overall compared to the composites although this may be attributed to environmental factors since they were tested on different days.

7.3.4.3 Time in Distilled Water

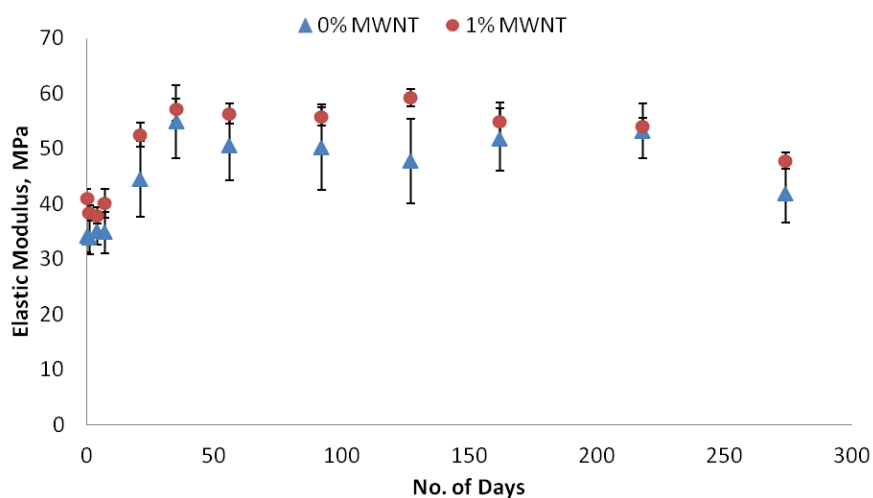


Figure 7.22 - Secant Modulus at 5% strain of Carbothane 95A after immersion in distilled water for several days (n=5).

The samples were immersed in distilled water for 9 months. The secant modulus of the pure and reinforced polymeric composites measured at intermittent dates is shown in Figure 7.22. The stiffness increased rapidly for both samples from Day 7 to Day 21 after which a plateau region was observed. The highest increase in stiffness was 61% for the pure polymer compared to a 44% increase in the 95A-MWNT composite. There was a significant ($p < 0.05$) increase between days 7 and 35 in the neat polymer and between days 7 and 21 in the composite. In this case, it is apparent that the composites reach saturation sooner than the neat polymer. There is also a greater variability in the elastic modulus of the neat polymers compared to the composites.

There was an initial drop in film thickness but there was no significant ($p > 0.05$) change over time, indicating that polymer swelling did not occur (Figure 7.23). The initial thickness of the neat polymer was 52.7 μm compared to a thickness of 50.5 μm , however the difference between the neat and composite films increased with time, with the neat polymer being 4.1 μm thicker than the composite. The percentage

stress relaxation was noted to decrease with increasing immersion time. A negative correlation existed between the elastic modulus and stress relaxation.

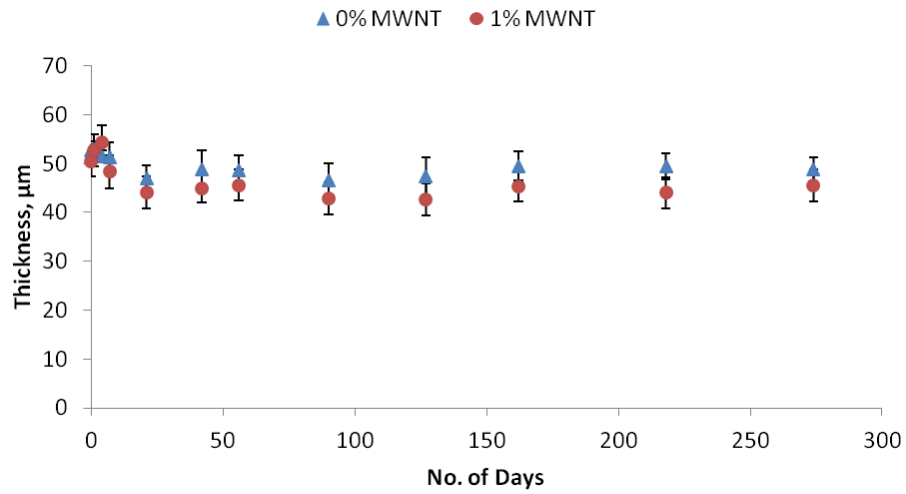


Figure 7.23 - Change of sample thickness (mm) with increasing time in water (n=6).

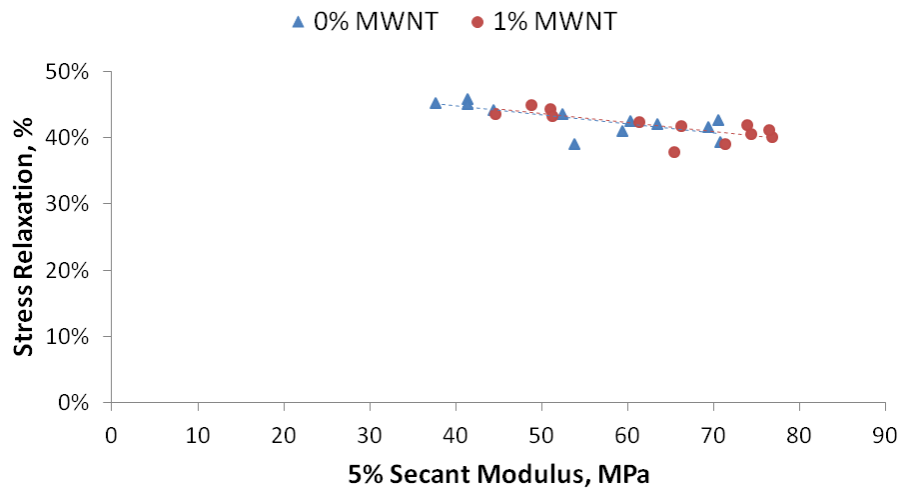


Figure 7.24 – Negative correlation between the percentage stress relaxation and the secant modulus.

7.3.4.4 Effect of Temperature on Composites

The results of the mechanical properties of the 0.5% and 1.0% 95A-MWNT composites that were used previously in the sonication studies at 1 hour are shown in Table 7.6. The elastic modulus was obtained between 0.1 and 0.5 MPa of stress which would give a higher stiffness than what would be reported if a secant modulus

at 5% strain was used. The elastic modulus and % stress relaxation are both significantly ($p < 0.05$) reduced following an increase in temperature.

Table 7.6 - Results of the mechanical properties of composites at 37°C

| Composite | N | Thickness (μm) | E.Modulus (MPa) | | % Stress Relaxation | |
|-----------|---|--------------------------------|-----------------|-----------------------------|---------------------|-----------------------------|
| | | | 25°C | 37°C* | 25°C | 37°C |
| Neat PCU | 6 | 49.3 \pm 3.1 | 62.5 \pm 3.6 | 10.9 \pm 1.0 ^a | 39.8 \pm 0.1 | 22.3 \pm 0.8 ^a |
| 0.5% MWNT | 6 | 49.5 \pm 1.4 | 73.0 \pm 2.8 | 12.2 \pm 0.5 | 41.2 \pm 0.1 | 21.2 \pm 0.2 |
| 1.0% MWNT | 6 | 51.0 \pm 1.0 | 76.1 \pm 3.0 | 15.0 \pm 0.6 | 41.1 \pm 0.1 | 22.2 \pm 0.2 |

^a batch tested is different to 25 °C batch, n=4

* $p < 0.05$ based on a one-way ANOVA at 95% CI compared to modulus at 25°C.

7.3.4.5 Tension-Tension Fatigue Life

There was a decrease in fatigue life with increasing carbon nanotube content (Figure 7.25). The composite with 0.125% MWNTs had similar fatigue to the clear polymer. SEM images of the ruptured specimens show surface cracking of the clear polymer which is not evident in the 0.125% and 0.25% MWNT composites. Evidence of fibre pull out was also not found in the failed composite. However the composites appeared to have a more frayed edge compared to the clean cut in the neat polymer. A summary of the properties of the samples cycled to failure is shown in Table 7.7.

Table 7.7 - Summary of results (Mean \pm SEM) for fatigue testing batches at 70.1% strain.

| % MWNT in PC3595A | N | Secant Mod (MPa) | SR (%) | Thickness (μm) | Cycles to Failure ($\times 10^6$) | |
|----------------------|----|---------------------|----------------|--------------------------------|--|-------------|
| | | | | | Mean | Range |
| 0.000%* | 11 | 30.5 \pm 3.7 | 42.3 \pm 0.3 | 56.6 \pm 0.5 | 1.04 \pm 0.12 | 0.36 - 1.70 |
| 0.125% | 6 | 24.7 \pm 1.1 | 41.5 \pm 0.1 | 39.4 \pm 2.3 | 0.99 \pm 0.19 | 0.48 - 1.61 |
| 0.250% | 5 | 28.6 \pm 1.0 | 42.1 \pm 0.1 | 41.1 \pm 1.3 | 0.69 \pm 0.10 | 0.48 - 0.94 |
| 0.500%* | 6 | 35.0 \pm 3.2 | 42.0 \pm 2.2 | 46.3 \pm 1.5 | 0.44 \pm 0.16 | 0.13 - 1.23 |
| 1.000%** | 16 | 38.2 \pm 1.2 | 43.4 \pm 0.4 | 52.8 \pm 1.5 | 0.30 \pm 0.05 | 0.03 - 0.59 |

* 2 solvent cast batches fatigue tested

** 3 solvent cast batches fatigue tested

SR = % Stress relaxation.

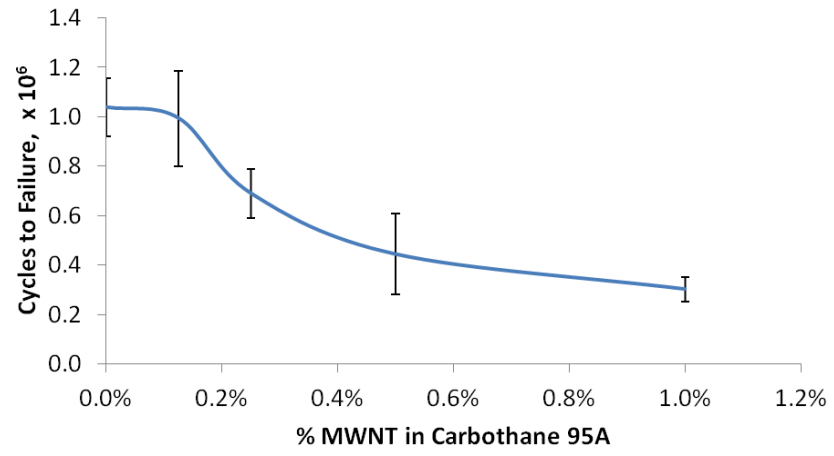


Figure 7.25 - Cycles to failure with increasing MWNT content.

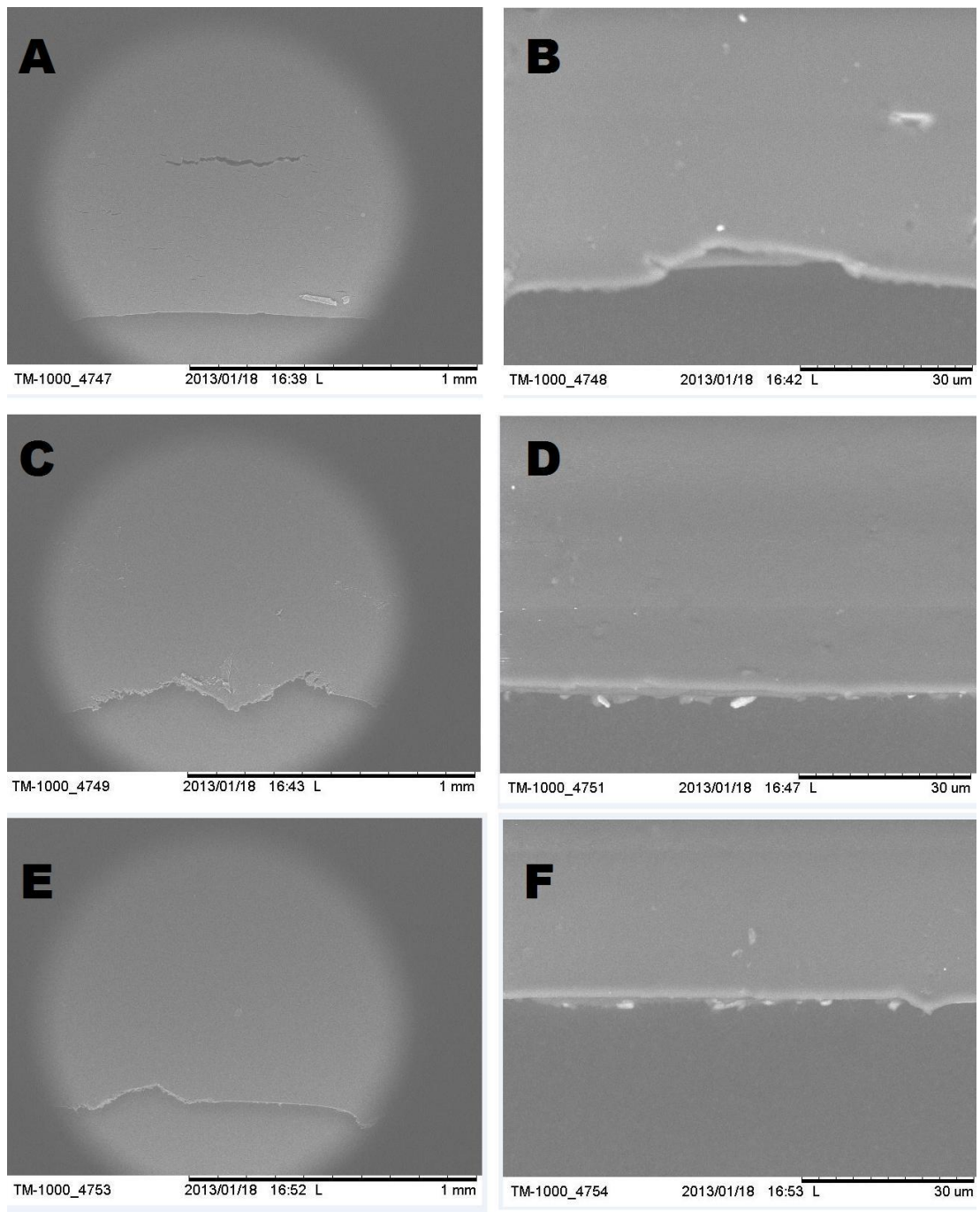


Figure 7.26 - SEM images of failed fatigue tested samples at two different magnifications of PC3595A with (a-b) 0%, (c-d) 0.125% and (e-f) 0.25% MWNTs.

7.3.4.6 Effect of Gamma Irradiation on the Tensile Properties

In the sterilization study, the secant modulus for the 1% MWNT composite was 40.1 MPa compared to 39.0 MPa for the neat polymer when taken at a 5% strain (Figure 7.27). Two days following irradiation, there was a drop in modulus in both the neat and composite material to the non-sterilized samples. There was an overall decrease in modulus in all polymers following 14 days which may be due to insufficient preconditioning of the polymer prior to testing or environmental factors. Based on a two-way ANOVA, there was no significant difference ($p > 0.05$) in the secant modulus of either the neat or composite polymer following days after sterilization.

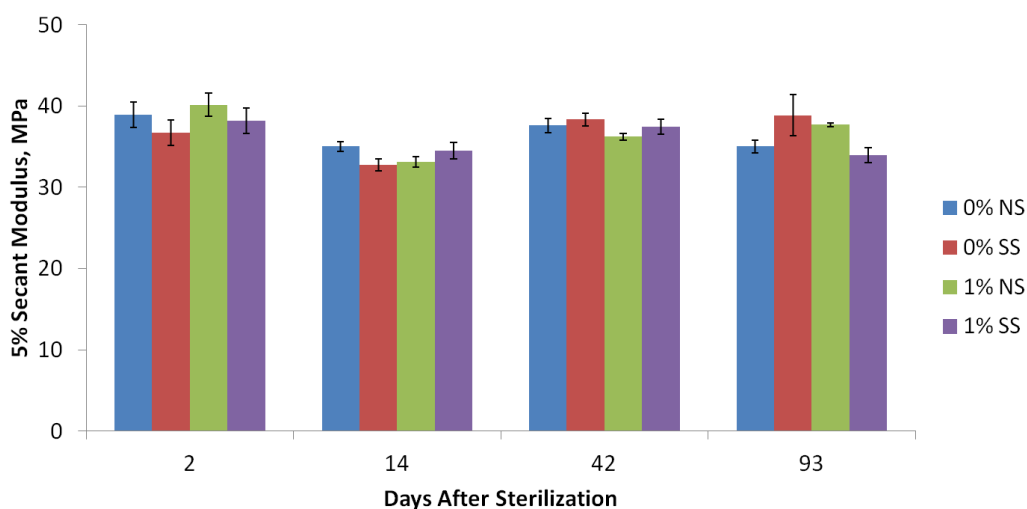


Figure 7.27 - Secant modulus at 5% strain for the pure, 0% and composite 1% films several days after gamma irradiation. NS - non sterile and SS – sterile.

Stress relaxation was highest in all samples 2 days following sterilization which may be due to inadequate preconditioning (Figure 7.28). The percentage stress relaxation following 30 seconds of hold at 45% strain was seen to increase in all samples following sterilization. Following 6 weeks after sterilization, the stress relaxation for the composite was similar to the control whereas the neat polymer still showed an increase compared to the control. Both the drop in stress relaxation with time and its increase following sterilization were significant ($p < 0.05$) following a two-way ANOVA test for both the neat and composite samples.

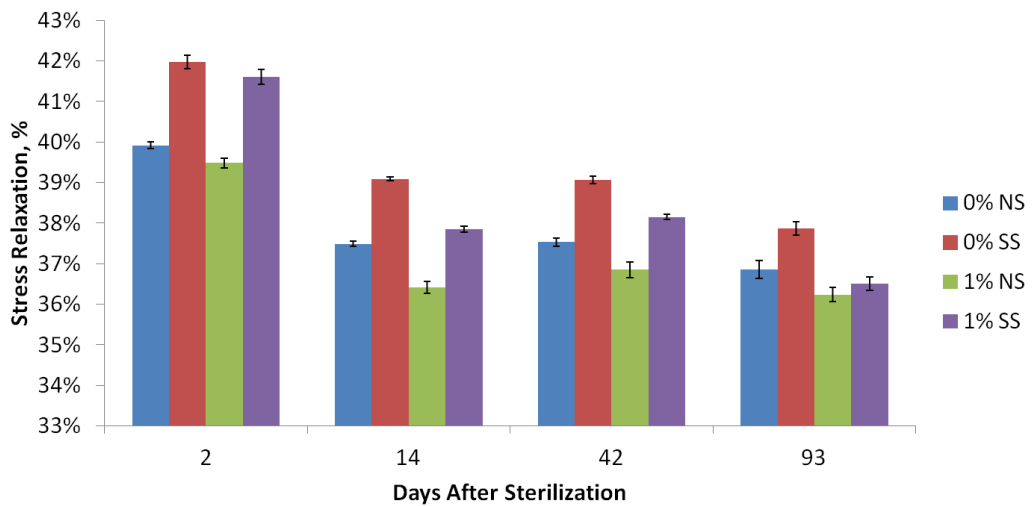


Figure 7.28 - Percentage stress relaxation in composites following sterilization.

7.3.4.7 Effect of Crimping on Tensile Properties

The secant modulus at 5% strain was seen to drop in the 0% and 1% 95A-MWNT samples following crimping although no change was observed with the 0.5% sample. The significant drop was apparent with the 1% fibre which dropped by 15.3% from 41.6 MPa to 35.2 MPa. The percentage stress relaxation correlated positively with the secant modulus of all the samples.

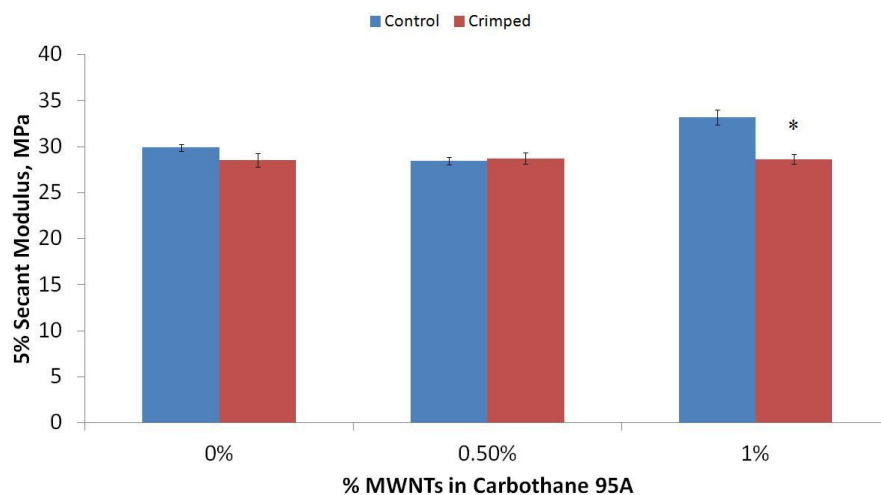


Figure 7.29 - Secant modulus at 5% strain for composites when crimped under a 1 kg load. * represents significant difference ($p < 0.05$) compared to control based on a one-way ANOVA study.

7.4 DISCUSSION

The reinforcement potential of the CNT/polymer composite depends on the choice of polymer, CNT aspect ratio, dispersion method, solvent used and nanotube-polymer interface, amongst other factors. The large variability in the mechanical properties of the composites following repeat testing demonstrates the technical challenges faced with reproducibility. Variables such as temperature, humidity and solvent evaporation rate can all affect the surface structure and mechanical performance of the composite. This is particularly problematic when working with DMAc solvent which is highly hygroscopic.

A higher concentration of MWNTs is likely to increase the stiffness of the polymer but would require a longer dispersion period to reduce the nanotube agglomerates. This was apparent with the Estane composite studies which showed an increase in modulus with increasing nanotube content, and an improvement of up to 63% in the 4% MWNT composite. Additionally, the incorporation of the nanotubes did not seem to compromise the ultimate tensile strain of the polymer which has often been noted in literature to decrease. However, with increasing nanotube content, an efficient dispersion is less likely to be achieved due to the decreased distance between bundles. A longer sonication period may be used to overcome this problem but this may subject the nanotubes to increased structural damage, shortening their aspect ratio which in turn reduces their stress transfer potential.

It is likely that the tackiness of the Estane provided an increased contact area between the nanotube and polymer, thereby allowing a greater load to be transferred from the polymer matrix to the nanotubes. However, Estane is a poly(ether) based polyurethane which meant it was susceptible to hydrolysis in haemodynamic environments. Neat Estane also had a reduced stiffness compared to neat Carbothane and Elast-Eon which would imply that the leaflets would undergo large deformations at low stresses. Carbothane is a PCU and therefore has a better resistance to oxidation than Estane. Due to their large extensibility, the UTS of the polyurethanes was not determined on the ELF tester, which has a maximum crosshead extension of

12 mm. However, the UTS of the Estane TPU was determined to be around 20 MPa which was comparable to the UTS of the porcine pericardium tested in Chapter 4. Carbothane and Elast-Eon are harder and stiffer than Estane and therefore their UTS would be greater than 20 MPa.

The highest improvement in stiffness was reported with the thick MWNTs in all polymers and Carbothane 95A with the thick impure MWNTs exhibited the highest stiffness, tear strength and creep modulus overall. The improved mechanical properties did not appear to compromise the flexibility of the composites as very thin films having thickness of 40 μm were used. In a study by Bernacca et al (2002), it was demonstrated that the leaflet thickness had more of an impact to the hydrodynamic function of the valve compared to the stiffness of the material and that leaflets had good opening dynamics up to a stiffness of 32 MPa, although in their case, the thicknesses studied were much higher than the 40 μm used here.

The poorest reinforcement was found with the thinner MWNTs when incorporated into the Carbothane polymers. Large nanotube agglomerates were noticeable with the naked eye, which implied that although their aspect ratio was higher than the thicker nanotubes, the bundles would have reduced their aspect ratio considerably. Additionally large clear regions containing no nanotubes were evident, indicating potential weakening points in the matrix which can actually reduce the stiffness rather than enhance it. With increasing sonication times, the size of bundles and the clear patches appeared to be larger suggesting reagglomeration. The dispersion of MWNT in Elast-Eon appeared to be significantly better than the Carbothane composites, particularly with the thinner nanotubes when observed both with the naked eye and an optical microscope. This may suggest that the surface wettability of MWNTs is better in Elast-Eon than in Carbothane; this favours the theory that MWNTs bond well to PDMS which was discussed in Chapter 6.

The stiffness of the polymer was expected to decrease upon immersion in water. This is due to the hydrogen in the water weakening the bonds between the polymer segments. However, the results from this test demonstrate an increase in modulus

with increasing time in water as well as an increase in the maximum stress at 45% strain. The peak rise in modulus may be due to the polymers reaching saturation as a plateau region was observed. In a study by Yang et al. (2006), it was noted that the elastic modulus of shape memory polymer decreased with increasing immersion time in water at room temperature which was below its glass transition temperature (T_g), but increased when tested above its T_g . In this study, the polycarbonate urethane is tested above its T_g , agreeing with the increase in stiffness of the films reported by Yang et al.

Higher temperatures decrease the stiffness of polymers. However, the 1.0% composite had the highest stiffness compared to the neat and 0.5% composite at 37°C. This value is comparable to human aortic valve leaflets which have a stiffness of 16.05 ± 2.02 MPa and 1.98 ± 0.15 MPa in the circumferential and radial directions respectively (Stradins et al. 2004), although the leaflets were considerably thicker at 605 ± 196 μm .

During the dip coating process (discussed in Chapter 8) the rheological properties of the composite need to be viscous enough to allow the polymer to settle on the hyperbolic – elliptical surface of the former. Additionally, larger volumes prepared in larger diameter bottles were required which would affect the sonication efficiency compared to the smaller bottles used previously. Initial studies on viscous composite solutions found difficulty obtaining a homogenous dispersion and improvement in mechanical integrity. It was decided that many factors influenced the dispersion state of the nanotubes. Firstly, the viscosity of the solution may reduce the energy absorbed by the bundles, so reduced solutions of 0.125%, 0.25% and 0.5% MWNT were developed alongside the 1% composite and the temperature of the bath water was raised. Secondly, the ideal sonication time needed to be established. If the time was too short, large clusters would still be present. Better dispersion would reduce the size of the bundles; however the nanotubes have been shown to break down after long sonication periods. In a study by Song and Youn (2005), the elastic modulus of epoxy with poorly dispersed nanotubes was higher than the well dispersed epoxy, suggesting that the material behaved as a solid in poor dispersion. However, ultimate

tensile strength was noted to be higher in the well dispersed epoxy which showed efficient load transfer.

Often, little to no improvement was noted when nanotubes were added to the polymer. Similar findings were reported in a study by Gkikas et al. (2012), who also reported little change in stiffness of 0.5% and 1% MWNTs in epoxy resin. However, the authors noted an increase in UTS and storage modulus compared to the neat resin, particularly at higher temperatures. Additionally, they found the storage modulus, E' of 0.5% and 1% MWNT/epoxy composites to be overall higher than the neat epoxy and was highest after 1 hour of sonicating when tested at 30 °C.

In all cases, crimping the composites using a 1 kg load led to a decrease in stiffness compared to the control samples. This decrease was greatest with the 1% composite and may imply that the nanotube-polymer interface was weakened following folding. It would be desirable to conduct further tests to determine if the change in stiffness was temporary and observe the impact that folding would have on the structure of the polymer. In one study looking at the crimping effects of leaflets from four Edwards Sapien valves, microscopic collagen disruption was apparent (Zegdi et al. 2011). In another study, collagen defects were noted on the surface and superficial layers of pericardial tissue which did not improve with time. However, the deeper layers appeared to be unaffected (Kheradvar and Alavi 2012). There is still no long term data on the effects that crimping has on pericardial tissue and it will be interesting to observe whether these defects can lead to early calcification and fatigue.

In a study by Rama Sreekanth et al. (2012), MWNTs incorporated in polymer were found to reduce the loss in elastic modulus compared with the neat polymer following irradiation due to the ability of the nanotubes to scavenge radicals mobilized in the radiation process. However, this study found no significant changes in the secant modulus of composites following sterilization although a higher increase in modulus was noted with the control neat polymer after 6 weeks. Interestingly, an increase in the percentage stress relaxation of samples was found to

be significant. It is possible that the nanotubes absorbed some of the radiation which helped reduce the detrimental effect it has on the polymer.

The incorporation of nanotubes into the polymer matrix was found to reduce the fatigue life, with durability decreasing with increasing nanotube content. There was a large variability between the numbers to cyclic failure of samples in the same batch with similar thicknesses, suggesting that film thickness did not affect the durability of the composite.

7.5 CHAPTER SUMMARY

1. Multi-walled carbon nanotubes can improve the stiffness of the polyurethane.
2. Increasing the purity of the nanotubes did not significantly improve their reinforcement potential and therefore the MWNTs will be used in their impure forms to avoid an unnecessary loss in yield.
3. Carbothane PC3595A with thick MWNTs exhibited high stiffness, tear strength and creep modulus without compromising its flexibility.
4. This composite will be used to develop dip-coated heart valves having thin leaflets.

CHAPTER 8:

VALVE DEVELOPMENT AND TESTING

8 VALVE DEVELOPMENT AND TESTING

8.1 VALVE FABRICATION

8.1.1 Dip Coating Process

Valves having a 22 mm diameter were developed through a dip coating process using 15% 95A neat or 95A-MWNT composite solutions, which were prepared as previously described in Section 6.2.2. A stent, having an inner diameter of 22.4 mm was mounted and aligned at the commissures on the stainless steel former which was heated on a hot plate to approximately 50 °C prior to applying the first coat. Polymeric coats were applied by downwardly driving the former into the bottle containing the polymeric solution and withdrawing slowly. Any bubbles that appeared were immediately burst carefully with the aid of a small spatula. A bubble level was used to ensure that the former remained vertically aligned when the coat was dried in an inverted position. The coats were applied approximately hourly to the former which was dried in altering positions as described below. This was to ensure an even thickness developed throughout the entire length of the leaflet:

1. The former was allowed to dry in an inverted position for 10 minutes prior to positioning upright on a hotplate to complete curing.
2. The former was immediately placed to dry in an upright position; excess polymer which settled at the base was carefully removed with the aid of a spatula.

Valves with 3, 4, 5 and 6 dips were developed and their thicknesses measured prior to durability testing. Since a 15% polymeric solution is fairly dilute, valves with 1 or 2 coats would be too thin. Stents were initially developed using rapid prototyping (Figure 8.2a) which was found to soften and deform when exposed to high temperatures and solvents. The stent was replaced with a rigid polycarbonate stent (manufactured by Brightwake Ltd, Nottingham, UK), an amorphous and highly transparent polymer. This stent bonded well with the polymeric solution due to its

poor solvent resistance but found to occasionally develop cracks during the dip coating process as a result. The final change was to develop the stent from Delrin, (also manufactured by Brightwake Ltd. Nottingham, UK) a semi-crystalline acetal homopolymer. The Delrin stent bonded less well with the polyurethane leaflets due to its excellent solvent resistance but was less brittle than the polycarbonate stent and therefore offered flexibility. An annular ring was created by super-gluing an elastic rubber strip around an elastic band to create a thickened ring. This was then super-glued to the base of the valves to allow attachment to the silicon ring which fits into the durability tester.

8.1.2 Leaflet Thicknesses

The thickness of the valve leaflets was measured at three points along the mid-line of each leaflet using a micrometer. Care was taken to ensure leaflet twisting did not occur during measurements, particularly when measuring at the base where straining may occur at the leaflet-stent interface. Leaflet thickness was seen to increase gradually particularly at the middle region of the leaflet. However, 5 and 6 dip coats lead to further thickening at the top and base of the leaflets, but little or no changes in the middle region.

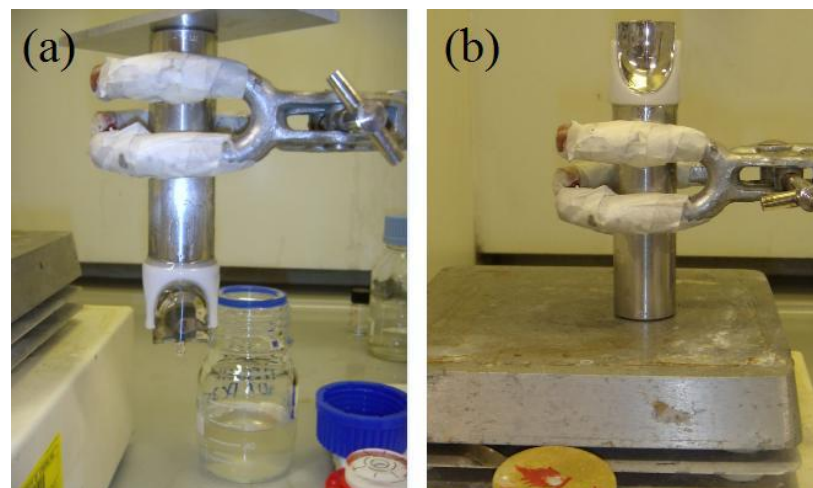


Figure 8.1 - Former with stent mounted and dipped in (a) an inverted and (b) upright position on the hotplate.

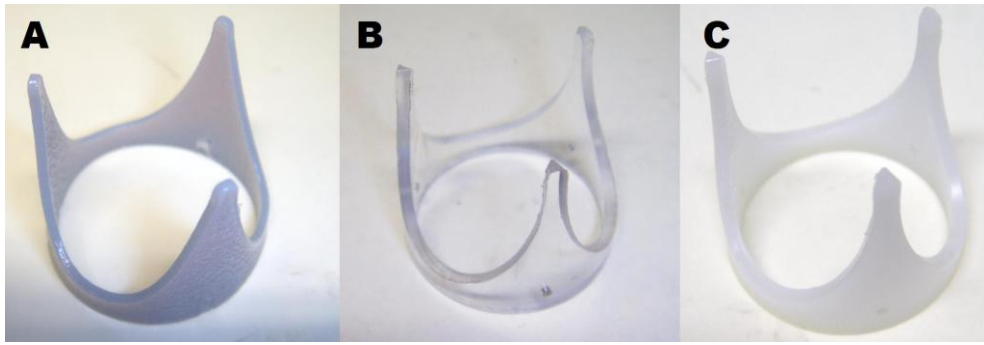


Figure 8.2 - Rigid stents used (a) rapid prototyping, (b) clear polycarbonate stent and (c) Delrin stent.

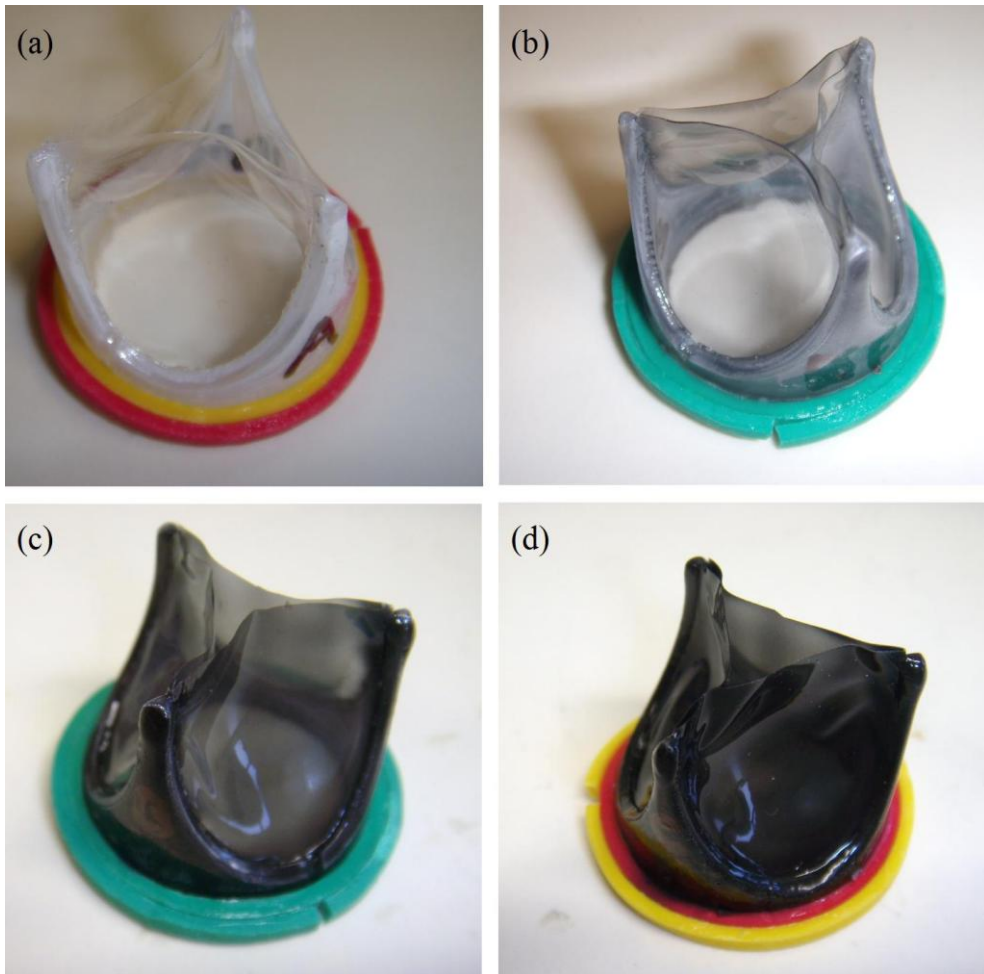


Figure 8.3 - Developed valves (a) clear polymer, (b) 0.125% 95A-MWNT, (c) 0.5% 95A-MWNT and (d) 1.0% P5A-MWNT.

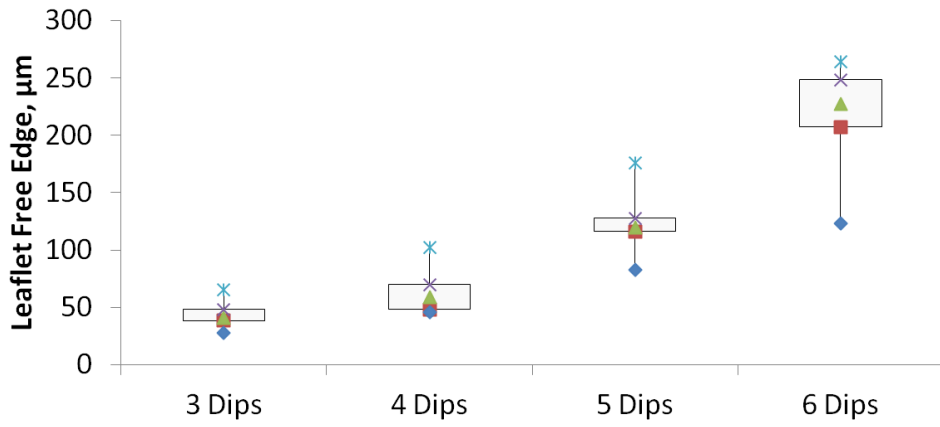


Figure 8.4 - Thickness distribution of the free edge of leaflets.

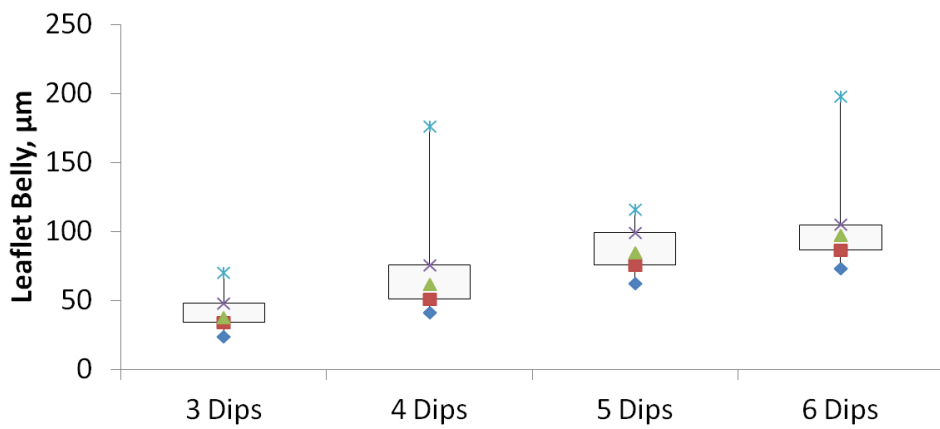


Figure 8.5 - Thickness distribution in the belly region of leaflets.

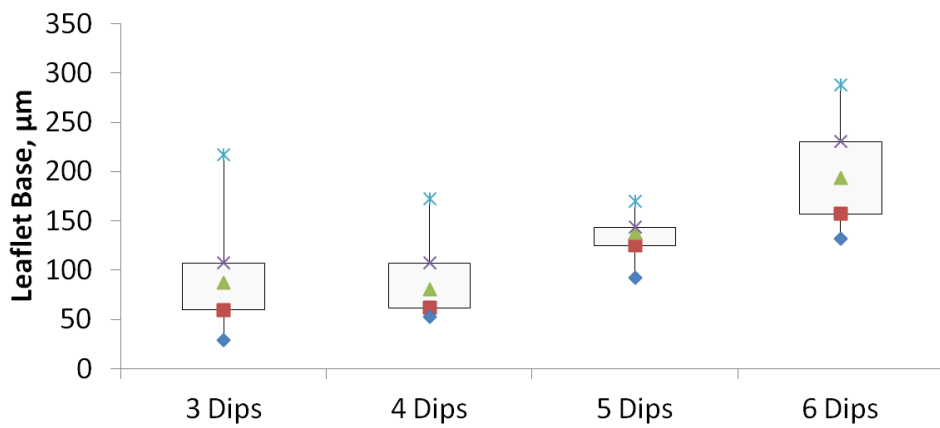


Figure 8.6 - Thickness distribution at the base of leaflets.

8.2 DURABILITY TESTING

In accordance with testing standard ISO 5840:2005, prosthetic heart valves are required to endure at least 200 million cycles for bioprosthetic valves and 400 million cycles for mechanical valves. Uni-axial tensile fatigue testing can help provide comparable information on the durability of several materials. However, it cannot factor in other parameters such as the stent-leaflet interface, stent flexibility and bi-axial leaflet flexion which all contribute to the durability of the valve. Accelerated fatigue testers, also known as durability testers are functioned to cyclically load the valves at several times their normal rate to achieve the desired cycles within several months rather than years. These systems can provide harsh environments for the prosthetic valve including cavitations and water hammer effects. Additionally, variability in different test models as well as variability in the fluid medium, temperature and frequency can lead to incomparable results. However, these tests provide an opportunity to examine any design or material faults which may have been missed out in mechanical testing or modelling studies to allow re-design prior to in vivo testing.

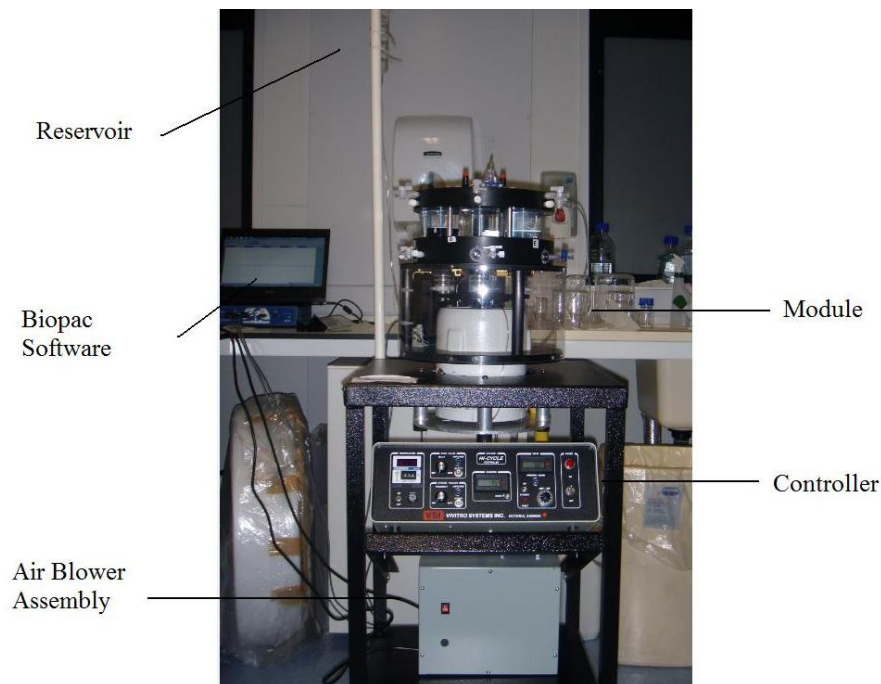


Figure 8.7 - General Vi-Vitro set up.

8.2.1 Set-Up

Durability testing was carried out on the valves using the ViVitro Hi-Cycle^{VSI} system which included a test module and an electronic controller. The test module consists of six chambers, enabling six valves to be tested at any one time. Each test valve is attached to a piston within each chamber filled with test fluid. A shaker plate connects 6 bellows to the piston rods, enabling the valves to oscillate in an upward and downward movement to flex the leaflets of the valves. The controller allows management of the frequency and amplitude of the drive and temperature control of the test fluid. It also includes an accumulated cycle counter and output for stroboscopic observation.

A blower assembly unit was developed to keep the system cool during cyclic loading. This consisted of a 155 cu.m/h centrifugal air blower (R.S. Components Ltd, UK) encased in a 7" x 8" x 10" steel enclosure box with a filter attached to the inlet and the outflow connected to the electrodynamic shaker by a rubber hose.

The durability tester was dormant for some time and therefore needed to be re-commissioned. The old silicone bellows had dried out and become brittle causing surface cracking and leakage and were therefore replaced with softer silicone bellows. The piston rods were then realigned to prevent chafing of the piston on the walls of the chambers. The valves were then mounted onto the piston rods by a piston cap and a silicone rubber ring which was casted from a stent with an annular ring (Figure 8.9). The chamber was filled with distilled water and allowed to heat to 37 °C. The stiffness of the polymeric leaflets decreases at high temperatures enabling them to coapt at low stresses. The system was run briefly to dislodge bubbles to the top window which were then removed through a syringe. The system was then left on standby for a few days to enable complete bubble dissipation.

A fluid reservoir fitted approximately 70 cm above the test module enables a positive pressure head to be maintained throughout the test. This was filled to a 50 ml level and capped to prevent evaporation. The pressure was measured using two blood

pressure transducers connected to the upper and lower luer ports of the test chambers and monitored using the Biopac Acquisition software. Two of each 0%, 0.5% and 1.0% MWNT/Polyurethane valve were mounted evenly to distribute the load on the shaker plate. Testing standards according to ISO 5840:2005 require that a transvalvular pressure gradient of 90 mmHg needs to be maintained for a minimum of 5% of each test cycle and for 95% of the total number of cycles.

Cyclic testing was carried out at 12 Hz (720 bpm) and the system was tuned by adjusting the amplitude of the pistons and the resistor on each chamber to achieve a pressure drop of 90 mmHg. If failure in one of the valves occurs, the pressure difference across the remaining valves increases to compensate for the load which may accelerate failure in the remaining valves. Therefore, tuning needed to be re-evaluated to ensure that the remaining valves functioned at the correct load.

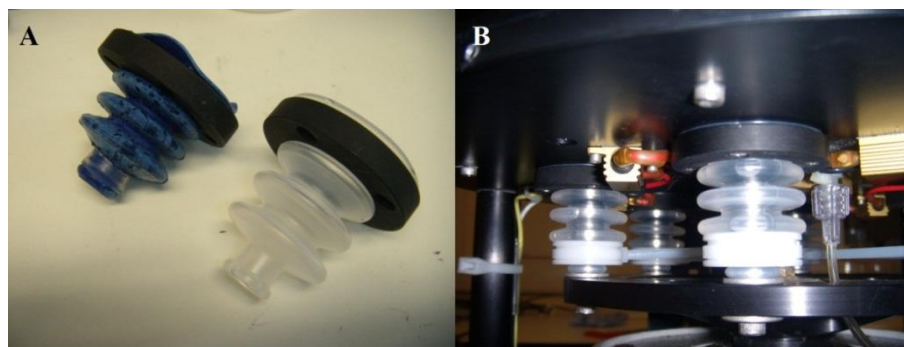


Figure 8.8 - Bellow replacement on durability tester (a) brittle old bellow (blue) alongside a softer new bellow (transparent) and (b) mounted on tester.

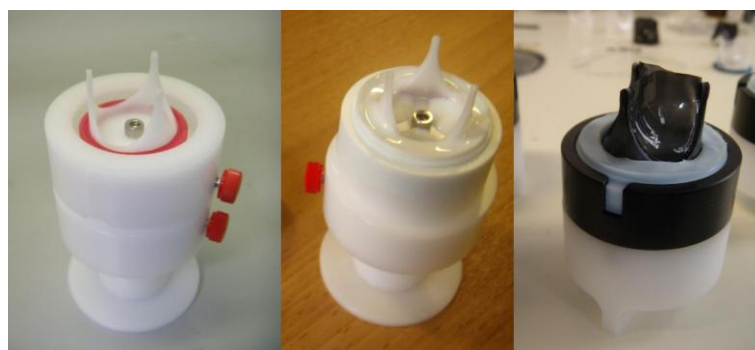


Figure 8.9 - Silicone ring mould with a valve-less stent before (a) and after (b) application of silicone. (c) Valve mounted in piston cap.

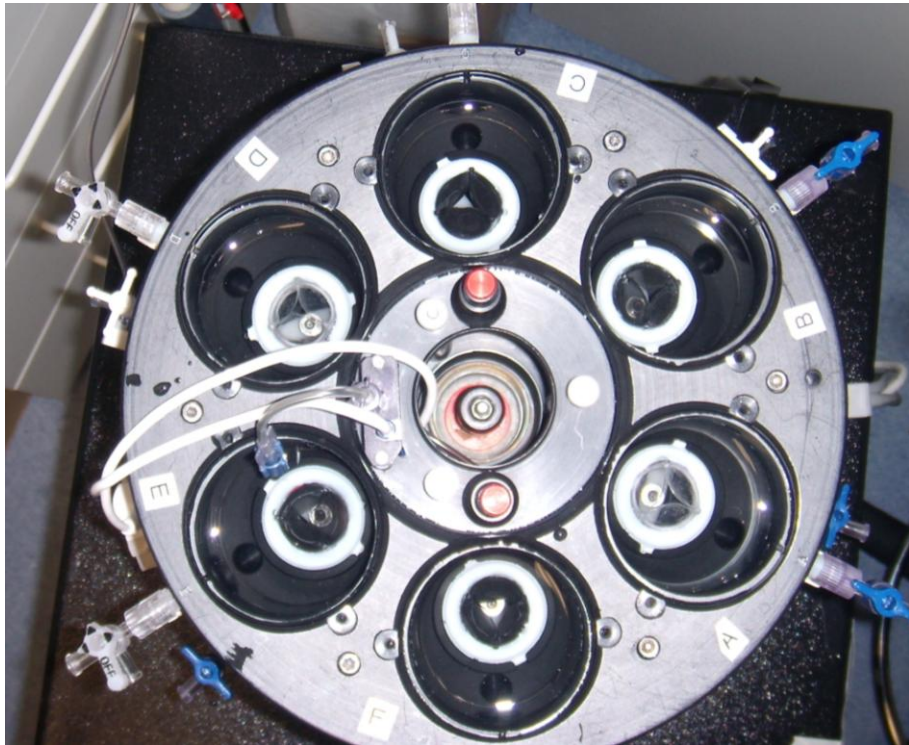


Figure 8.10 - Top view of Vi-Vitro tester with all 6 valves in situ.

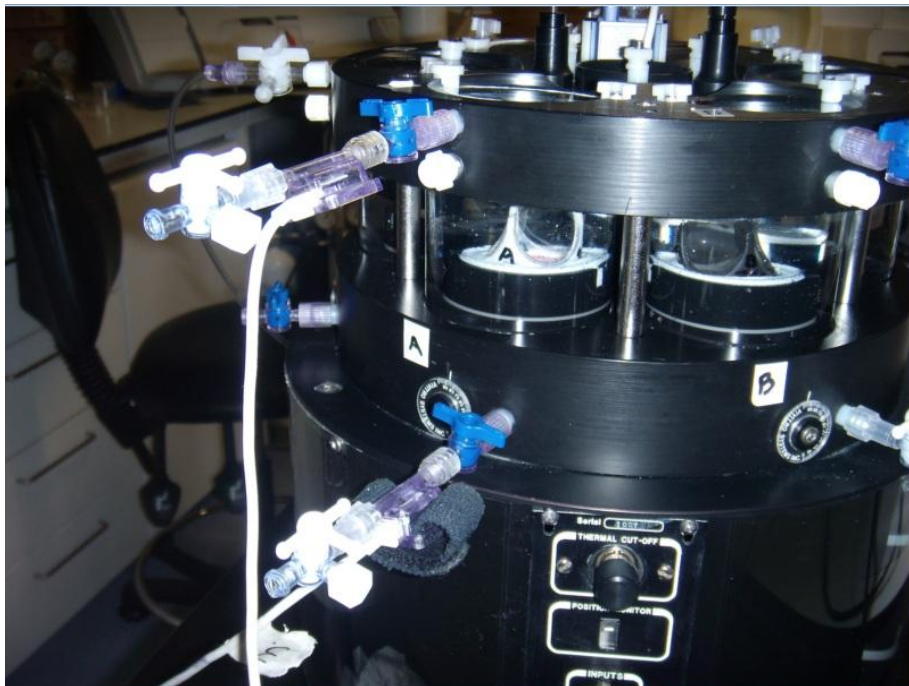


Figure 8.11 - Pressure transducers mounted to top and bottom of valve chambers.

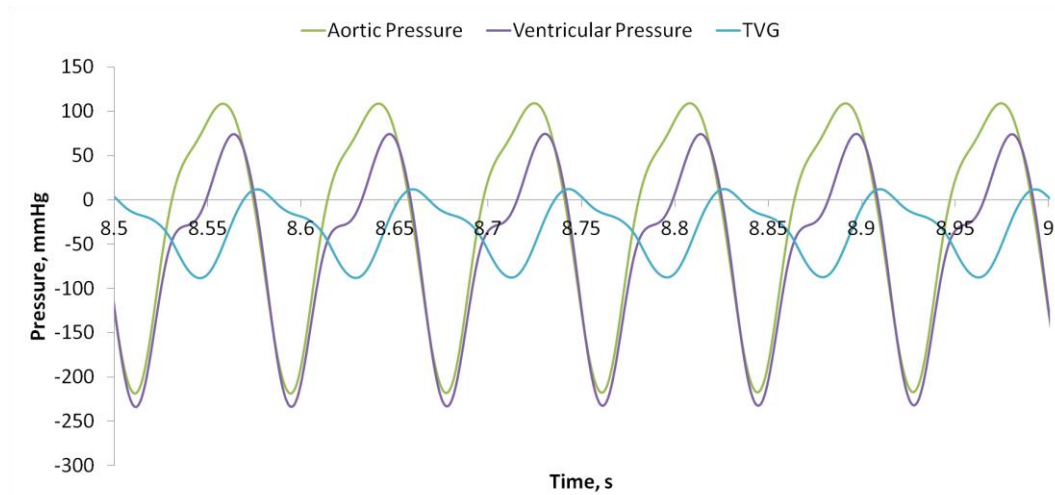


Figure 8.12 - Typical pressure curves in HiCycle chamber displaying a 90 mmHg pressure drop. TVG – transvalvular gradient.

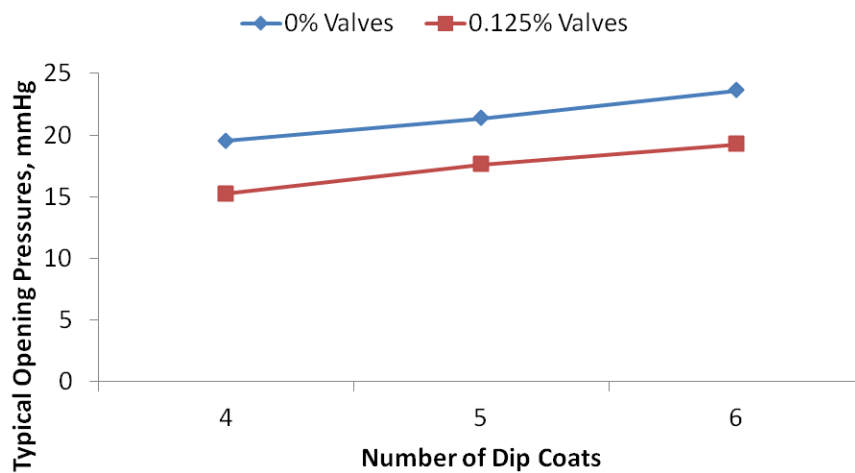


Figure 8.13 - Typical opening pressures of 0% and 0.125% 95A-MWNT valves with varying number of coats.

Several problems were encountered with bubbles and leakage within the chambers during testing. This was more prevalent when all six valves were tested as the amplitude of the pistons needed to be as high as 7 mm to allow a pressure gradient of 90 mmHg to be established. Therefore comparative tests of a neat and composite valve were carried out, using two chambers rather than all six to reduce the complications. A slight increase in opening pressures was noted with increasing

leaflet thickness (Figure 8.13). The neat polymer valve appeared to have a higher opening pressure than the composite valve although this may be attributed to the composite valve having slightly thinner leaflets.

8.2.2 Valves with the Delrin Stent

The initial test valves were formed from 3 dip coats in the polymer on a Delrin stent and peeled off the stent at the commissures within 10 minutes of testing (less than 10,000 cycles). Following these findings, the stents were sanded down to increase the contact surface area between the polymer and stent. However, the leaflets were also found to peel off the commissures in some of these stents. This occurred in all cases except for the 1% MWNT/Polymer valves where the leaflets remained attached to the stent but had ruptured vertically along the middle. It is likely that this rupture was due to thinning of the leaflets at the belly region where the surface was at its highest degree of curvature. Additionally, small bubbles in the leaflets may have created weak interfaces. Failure in all these valves occurred between 200,000 and 800,000 cycles. SEM images of the leaflets of the failed valves were taken to determine cause of failure.



Figure 8.14 - Initial failure modes of valves with a Delrin stent; leaflet de-bonding from stent.

Finally, the Delrin stents were coated in a harder grade PCU, dried and then dipped in the respective polymeric solution prior to mounting on the former and dip forming the leaflets. These valves were dipped 5 times to create a sufficiently thick valve. The valve survived 4.4 million cycles before a small tear was noticed in one of the

leaflets. During cyclic testing, the stent posts could be seen to flex inward and outwardly which helped reduce the stresses at the leaflet-stent interface.

SEM images are shown below of the valves which peeled off at the stent posts. The leaflets near the stent post region appeared to exhibit severe thinning and an uneven thickness distribution. Thinning was particularly evident in Figure 8.15c, which appeared to have a thickness less than 10 μm .

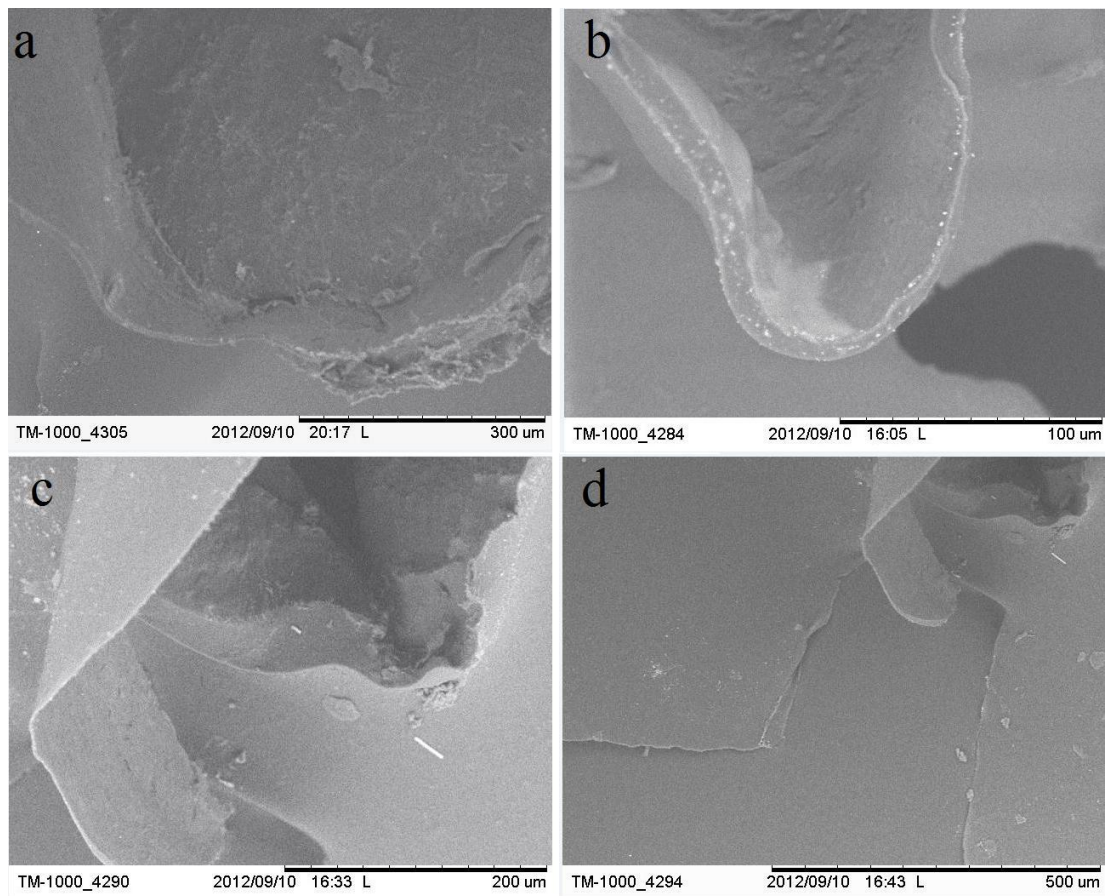


Figure 8.15 - SEM images of failed samples around the stent post region; (a)-(b) 0% and (c) 1.0% valves, (d) free edge at stent post.

An attempt was made to determine the effect that polymer hardness has on the durability of the valve leaflets. Carbothane PC3585A was used to produce two valves having 5 dip coats each; in an effort to see if a softer material being susceptible to

larger deformations would enable leaflet coaptation with less stress. In both cases, the valves were found to fail below 800,000 cycles. Therefore valves were developed and tested from a harder grade of Carbothane (PC3555D) having a Shore hardness of 55D and a valve with this polymer, having a thickness of 130 μm has endured 23 million cycles to date.

8.2.3 Valves with Polycarbonate Stents

Valves with polycarbonate stents were tested to avoid the initial complications of peeling with the Delrin stents as they had better adhesion with the polyurethane due to the polycarbonate having little solvent resistance to DMAc. However, the valves also ruptured along the middle of the leaflet which may be due to clusters of the nanotubes or due to the leaflet being too thin. In other instances, the polycarbonate stent fractured down the base at its smallest thickness. This occurred due to cracking that had been caused by the solvent during the dip coating process. This problem was overcome by increasing the thickness of the base of the stent by 2 mm. Failure in 3 and 4 dip coated valves lead to the production of 5 and 6 dip coated valves with thicknesses of approximately 80-120 μm and 200-300 μm respectively. These valves all failed due to a fracture at the stent posts with the exception of the 5 dip coated 0.125% MWNT valve which developed a tear near the base region at the leaflet-stent interface.



Figure 8.16 - Primary failure mode of valves with a polycarbonate stents; leaflet rupture across belly region.

It was realised that the rigidity of the stent prevented the posts from deflecting inwardly during cyclic testing which created leaflet strains and eventual ruptures particularly at their base. Additionally, with the thicker leaflets, a large strain was placed on the stent posts to deflect inwardly which lead to their fracture at around 2 million cycles (~20 days). These findings highlighted the importance of having a stent that is flexible enough to flex inwardly but not too soft that permanent deformation occurs due to creep.

SEM images taken of the failed valves showed very porous edges at the leaflet-stent interface which may have been the cause of failures at the stent post. It is possible that the solubility of the polycarbonate stent allowed it to react with the dipping polymeric solution, creating a brittle interface.

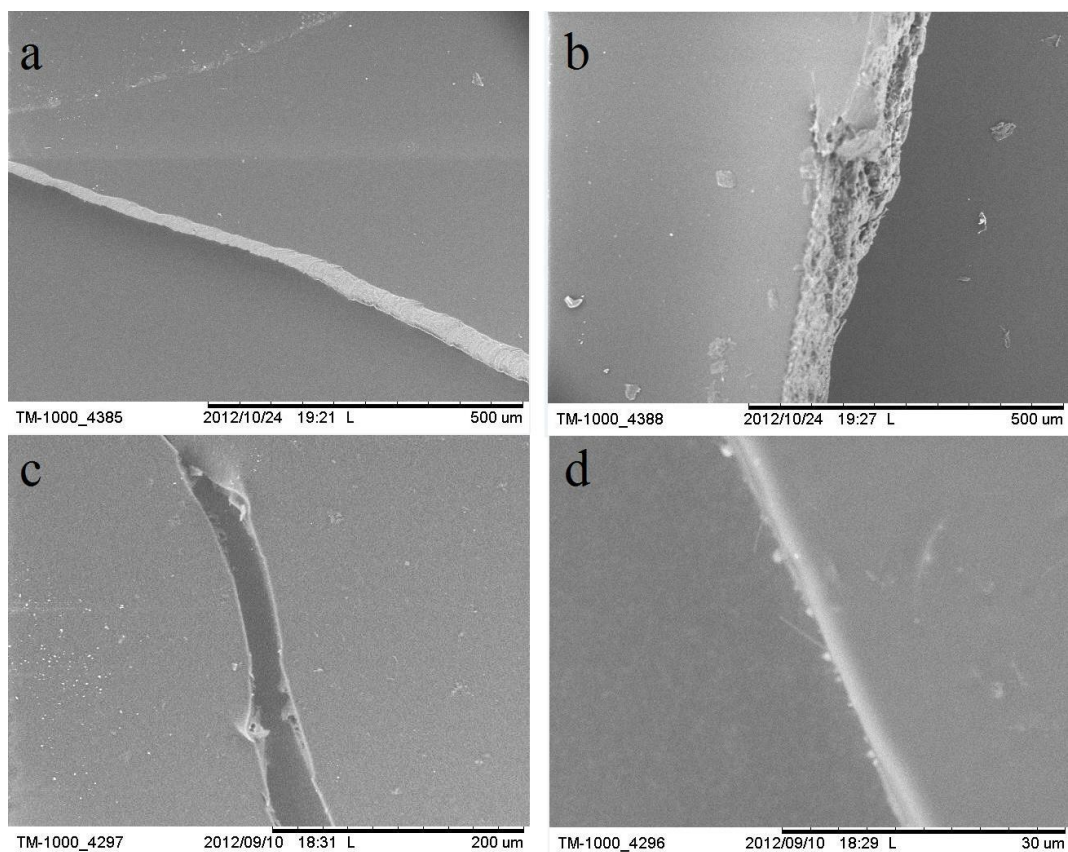


Figure 8.17 - Failed 0% (a-b) and 1% (c-d) MWNT valves with leaflet ruptures (a) leaflet near base of valve, (b) at polycarbonate stent post, (c) split along the middle and (d) close-up of (c) with evidence of fibre pull-out.

From these preliminary findings, it appears that the carbon nanotube in concentrations higher than 0.125% can contribute to early leaflet failure. The Delrin stent has been found to be the more suitable for valve development due to its flexibility. The issue of leaflet de-bonding has been resolved by coating the stent prior to mounting on the former for dip-coating. A leaflet thickness of 5 dip coats of the PC3595A polymer with a coated Delrin stent was seen to produce the most durable valve to date, lasting 4.4 million cycles. Although a thicker belly region may compromise on leaflet flexion, it is considered necessary to prevent leaflet tears.

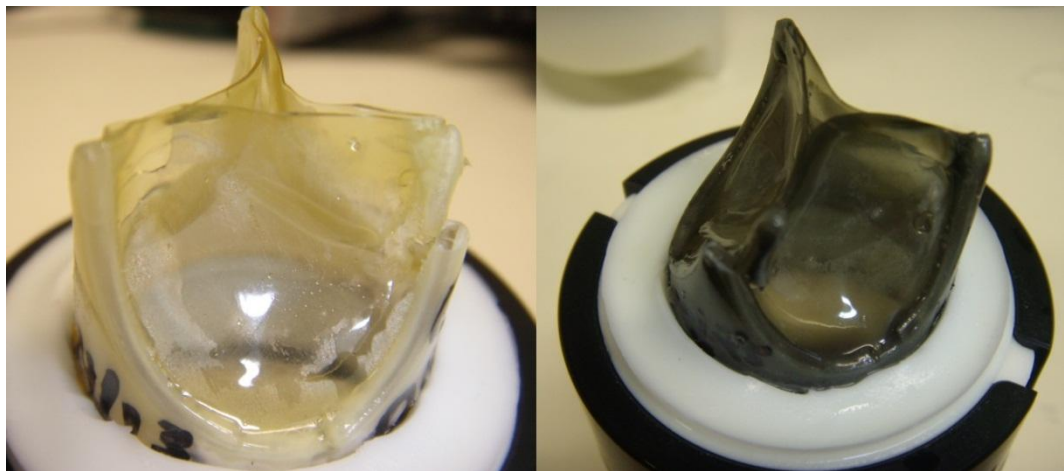


Figure 8.18 - Polycarbonate stent fracture with valves. Leaflet ruptured occurred as a secondary failure mode.

8.3 COMPUTATIONAL FLUID DYNAMICS

8.3.1 Introduction to Fluid Dynamics

Fluid dynamics relies on the ‘Laws of Conservation’ to identify the relationships between property variables of a fluid (Chandran et al. 2006). Flow is usually defined as laminar or turbulent depending on the Reynolds number, Re which is the ratio of the inertial force to the viscous force in fluid flow:

$$Re = \frac{\text{Inertial Force}}{\text{Viscous Force}} = \frac{\rho VD}{\mu}$$

Where,

ρ is the density of the fluid,

V is the average velocity,

D is the diameter of the pipe and

μ is the dynamic viscosity.

In laminar flow, Re is < 2100 and above this number the flow starts to become turbulent. Due to the no-slip boundary condition at the walls of the aorta, viscous forces slow down the flow of the layers adjacent to the wall to create a parabolic velocity profile. Therefore, in laminar flow the boundary layer thickens with time as the flow becomes fully developed (Figure 8.19). When the Re value is calculated for the ascending aorta, the Re would give a high value indicating turbulent flow. However, flow in the ascending aorta has been observed to be laminar and flat, partially due to the systolic accelerated flow creating stability (Temple et al. 1964, Chandran et al. 2006).

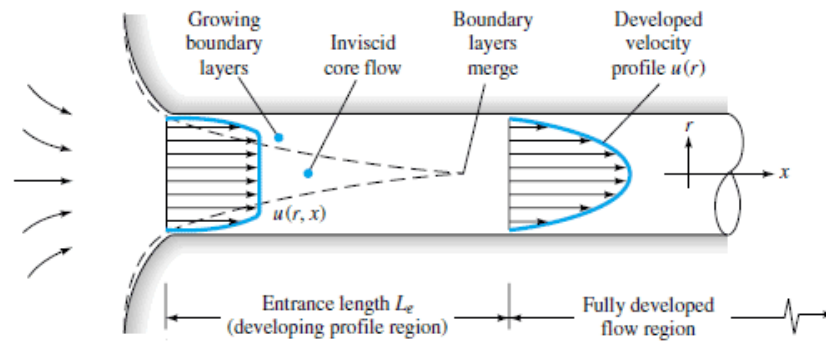


Figure 8.19 - Velocity profile of fluid in a pipe; flow is fully developed when the boundary layers merge. The initial plug velocity profile is like that of the aorta (www.learneasy.info).

A better representation of the pulsatile flow through the aorta would be given by the Womersley number, α :

$$\alpha = R \sqrt{\frac{\omega}{\nu}}$$

Where

R is the inlet radius of the aorta,

ν is the kinematic viscosity (calculated as the dynamic viscosity, μ / density, ρ),

ω is the angular frequency or heart rate

When $\alpha < 1.0$, as in small arteries, viscous forces dominate and the frequency is low enough to enable flow to fully develop. When it is larger than 1.0, inertial forces dominate and the flow has insufficient time to fully develop, leading to a flat velocity profile as is the case in the aorta.

Fluid flow can be described as steady or unsteady. In steady flow, the properties of the fluid do not change with time whereas in unsteady flow they do; as is the case for pulsatile blood flow and oscillatory flows. In pulsatile flow through the aortic valve, the velocity profile does not have a chance to fully develop thus leading to a flat, 'plug-like' profile with a very thin boundary layer.

Flow through a prosthetic heart valve can be likened to flow through a stenosed pipe. It is essential to determine the properties of the fluid as it exits the stenosed region for several reasons:

1. An increased ventricular work load may be created to overcome the increased resistance due to
 - a. a reduced effective orifice area and
 - b. an increased transvalvular pressure gradient
2. High shear forces will lead to an increased risk of haemolysis and platelet activation which can lead to thrombogenicity and calcification.
3. Disturbed flow patterns may affect the flow of blood several centimetres downstream of the valve.
4. An increased ventricular force may cause downstream migration of the percutaneous heart valve and,
5. Increase the possibility for paravalvular leakage.

With artificial valves, the leaflet structure, orifice area and geometry influence the flow profile. Complex fluid problems such as flow of blood in a valve or stenosed pipe can be solved through Computational Fluid Dynamics (CFD). Although CFD should never replace experimental studies, it is a very useful tool to implement when looking at preliminary design specifications and can save on costs when experimenting with several design parameters. For example step by step alterations can be carried out to the leaflet shape, commissural height and stent angle to optimise the valve without having to manufacture a prototype for each design alteration. Additionally, data on pressure, velocity and shear forces can be collected in a matter of hours, thereby saving on time that would have otherwise been spent in the laboratory.

CFD relies on a series of governing Navier-Stokes equations to solve complex fluid dynamic problems. The model of the fluid is discretized into a series of finite volumes to form a mesh and generally, the finer the mesh the more accurate a solution to the fluid problem. However, a finer mesh leads to an increased CPU time

so a balance between the mesh density and processing time needs to be established. This is usually achieved by running the simulation across various mesh densities until a negligible difference in the results between one mesh density and another is observed. The boundary conditions of the fluid are then applied and the model is run using a CFD software package such as Ansys Fluent.

In the following sections, two 3D fluid problems were solved using Fluent. The first problem looked into the influence that leaflet curvature has on the flow properties and was modelled as a steady flow. In the second model, an unsteady velocity profile was inputted to examine how the flow changes with time downstream of the valve. In both cases, the blood was modelled as an incompressible Newtonian laminar fluid, having a viscosity of $0.004 \text{ pa}\cdot\text{s}$ and a density of 1060 kg/m^3 (Formaggia et al. 2009). Blood is non-Newtonian meaning that its properties are dependent on the shear rate due to the deformability of the cells. However, blood flowing through large arteries can be considered to behave as a Newtonian fluid since the diameter of the blood cells are significantly smaller than the diameter of the vessel, allowing viscosity to be almost independent of shear rate.

A preliminary solver was defined for a steady flow problem with an initial inlet velocity of 0.4 m/s . A low initial velocity was used to ensure the stability of the iterative solution process. The volume mesh was refined to interval sizes of 0.8, 0.6 and 0.4 compared to the original interval size of 1.0 and the results from the preliminary simulations were used to determine the optimal grid size to use. The results appeared to deviate from the original grid size which may imply that a finer mesh introduces errors such as skewed elements. Skewed elements were particularly problematic with the curved leaflet valve compared to the flat. Therefore it was decided to stick with the original grid dimensions.

8.3.2 Steady Flow through a Valve

Two three-dimensional models were created of a valve enclosed in a pipe having a diameter of 22 mm and a length of 40 mm. In one of the models, the valve had

leaflets in the circumferential direction only and in the other valve, the leaflets were curved in both the radial and circumferential directions. Both valves were modelled in an open configuration, having the same aperture cross-sectional area and leaflet thickness. The aim was to determine if leaflet curvature in the radial direction influenced the flow rate and shear stress, since high shear forces can activate thrombus formation and early calcification.

A pipe was created around the valve to enable inflow and outflow boundary conditions to be set, which would represent the ventricular and aortic outflow tracts respectively. A hybrid mesh with predominately tetrahedral volume elements was then created for both models using Gambit meshing and modelling software. A total of 73,819 elements were defined for the valve with the flat leaflets and 54,107 elements for the curved leaflet valve. The meshes were imported into a computational fluid dynamic (CFD) package; Ansys Fluent v6.3.

A velocity of 1.35 m/s corresponding to the maximal peak velocity of flow obtained from Chandran et al. (2006) was applied at the pipe inlet. Operating pressures were assumed to be 0 mmHg and gravity was neglected. The model was considered solved when the residual difference between iterations was less than 1×10^{-4} .

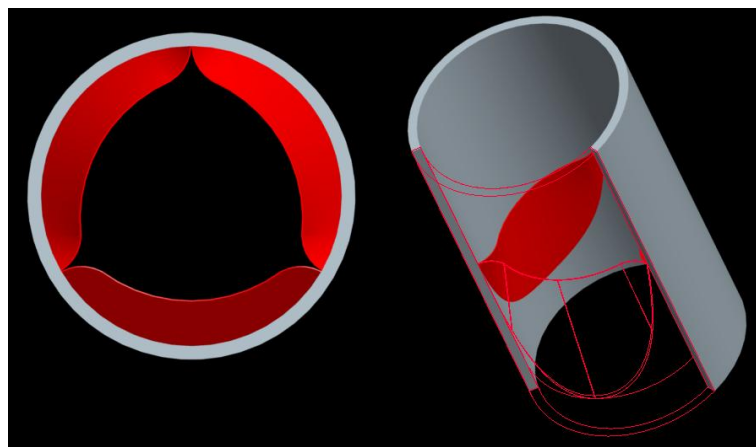


Figure 8.20 - Top and isometric view of the valve in pipe model with leaflets flat in the radial direction. Third of valve hidden in isometric view to show leaflets.

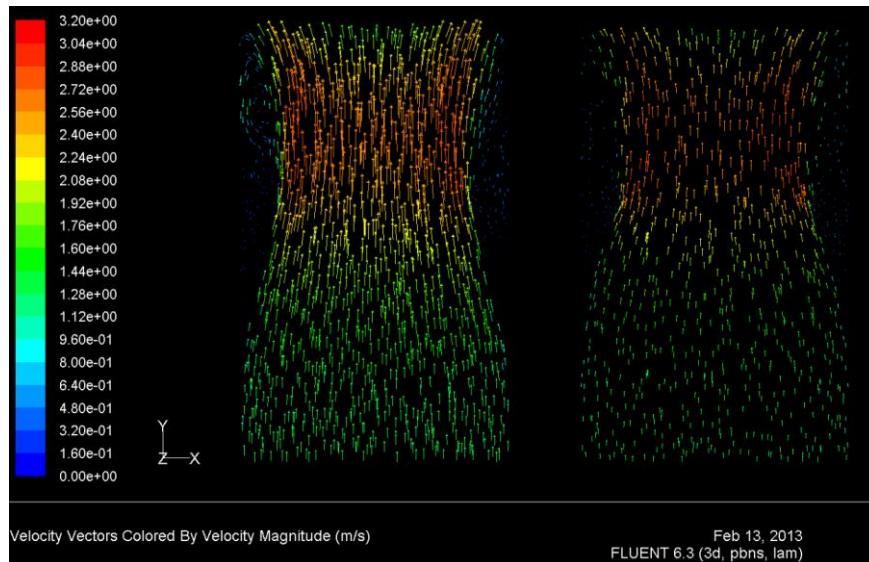


Figure 8.21 - Velocity vectors of flat and curved leaflet at a cross-section of the pipe at $z=0$.

The vectors of the velocity magnitude are shown in Figure 8.21 at a cross-section of the pipe at $z=0$ for both the flat and curved leaflets. The velocity vectors were modelled at the same scale; however the curved leaflets appear to have fewer vectors. A vortex formation is observed in the flat leaflets downstream of the valve which is not apparent in the curved leaflets. The peak velocity reached is also slightly lower in the valve with the flat leaflets at 2.88 m/s compared to 3.13 m/s in the curved leaflets.

Assuming a conservation of mass:

$$\frac{A_1}{A_2} = \frac{V_2}{V_1}$$

Where A_1 and V_1 are the area and velocity at the inlet, and A_2 and V_2 are the area and velocity of the *vena contracta*, which is the narrowest point of the downstream flow. Assuming that the maximum velocity is at the *vena contracta*, this equation can be used to determine A_2 from the results of the flat and curved models to be 1.78 cm² and 1.64 cm² respectively.

The contours of the total pressure are shown in Figure 8.22 taken at a cross-section of the pipe at $z=0$. It can be seen that the pressures on both the interior and exterior of the valve walls are slightly higher with the flat leaflets compared to the curved.

The Bernoulli equation (neglecting gravitational forces) states that:

$$\Delta P = p_1 - p_2 = \frac{1}{2}\rho(V_2^2 - V_1^2)$$

Thus from the velocity data, the change in pressure can be calculated from the above velocities to be 25.7 mmHg and 31.7 mmHg for the flat and curved leaflets respectively.

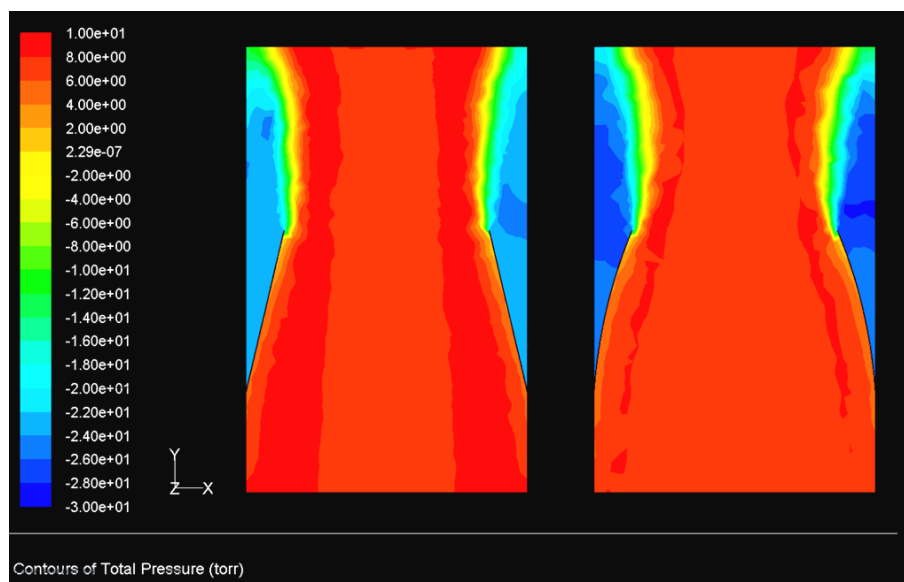


Figure 8.22 - Pressure contours of flat and curved leaflet at a cross-section of the pipe at $z=0$.

The shear stress at the leaflets of the valves is shown in Figure 8.23. It can be seen that although the stresses appear to be higher in the curved leaflets, the stress regions are much more concentrated compared to the flat leaflets. On the other hand, because the stress is concentrated, it leads to a higher shear stress gradient which can potentially cause weak points. It would be better to evenly distribute the load across the entire leaflet surface. Figure 8.24 shows the contours of shear stress on the

leaflets of the flat valve. It can be seen that the highest points of stress are at the commissures and free edge.

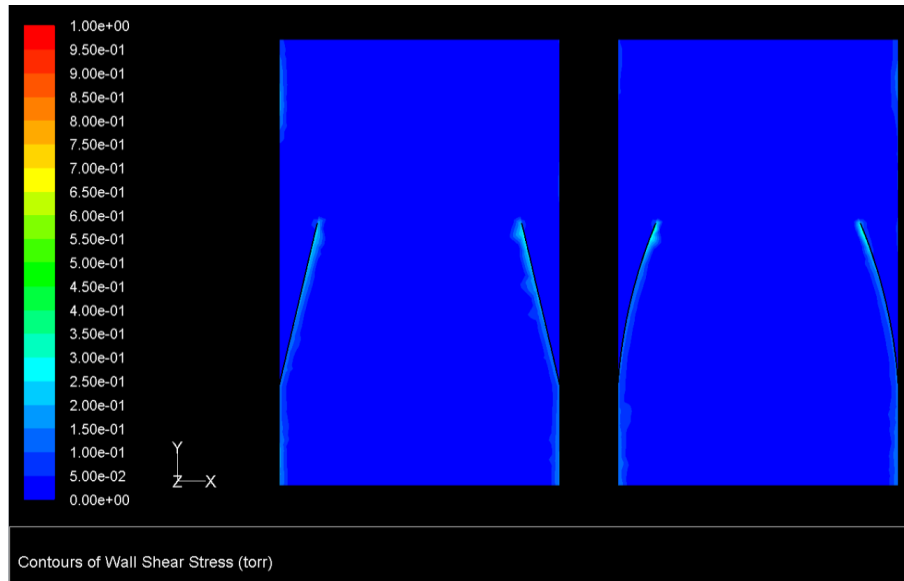


Figure 8.23 - Shear stresses across walls in flat and curved leaflets.

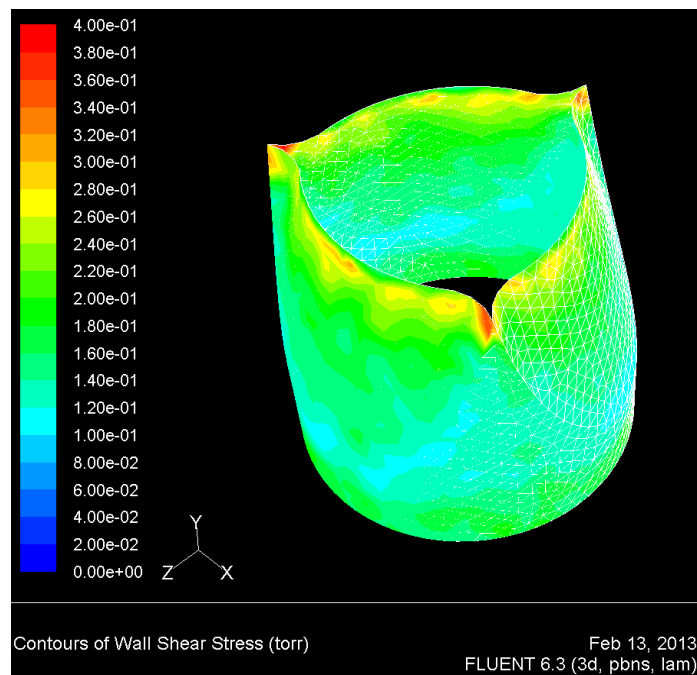


Figure 8.24 - Contours of the wall shear stress in the flat valve.

8.3.3 Unsteady Flow through a Valve

It was also desirable to determine flow behaviour changing with time through an open valve. Additionally, from the images of the steady flow study, it can be seen that flow has not fully recovered downstream of the pipe at a length of 40 mm. The length of the pipe of the flat valve model was therefore extended to 70 mm from the leaflet base in Gambit.

A time-dependant user defined function (UDF) for the velocity inlet of blood was defined as:

$$v_y(t) = 1.35 \sin\left(\frac{\pi}{0.280} t\right)$$

Where $v_y(t)$ is the velocity magnitude in the y axis. This enabled a parabolic velocity profile to be created, with a peak velocity of 1.35 m/s at 140 ms and a systolic cycle period of 280 ms. This was calculated as being approximately a third of the cardiac cycle. Atmospheric and operating pressures were defined as 0 mmHg and gravity was neglected. The iteration of the unsteady flow of blood was carried out with a time step of 0.0028 seconds and 20 times steps per iteration. This enabled the solution to converge to a residual of $<10^{-3}$ per iteration which would enable it to be considered solved. Images of the total pressures, velocity magnitudes and shear stress at the inflow and outflow and the velocity magnitude were taken periodically at 0.14, 0.21, and 0.28 seconds of the flow time.

The maximum facet values for the total pressure across the inlet, and valve and pipe outlets are shown in Figure 8.26. The pressure drop obtained using Bernoulli's equation was found to be 27.1 mmHg which is only slightly higher the value obtained for the steady flow model. However from the maximum facet data, the peak pressure drop was calculated to be 8.2 mmHg as the blood flows through the open valve.

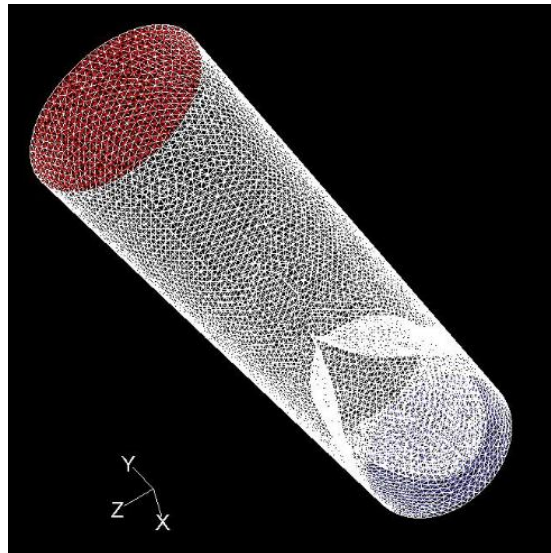


Figure 8.25 - Fluent grid model of the valve in pipe with a velocity inlet (blue) and pressure outlet (red).

The maximum velocity of the blood is shown in Figure 8.27 as it exists at the valve and at the pipe outlet. It can be seen that the velocity peaks at the valve outlet to 2.94 m/s and remains slightly higher at the pipe outlet. This shows that even 70 mm downstream of the pipe where the velocity decreases as the area increases, the velocity still remains slightly higher than it was at the inlet. Images of the velocity profiles across the pipe through its cross-sectional area at $z=0$ are shown in Figure 8.29. These images implicitly highlight how flow downstream of a valve is not symmetrical and is in fact complex. Therefore is it essential to model the valve and pipe in 3D and complete, rather than in 2D or mirrored through a plane of symmetry, to provide a more accurate representation of the flow patterns.

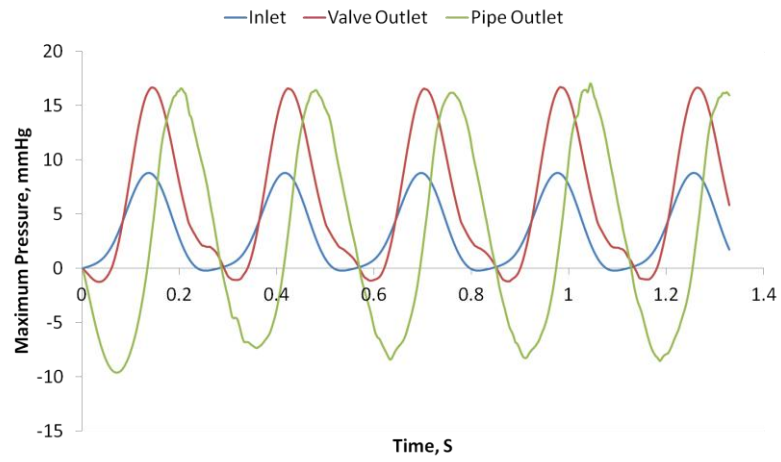


Figure 8.26 - Maximum facet total pressure in mm of mercury at the inlet, and valve and pipe outlets.

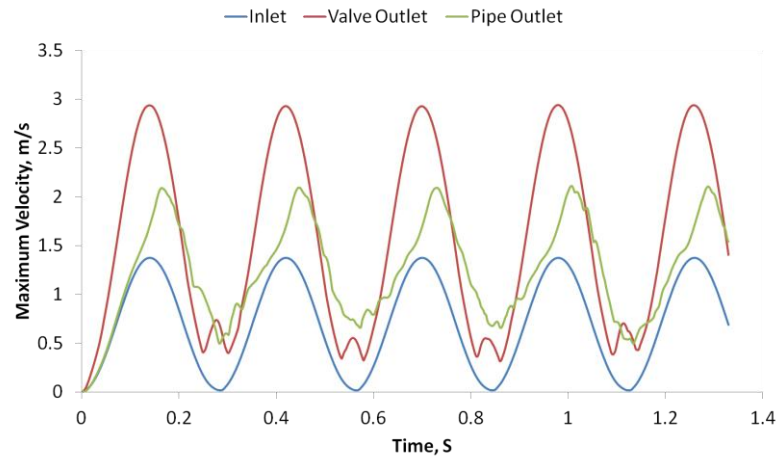


Figure 8.27 - Maximum facet velocity in m/s at the inlet and valve and pipe outlets.

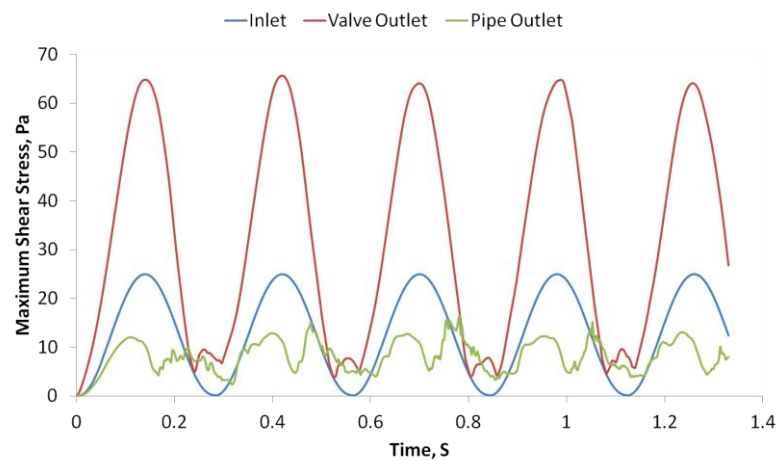


Figure 8.28 - Maximum facet shear stress in Pascals at the inlet and valve and pipe outlets.

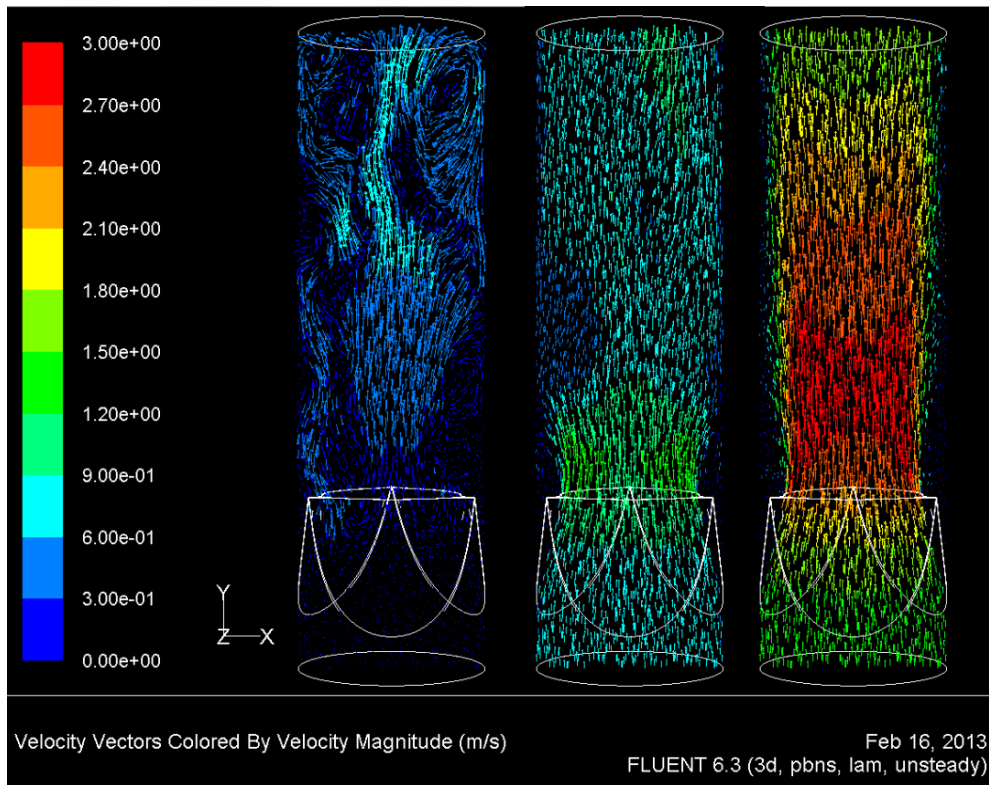


Figure 8.29 - Velocity magnitude at an iso-surface of $z=0$ for times of 280 ms, 350 ms and 420 ms

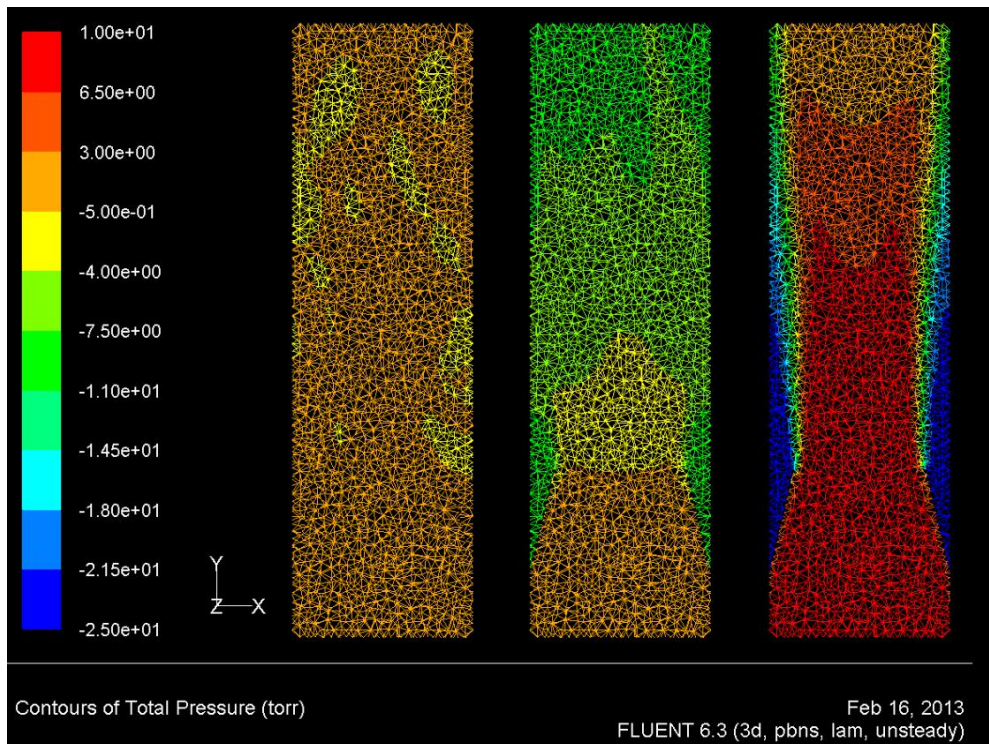


Figure 8.30 - Pressure and velocity profiles at at an iso-surface of $z=0$ for times of 280 ms, 350 ms and 420 ms.

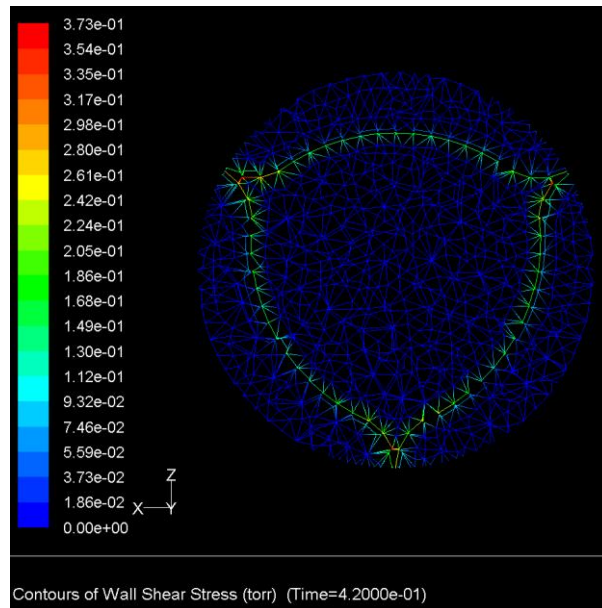


Figure 8.31 - Contours of wall shear stress (mmHg) at valve outlet.

From the data of maximum facet values (Figure 8.28), the maximum shear stress was 65.5 Pa when velocity was at a maximum. This was just over 2.5 times the shear stress at the inlet. The contours of shear stress at the valve outlet at maximum velocity (when $t = 420$ ms) are shown in Figure 8.31 and can be seen to be greatest at the commissures. This is likely due to the narrowed region of flow through the leaflets at the stent post and the initial point for haemolysis and platelet activation. Based on the maximum velocity, the calculated orifice area was observed to be 1.91 cm^2 .

8.3.4 Model Limitations

There were several limitations to the models in this work:

1. The aortic diameter was assumed to be circular although anatomically, it is asymmetrical and this would influence the flow. Additionally, the sinuses had been eliminated which prevented the flow from forming vortexes behind the leaflets.
2. The valve was only modelled in an open configuration so diastolic flow was not observed.

3. A more accurate representation would be to carry out a fluid structure interaction (FSI) model which would allow hemodynamic evaluation of the fluid flow as the valve opens and closes during the cycle. This will also enable the model to factor in the aortic wall elasticity which would influence flow and help determine valve opening and closing times.
4. The gravitational and operational forces were neglected.

8.4 DISCUSSION

Dip coated valves were developed having thicknesses ranging from 30 μm to 250 μm . Despite trying to ensure an even coat was applied to each leaflet by levelling the former using a bubble level, variations in thickness between the three leaflets were still observed. However, the aperture of the valve when open and coaptation when closed appeared to be almost symmetrical. The only exception was the 6 dip coated valves which did not coapt symmetrically and this may be due to their exceptionally high thicknesses. D'Souza et al. (2003) examined the bending strains on polyurethane heart valves during accelerated tests and found one leaflet to always deform more greatly than the others.

The largest contributing factor to the failure of the valves was due to leaflet debonding at the stent posts of the Delrin stents. SEM images showed severe thinning of the leaflets at the commissures which contributed to their detachment from the stent. This issue was resolved by completely coating the Delrin stents initially in a harder polymer, then again in the leaflet polymer prior to mounting on the former. This led to a significant increase in durability by up to 4.4 million cycles, which was more than twice the durability of the previous valves.

Two features of the valve contribute significantly to its failure; the commissural region and the belly region as they bear a greater portion of the load. Leaflets formed through the current dip coating technique are significantly thinner in the belly region

compared to the base and free edge. Future work will focus on developing a thicker base, perhaps by increasing the number of coats produced in the upward position or by using a more concentrated solution. Stent flexure was found to be fundamental to the durability of the heart valves and this was evident from the fracture of the rigid polycarbonate stents at the commissural interface.

The mathematical model was able to show the influence of leaflet curvature on flow behaviour. Despite both valves having the same aperture and leaflet thickness, the leaflets that were curved radially had a reduced effective orifice area and an increased transvalvular pressure gradient compared to the flat leaflet valve. Additionally, the shear stresses across the walls of the valve were evenly distributed in the flat leaflets whereas they were concentrated at the commissures of the curved leaflets. However, the pressures were reduced in the curved leaflet compared to the flat valve. This may be due to the increased surface area of the curved leaflet.

Lim et al. (2004) conducted a finite element analysis (FEA) on the von Mises stresses across 4 leaflets with varying curvatures in the circumferential region. The flat leaflet was found to exhibit the greatest degree of stress at the commissures due to the excessive strain required to enable complete coaptation. An increase in the leaflet curvature lead to an increased surface area which reduced the von Mises stresses in the belly region. This led the authors to suggest that the belly region of the leaflet bore an effective part of the load. This would agree with the findings from the valve durability tests carried out in this thesis since the ruptures in the leaflets originated at the belly region.

Dywer et al. (2009) looked into a CFD model of transcatheter aortic valves which had degenerated due to stenoses. The authors found that a reduction in the orifice area by 35% and 78% lead to a increase in ventricular force of 63% and 86% respectively. They reported higher values for the wall shear stress of 87 Pa and 115 Pa respectively, compared to 65.6 Pa reported here. The authors also found that the systolic force due to an increased ventricular load caused by stenosis to be only a third of that in diastole and would therefore be unlikely to cause stent migration.

Polyurethane is strain rate dependant and this viscoelastic nature is likely to influence the fatigue life depending on the rate of cyclic testing. D'Souza et al. (2003) found the leaflet free edge of polyurethane heart valves to be independent of the cyclic rate. However, the bending strains at the belly region of the valves were found to increase with increasing heart rate, mainly as leaflets were more constrained at the belly than at the free edge. This implicates that accelerated testing on polymeric heart valves may lead to accelerated fatigue due to its dependence on strain and time.

8.5 CHAPTER SUMMARY

1. Dip coated valves were developed having varying thicknesses from 30 μm to 250 μm .
2. With the exception of the 0.125% 95A-MWNT valve, the 0.5% and 1.0% valves did not survive beyond 1 million cycles (10 days) in the fatigue tester.
3. Durable valves can be developed by coating Delrin stents prior to dipping with the former and by applying a sufficient number of coats. 5 coats were found to produce durable leaflets whilst still remaining relatively thin compared to bioprosthetic valves.
4. The durability of the leaflets can be extensively improved by using a harder grade of polyurethane and a reasonably thin leaflet with this polymer has achieved 23 million cycles to date.
5. Mathematical models have highlighted that leaflet shape plays a large role in determining the flow behaviour downstream of the valve.

CHAPTER 9:

DISCUSSION AND CONCLUSIONS

9 DISCUSSION AND CONCLUSIONS

9.1 DISCUSSION

The aortic valve is subjected to well over 100,000 cycles a day and 3.7 billion cycles in a lifetime, enduring harsh hydrodynamic environments to ensure unidirectional flow of blood within the heart. The elastin fibres in the native valve enable the leaflet to stretch radially with minimal stress and the collagen fibres provide the mechanical integrity and commissural support to the valve. The valvular interstitial and endocardial cells work together in a complex manner to regulate the constituents of the valve (Butcher and Nerem 2006). When designing a prosthetic heart valve, one aspires to develop a valve that is as durable and as functionally similar to the native valve as possible; for example by having a low pressure drop in forward flow, minimal regurgitation, low energy loss, and low thrombogenicity. Although it is extremely difficult to achieve a leaflet that is as adaptable as the native valve, certain features of the valve are sought. For example, achieving a durable leaflet with improved hemodynamic flow compared to the diseased valve or a leaflet with a reduced propensity to calcification. The development of artificial heart valves has progressed from the initial concepts of a ball and cage valve, to pyrolytic carbon mechanical valves such as the tilting disc and bi-leaflet valves (with a parallel development of glutaraldehyde treated xenograft aortic valves), to polymeric valves and finally percutaneous heart valves.

Transcatheter aortic valve intervention has enabled patients who are currently refused conventional surgery on the grounds of high risk or technical complications to become candidates for valve replacement. From their initial development in 1992, progress in TAVI has increased exponentially and clinical trials have highlighted the significance of reducing the profile of percutaneous heart valves to minimise post-procedural complications such as vascular bleeding. Delivery may also be complicated due to diseased or tortuous femoral arteries or in cases where a femoral pulse is absent (Heenan et al. 1996). Therefore it is desirable to steer away from the femoral artery and consider delivery through a super-peripheral access vessel such as

the radial or brachial arteries. Baseline data from literature has found the mean radial artery diameter to be 2.3 mm and the brachial artery to be 4.2 mm, measured using B-mode ultrasound or pulsed Doppler imaging (Safar et al. 1981). These dimensions would require an 8 Fr or 12 Fr sheath to be used for transcatheter delivery through the radial or brachial artery respectively. If the thickness of the stent is limited, then the profile needs to be reduced by decreasing the thickness of the leaflets.

Leading percutaneous heart valves such as the CoreValve and the Edwards SAPIEN valve are constructed from glutaraldehyde-treated allograft pericardium such as calf, sheep or horse pericardium. The thickness of pericardium limits the size of the valve in a compressed state, which presents a challenge in achieving a low delivery profile. Even porcine pericardium with an approximate thickness of 200 μm and being substantially thinner than bovine pericardium is still too thick to reduce the profile below 18 Fr. This makes them difficult to compress into a small vessel and limits their delivery to the larger femoral artery rather than a peripheral artery which is desirable in order to reduce vascular complications such as bleeding or to bypass delivery in tortuous arteries. From the test results in Chapter 4, it is clear that glutaraldehyde (GA) treatment increases the thickness of the pericardial tissue, as well as affects its mechanical properties by increasing its extensibility and decreasing the percentage stress relaxation. Pericardium is also prone to calcification due to their glutaraldehyde fixation and their method of attachment involving sutures creates regions for stress concentration.

Polymeric valves have shown promise of combining the durability of mechanical valves with the hemodynamics of bioprosthetic valves (Wheatley et al. 2000). Initial polymeric valve designs had complications with durability and calcification and were used predominately short term and in bridge-to-transplant devices such as LVADs and artificial hearts. However, improvements in material science have enabled the development of polymers with increased biostability and oxidative resistance. There is large potential in developing a polymeric heart valve; their hemodynamic performance is similar to that of currently used bioprosthetic valves, the leaflets do not cause cavitation as is the case with mechanical valves, and there is a reduced

need for anti-coagulants. Additionally complex leaflet designs can be cost effectively manufactured, and although current laboratory dip coating techniques are laborious, they can be developed on a large scale on an automated manufacturing line. The thickness can also be controlled by managing the polymer viscosity and number of dip coats such that an ultra-thin leaflet less than 50 μm can be developed.

The development of a polymeric heart valve requires the challenging task of balancing design, material and stent considerations to ensure a highly durable and functional valve requirement is met. Design of a polymeric valve is very different to that of a pericardial valve. For example, polymers are strain rate and temperature dependant and their geometry should account for creep deformation, plasticization or softening. It is advantageous that the design of a polymeric heart valve is not restricted and can be developed in various configurations such as whether the leaflets are open, closed, or in a neutral position or whether the leaflets are flat or curved. Additionally, mathematical modelling such as Finite Element Analysis (FEA) enables the user to determine the stresses across the valve when exposed to hemodynamic loads to optimise valve design.

The focus on developing a valve with leaflet reinforcement adds another factor to the design matrix. The aortic valve is naturally reinforced with elastin and collagen fibres and there is common agreement that reinforcement of the leaflets helps to minimise the stresses endured during harsh hemodynamic environments. Reinforcement is also anticipated to prevent tear propagation by bridging cracks in polymeric leaflets with reduced thicknesses. The success of a developed reinforced leaflet depends on the polymer matrix interface with the filler, the filler and matrix mechanical properties and the size and orientation of the fibres which all influence the final leaflet properties.

Whilst there have been many mathematical models that have addressed the issue of reinforcement, there are only two other studies that have reported experimental work on the reinforcement of polymeric heart valves. The first group, De Hart et al. (Cacciola 1998, 1998), developed a stented and stentless valve with fibres that ran

sinusoidally along its leaflets, sandwiched between layers of neat polymer. Their study did not focus on the durability of the valves, choosing instead to focus on the hydrodynamic function of the valve. They did however focus on fatigue design and tensile fatigue testing and found fibres (both chopped and long) to significantly improve the fatigue life of the polymer. Chopped fibres were determined to have a reduced reinforcement efficiency compared to continuous fibres since a larger proportion of their lengths is not loaded (Cacciola 1998). Additionally, crack propagation was assumed to be reduced in fibres with a cross ply layout. The authors had aimed to improve fatigue life by adjusting the angle of the cross-ply of continuous fibres such that the leaflets can be stiffer in the circumferential direction than the radial.

The second group were a little more successful with their valves, now marketing it under the brand Innovia LLC (Gallocher et al. 2006, Gallocher 2007, Claiborne et al. 2009). The valve, which used Dacron as its reinforcement material, underwent several design changes before one successfully endured a fatigue life-span of just over 10 years in an accelerated fatigue tester (Gallocher 2007). Initial design problems were due to leaflet-stent de-bonding, polymer blow-out at the unreinforced areas and tearing at the free edge which were similar to some of the complications reported in this thesis.

This thesis has the objective of addressing the problem of reinforcing polymeric heart valves with multi-walled carbon nanotubes (MWNTs). Carbon nanotubes have nanometer diameters and been found to have stiffness's as high as 1 TPa, as well as high flexibility. This made them ideal candidates in the reinforcement of polymeric leaflets since it was envisaged that they can enable ultra-thin leaflets to be developed with excellent mechanical properties and durability.

Multi-walled carbon nanotubes were incorporated into various grades of polyurethane to create composite films that were approximately 40 μm thick. Initial tests with up to 4% MWNTs in Estane highlighted the excellent reinforcement potential of nanotubes in improving the composite stiffness, with the stiffness

generally increasing with increasing nanotube content. However, high concentrations of carbon nanotubes can compromise the ultimate tensile strain as well as be difficult to disperse efficiently. It was decided that a 1% w/w content of MWNTs was optimal to improve the stiffness of the polymer substantially.

It was anticipated that the carbon nanotubes would halt crack propagation or bridge cracks due to their superior strength compared to the matrix material. Unfortunately, a 1% w/w MWNT concentration was found to significantly reduce the fatigue properties of the material. Therefore 0.125%, 0.25% and 0.5% w/w 95A-MWNT composites were created in order to improve the fatigue life of composites. However it was only the 0.125% MWNT content that appeared to show similar fatigue life to the neat polymer. Similar findings were reported by Jen et al. (2012) who tested the fatigue life of 0.5% and 1.0% as-received and acid treated MWNTs in epoxy matrix. The 1.0% composites were also found to have a fatigue life that was less than the polymer and this was attributed to poor dispersion. Additionally, the 0.5% acid-treated composite had a higher fatigue life than its as-received counter-part which led the authors to conclude that functional end groups increased the adhesion between the nanotubes and matrix.

Some authors have reported carbon nanotubes to enhance the fatigue life of composites exposed to low stress, high cycle numbers due to an efficient stress transfer between the matrix and nanotube (Grimmer and Dharan 2009). Conversely, others found fatigue life to improve in high stress, low cycle numbers (Loos et al. 2012). Regardless, in reported cases of fatigue life improvement, nanotube bridging was shown to dissipate the energy of the crack. Cracking is not only a predecessor to tearing but can also be the initial region for calcification to form.

Although fatigue life was improved with a decrease in nanotube content, the tensile stiffness of the 0.125% and 0.25% 95A-MWNT composites were less than that of the neat polymer. This conflicted with the initial hypothesis since it was assumed a reduced concentration would allow sufficient space for the bundles in the polymer matrix to break apart, hence providing better dispersion. On the other hand, the

increased space between the nanotubes may reduce the stress transfer between them which in fact would make the fillers act as defects in the polymeric matrix, reducing their mechanical integrity.

Reproducibility with the carbon nanotube composites was found to be difficult to achieve, mainly due to environmental variables such as temperature, humidity and dispersion efficiency that are difficult to control. The time the solutions were left in the ultrasonic bath was found to influence the stiffness, with increased sonication rates leading to a decrease in stiffness. This may show signs of nanotube breakdown which may make them act like defects rather than fillers. An ultrasonic probe has a higher intensity focused on a smaller range and has been alternatively used to the water bath (Gkikas et al. 2012). However, exposing the composite solution for too long can lead to overheating and destruction of the nanotube layers. Authors therefore resort to using the probe in short intervals under an ice bath to cool the solution down. Canebal et al. (2010) reported improved dispersion efficiency through inserting the high intensity ultrasonic probe in the ultrasonic bath rather than directly into the solution.

The hemocompatibility of carbon nanotube composites still needs to be established. From previous studies, carbon nanotubes have been found to reduce platelet activation on composite surfaces (Meng et al. 2005, Takahashi et al. 2009). This reduced thrombogenic potential can be beneficial in heart valves particularly in regions such as the commissures which experience high rates of shear or stagnant flow. Additionally, if nanotubes promote growth of an endothelial lining, not only will this thicken the leaflets in situ, thereby reinforcing their strength, but it could also prevent haemolysis and calcification.

Initial dip coating techniques were applied only in an inverted position and this led to two issues. The first was that the valve that formed had a thicker free edge than the base and although the belly flexed further, the angle of the free edge at the commissures was found to be restricted from flexing far. This led to a reduced valve aperture which can increase transvalvular pressure gradient and ventricular load. The

second problem was that the former needed to be heated to prevent hygroscopic conditions from affecting the polymer during curing. These issues were resolved by dipping in alternate positions (with the outflow up or down) to enable an evenly thick coat to be applied to the former. Additionally, it enabled the former to be mounted on a hot plate to prevent moisture from affecting the polymer curing process.

The success of the durability of heart valves depends on several factors including the leaflet fatigue strength, leaflet thickness, leaflet-stent interface, stent flexibility, leaflet curvature and coaptation. The leaflet-stent interface and the material choice were found to be the two most detrimental factors to the fatigue life of the valve. Leaflets peeled off the stent posts within the first few thousand cycles when dip coated on the Delrin stent without prior stent coating. The polycarbonate stent provided a better bond but its rigidity led to leaflet tears at the belly region, originating from the stent interface. Regarding material influences, it was thought that softer grade polymers would lead to increased creep but would provide a better coaptation. However, their durability was found to be less than 800,000 cycles both times they were tested. Conversely, when a higher grade polymer was used to develop a valve with a similar thickness to the prior valves, the durability was found to drastically improve and 23 million cycles have been run with this valve to date. The third factor was the leaflet thickness. The valves that were dip-coated 4 times were found to have increased durability compared to the valves with 3 coats.

Initial tests with the Delrin stents having 3 dip coats were found to fail below 1 million cycles. It was noted from the mechanical tests in Chapter 7 that the fatigue life of the composite is compromised with increasing nanotube content. Only at a 0.125% MWNT concentration did the durability of the composite match that of the neat polymer. Failure in the 1% MWNTs were predominately caused by a radial rupture along the leaflet mid-line. Belly ruptures were also evident in the 0.5% valve but the neat polymeric valve did not appear to have any ruptures in initial tests, failing instead due to leaflet de-bonding at the stent interface.

Mathematical models supported the findings on the belly region of the leaflets bearing most of the load. Despite both the flat leaflet and curved leaflet valves having the same aperture and leaflet thickness, the flat valve had a larger effective orifice area and lower transvalvular pressure gradient compared to the curved leaflet. The increased gradient in the curved leaflets may be due to the increased surface area which would increase the shear stress. However, an increased surface area was advantageous in reducing the pressures across the leaflet on both the aortic and ventricular sides.

Unlike flow through a native valve, flow through a prosthetic heart valve will be similar to flow through a stenosed aorta. The dip coated valves had a hyperbolic and elliptical curvature which enabled the valve to have a semi-open configuration, restricting its orifice area. However, this enabled the leaflets to coapt readily with minimal stress, and minimised buckling when opened. Additionally, the leaflets were found to open smoothly to allow sufficient flow through. The exception was with the thickest leaflet which significantly reduced the orifice area to a triangular cross-section. The fatigue life of polymeric valves is likely to be improved by increasing the thickness of the belly portion of the leaflets. This may be achieved by reversing the dip coating positions so that more dip coats are applied in an upright position rather than inverted.

9.2 FUTURE WORK

The limitations of this study meant that only two types of carbon nanotubes and three different polymeric materials were considered for composite development. Composites containing nanotubes have huge potential in providing a thin flexible leaflet without compromising its mechanical integrity. However the potential for a strong interfacial bond to enable sufficient load transfer depends on the type of polymer and nanotube used. Follow up studies would look into functionalized nanotubes that bond with the polymer during polymerization such as by grafting onto the soft or hard segments of the polymer. These nanotubes are envisaged to provide a greater polymer-nanotube interface which would allow for a greater load transfer.

Additionally, it is believed that the greater interface would lead to improved fatigue properties due to crack bridging. As well as using functionalized nanotubes, reinforcement work may also focus on single-walled nanotubes (SWNTs). These nanotubes have significantly high aspect ratios compared to multi-walled nanotubes and can transfer load more efficiently. Their main obstacle is their difficulty to be effectively dispersed due to their entanglement but this may be resolved by using an ultrasound probe alongside an ultrasonic bath.

Material characterization studies will also be carried out such as dynamic mechanical analysis through a spectrum of frequencies which help to determine the glass transition temperature of composites. An increase in the T_g increases the crystallinity of the materials which improves their mechanical integrity. Xiong et al. (2006) found an increase of 10 °C in the T_g following grafting nanotubes in polyurethane, demonstrating increased thermo-stability compared to the neat. Additionally a differential scanning calorimeter, DSC can be used instead to determine these parameters. Fourier transform infrared (FTIR) characterization would also show evidence of functionalization such as the presence of COOH^- bonds on the walls and ends of nanotubes.

Other polymeric materials will be experimented with to determine if other polymers can provide a better interfacial bonding between the material and nanotube. These polymers may be harder grades than the Carbothane PC3595A as from the durability tests, it is apparent that the harder polymers have a much greater resistance to fatigue than the softer grades. Further work would be carried out on composite film development prior to valve production, to determine optimal reinforcement properties. Finally valves are currently developed by dipping a stent mounted on a valve former into a polymeric solution. Other manufacturing methods such as solvent bonding cast leaflets to the stent or through injection moulding may also be considered. Hydrodynamic testing will then be carried out to determine the valve properties such as pressure gradients, leakage and regurgitation.

The lessons learned in this work suggest that if the identified issues can be met, then the objective of an ultra-thin reinforced polymeric valve leaflet apparatus is realistic if somewhat challenging. This work has provided the necessary direction to allow subsequent research towards this case.

9.3 CONCLUSION

Polyurethane composite heart valves reinforced with 0.125% to 1% w/w multi-walled carbon nanotubes have been developed, with the former concentration having similar durability to neat polymeric valves. Carbon nanotubes have shown potential in improving the mechanical integrity of thin films and with their potential to reduce platelet activation, have offered a way for the development of thin valves with anti-thrombogenic properties. This work has established the basis for the reinforcement of synthetic leaflets with carbon nanotubes and has answered key questions involving the impact that nanotube concentration and matrix property has on the durability of synthetic heart valve leaflets. A higher grade of polyurethane improves the durability drastically and a reasonably thin leaflet (130 μm) has achieved 23 million cycles to date. As 0.125% w/w MWNTs have shown similar durability to the neat polymer, it is interesting to determine the impact that their incorporation in the harder polymer would have at higher cycle counts in terms of bridging cracks and in improving hemocompatibility. It is envisaged that this following line of work will one day lead to the development of a durable synthetic heart valve for low profile percutaneous delivery through a peripheral artery.

CHAPTER 10:

REFERENCES

10 REFERENCES

- Alavi, S. H., V. Ruiz, T. Krasieva, E. L. Botvinick and A. Kheradvar (2012). "Characterizing the Collagen Fiber Orientation in Pericardial Leaflets Under Mechanical Loading Conditions." Annals of biomedical engineering: 1-15.
- Andersen, H. R., L. L. Knudsen and J. M. Hasenkam (1992). "Transluminal implantation of artificial heart valves. Description of a new expandable aortic valve and initial results with implantation by catheter technique in closed chest pigs." Eur Heart J **13**(5): 704-708.
- Anderson, R. H. (2007). "The surgical anatomy of the aortic root." Multimedia Manual of Cardio-Thoracic Surgery **2007**(0219).
- Anderson, R. H., W. A. Devine, S. Y. Ho, A. Smith and R. McKay (1991). "The myth of the aortic annulus: The anatomy of the subaortic outflow tract." The Annals of Thoracic Surgery **52**(3): 640-646.
- Antunes, M. J. (2012). "Editorial Comment: Aortic stenosis in octogenarians and other high-risk groups: what can surgical valve replacement offer?" European Journal of Cardio-Thoracic Surgery **42**(6): 940-941.
- Arbeiter, D., N. Grabow, Y. Wessarges, K. Sternberg and K. P. Schmitz (2012). "Suitability of porcine pericardial tissue for heart valve engineering: Biomechanical properties." Biomed Tech (Berl).
- Banerjee, S., T. Hemraj-Benny and S. S. Wong (2005). "Covalent Surface Chemistry of Single-Walled Carbon Nanotubes." Advanced Materials **17**(1): 17-29.
- Barber, A. H., S. R. Cohen and H. D. Wagner (2004). "Static and Dynamic Wetting Measurements of Single Carbon Nanotubes." Physical Review Letters **92**(18): 186103.
- Barsanti, S. (1998). Observations on the mechanical behaviour of polyurethane heart valves. Doctor of Philosophy, University of Paisley.
- Baughman, R. H., A. A. Zakhidov and W. A. de Heer (2002). "Carbon Nanotubes--the Route Toward Applications." Science **297**(5582): 787-792.
- Bellhouse, B. J. and L. Talbot (1969). "The fluid mechanics of the aortic valve." Journal of Fluid Mechanics **35**: 721-735.
- Bernacca, G. M., T. G. Mackay, R. Wilkinson and D. J. Wheatley (1997). "Polyurethane heart valves Fatigue failure, calcification, and polyurethane structure, Journal of Biomedical Materials Research Volume 34, Issue 3." Journal of Biomedical Materials Research **34**(3): 371-379.
- Bernacca, G. M., B. O'Connor, D. F. Williams and D. J. Wheatley (2002). "Hydrodynamic function of polyurethane prosthetic heart valves: influences of Young's modulus and leaflet thickness." Biomaterials **23**(1): 45-50.
- Bianco, R. W., R. Phillips, J. Mrachek and J. Witson (1996). "Feasibility evaluation of a new pericardial bioprosthesis with dye mediated photo-oxidized bovine pericardial tissue." J Heart Valve Dis **5**(3): 317-322.

- Bijuklic, K., T. Tuebler, H. Reichenspurner, H. Treede, A. Wandler, J. H. Harreld, R. I. Low and J. Schofer (2011). "Midterm stability and hemodynamic performance of a transfemorally implantable nonmetallic, retrievable, and repositionable aortic valve in patients with severe aortic stenosis. Up to 2-year follow-up of the direct-flow medical valve: a pilot study." Circulation. Cardiovascular interventions **4**(6): 595-601.
- Bloomfield, P. (2002). "Choice of heart valve prosthesis." Heart **87**(6): 583-589.
- Bolling, S. F., J. H. Rogers, V. Babaliaros, N. Piazza, P. A. Takeda, R. I. Low and P. C. Block (2008). "Percutaneous aortic valve implantation utilising a novel tissue valve: preclinical experience." EuroIntervention **4**(1): 148-153.
- Bonard, J. M., T. Stora, J. P. Salvetat, F. Maier, T. Stöckli, C. Duschl, L. Forró, W. A. de Heer and A. Châtelain (1997). "Purification and size-selection of carbon nanotubes." Advanced Materials **9**(10): 827-831.
- Bonow, R. O., B. A. Carabello, K. Chatterjee, A. C. de Leon, D. P. Faxon, M. D. Freed, W. H. Gaasch, B. W. Lytle, R. A. Nishimura and P. T. O'Gara (2008). "2008 Focused Update Incorporated Into the ACC/AHA 2006 Guidelines for the Management of Patients With Valvular Heart Disease: A Report of the American College of Cardiology/American Heart Association Task Force on Practice Guidelines (Writing Committee to Revise the 1998 Guidelines for the Management of Patients With Valvular Heart Disease) Endorsed by the Society of Cardiovascular Anesthesiologists, Society for Cardiovascular Angiography and Interventions, and Society of Thoracic Surgeons." Journal of the American College of Cardiology **52**(13): e1-e142.
- Bonow, R. O., B. A. Carabello, K. Chatterjee, A. C. de Leon, D. P. Faxon, M. D. Freed, W. H. Gaasch, B. W. Lytle, R. A. Nishimura, P. T. O'Gara, R. A. O'Rourke, C. M. Otto, P. M. Shah, J. S. Shanewise, S. C. Smith, A. K. Jacobs, C. D. Adams, J. L. Anderson, E. M. Antman, D. P. Faxon, V. Fuster, J. L. Halperin, L. F. Hiratzka, S. A. Hunt, B. W. Lytle, R. Nishimura, R. L. Page, B. Riegel and H. Amer Col CardiologyAmer (2006). "ACC/AHA 2006 guidelines for the management of patients with valvular heart disease." Circulation **114**(5): E84-E231.
- Boudjemline, Y. and P. Bonhoeffer (2002). "Percutaneous implantation of a valve in the descending aorta in lambs." European Heart Journal **23**(13): 1045-1049.
- Braunwald, N. S. (1989). "It will work: The first successful mitral valve replacement." The Annals of Thoracic Surgery **48**(3, Supplement): S1-S3.
- Bridgewater, B., B. Keogh, R. Kinsman and P. Walton (2008). "The Society for Cardiothoracic Surgery in Great Britain and Ireland. Sixth National Adult Cardiac Surgical Database Report. Demonstrating quality."
- Brodsky, A. M. (2004). "Percutaneous approaches to aortic valve replacement." Cardiac Interventions: 4-9.
- Buellesfeld, L., U. Gerckens and E. Grube (2008). "Percutaneous implantation of the first repositionable aortic valve prosthesis in a patient with severe aortic stenosis." Catheterization and Cardiovascular Interventions **71**(5): 579-584.

- Butcher, J. T. and R. M. Nerem (2006). "Valvular endothelial cells regulate the phenotype of interstitial cells in co-culture: effects of steady shear stress." Tissue Eng. **12**(4): 905-915.
- Cacciola, G. R. (1998). Design, Simulation and Manufacturing of Fiber Reinforced Polymer Heart Valves, Technische Universiteit Eindhoven.
- Cai, C. Q., S. D. Kruse, J. L. Kurk and Y.-r. Woo (2003). Polymer leaflet designs for medical devices. United States, St. Jude Medical, Inc. (St. Paul, MN)
- Campbell, M. (2011). "Nanotubes help cloak objects in a mirage." New Scientist **212**(2833): 24.
- Canebal, G. T., C. Dutta, V. Agrawal and M. Rao (2010). "Novel ultrasonic dispersion of carbon nanotubes." Journal of Minerals and Materials Characterization and Engineering **9**(3): 165-181.
- Chachra, D., P. F. Gratzner, C. A. Pereira and J. M. Lee (1996). "Effect of applied uniaxial stress on rate and mechanical effects of cross-linking in tissue-derived biomaterials." Biomaterials **17**(19): 1865-1875.
- Chandran, K. B., A. P. Yoganathan and S. E. Rittgers (2006). Biofluid Mechanics: The Human Circulation, Taylor & Francis.
- Chen, H., H. Muthuraman, P. Stokes, J. Zou, X. Liu, J. Wang, Q. Huo, S. I. Khondaker and L. Zhai (2007). "Dispersion of carbon nanotubes and polymer nanocomposite fabrication using trifluoroacetic acid as a co-solvent." Nanotechnology **18**(41): 415606.
- Chen, R., Y. Morsi, S. Patel, Q.-f. Ke and X.-m. Mo (2009). "A novel approach via combination of electrospinning and FDM for tri-leaflet heart valve scaffold fabrication." Frontiers of Materials Science in China **3**(4): 359-366.
- Chen, S., L. Xu, Y. Liu, Q. Li, D. Wang, X. Wang and T. Liu (2013). "Donkey Pericardium as an Alternative Bioprosthetic Heart Valve Material." Artificial Organs **37**(3): 248-255.
- Chen, X. H., C. S. Chen, Q. Chen, F. Q. Cheng, G. Zhang and Z. Z. Chen (2002). "Non-destructive purification of multi-walled carbon nanotubes produced by catalyzed CVD." Materials Letters **57**(3): 734-738.
- Chen, Z., W. Thiel and A. Hirsch (2003). "Reactivity of the Convex and Concave Surfaces of Single-Walled Carbon Nanotubes (SWCNTs) towards Addition Reactions: Dependence on the Carbon-Atom Pyramidalization." ChemPhysChem **4**(1): 93-97.
- Chester, A. H. and P. M. Taylor (2007). "Molecular and functional characteristics of heart-valve interstitial cells." Philosophical Transactions of the Royal Society B: Biological Sciences **362**(1484): 1437-1443.
- Chiam, P. T. L. and C. E. Ruiz (2009). "Percutaneous transcatheter aortic valve implantation: Evolution of the technology." American Heart Journal **157**(2): 229-242.
- Chinchoy, E., M. Ujhelyi, A. Hill, N. Skadsberg and P. Iaizzo (2005). The Pericardium. Handbook of Cardiac Anatomy, Physiology, and Devices. P. Iaizzo, Humana Press: 101-110.
- Christenson, E. M., M. Dadsetan, M. Wiggins, J. M. Anderson and A. Hiltner (2004). "Poly(carbonate urethane) and poly(ether urethane) biodegradation: In vivo studies." Journal of Biomedical Materials Research Part A **69A**(3): 407-416.

- Ciselli, P. (2007). The Potential of Carbon Nanotubes in Polymer Composites. PhD, Eindhoven University of Technology.
- Claiborne, T. E., D. Bluestein and R. T. Schoepfoerster (2009). "Development and evaluation of a novel artificial catheter-deliverable prosthetic heart valve and method for in vitro testing." International Journal of Artificial Organs **32**(5): 262-271.
- Claiborne, T. E., G. Girdhar, S. Gallocher-Lowe, J. Sheriff, Y. P. Kato, L. Pinchuk, R. T. Schoepfoerster, J. Jesty and D. Bluestein (2011). "Thrombogenic potential of Innovia polymer valves versus Carpentier-Edwards Perimount Magna aortic bioprosthetic valves." ASAIO J **57**(1): 26-31.
- Coleman, J. N., U. Khan, W. J. Blau and Y. K. Gun'ko (2006). "Small but strong: A review of the mechanical properties of carbon nanotube-polymer composites." Carbon **44**(9): 1624-1652.
- Crawford, D. M., R. G. Bass and T. W. Haas (1998). "Strain effects on thermal transitions and mechanical properties of thermoplastic polyurethane elastomers." Thermochimica Acta **323**(1&2): 53-63.
- Crawford, R. J. (1998). Plastics Engineering, Elsevier Science.
- Cribier, A., H. Eltchaninoff, A. Bash, N. Borenstein, C. Tron, F. Bauer, G. Derumeaux, F. Anselme, F. Laborde and M. B. Leon (2002). "Percutaneous transcatheter implantation of an aortic valve prosthesis for calcific aortic stenosis - First human case description." Circulation **106**(24): 3006-3008.
- Cribier, A., H. Eltchaninoff, C. Tron, F. Bauer, C. Agatiello, L. Sebah, A. Bash, D. Nusimovici, P. Y. Litzler, J. P. Bessou and M. B. Leon (2004). "Early experience with percutaneous transcatheter implantation of heart valve prosthesis for the treatment of end-stage inoperable patients with calcific aortic stenosis." J Am Coll Cardiol **43**(4): 698-703.
- D'Souza, S. S., M. Butterfield and J. Fisher (2003). "Kinematics of synthetic flexible leaflet heart valves during accelerated testing." The Journal of heart valve disease **12**(1): 110-119; discussion 119-120.
- Dabagh, M., M. Abdekhodaie and M. Khorasani (2005). "Effects of polydimethylsiloxane grafting on the calcification, physical properties, and biocompatibility of polyurethane in a heart valve." Journal of Applied Polymer Science **98**(2): 758-766.
- Daebritz, S. H., B. Fausten, B. Hermanns, J. Schroeder, J. Groetzner, R. Autschbach, B. J. Messmer and J. S. Sachweh (2004). "Introduction of a flexible polymeric heart valve prosthesis with special design for aortic position." Eur J Cardiothorac Surg **25**(6): 946-952.
- Davies, H. (1965). "Catheter-mounted valve for temporary relief of aortic insufficiency." The Lancet **285**(7379): 250.
- de Buhr, W., S. Pfeifer, J. Slotta-Huspenina, E. Wintermantel, G. Lutter and W. A. Goetz (2012). "Impairment of pericardial leaflet structure from balloon-expanded valved stents." The Journal of Thoracic and Cardiovascular Surgery **143**(6): 1417-1421.
- De Hart, J., G. Cacciola, P. J. G. Schreurs and G. W. M. Peters (1998). "A three-dimensional analysis of a fibre-reinforced aortic valve prosthesis." Journal of Biomechanics **31**(7): 629-638.

- Del Gaudio, C., M. Grigioni, A. Bianco and G. De Angelis (2008). "Electrospun bioresorbable heart valve scaffold for tissue engineering." Int J Artif Organs **31**(1): 68-75.
- Duncan, A. C., D. Boughner and I. Vesely (1997). "Viscoelasticity of dynamically fixed bioprosthetic valves. II. Effect of glutaraldehyde concentration." The Journal of Thoracic and Cardiovascular Surgery **113**(2): 302-310.
- Dwyer, H. A., P. B. Matthews, A. Azadani, N. Jaussaud, L. Ge, T. S. Guy and E. E. Tseng (2009). "Computational fluid dynamics simulation of transcatheter aortic valve degeneration." Interactive cardiovascular and thoracic surgery **9**(2): 301-308.
- El-Hamamsy, I., A. H. Chester and M. H. Yacoub (2010). "Cellular regulation of the structure and function of aortic valves." Journal of Advanced Research **1**(1): 5-12.
- El-Hamamsy, I., M. H. Yacoub and A. H. Chester (2009). "Neuronal regulation of aortic valve cusps." Current vascular pharmacology **7**(1): 40-46.
- Ellis, J. T., T. M. Healy, A. A. Fontaine, R. Saxena and A. P. Yoganathan (1996). "Velocity measurements and flow patterns within the hinge region of a Medtronic Parallel bileaflet mechanical valve with clear housing." J Heart Valve Dis **5**(6): 591-599.
- Eltchaninoff, H., A. Zajarias, C. Tron, P. Y. Litzler, B. Baala, M. Godin, J. P. Bessou and A. Cribier (2008). "Transcatheter aortic valve implantation: technical aspects, results and indications." Archives of Cardiovascular Diseases **101**(2): 126-132.
- Fedak, P. W. M., S. Verma, T. E. David, R. L. Leask, R. D. Weisel and J. Butany (2002). "Clinical and Pathophysiological Implications of a Bicuspid Aortic Valve." Circulation **106**(8): 900-904.
- Filip, D. A., A. Radu and M. Simionescu (1986). "Interstitial cells of the heart valves possess characteristics similar to smooth muscle cells." Circulation Research **59**(3): 310-320.
- Flanagan, T. C. and A. Pandit (2003). "Living artificial heart valve alternatives: a review." European cells & materials **6**: 28-45; discussion 45.
- Formaggia, L., A. M. Quarteroni and A. Veneziani (2009). Cardiovascular Mathematics: Modeling and Simulation of the Circulatory System, Springer-Verlag Milan.
- Foster, J., S. Singamaneni, R. Kattumenu and V. Bliznyuk (2005). "Dispersion and phase separation of carbon nanotubes in ultrathin polymer films." Journal of Colloid and Interface Science **287**(1): 167-172.
- Freeman, R. V. and C. M. Otto (2005). "Spectrum of Calcific Aortic Valve Disease." Circulation **111**(24): 3316-3326.
- Gallocher, S. L. (2007). Durability Assessment of Polymer Trileaflet Heart Valves, Florida International University.
- Gallocher, S. L., A. F. Aguirre, V. Kasyanov, L. Pinchuk and R. T. Schoepfoerster (2006). "A novel polymer for potential use in a trileaflet heart valve." Journal of Biomedical Materials Research Part B: Applied Biomaterials **79B**(2): 325-334.
- Garcia, D. and L. Kadem (2006). "What do you mean by aortic valve area: geometric orifice area, effective orifice area, or gorlin area?" J Heart Valve Dis **15**(5): 601-608.

- García Páez, J. M., E. Jorge, A. Rocha, J. L. Castillo-Olivares, I. Millan, A. Carrera, A. Cordon, G. Tellez and R. Burgos (2002). "Mechanical effects of increases in the load applied in uniaxial and biaxial tensile testing. Part II. Porcine pericardium." Journal of Materials Science: Materials in Medicine **13**(5): 477-483.
- Gauvin, R., G. Marinov, Y. Mehri, J. Klein, B. Li, D. Larouche, R. Guzman, Z. Zhang, L. Germain and R. Guidoin (2012). "A comparative study of bovine and porcine pericardium to highlight their potential advantages to manufacture percutaneous cardiovascular implants." J Biomater Appl.
- Généreux, P., S. J. Head, D. A. Wood, S. K. Kodali, M. R. Williams, J.-M. Paradis, M. Spaziano, A. P. Kappetein, J. G. Webb, A. Cribier and M. B. Leon (2012). "Transcatheter aortic valve implantation 10-year anniversary: review of current evidence and clinical implications." European Heart Journal.
- Ghanbari, H., A. G. Kidane, G. Burriesci, B. Ramesh, A. Darbyshire and A. M. Seifalian (2010). "The anti-calcification potential of a silsesquioxane nanocomposite polymer under in vitro conditions: Potential material for synthetic leaflet heart valve." Acta Biomaterialia **6**(11): 4249-4260.
- Ghanbari, H., H. Viatge, A. G. Kidane, G. Burriesci, M. Tavakoli and A. M. Seifalian (2009). "Polymeric heart valves: new materials, emerging hopes." Trends in Biotechnology **27**(6): 359-367.
- Gkikas, G., N. M. Barkoula and A. S. Paipetis (2012). "Effect of dispersion conditions on the thermo-mechanical and toughness properties of multi walled carbon nanotubes-reinforced epoxy." Composites Part B: Engineering **43**(6): 2697-2705.
- Gott, V. L., D. E. Alejo and D. E. Cameron (2003). "Mechanical heart valves: 50 years of evolution." Ann Thorac Surg **76**(6): S2230-2239.
- Grimmer, C. S. and C. K. Dharan (2009). "High-cycle fatigue life extension of glass fiber/polymer composites with carbon nanotubes." Journal of Wuhan University of Technology--Materials Science Edition **24**(2): 167-173.
- Gross, L. and M. A. Kugel (1931). "Topographic Anatomy and Histology of the Valves in the Human Heart." Am J Pathol **7**(5): 445-474 447.
- Grube, E., L. Buellesfeld, R. Mueller, B. Sauren, B. Zickmann, D. Nair, H. Beucher, T. Felderhoff, S. Iversen and U. Gerckens (2008). "Progress and Current Status of Percutaneous Aortic Valve Replacement: Results of Three Device Generations of the CoreValve Revalving System." Circulation: Cardiovascular Interventions **1**(3): 167-175.
- Grube, E., J. C. Laborde, B. Zickmann, U. Gerckens, T. Felderhoff, B. Sauren, A. Bootsvelde, L. Buellesfeld and S. Iversen (2005). "First report on a human percutaneous transluminal implantation of a self-expanding valve prosthesis for interventional treatment of aortic valve." Catheterization and Cardiovascular Interventions **66**(4): 465-469.

- Grube, E., C. Naber, A. Abizaid, E. Sousa, O. Mendiz, P. Lemos, R. Kalil Filho, J. Mangione and L. Buellesfeld (2011). "Feasibility of Transcatheter Aortic Valve Implantation Without Balloon Pre-Dilation A Pilot Study." JACC: Cardiovascular Interventions **4**(7): 751-757.
- Gunatillake, P. A., G. F. Meijs, S. J. McCarthy and R. Adhikari (2000). "Poly(dimethylsiloxane)/poly(hexamethylene oxide) mixed macrodiol based polyurethane elastomers. I. Synthesis and properties." Journal of Applied Polymer Science **76**(14): 2026-2040.
- Hanzel, G. S., P. J. Harrity, T. L. Schreiber and W. W. O'Neill (2005). "Retrograde percutaneous aortic valve implantation for critical aortic stenosis." Catheterization and Cardiovascular Interventions **64**(3): 322-326.
- Heenan, S. D., S. Grubnic, T. M. Buckenham and A. M. Belli (1996). "Transbrachial arteriography: indications and complications." Clin Radiol **51**(3): 205-209.
- Hiester, E. D. and M. S. Sacks (1998). "Optimal bovine pericardial tissue selection sites. I. Fiber architecture and tissue thickness measurements." Journal of Biomedical Materials Research **39**(2): 207-214.
- Holmes Jr, D. R., M. J. Mack, S. Kaul, A. Agnihotri, K. P. Alexander, S. R. Bailey, J. H. Calhoun, B. A. Carabello, M. Y. Desai, F. H. Edwards, G. S. Francis, T. J. Gardner, A. P. Kappetein, J. A. Linderbaum, C. Mukherjee, D. Mukherjee, C. M. Otto, C. E. Ruiz, R. L. Sacco, D. Smith and J. D. Thomas (2012). "2012 ACCF/AATS/SCAI/STS Expert Consensus Document on Transcatheter Aortic Valve Replacement." Journal of the American College of Cardiology **59**(13): 1200-1254.
- Hou, P.-X., C. Liu and H.-M. Cheng (2008). "Purification of carbon nanotubes." Carbon **46**(15): 2003-2025.
- Hulsmann, J., K. Grun, S. El Amouri, M. Barth, K. Hornung, C. Holzfluss, A. Lichtenberg and P. Akhyari (2012). "Transplantation material bovine pericardium: biomechanical and immunogenic characteristics after decellularization vs. glutaraldehyde-fixing." Xenotransplantation **19**(5): 286-297.
- Iijima, S. (1991). "Helical microtubules of graphitic carbon." Nature **354**(6348): 56-58.
- Iijima, S. and T. Ichihashi (1993). "Single-shell carbon nanotubes of 1-nm diameter." Nature **363**(6430): 603-605.
- Imachi, K., T. Chinzei, Y. Abe, K. Mabuchi, H. Matsuura, T. Karita, K. Iwasaki, S. Mochizuki, Y.-p. Son, I. Saito, A. Kouno and T. Ono (2001). "A new hypothesis on the mechanism of calcification formed on a blood-contacted polymer surface." Journal of Artificial Organs **4**(1): 74-82.
- Ishihara, T., V. J. Ferrans, M. Jones, S. W. Boyce and W. C. Roberts (1981). "Structure of bovine parietal pericardium and of unimplanted Ionescu-Shiley pericardial valvular bioprostheses." J Thorac Cardiovasc Surg **81**(5): 747-757.
- Lung, B., G. Baron, E. G. Butchart, F. Delahaye, C. Gohlke-Bärwolf, O. W. Levang, P. Tornos, J.-L. Vanoverschelde, F. Vermeer, E. Boersma, P. Ravaut and A. Vahanian (2003). "A

- prospective survey of patients with valvular heart disease in Europe: The Euro Heart Survey on Valvular Heart Disease." European Heart Journal **24**(13): 1231-1243.
- Lung, B., A. Cachier, G. Baron, D. Messika-Zeitoun, F. Delahaye, P. Tornos, C. Gohlke-Bärwolf, E. Boersma, P. Ravaud and A. Vahanian (2005). "Decision-making in elderly patients with severe aortic stenosis: why are so many denied surgery?" European Heart Journal **26**(24): 2714-2720.
- Jen, Y.-M. and C.-Y. Huang (2012). "Fatigue characterization of acid-treated carbon nanotube/epoxy composites." Journal of Composite Materials.
- Jiang, H., G. Campbell, D. Boughner, W.-K. Wan and M. Quantz (2004). "Design and manufacture of a polyvinyl alcohol (PVA) cryogel tri-leaflet heart valve prosthesis." Medical Engineering & Physics **26**(4): 269-277.
- Joshi, R. R., J. R. Frautschi, R. E. Phillips and R. J. Levy (1994). "Phosphonated polyurethanes that resist calcification." J Appl Biomater **5**(1): 65-77.
- Kagan, V. E., N. V. Konduru, W. Feng, B. L. Allen, J. Conroy, Y. Volkov, I. I. Vlasova, N. A. Belikova, N. Yanamala, A. Kapralov, Y. Y. Tyurina, J. Shi, E. R. Kisin, A. R. Murray, J. Franks, D. Stolz, P. Gou, J. Klein-Seetharaman, B. Fadeel, A. Star and A. A. Shvedova (2010). "Carbon nanotubes degraded by neutrophil myeloperoxidase induce less pulmonary inflammation." Nat Nano **5**(5): 354-359.
- Kahlert, P., S. C. Knipp, M. Schlamann, M. Thielmann, F. Al-Rashid, M. Weber, U. Johansson, D. Wendt, H. G. Jakob, M. Forsting, S. Sack, R. Erbel and H. Eggebrecht (2010). "Silent and Apparent Cerebral Ischemia After Percutaneous Transfemoral Aortic Valve Implantation." Circulation **121**(7): 870-878.
- Kalejs, M., P. Stradins, R. Lacis, I. Ozolanta, J. Pavars and V. Kasyanov (2009). "St Jude Epic heart valve bioprostheses versus native human and porcine aortic valves – comparison of mechanical properties." Interactive CardioVascular and Thoracic Surgery **8**: 553-557.
- Kempfert, J., A. Rastan, D. Holzhey, A. Linke, G. Schuler, A. van Linden, J. Blumenstein, F. W. Mohr and T. Walther (2011). "Transapical Aortic Valve Implantation. Analysis of Risk Factors and Learning Experience in 299 Patients." Circulation **124**(11 suppl 1): S124-S129.
- Khare, R. and S. Bose (2005). "Carbon Nanotube Based Composites- A Review." Journal of Minerals & Materials Characterization & Engineering **4**(1): 31-46.
- Kheradvar, A. and H. Alavi (2012). "TCT-830 Immediate and Delayed Effects of Stent Crimping on Pericardial Leaflets of Transcatheter Valves." Journal of the American College of Cardiology **60**(17_S).
- Kidane, A. G., G. Burriesci, P. Cornejo, A. Dooley, S. Sarkar, P. Bonhoeffer, M. Edirisinghe and A. M. Seifalian (2009). "Current Developments and Future Prospects for Heart Valve Replacement Therapy." Journal of Biomedical Materials Research Part B-Applied Biomaterials **88B**(1): 290-303.
- Kroto, H. W., J. R. Heath, S. C. O'Brien, R. F. Curl and R. E. Smalley (1985). "C60: Buckminsterfullerene." Nature **318**(6042): 162-163.

- Krumsdorf, U., R. Bekeredjian, G. Korosoglou, J. Kreuzer, B. J. Rieck, K. Kallenbach, H. A. Katus and W. Rottbauer (2010). "Percutaneous Aortic "Valve in Valve" Implantation for Severe Aortic Regurgitation in a Degenerated Bioprosthesis." Circulation: Cardiovascular Interventions **3**(3): e6-e7.
- Kunzelman, K. S., R. P. Cochran, S. S. Murphree, W. S. Ring, E. D. Verrier and R. C. Eberhart (1993). "Differential collagen distribution in the mitral valve and its influence on biomechanical behaviour." J Heart Valve Dis **2**(2): 236-244.
- Kuronuma, Y., Y. Shindo, T. Takeda and F. Narita (2011). "Crack growth characteristics of carbon nanotube-based polymer composites subjected to cyclic loading." Engineering Fracture Mechanics **78**(17): 3102-3110.
- Lam, C.-W., J. T. James, R. McCluskey and R. L. Hunter (2004). "Pulmonary Toxicity of Single-Wall Carbon Nanotubes in Mice 7 and 90 Days After Intratracheal Instillation." Toxicological Sciences **77**(1): 126-134.
- Langdon, S. E., R. Chernecky, C. A. Pereira, D. Abdulla and J. Michael Lee (1999). "Biaxial mechanical/structural effects of equibiaxial strain during crosslinking of bovine pericardial xenograft materials." Biomaterials **20**(2): 137-153.
- Leat, M. E. and J. Fisher (1994). "A synthetic leaflet heart valve with improved opening characteristics." Medical Engineering & Physics **16**(6): 470-476.
- Leat, M. E. and J. Fisher (1995). "The influence of manufacturing methods on the function and performance of a synthetic leaflet heart valve." Proceedings of the Institution of Mechanical Engineers, Part H: Journal of Engineering in Medicine **209**(1): 65-69.
- Lee, J. M., S. A. Haberer, C. A. Pereira, W. A. Naimark, D. W. Courtman and G. J. Wilson (1994). High strain rate testing and structural analysis of pericardial bioprosthetic materials. Biomaterials' mechanical properties. H. E. Kambic and A. T. Yokobori, ASTM International. **1173**: 19-42.
- Lee, J. M. and S. E. Langdon (1996). "Thickness measurement of soft tissue biomaterials: A comparison of five methods." Journal of biomechanics **29**(6): 829-832.
- Leon, M. B., C. R. Smith, M. Mack, D. C. Miller, J. W. Moses, L. G. Svensson, E. M. Tuzcu, J. G. Webb, G. P. Fontana, R. R. Makkar, D. L. Brown, P. C. Block, R. A. Guyton, A. D. Pichard, J. E. Bavaria, H. C. Herrmann, P. S. Douglas, J. L. Petersen, J. J. Akin, W. N. Anderson, D. Wang and S. Pocock (2010). "Transcatheter Aortic-Valve Implantation for Aortic Stenosis in Patients Who Cannot Undergo Surgery." New England Journal of Medicine **363**(17): 1597-1607.
- Li, K. and W. Sun (2010). "Simulated thin pericardial bioprosthetic valve leaflet deformation under static pressure-only loading conditions: implications for percutaneous valves." Ann **38**(8): 2690-2701. Epub 2010 Mar 2625.
- Liao, J., L. Yang, J. Grashow and M. S. Sacks (2005). "Molecular orientation of collagen in intact planar connective tissues under biaxial stretch." Acta Biomater **1**(1): 45-54.

- Lichtenstein, S. V., A. Cheung, J. Ye, C. R. Thompson, R. G. Carere, S. Pasupati and J. G. Webb (2006). "Transapical transcatheter aortic valve implantation in humans - Initial clinical experience." Circulation **114**(6): 591-596.
- Lim, K. H., J. Candra, J. H. Yeo and C. M. Duran (2004). "Flat or curved pericardial aortic valve cusps: a finite element study." J Heart Valve Dis **13**(5): 792-797.
- Lim, K. H., J. Candra, J. H. Yeo and C. M. Duran (2004). "Flat or curved pericardial aortic valve cusps: a finite element study." The Journal of heart valve disease **13**(5): 792-797.
- Liu, Y., V. Kasyanov and R. T. Schoepfoerster (2007). "Effect of fiber orientation on the stress distribution within a leaflet of a polymer composite heart valve in the closed position." Journal of Biomechanics **40**(5): 1099-1106.
- Loos, M. R., J. Yang, D. L. Feke, I. Manas-Zloczower, S. Unal and U. Younes (2012). "Enhancement of fatigue life of polyurethane composites containing carbon nanotubes." Composites Part B: Engineering **44**(1): 740-744.
- Love, J. W. (1993). Autologous Tissue Heart Valves. London, CRC Press.
- Low, R. I., S. F. Bolling, K. K. Yeo and A. Ebner (2008). "Direct flow medical percutaneous aortic valve: proof of concept." EuroIntervention **4**(2): 256-261.
- Lutter, G., D. Kuklinski, G. Berg, P. von Samson, J. Martin, M. Handke, P. Uhrmeister and F. Beyersdorf (2002). "Percutaneous aortic valve replacement: An experimental study. I. Studies on implantation." Journal of Thoracic and Cardiovascular Surgery **123**(4): 768-776.
- Mackay, T. G. (1992). Towards a Tri-leaflet Polyurethane Heart Valve Prosthesis, University of Strathclyde.
- Mackay, T. G., D. J. Wheatley, G. M. Bernacca, A. C. Fisher and C. S. Hindle (1996). "New polyurethane heart valve prosthesis: design, manufacture and evaluation." Biomaterials **17**(19): 1857-1863.
- Martin, D. J., G. F. Meijs, P. A. Gunatillake, S. P. Yozghatlian and G. M. Renwick (1999). "The influence of composition ratio on the morphology of biomedical polyurethanes." Journal of Applied Polymer Science **71**(6): 937-952.
- Martin, D. J., L. A. Poole Warren, P. A. Gunatillake, S. J. McCarthy, G. F. Meijs and K. Schindhelm (2000). "Polydimethylsiloxane/polyether-mixed macrodiol-based polyurethane elastomers: biostability." Biomaterials **21**(10): 1021-1029.
- Melrose, D. G., B. Dreyer, H. H. Bentall and J. B. Baker (1955). "Elective cardiac arrest." Lancet **269**(6879): 21-22.
- Mendelson, K. and F. J. Schoen (2006). "Heart valve tissue engineering: concepts, approaches, progress, and challenges." Annals of biomedical engineering **34**(12): 1799-1819.
- Meng, J., H. Kong, Z. Han, C. Wang, G. Zhu, S. Xie and H. Xu (2009). "Enhancement of nanofibrous scaffold of multiwalled carbon nanotubes/polyurethane composite to the fibroblasts growth and biosynthesis." Journal of Biomedical Materials Research Part A **88A**(1): 105-116.

- Meng, J., H. Kong, H. Y. Xu, L. Song, C. Y. Wang and S. S. Xie (2005). "Improving the blood compatibility of polyurethane using carbon nanotubes as fillers and its implications to cardiovascular surgery." Journal of Biomedical Materials Research Part A **74A**(2): 208-214.
- Meyer, J. A. (1990). "Werner Forssmann and catheterization of the heart, 1929." Ann Thorac Surg **49**(3): 497-499.
- Migliarese, C. (2013). Chapter I.2.9 - Composites. Biomaterials Science (Third Edition). D. R. Buddy, S. H. Allan, A. S. H. F. J. S. Frederick J. Schoen and Jack E. LemonsA2 - Buddy D. Ratner and E. L. Jack, Academic Press: 223-241.
- Mirnajafi, A., J. Raymer, M. J. Scott and M. S. Sacks (2005). "The effects of collagen fiber orientation on the flexural properties of pericardial heterograft biomaterials." Biomaterials **26**(7): 795-804.
- Mirnajafi, A., J. M. Raymer, L. R. McClure and M. S. Sacks (2006). "The flexural rigidity of the aortic valve leaflet in the commissural region." Journal of Biomechanics **39**(16): 2966-2973.
- Mohammadi, H., D. Boughner, L. E. Millon and W. K. Wan (2009). "Design and simulation of a poly(vinyl alcohol)-bacterial cellulose nanocomposite mechanical aortic heart valve prosthesis." Proc Inst Mech Eng H **223**(6): 697-711.
- Mohammadi, H. and K. Mequanint (2011). "Prosthetic aortic heart valves: modeling and design." Med Eng Phys **33**(2): 131-147.
- Mol, A., M. C. M. Rutten, N. J. B. Driessen, C. V. C. Bouten, G. Zünd, F. P. T. Baaijens and S. P. Hoerstrup (2006). "Autologous Human Tissue-Engineered Heart Valves." Circulation **114**(1 suppl): I-152-I-158.
- Moniruzzaman, M. and K. I. Winey (2006). "Polymer Nanocomposites Containing Carbon Nanotubes." Macromolecules **39**(16): 5194-5205.
- Naimark, W. A., J. Lee, H. Limeback and D. T. Cheung (1992). "Correlation of structure and viscoelastic properties in the pericardia of four mammalian species." American Journal of Physiology-Heart and Circulatory Physiology **263**(4): H1095-H1106.
- Ng, A. C. T., V. Delgado, F. van der Kley, M. Shanks, N. R. L. van de Veire, M. Bertini, G. Nucifora, R. J. van Bommel, L. F. Tops, A. de Weger, G. Tavilla, A. de Roos, L. J. Kroft, D. Y. Leung, J. Schuijff, M. J. Schaliij and J. J. Bax (2010). "Comparison of Aortic Root Dimensions and Geometries Before and After Transcatheter Aortic Valve Implantation by 2- and 3-Dimensional Transesophageal Echocardiography and Multislice Computed Tomography / CLINICAL PERSPECTIVE." Circulation: Cardiovascular Imaging **3**(1): 94-102.
- Nkomo, V. T., J. M. Gardin, T. N. Skelton, J. S. Gottdiener, C. G. Scott and M. Enriquez-Sarano (2006). "Burden of valvular heart diseases: a population-based study." The Lancet **368**(9540): 1005-1011.
- O'Connor, B., D. J. Wheatley, G. M. Bernacca and W. S. Haworth (2012). Heart valve prosthesis and method of manufacture. United States, Aortech International PLC.
- Otto, C. M. (2006). "Valvular aortic stenosis: disease severity and timing of intervention." J Am Coll Cardiol **47**(11): 2141-2151.

- Paez, J. M. G. and E. Jorge-Herrero (1999). "Assessment of pericardium in cardiac bioprostheses. A review." Journal of Biomaterials Applications **13**(4): 351-388.
- Paniagua, D., J. A. Condado, J. Besso, M. VÁ©lez, B. Burger, S. Bibbo, D. Cedeno, H. Acquatella, C. Mejia and E. Induni (2005). "First human case of retrograde transcatheter implantation of an aortic valve prosthesis." Texas Heart Institute Journal **32**(3): 393.
- Park, J. C., M. J. Song, Y. S. Hwang and H. Suh (2001). "Calcification comparison of polymers for vascular graft." Yonsei Med J **42**(3): 304-310.
- Pavcnik, D., K. C. Wright and S. Wallace (1992). "Development and Initial Experimental Evaluation of a Prosthetic Aortic-Valve for Transcatheter Placement - Work in Progress." Radiology **183**(1): 151-154.
- Piazza, N., P. de Jaegere, C. Schultz, A. E. Becker, P. W. Serruys and R. H. Anderson (2008). "Anatomy of the Aortic Valvar Complex and Its Implications for Transcatheter Implantation of the Aortic Valve." Circulation: Cardiovascular Interventions **1**(1): 74-81.
- Piazza, N., R. Lange, G. Martucci and P. W. Serruys (2012). "Patient selection for transcatheter aortic valve implantation: Patient risk profile and anatomical selection criteria." Archives of Cardiovascular Diseases **105**(3): 165-173.
- Pinchuk, L. (1994). "A review of the biostability and carcinogenicity of polyurethanes in medicine and the new generation of 'biostable' polyurethanes." J Biomater Sci Polym Ed **6**(3): 225-267.
- Podesser, B. K., D. J. Chambers, S. Gunnes and P. Jynge (2011). Fundamentals of the Past: Cardioplegia: The First Period Revisited. New Solutions for the Heart, Springer Vienna: 15-40.
- Qian, D., E. C. Dickey, R. Andrews and T. Rantell (2000). "Load transfer and deformation mechanisms in carbon nanotube-polystyrene composites." Applied Physics Letters **76**(20): 2868-2870.
- Rama Sreekanth, P. S., N. Naresh Kumar and S. Kanagaraj (2012). "Improving post irradiation stability of high density polyethylene by multi walled carbon nanotubes." Composites Science and Technology **72**(3): 390-396.
- Ramaraj, R. and V. L. Sorrell (2008). "Degenerative aortic stenosis." BMJ **336**(7643): 550-555.
- Rao, P. S. (2012). "Historical Aspects of Transcatheter Treatment of Heart Disease in Children." Pediat Therapeut **S5**(002).
- Ratner, B. D., A. S. Hoffman, F. J. Schoen and J. Lemons (2004). "Biomaterials science: a multidisciplinary endeavor."
- Reibold, M., P. Paufler, A. A. Levin, W. Kochmann, N. Patzke and D. C. Meyer (2006). "Materials: Carbon nanotubes in an ancient Damascus sabre." Nature **444**(7117): 286-286.
- Reilly, R. M. (2007). "Carbon Nanotubes: Potential Benefits and Risks of Nanotechnology in Nuclear Medicine." Journal of Nuclear Medicine **48**(7): 1039-1042.
- Rémi, E., N. Khelil, I. Di Centa, C. Roques, M. Ba, F. Medjahed-Hamidi, F. Chaubet, D. Letourneur, E. Lansac and A. Meddahi-Pellé (2011). "Pericardial Processing: Challenges, Outcomes and Future Prospects."

- Reynolds, M. R., E. A. Magnuson, Y. Lei, K. Wang, K. Vilain, H. Li, J. Walczak, D. S. Pinto, V. H. Thourani, L. G. Svensson, M. J. Mack, D. C. Miller, L. E. Satler, J. Bavaria, C. R. Smith, M. B. Leon and D. J. Cohen (2012). "Cost-Effectiveness of Transcatheter Aortic Valve Replacement Compared With Surgical Aortic Valve Replacement in High-Risk Patients With Severe Aortic Stenosis: Results of the PARTNER (Placement of Aortic Transcatheter Valves) Trial (Cohort A)." Journal of the American College of Cardiology(0).
- Robicsek, F. (1991). "Leonardo da Vinci and the sinuses of Valsalva." Ann Thorac Surg **52**(2): 328-335.
- Rodes-Cabau, J. (2012). "Transcatheter aortic valve implantation: current and future approaches." Nat Rev Cardiol **9**(1): 15-29.
- Rosca, I. D., F. Watari, M. Uo and T. Akasaka (2005). "Oxidation of multiwalled carbon nanotubes by nitric acid." Carbon **43**(15): 3124-3131.
- Ruiz, C. E., J. C. Laborde, J. F. Condado, P. T. L. Chiam and J. A. Condado (2008). "First percutaneous transcatheter aortic valve-in-valve implant with three year follow-up." Catheterization and Cardiovascular Interventions **72**(2): 143-148.
- Sabet, H. Y., W. D. Edwards, H. D. Tazelaar and R. C. Daly (1999). "Congenitally bicuspid aortic valves: a surgical pathology study of 542 cases (1991 through 1996) and a literature review of 2,715 additional cases." Mayo Clin Proc **74**(1): 14-26.
- Sacks, M. S. (2000). "Biaxial mechanical evaluation of planar biological materials." Journal of Elasticity **61**(1-3): 199-246.
- Sacks, M. S., D. W. Merryman and D. E. Schmidt (2009). "On the biomechanics of heart valve function." Journal of biomechanics **42**(12): 1804-1824.
- Sacks, M. S., D. B. Smith and E. D. Hiester (1998). "The aortic valve microstructure: Effects of transvalvular pressure." Journal of Biomedical Materials Research **41**(1): 131-141.
- Sacks, M. S. and A. P. Yoganathan (2007). "Heart valve function: a biomechanical perspective." Philosophical Transactions of the Royal Society B: Biological Sciences **362**(1484): 1369-1391.
- Safadi, B., R. Andrews and E. A. Grulke (2002). "Multiwalled carbon nanotube polymer composites: Synthesis and characterization of thin films." Journal of Applied Polymer Science **84**(14): 2660-2669.
- Safar, M. E., P. A. Peronneau, J. A. Levenson, J. A. Toto-Moukouo and A. C. Simon (1981). "Pulsed Doppler: diameter, blood flow velocity and volumic flow of the brachial artery in sustained essential hypertension." Circulation **63**(2): 393-400.
- Sandgren, T., B. Sonesson, A. R. Ahlgren and T. Lanne (1999). "The diameter of the common femoral artery in healthy human: Influence of sex, age, and body size." Journal of Vascular Surgery **29**(3): 503-510.
- Shabetai, R. (2004). The Pericardium. Massachusetts, Kluwer Academic Publishers.
- Shvedova, A. A., E. Kisin, A. R. Murray, V. J. Johnson, O. Gorelik, S. Arepalli, A. F. Hubbs, R. R. Mercer, P. Keohavong, N. Sussman, J. Jin, J. Yin, S. Stone, B. T. Chen, G. Deye, A.

- Maynard, V. Castranova, P. A. Baron and V. E. Kagan (2008). "Inhalation vs. aspiration of single-walled carbon nanotubes in C57BL/6 mice: inflammation, fibrosis, oxidative stress, and mutagenesis." American Journal of Physiology - Lung Cellular and Molecular Physiology **295**(4): L552-L565.
- Simmons, A., J. Hyvarinen, R. A. Odell, D. J. Martin, P. A. Gunatillake, K. R. Noble and L. A. L. A. Poole-Warren (2004). "Long-term in vivo biostability of poly(dimethylsiloxane)/poly(hexamethylene oxide) mixed macrodiol-based polyurethane elastomers." Biomaterials **25**(20): 4887-4900.
- Sinha, P., D. Zurakowski, T. K. Susheel Kumar, D. He, C. Rossi and R. A. Jonas (2012). "Effects of glutaraldehyde concentration, pretreatment time, and type of tissue (porcine versus bovine) on postimplantation calcification." The Journal of Thoracic and Cardiovascular Surgery **143**(1): 224-227.
- Sinning, J. M., N. Werner, G. Nickenig and E. Grube (2012). "Next-generation transcatheter heart valves: current trials in Europe and the US." Methodist Debaquey Cardiovasc J **8**(2): 9-12.
- Siu, S. C. and C. K. Silversides (2010). "Bicuspid Aortic Valve Disease." Journal of the American College of Cardiology **55**(25): 2789-2800.
- Smart, S. K., A. I. Cassady, G. Q. Lu and D. J. Martin (2006). "The biocompatibility of carbon nanotubes." Carbon **44**(6): 1034-1047.
- Smith, C. R., M. B. Leon, M. J. Mack, D. C. Miller, J. W. Moses, L. G. Svensson, E. M. Tuzcu, J. G. Webb, G. P. Fontana, R. R. Makkar, M. Williams, T. Dewey, S. Kapadia, V. Babaliaros, V. H. Thourani, P. Corso, A. D. Pichard, J. E. Bavaria, H. C. Herrmann, J. J. Akin, W. N. Anderson, D. Wang and S. J. Pocock (2011). "Transcatheter versus Surgical Aortic-Valve Replacement in High-Risk Patients." New England Journal of Medicine **364**(23): 2187-2198.
- Song, Y. S. and J. R. Youn (2005). "Influence of dispersion states of carbon nanotubes on physical properties of epoxy nanocomposites." Carbon **43**(7): 1378-1385.
- Spitalsky, Z., D. Tasis, K. Papagelis and C. Galiotis (2010). "Carbon nanotube-polymer composites: Chemistry, processing, mechanical and electrical properties." Progress in Polymer Science **35**(3): 357-401.
- Spodick, D. H. (1997). The Pericardium: A Comprehensive Textbook. New York, Marcel Dekker.
- Stephenson, L. W. (2008). "History of cardiac surgery." Surgery: 1471-1479.
- Stradins, P., R. Lacis, I. Ozolanta, B. Purina, V. Ose, L. Feldmane and V. Kasyanov (2004). "Comparison of biomechanical and structural properties between human aortic and pulmonary valve." European Journal of Cardio-Thoracic Surgery **26**(3): 634-639.
- Sutton Iii, J. P., S. Y. Ho and R. H. Anderson (1995). "The forgotten interleaflet triangles: A review of the surgical anatomy of the aortic valve." The Annals of Thoracic Surgery **59**(2): 419-427.
- Swanson, W. M. and R. E. Clark (1974). "Dimensions and Geometric Relationships of the Human Aortic Value as a Function of Pressure." Circulation Research **35**(6): 871-882.
- Takahashi, K., R. Shizume, K. Uchida and H. Yajima (2009). "Improved blood biocompatibility of composite film of chitosan/carbon nanotubes complex." Journal of Biorheology **23**(1): 64-71.

- Taylor, J. E., P. R. Laity, S. S. Wong, K. Norris, P. Khunkamchoo, M. Cable, G. Andrews, A. F. Johnson and R. E. Cameron (2006). "Examination of hard segment and soft segment phase separation in polyurethane medical materials by electron microscopy techniques." Microsc Microanal **12**(2): 151-155.
- Temple, L. J., R. Serafin, N. G. Calvert and J. M. Drabble (1964). "Principles of fluid mechanics applied to some situations in the human circulation and particularly to the testing of valves in a pulse duplicator." Thorax **19**(3): 261-267.
- Thomas, M., G. Schymik, T. Walther, D. Himbert, T. Lefèvre, H. Treede, H. Eggebrecht, P. Rubino, A. Colombo, R. Lange, Schwarz, R. R. and O. Wendler (2011). "One-Year Outcomes of Cohort 1 in the Edwards SAPIEN Aortic Bioprosthesis European Outcome (SOURCE) Registry / Clinical Perspective." Circulation **124**(4): 425-433.
- Thostenson, E. T., Z. Ren and T. W. Chou (2001). "Advances in the science and technology of carbon nanotubes and their composites: a review." Composites Science and Technology **61**: 1899-1912.
- Thubrikar, M. (1990). The Aortic Valve. Boca Raton, CRC Press.
- Thubrikar, M., W. C. Piepgrass, T. W. Shaner and S. P. Nolan (1981). "The design of the normal aortic valve." American Journal of Physiology - Heart and Circulatory Physiology **241**(6): H795-H801.
- Thubrikar, M. J. (1990). The Aortic Valve, Taylor & Francis.
- Toggweiler, S., R. Gurvitch, J. Leipsic, D. A. Wood, A. B. Willson, R. K. Binder, A. Cheung, J. Ye and J. G. Webb (2012). "Percutaneous Aortic Valve Replacement: Vascular Outcomes With a Fully Percutaneous Procedure." Journal of the American College of Cardiology **59**(2): 113-118.
- Vahanian, A., O. Alfieri, N. Al-Attar, M. Antunes, J. Bax, B. Cormier, A. Cribier, P. De Jaegere, G. Fournial, A. P. Kappetein, J. Kovac, S. Ludgate, F. Maisano, N. Moat, F. Mohr, P. Nataf, L. PiÅ©ard, J. L. Pomar, J. Schofer, P. Tornos, M. Tuzcu, B. van Hout, L. K. Von Segesser and T. Walther (2008). "Transcatheter valve implantation for patients with aortic stenosis: a position statement from the European Association of Cardio-Thoracic Surgery (EACTS) and the European Society of Cardiology (ESC), in collaboration with the European Association of Percutaneous Cardiovascular Interventions (EAPCI)." European Heart Journal **29**(11): 1463-1470.
- Vahanian, A., D. Himbert, É. Brochet, J.-P. Depoix, B. Iung and P. Nataf (2012). "Transcatheter aortic valve implantation: Our vision of the future." Archives of Cardiovascular Diseases **105**(3): 181-186.
- Vaisman, L., H. D. Wagner and G. Marom (2006). "The role of surfactants in dispersion of carbon nanotubes." Advances in Colloid and Interface Science **128-130**: 37-46.
- Verbrugge, P., B. Meuris, W. Flameng and P. Herijgers (2009). "Reconstruction of atrioventricular valves with photo-oxidized bovine pericardium." Interactive CardioVascular and Thoracic Surgery **9**(5): 775-779.

- Vesely, I. (1998). "The role of elastin in aortic valve mechanics." Journal of Biomechanics **31**(2): 115-123.
- Vesely, I. (2003). "The evolution of bioprosthetic heart valve design and its impact on durability." Cardiovascular Pathology **12**(5): 277-286.
- Vitale, N., M. De Feo, P. De Siena, G. Cappabianca, F. Onorati, R. Gregorio, S. Branzoli, L. de Luca, T. Schinosa, M. Vigano, M. Scardone and M. Cotrufo (2004). "Tilting-disc versus bileaflet mechanical prostheses in the aortic position: a multicenter evaluation." J Heart Valve Dis. **13**(Suppl 1): S27-34.
- Vyavahare, N., M. Ogle, F. J. Schoen, R. Zand, D. C. Gloeckner, M. Sacks and R. J. Levy (1999). "Mechanisms of bioprosthetic heart valve failure: Fatigue causes collagen denaturation and glycosaminoglycan loss." Journal of Biomedical Materials Research **46**(1): 44-50.
- Walther, T., H. Möllmann, A. v. Linden and J. Kempfert (2011). "Transcatheter Aortic Valve Implantation Transapical: Step by Step." Seminars in thoracic and cardiovascular surgery **23**(1): 55-61.
- Ward, C. (2000). "Clinical significance of the bicuspid aortic valve." Heart **83**(1): 81-85.
- Webb, J. G. and R. K. Binder (2012). "Transcatheter aortic valve implantation: The evolution of prostheses, delivery systems and approaches." Archives of Cardiovascular Diseases **105**(3): 153-159.
- Webb, J. G., M. Chandavimol, C. R. Thompson, D. R. Ricci, R. G. Carere, B. I. Munt, C. E. Buller, S. Pasupati and S. Lichtenstein (2006). "Percutaneous Aortic Valve Implantation Retrograde From the Femoral Artery." Circulation **113**(6): 842-850.
- Webb, J. G., D. A. Wood, J. Ye, R. Gurvitch, J.-B. Masson, J. Rodés-Cabau, M. Osten, E. Horlick, O. Wendler, E. Dumont, R. G. Carere, N. Wijesinghe, F. Nietlispach, M. Johnson, C. R. Thompson, R. Moss, J. Leipsic, B. Munt, S. V. Lichtenstein and A. Cheung (2010). "Transcatheter Valve-in-Valve Implantation for Failed Bioprosthetic Heart Valves." Circulation **121**(16): 1848-1857.
- Webster, T. J., M. C. Waid, J. L. McKenzie, R. L. Price and J. U. Ejiófor (2004). "Nanobiotechnology: carbon nanofibres as improved neural and orthopaedic implants." Nanotechnology **15**(1): 48.
- Wheatley, D. J., G. M. Bernacca, M. M. Tolland, B. O'Connor, J. Fisher and D. F. Williams (2000). "Hydrodynamic function of a biostable polyurethane flexible leaflet heart valve after 6 months in sheep." International Journal of Artificial Organs **23**(8): 19.
- Wheatley, D. J., J. Fisher and D. Williams (1998). HEART VALVE PROSTHESIS.
- Wheatley, D. J., L. Raco, G. M. Bernacca, I. Sim, P. R. Belcher and J. S. Boyd (2000). "Polyurethane: material for the next generation of heart valve prostheses?" Eur J Cardiothorac Surg **17**(4): 440-448.
- Williams, D. F. (1999). The Williams dictionary of Biomaterials. Liverpool, Liverpool University Press.

- Willson, A., S. Toggweiler and J. G. Webb (2011). Transfemoral aortic valve replacement with the SAPIEN XT valve: step-by-step. Seminars in Thoracic and Cardiovascular Surgery, Elsevier.
- Xie, X.-L., Y.-W. Mai and X.-P. Zhou (2005). "Dispersion and alignment of carbon nanotubes in polymer matrix: A review." Materials Science and Engineering: R: Reports **49**(4): 89-112.
- Xiong, J., Z. Zheng, X. Qin, M. Li, H. Li and X. Wang (2006). "The thermal and mechanical properties of a polyurethane/multi-walled carbon nanotube composite." Carbon **44**(13): 2701-2707.
- Yang, B., W. M. Huang, C. Li and L. Li (2006). "Effects of moisture on the thermomechanical properties of a polyurethane shape memory polymer." Polymer **47**(4): 1348-1356.
- Ye, J., A. Cheung, S. V. Lichtenstein, F. Nietlispach, S. Albugami, J. B. Masson, C. R. Thompson, B. Munt, R. Moss, R. G. Carere, W. R. Jamieson and J. G. Webb (2010). "Transapical transcatheter aortic valve implantation: follow-up to 3 years." The Journal of thoracic and cardiovascular surgery **139**(5): 1107-1113, 1113.e1101.
- Yin, W., S. Gallocher, L. Pinchuk, R. T. Schoepfoerster, J. Jesty and D. Bluestein (2005). "Flow-induced Platelet Activation in a St. Jude Mechanical Heart Valve, a Trileaflet Polymeric Heart Valve, and a St. Jude Tissue Valve
Artificial Organs Volume 29, Issue 10." Artificial Organs **29**(10): 826-831.
- Yu, M.-F., B. S. Files, S. Arepalli and R. S. Ruoff (2000). "Tensile Loading of Ropes of Single Wall Carbon Nanotubes and their Mechanical Properties." Physical Review Letters **84**(24): 5552.
- Yu, M.-F., O. Lourie, M. J. Dyer, K. Moloni, T. F. Kelly and R. S. Ruoff (2000). "Strength and Breaking Mechanism of Multiwalled Carbon Nanotubes Under Tensile Load." Science **287**(5453): 637-640.
- Zegdi, R., P. Bruneval, D. Blanchard and J.-N. I. Fabiani (2011). "Evidence of leaflet injury during percutaneous aortic valve deployment." European Journal of Cardio-Thoracic Surgery **40**(1): 257-260.
- Zilla, P., J. Brink, P. Human and D. Bezuidenhout (2008). "Prosthetic heart valves: Catering for the few." Biomaterials **29**(4): 385-406.
- Zioupos, P. (1989). Mechanical Properties and Structure of Bovine Pericardium. PhD, University of Strathclyde.
- Zioupos, P., J. C. Barbenel and J. Fisher (1992). "Mechanical and Optical Anisotropy of Bovine Pericardium." Medical & Biological Engineering & Computing **30**(1): 76-82.
- Zioupos, P., J. C. Barbenel and J. Fisher (1994). "Anisotropic Elasticity and Strength of Glutaraldehyde Fixed Bovine Pericardium for Use in Pericardial Bioprosthetic Valves." Journal of Biomedical Materials Research **28**(1): 49-57.